Ultra-Fast Transient Pool Boiling under High Pressure and Subcoolings

by

Ezekiel Thomas Villarreal

BS Mechanical Engineering, Utah State University, 2016

MS Mechanical Engineering, University of Pittsburgh, 2022

Submitted to the Graduate Faculty of the

Swanson School of Engineering in partial fulfillment

of the requirements for the degree of

Doctor of Philosophy

University of Pittsburgh

2023

UNIVERSITY OF PITTSBURGH

SWANSON SCHOOL OF ENGINEERING

This dissertation was presented

by

Ezekiel Thomas Villarreal

It was defended on

March 29, 2023

and approved by

Thomas Vincent Congedo, PhD, Adjunct Professor, Department of Mechanical Engineering and Materials Science, University of Pittsburgh

Katherine Mary Hornbostel, PhD, Assistant Professor, Department of Mechanical Engineering and Materials Science, University of Pittsburgh

Minghui Chen, PhD, Assistant Professor, Department of Nuclear Engineering, University of New Mexico

Heng Ban, PhD, Professor, Richard K. Mellon Professor & Associate Dean for Strategic Initiatives, Department of Mechanical Engineering and Materials Science, University of Pittsburgh

Ultra-Fast Transient Pool Boiling under High Pressure and Subcoolings

Ezekiel Thomas Villarreal, PhD

University of Pittsburgh, 2023

Growing global energy consumption and demand has led to growing interest in a variety of energy options and new technologies for various applications. A fundamental understanding of the foundational physics is essential in being able to design and safely operate future energy options and technologies. Of particular interest presently are energy sources that produce little to no carbon emissions. Nuclear energy is a vital component of the repertoire of zero-carbon energy sources. Under accident conditions nuclear reactors can undergo high-energy, fast power transients. In addition, advancing technologies are required to dissipate larger quantities of heat at shorter timescales. The goal of this work is to investigate ultra-fast transient pool boiling regimes to enhance the fundamental understanding of this phenomenology and to establish a basis for future energy and technological application.

In this work, temperature, heat transfer, and high-speed imagery of transient boiling events are collected during ultra-fast (up to 250,000°C/s) heating pulses to define the behavior and mechanisms occurring. While pool boiling responses have been studied previously at longer time scales, this work provides fundamental understanding of the mechanisms in the ultra-fast timescale. To accomplish this a high-pressure, variable temperature, transient boiling system is created to experimentally study a variety of factors related to ultra-fast transient boiling. These factors include combinations of pressures and water subcoolings, the heater surface condition, the heating shape, and the heating level. The water is heated by, and measurement are taken from, a thin wire inside a pressure vessel. Parameter comparison studies are performed to provide a relative

importance of the tested parameters on a variety of experimental outcomes. Additional investigations of the material failure mechanisms under extreme heating rates are presented.

Ultimately, this work presents the transient boiling heat transfer and associated phenomena of numerous experimental conditions under ultra-fast heating. This will provide a fundamental evaluation of an area of pool boiling that has not been previously explored. The results can provide a basis to drive growth and future study both in the nuclear industry and in the heat transfer industry, where there is an ever-increasing demand for higher heat transfer and controllable configurations.

Table of Contents

List of Tables

List of Figures

Preface

I, Ezekiel, having been born of goodly parents therefore I was taught somewhat in all the learning of my fathers, and it is largely to my parents and the diverse learning that they gave me that I owe my desire to pursue endless education. To my parents and my family, both biological and by marriage, I am endlessly grateful. Throughout the course of my graduate career no one has been more supportive and motivating to me than my dear wife, Paige. She saw me through the times when it seemed like things wouldn't work and encouraged me to do what it took to get things finished. She, together with our four children, Franklin, Ralph, Ramona, and Lewis, have been the biggest source of comfort and joy to me throughout this process. To you five I owe my future and all that I have grown to be.

Sir Isaac Newton is quoted as saying, "If I have seen further, it is by standing on the shoulders of giants." To the many giants who came before me and worked around me, I give my thanks. I thank Dr Heng Ban for his guidance, his foresight, and his care for me and my family throughout a journey that started almost 2,000 miles away. Thank you for caring about us and helping me realize that there was more inside of me. I thank Dr Alison Hake for the painstaking effort that was the in-depth review of this dissertation and the hours of work and discussion ranging from boiling to electronics to computations. I am grateful to the members of my thesis committee Dr Thomas Congedo, Dr Katherine Hornbostel, and Dr Minghui Chen for their willingness to see me through this process and for their support and encouragement throughout. I am grateful to all the members of the Pitt Multiscale Thermophysics Lab throughout the years. Thank you all for the memories. In particular, I want to acknowledge Duane DiCenzo, Philip Santillo, Joseph Martino,

Gregory Kinzler, Tomas Mayer-Costa, Dr Tess Zangrilli, Yuan Gao and Dr Mingfu He for their direct work in this and other boiling ventures. You, and all of my lab mates and collaborators in multiple states and multiple countries, have made my graduate work a joy.

And finally, as a deeply religious individual, I would be remiss to not acknowledge the goodness of a God who got me through it all and helped me become more than I ever thought I would be. To all these people, so many others, and you for reading this, I am grateful!

~Ezekiel Villarreal

Nomenclature – (with units unless otherwise specified in the text)

Bi – Biot Number

c_p – Specific heat capacity at constant pressure, $[J \cdot kg^{-1} \cdot K^{-1}]$

d – Diameter, [m]

Gr – Grashof Number

h – Convective Heat Transfer Coefficient, $[W \cdot m^{-2} \cdot K^{-1}]$

I – Current, [A]

J_n – Bessel Function of the first kind, order n

k – Thermal conductivity, $[W \cdot m^{-1} \cdot K^{-1}]$

l – length, [m]

P – Power, [W]

Pr – Prandtl Number

q'' – Heat Transfer per Unit Area, $[W \cdot m^{-2}]$

q''' – Volumetric Heat Generation, $[W \cdot m^{-3}]$

r – Cylindrical Variable (radius [m])

R – Resistance [Ω]

r_0 – Full Wire Radius, [m]

R_0 – Resistance at 0 °C, [Ω]

Ra – Rayleigh Number

Re – Reynolds Number

T – Temperature, [°C]

T_∞ - Ambient Surrounding Temperature, [°C]

t – time, [s]

V – Voltage, [V]

$\forall$ – Total volume, [m^3]

x – Cartesian Variable

y – Cartesian Variable

z – Cartesian Variable

α – Thermal diffusivity, [$m^2 \cdot s^{-1}$]

ϵ – Emissivity

λ – Numerical Weighting Factor

λ_k – Eigenvalue (square root of the Separation Constant, λ_k^2)

ρ – Density, [$kg \cdot m^{-3}$]

ρ_e – Electrical Resistivity, [$\Omega \cdot cm$]

σ – Stephan Boltzmann constant, [$W \cdot m^{-2} \cdot K^{-4}$]

θ – Cylindrical Variable (azimuth)

Acronyms

BWR	Boiling Water Reactor
CHF	Critical Heat Flux
CVD	Callendar-Van Dusen
CSR	Current Sense Resistor
DI	Deionized
DNB	Departure from Nucleate Boiling
DOE	Department of Energy
FWHM	Full Width Half Maximum
HTC	Heat Transfer Coefficient
IR	Infrared
LWR	Light Water Reactor (a common nuclear reactor type in the USA)
MTL	Multiscale Thermophysics Laboratory
PWR	Pressurized Water Reactor
RIA	Reactivity Initiated Accident
TRT	Temperature Resistance Thermometer

1.0 Introduction

Characterizing heat transfer in many contexts and processes is essential to generate electricity, to manufacture a great variety of products, and to develop new technologies to better serve the world and its people. Within the energy sector, there is significant interest in the heat transfer behavior of nuclear reactors, particularly under sudden accident conditions. This work presents a detailed experimental analysis of ultrafast transient boiling heat transfer under elevated pressure and subcooling similar to the conditions seen in a nuclear reactor. Subcooling is defined as the difference between the liquid temperature and the boiling point. This chapter will present the motivation and broad overview of the work. A full description of the work, as well as the state of the art will be presented in later chapters.

1.1 Motivation

Growing global energy consumption and demand has led to increased interest in a variety of energy generation options. Of particular interest presently are energy sources that produce little to no carbon emissions. Among the most prominent of these low-carbon energy sources are solar panels, wind turbines, hydropower, geothermal energy, and nuclear reactors. Nuclear reactors present key advantages in their ability to operate independent of time and weather, scale energy production to meet fluctuating demand, and their functional longevity. Despite these benefits, nuclear reactors have a unique set of challenges and potential behaviors to understand.

In the United States, commercial nuclear reactors are Light Water Reactors (LWRs), of which there are two kinds, Pressurized Water Reactors (PWRs) and Boiling Water Reactors (BWRs). “Light water” that the reactor uses regular water (as opposed to heavy water, in which the hydrogen is replaced with deuterium) as a moderator to slow down and absorb energy from neutrons produced by nuclear fission in the reactor core. The coolant water is kept at very high pressure (150-160 Bar) for PWRs in order to allow the moderating water to reach high temperatures without boiling. This high temperature water then transfers its energy as heat to a secondary water loop at lower pressure to create steam and drive a turbine-generator, ultimately producing electricity. Throughout the operation of the PWR it is assumed that the moderating water does not boil, being maintained at a temperature approximately 50 °C below the point of boiling. However, the moderator *can* boil under certain conditions. It is therefore critical to understand the impact that this boiling may have on the safety and efficiency of the reactor.

The pioneering work on boiling heat transfer characterization was performed by S. Nukiyama in 1934 [1]. Since that time, many experiments have been performed to understand boiling behavior in many different scenarios. However, there remain unexplored areas of the characterization and parameter comparison. In particular, the ultra-fast transient pool boiling heat transfer of a thin cylindrical heating source under increased pressure and water subcooling has not been studied to provide fundamental phenomena and behavior. This transient behavior, however, is an accurate description of the heating that can occur in the long, thin fuel rods of a nuclear reactor during a Reactivity-Initiated Accident (RIA), which condition was the initial idea that led to the conception of the study presented in this dissertation

A RIA occurs when a sudden, unwanted increase in the fission rate occurs, and results in a near instantaneous increase in reactor power [2]. In general, the fission rate is partially managed

by control rods which absorb excess neutrons from the reactor core. However, if the control rod is suddenly ejected, rapid fission and heat production occur causing a RIA. This accident is characterized by a peak in the core output power, which occurs over a very short time period, usually on the order of 30 ms Full Width Half Maximum (FWHM) [3]. This energy is transmitted to the primary coolant, which can be near-instantaneously vaporized; this, in effect, insulates the nuclear fuel leading to increased temperatures. The insulation reduces the heat transfer between fluid and fuel and can weaken the cladding material [4 – 9]. In severe cases, the fuel can shatter, and the fuel cladding can rupture [10].

Currently, there exists a lack of consensus between several global regulatory agencies regarding the heat transfer behavior under RIA-like conditions [3]. This is illustrated in Figure 1, which shows the various models used to predict the cladding outer surface temperature due to a RIA under one of 10 simplified cases for modeling comparison. Similar variability exists in many of the other cases [3]. The predicted behaviors range from a 1 second temperature increase of 500 °C, to a prolonged temperature increase of 1,800 °C. This figure clearly indicates how different modeling assumptions lead to significant divergence in predicted accident behaviors and outcomes. Variation in model assumptions will persist unless the transient heating behavior under RIA-like conditions is more thoroughly quantified. This led to the ideation of the work presented here.

The primary motivation for this work is to understand the fundamental science and mechanisms of ultra-fast heating, pool boiling under high pressure and subcooling conditions. This will allow future work to elucidate the fundamental transient boiling behavior under RIA-like pulses and time scales. The outcomes of this work will provide a first principles understanding from which future theoretical and simulation models can be developed.

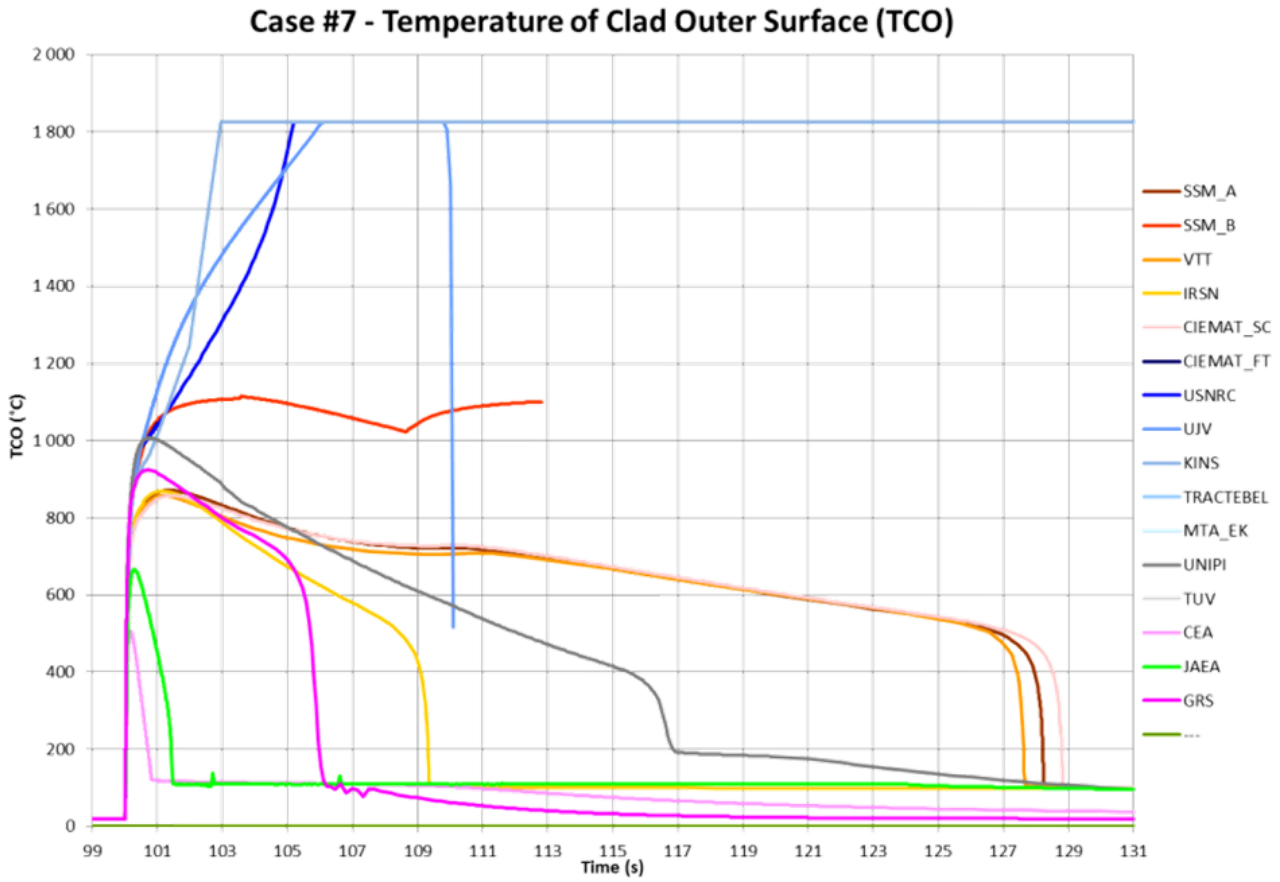

Figure 1: Modeled results used by a variety of agencies for the cladding wall temperature after a RIA are quite spread [3].

The broader application and additional motivations of this work are much more varied than a single nuclear application. Pool boiling heat transfer has been studied for a wide range of potential uses in areas ranging from power generation to chemical and food processing, and from space applications to microelectronics and cooling devices. An understanding of transient boiling heat transfer, and the various mechanisms which affect it will allow for effective and informed design and utilization of boiling over a range of new research areas and applications of heat management.

1.2 Overview and Broader Approach

Traditional boiling characterization primarily focuses on two parameters. The first is the temperature of the heating surface, usually called the wall or surface temperature and given as a delta temperature above the boiling point of the fluid. The second is the heat transferred to the water at the associated temperature. A multitude of methods for measuring these two parameters exist, including various combinations of Temperature Resistance Thermometry (TRT) [11-24], infrared thermometry[25-27], direct thermocouple measurement[28-30], laser holographic interferometry [16], and high-speed imagery[11-14, 17-18, 20-24, 31]. These methods are compared in Table 1 of the work presented by the author in [10]. Due to the relative ease in finding resistive surfaces and their general applicability, the bulk of the research is performed using TRT, as demonstrated above.

The TRT adaptation used in this work involves measuring the voltage across a Joule-heated wire. This technique is employed under novel scenarios, including combinations of fast timescales, temperature, and pressure, to elucidate the physics and impact of various parameters on transient pool boiling. These studied parameters are the system pressure and subcooling pair (more especially the impact of the overall vs relative state), the heating pulse shape, and the heating wire physical and surface condition. A study on the failure mechanism of wires under fast transients is also presented.

The intent of this work is to explore the ultra-fast heating (over 9,000°C/s) pool boiling behavior under the temperature and pressure loading conditions of a nuclear LWR, and to highlight similarities and differences to the boiling behavior seen at standard atmospheric temperature and pressure conditions. This fundamental understanding will serve as a basis for future research to

inform modeling and simulation work in the nuclear industry, particularly under accident conditions when such fast transient boiling is most likely to occur. The work presented here was performed at the Multiscale Thermophysics Laboratory (MTL) in the Mechanical Engineering and Material Science department of the Swanson School of Engineering at the University of Pittsburgh, in Pittsburgh Pennsylvania.

1.3 Layout

The remainder of this work will proceed according to the following outline: The objectives of the work will be established (Chapter 2), the needed background information and state of the art previous to this work will be presented (Chapter 3), the methodology and approach will be highlighted along with a details of the plan pursued (Chapters 4-5), the results of individual studies along with their considerations and impacts will be presented (Chapters 6-9), and finally a general conclusion and discussion will be given. Appendices with additional data and code are provided after the work.

2.0 Objectives

The purpose of this research is to provide a fundamental understanding of the unknown boiling and heat transfer behavior from high power, short duration pulses supplied to thin wires in a water pool under atmospheric and increased pressure and two levels of water subcooling. The successful completion of this work allows us to:

1. Experimentally measure the temperature of, and heat transfer from, a thin wire subject to various states of pressure and water subcooling.
2. Correlate boiling behavior and the regime seen at temperature vs heat transfer locations to define the transient pool boiling heat transfer curve for ultrafast heating.
3. Quantify the impact of various experimental parameters on the heat transfer at a given heater temperature to inform and improve design and modeling of future systems.

In combination, these objectives aim to define the behavior of an unknown area of boiling heat transfer. Furthermore, quantifying the impact of various physical parameters on the heat transfer behavior will identify potential methods for heat transfer enhancement. Overall, data-informed thermal management is broadly applicable to various situations, ranging from nuclear accidents to energy generation to space applications.

2.1 Objective 1: Experimentally measure the temperature of, and heat transfer from, a thin wire subject to various states of pressure and water subcooling.

Fundamentally, the simultaneous measurement of the thin wire surface temperature and the heat transfer from the wire were necessary for the success of this research. In steady state boiling, knowledge of the heated surface temperature corresponds to the expected heat transfer values and the boiling behavior. Under transient conditions the correlation between these values and their behavior changes. Thus, it is crucial to measure both values simultaneously and independently to establish the correlation between temperature and heat transfer and compare the transient behavior to the steady state boiling curve. This relative values between heat transfer and temperature allow for comparisons to be made to the current state of the art, and it provide a basis for design decisions.

The demands for thermal control and predictive behavior are ever increasing, as seen in growing heat generation and dissipation needs, energy safety and reliability, and controlled thermal environments. Because of these demands it becomes increasingly important to understand what options exist for thermal management and control and especially the factors that influence these options. This highlights the importance of establishing the temperature and heat transfer relationship of new transient boiling regimes and probing what factors influence it.

2.2 Objective 2: Correlate boiling behavior and the regime seen at temperature vs heat transfer locations to define the transient pool boiling heat transfer curve for ultrafast heating.

The full impact of the boiling event cannot be calculated using only the heat flux and temperature. One shortcoming of only knowing the heat transfer and temperature is found in the hysteresis demonstrated in the original boiling curve. In order to better understand the total effect of the boiling along with the driving mechanisms, the specific boiling state that is occurring also needs to be known. The standard, steady state boiling curve with labeled boiling regimes is shown in Figure 2. The relationship between boiling state and the location on this curve is particularly instructive in determining the mechanism driving changes observed in the collected data. To illustrate this point, a thought experiment is presented, as follows:

Imagine how the surface temperature of a wire with current running through it would change if the surrounding water were to suddenly transition from a liquid to a vapor. Would this bubble, and potential oscillations, have a simultaneous effect on heat transfer and temperature, or would one lag the other? Imagine, again, the change that would occur due to the expansion of the bubble layer, and ultimately the change when the bubble lifts off from the wire. What would the wire state be after bubble lift off in relation to the previous states? Would it return to the same state or would the amount of heat being released result in a new, unique state? In order to adequately determine these effects, observation of the precise boiling behavior is ancillarily necessary to the temperature and heat transfer. This behavior also clarifies anomalies that may occur during the boiling process.

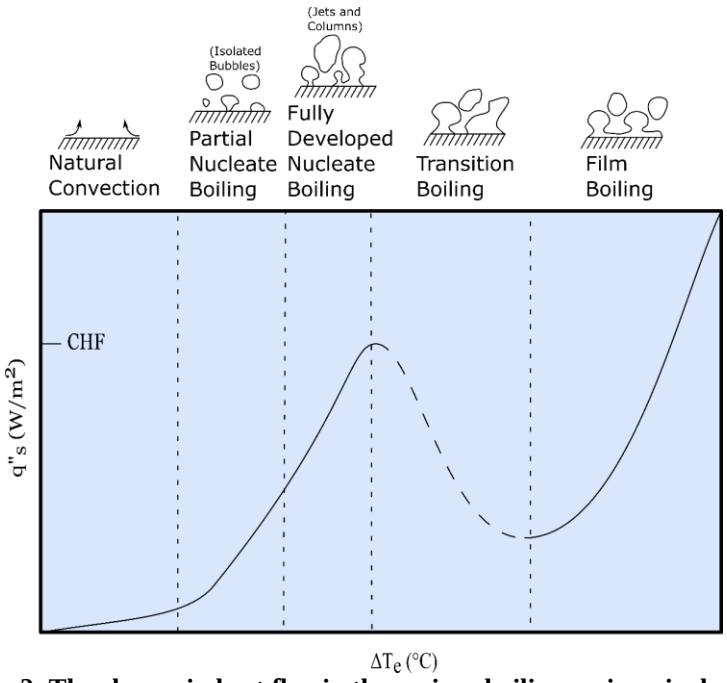

Figure 2: The change in heat flux in the various boiling regimes is shown. [37]

The steady state, pool boiling curve shown in Figure 2 is well defined and understood. This same understanding does not extend to the numerous conditions of transient boiling. While the heat transfer in transient conditions is shown to be larger than steady state [10,32-34], it is still unclear how pressure and subcooling will change the boiling curve under ultra-fast time scales and what factors will influence the behavior. To date, a fundamental understanding of boiling under these conditions remains unknown.

2.3 Objective 3: Quantify the impact of various experimental parameters on the heat transfer at a given heater temperature to inform and improve design and modeling of future systems.

The final piece to this work is to evaluate and quantify the impact of combinations of pressures and water subcoolings, the heater surface condition, the heating shape, and the heating level on the captured heat transfer, temperature, and boiling behavior. The acquired knowledge can establish a guide for making heat transfer decisions over various applications, such as designing systems to optimize heat transfer (to a maximum or minimum depending on the application), designing accident resistant systems, and informing simulation work.

When complete, this research will provide a basis on which to make decisions regarding the safety and optimization of systems undergoing ultra-fast transient pool boiling at elevated pressures and subcooling. This is imperative to both present and future safety, as in the case of the behavior of nuclear fuel, and the design and utilization of future technologies. Currently there is an accelerated need for data to inform decisions that will have lasting impact on our clean energy future and on future technological capabilities.

3.0 State of the Art, Theoretical Background, and Considerations

In order to facilitate uniform understanding of the concepts that will be discussed in this work, a wide array of underlying principles is presented. These principles range from fundamental and transient boiling phenomena to heat transfer to mathematical considerations in numerical processing. These topics are presented up front to orient the discussions in later chapters.

3.1 Boiling and Boiling Heat Transfer

The boiling phenomenon will be broken into two major branches for consideration: 1) Fundamental and Steady State Boiling and 2) Transient Boiling.

3.1.1 **Fundamental and Steady State Boiling**

As noted previously, the founding work on boiling characterization was performed by S. Nukiyama in 1934 and translated to English in 1966 [1] [1]. In this work, he initially used an electrically heated (via the Joule effect) nichrome wire across which the voltage drop was measured, along with the supplied current. The resistance of the wire could be calculated according to Ohm's law, $V = I \cdot R$, and, with a calibration of the wire resistance value as a function of the temperature, the wire temperature could be easily calculated. In addition to the temperature, the power produced by the system also becomes plain using the electronic power, $P = I \cdot V$. Under such steady-state conditions the total power produced across the wire is assumed to be completely

transferred to the water (there are only two options available for the heat; it can stay in the wire raising the wire temperature or it can leave the wire and be transferred to the surroundings). As the wire temperature in this case was steady, it is assumed that a thermal equilibrium is reached, and all the power is transferred out of the system as heat. The heat transfer can then be generalized by solving in a per unit area form.

Nukiyama observed that different boiling regimes existed depending upon the temperature of the heating surface (the wire in his setup). It should be noted that, in this work, the directly controlled parameter was not the wire temperature, but rather the system current. For most intents and purposes this distinction is of trivial importance (the power level determines the temperature of the wire). However, Nukiyama observed that above a certain power level, a rapid temperature excursion occurred, and the nichrome wire melted. To better understand the phenomenon at play, he subsequently used a platinum wire in place of nichrome since platinum has a higher melting temperature and could be used to probe deeper into the behavior.

With the platinum wire, it was observed that in order to reach a heat transfer level above a certain value, later to be known as the Critical Heat Flux (CHF), the temperature would need to increase drastically. The phenomenon was found to exist hysteretically in reverse. As the power level was reduced, the system fell below the CHF point at high temperature to a certain heat transfer value, later to be known as the Leidenfrost point, where again a temperature excursion occurred, in the negative direction this time, would occur. This curve is recreated in this work as seen in Figure 3.

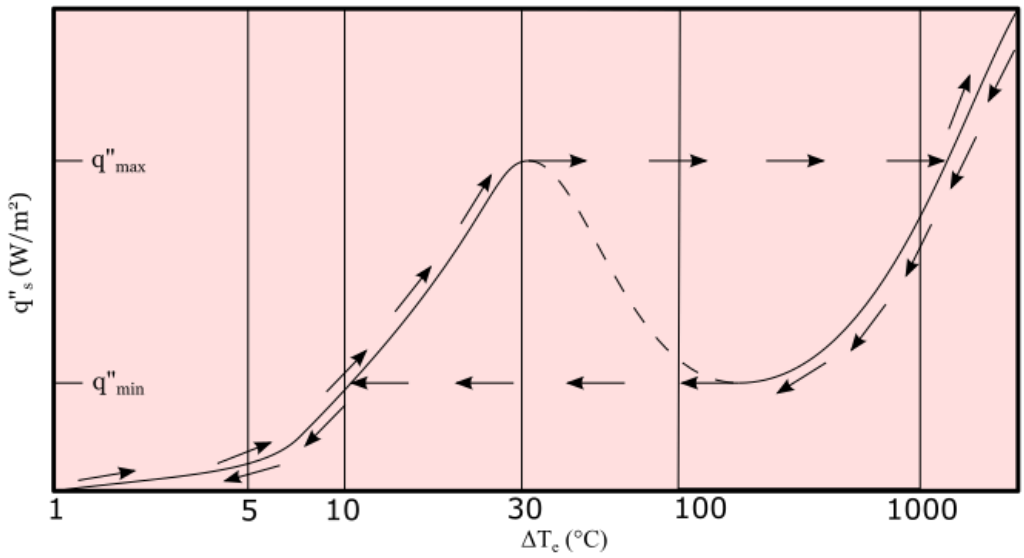

Figure 3: Hysteresis seen in the steady-state boiling curve found by Nukiyama. [1]

Nukiyama noted that the part of the curve between the $q"_{min}$ and $q"_{max}$, shown with the dashed lines in Figure 3, was "so unstable that it is hard to obtain in practice." [1] This curve, with the subsequent discoveries, clarifications, and equations form the basis of boiling and provide a comparison for all studies performed later.

3.1.2 **Transient Boiling and Present State of the Art**

Since the initial work in boiling was completed, extensive research in the field of transient pool boiling has occurred using a variety of heating source geometries (wires [15-16, 24], ribbons [11-15], rods and rodlets [17, 19-20, 23, 31, 35], and films, plates, and discs [21-22, 25-26, 28-20, 36]), a variety of diagnostic techniques (TRT [11-24, 31, 35-36], laser holographic interferometry [16], infrared thermometry [25-26], and thermocouple measurement [28-30]), and a variety of working fluids (water [11-18, 20-28], freon-113 [31], FC-72 [19, 29-30, 35], and ethyl alcohol and

toluene [36]). In addition to these variations, many fluid subcooling levels, which is defined as the difference between the liquid temperature and the boiling point, and some pressures have been explored to elucidate fluid boiling behavior. Specific trends and limitations in the previous work are presented in the following sections.

3.1.2.1 Elevated Pressure

The impact of pressure on pool boiling heat transfer in water, including pressures above and below standard atmospheric pressure has been studied extensively [15-16, 19, 22-23, 26, 28, 31, 37-40]. Three articles in particular will be highlighted for their results and similarity to the work completed in this dissertation.

In 2019, Dahariya and Betz [40] studied high pressure pool boiling on a polished copper surface to determine mechanisms for heat transfer enhancement. They varied the pressure from 0 psig to 60 psig in intervals of 15 psi. It was found that, under high flux power pulses, the heat transfer coefficient increased 50%, 75%, 125% and 175% respectively for each step. In addition, heat flux behavior and bubble formation and dynamics were observed, and a new mechanistic bubble lift model was presented.

LIMITATION: This work was performed under steady state conditions. The references included above demonstrate that transient boiling heat transfer is higher than steady state heat transfer. Thus, additional heat transfer enhancement can be assumed in the transient case over the steady state boiling. In addition, this work was performed solely under saturated conditions, which does not illuminate the impact of water subcooling on the heat transfer. The final limitation of this work is that this heating rod top surface acts as a plate heater as opposed to a cylindrical heating

source. This will impact the bubble formation and liftoff, which, presumably, will affect the heat transfer.

In 1995 Fukuda et al [17] presented an in-depth study about the impact of increased pressure and subcooling on both steady state and transient boiling, with specific emphasis placed on determining the maximum transient heat transfer, q_{max}. This study was completed with varying width power pulses. They found that the heat transfer increased with the increase in water subcooling, but that the effect decreased with increasing pressure. Furthermore, time lag in hydrodynamic instability and the occurrence of heterogeneous spontaneous nucleation were the dominating mechanisms affecting q_{max}.

LIMITATION: This work emphasized the impact of pressure, subcooling, and pulse width on the maximum heat transfer. Little detail or analysis is given on the heat transfer vs temperature behavior as pressure and temperature increase nor on the boiling phenomena. In addition, the impacts of heater geometry, surface condition, and pulse height are not analyzed. The heating time scale is also much longer than the time scales in this dissertation. The conclusions of this work regarding the impact of increasing pressure on the heat transfer coefficient contradict those from Dahariya and Betz.

In 2015, Su et al [26]performed transient pool boiling experiments on a plate heater under very fast power transients. Temperature and boiling phenomena were captured with an infrared (IR) camera and a high-speed camera to allow for spatial resolution over the heating plate employed. This work considered the transient pool boiling heat transfer at subcoolings between 0 and 75 °C, and pressures between atmosphere and 15.7 Bar. The heat generation rate was varied, with exponential periods ranging between 5 – 500 ms.

LIMITATION: A plate heater was used for this work, facing the same limitations noted for the work of Dahariya and Betz. In addition, the experimental pressures were limited to 1/10 the standard PWR pressure. Although the experiments are performed on a fast time scale, the actual heating event is significantly slower than the region probed by this dissertation. Under the fastest presented heating rate, it was found to take 6 time constants, or 30 ms, to heat up the first 10 °C.

In conclusion, despite the amount of research on the impact of pressure on various aspects of boiling under a number of conditions, there remains a lack of information, clarity, and understanding on the impact of increased pressure transient boiling heat transfer together with other factors, (i.e. surface geometry and roughness, and pulse variations). In addition, there remain some trends in literature that appear to contradict each other, such as the impact of pressure on the heat transfer coefficient as presented above in steady state vs transient cases. There also is a limit to the maximum system heating rate that has been explored.

3.1.2.2 Wire Material and Surface Conditions

Many researchers have published research on the effects of heater surface property changes on boiling and heat transfer. Kang [41] studied a tube under various orientations with surface roughness between 15 nm and 61 nm. The results indicated that an increase in surface roughness led to higher heat transfer at a given surface superheat due to higher nucleation site density for bubble formation.

LIMITATION: These tests were performed for steady state boiling. In addition, the impact of pressure and temperature were not tested.

A majority of the work on how material changes impact boiling has been on the impact of nanofluids (in which nanoparticle are added to the fluid to derive some desired benefit) on boiling

heat transfer and on wettability changes as highlighted in the reviews written by Drelich et al [42] (on hydrophilic and superhydrophilic surfaces and the related impact), Mori and Utaka [32] (on CHF enhancement through surface modification up to 2016), and Singh and Sharma [34] (on general boiling heat transfer enhancement through surface modification up to 2021). The overwhelming majority of the work presented in these three reviews pertain to the impact of various surface structure and/or liquid/liquid-particle interactions under ambient conditions. The noted exception to this is the work of Liu et al under various pressure conditions [43-44]. In both of these studies the impact of a nanofluid was studied under pressure and it was found that increase in CHF values diminished with increasing pressure.

Jo et al [45] studied the impact of surface wettability changes and the inclusion of nano/micro surface features on boiling and heat transfer. Identical nanostructures were fabricated using materials of differing wettability, namely oxidized silicon and Teflon. An increase in boiling heat transfer and critical heat flux was found independent of wettability. However, the amount of increase was dependent on the wettability, with Teflon showing a larger increase in boiling heat transfer but a lower increase in critical heat flux than the oxidized silicon.

LIMITATION: These two studies relate to steady state boiling. The also both include the introduction of materials not currently in use in nuclear power generation (the nano particles in the nanofluid or the Teflon and oxidized silicon).

Fukuda et al [18] and Sakurai [46] also investigated surface conditions, including roughness scales to determine the effect on transient critical heat flux. They determined that the impact of roughness was conditional on the time scale due to the competing heterogeneous spontaneous nucleation and hydrodynamic instability mechanisms. In slow transients, the heat transfer was independent of surface conditions due to the hydrodynamic instability, while fast

transients saw increased critical heat flux due to phenomenological domination of the heterogeneous spontaneous nucleation.

LIMITATION: The impact of increased pressure and variations in water subcooling on pool boiling with different surface conditions is not explored. This is of particular interest as the hydrodynamic stability of water is dependent on pressure. In addition, no testing is performed into the ultra-fast heating time scales.

3.1.2.3 Differing Pulse Shapes and Step Changes

The majority of previous transient boiling work has employed an exponential heating model [12, 14-15, 17, 19-20, 22-23, 25-28, 31, 35] or a step power increase [11, 13-16, 21, 24]. An exponential model is the natural tendency of an unconstrained Joule heated surface under constant current because the resistance increases with temperature in a positive feedback loop. Because nuclear reactors are typically designed to produce negative feedback to increase reactivity, another heating model, the Fuchs-RIA, has been proposed in the literature. This model is less used as it requires greater complexity in the power production [2-3, 10, 25, 47].

Kingston et al [48] performed experiments with pulsed power increases, where the power was increased from an initial, non-zero level to an elevated state for a specified duration. Under such conditions, the dynamic response of the system at the onset of boiling resembled an underdamped spring-mass-damper system subject to a unit step input. This novel heating model has been unexplored previously and represents a true-to-situation analog for an operating power system that experiences a sudden power increase.

LIMITATIONS: The impact of the heating shape in combination with other experimental parameters (e.g., pressure, and subcooling) has not been explored and remains unknown, but it

represents a potentially useful area of tuning for designing heat transfer systems. This is particularly interesting as the various heating models exist for simulating a RIA, but studies with a direct comparison have not been made. In addition, the pulse step-increase present by Kingston et al has not been explored in any pool boiling conditions apart from atmospheric pressure and saturated temperature. The influence of the heating rate on these tests remains to be explored.

3.2 Heat Transfer

Methods for quantifying and calculating the amount of heat transferred from a system or event are vast in number and specific application; this can be seen by the number of academic journals directly covering heat transfer and its various aspects. In general, and in this work, there are three main mechanisms for heat transfer: 1) Convection, or heat transferred from a surface by a moving fluid, 2) Conduction, or heat moving through or between solids and or stationary fluids, and 3) Radiation, or the net heat exchanged radiatively between two surfaces. These mechanisms, particularly as they relate to this work, will be discussed in the following sections.

3.2.1 **Convection Heat Transfer**

As noted above, convection heat transfer deals primarily with the heat transferred from a surface due to the movement of fluid. This can take the form of forced convection, where a fluid is moving at a noted velocity around the heated surface, or free convection, where the fluid in contact with the surface is initially static but begins to move due to buoyancy forces induced by

the change in density as the fluid heats up. A number of dimensionless parameters have been created to assess the relative importance of various interactions in the heat transfer and flow of the fluid. Of these parameters a few will be highlighted for future discussion in this work. These are as follows:

- Reynolds number (Re) – This number provides a ratio of the inertial vs viscous forces. This is often used to describe whether flow is laminar, turbulent or transitioning between the two.
- Grashof number (Gr) – This number provides a ratio of buoyancy to viscous forces. This is useful in determining the impact and importance of natural convection.
- Prandtl number (Pr) – This number provides a ratio of momentum diffusivity and thermal diffusivity.
- Rayleigh number (Ra) – This number is the product of the Grashof and Prandtl numbers and provides an additional characterization of the flow regime. Below a certain, critical value there is assumed to be no fluid motion and conduction becomes the dominant heat transfer mechanism.

In order to determine the importance of the buoyancy driven convection that will be present in this work, the Rayleigh number was calculated as well as a comparison between the Grashoff number and the Reynolds number. The Rayleigh number was found to be on the order of ones and tens, while this is much lower than the value for driven flow, it is not much, much less than one where the factor might be neglected. This was confirmed in the comparison of the Grashoff and Reynolds numbers. If $Gr/Re^2 \ll 1$ then natural convection can be neglected. Again, this criterion is not met, and thus, numerical models to solve the temperature will need to include convection on the outside surface.

3.2.2 **Conduction Heat Transfer**

Conduction heat transfer is often thought of as occurring between two solid bodies, but it occurs as heat is transferred between any two stationary media. It should be noted that fluids often do not remain stationary as they are heated because of buoyancy effects, as briefly noted above. A dimensionless parameter of note for conduction heat transfer is the Biot number which will be defined as follows:

- Biot number (Bi) – This number provides a ratio of the internal thermal resistance of a solid to the boundary layer thermal resistance. In principle, this defines whether it is easier for the heat to move through a body or out of it.

As established in the previous section, 3.2.1, the heat convection is not negligible on the outer surface. In the work of this dissertation, an evaluation of the influence of conduction on the ends of the system was necessary to determine for modeling. The impact of end conduction under the setup of this work was evaluated in accordance with the theory presented by Xing et al [49]. It was determined that conduction out the fixed ends of the heating surface was less than 5% of the heat transfer from the heater to the water and could therefore be neglected.

3.2.3 **Radiation Heat Transfer**

The radiation heat transfer of any body is compared to that of a perfect radiator, known as a blackbody. The blackbody radiation is given as proportional to the temperature differential between the two surfaces raised to the fourth power. In the case of non-perfect emission and emissivity value is needed to provide how similar the actual body is to the blackbody emission.

Radiation heat transfer remains small for small temperature differentials and can therefore often be negligible. Such is the case of this work. The equation for radiation between two bodies is given as follows:

$$q''_{Rad} = \sigma\epsilon\left(T^4_{Body} - T^4_{Surrounding}\right) \tag{3.1}$$

where σ is the StefanBoltzmann constant, ϵ is the emissivity, and the temperatures are given in absolute units (K or R). A comparison study was made on this work to determine the impact of the radiation heat transfer. An example test approaches a temperature of approximately 800 °C with a surrounding temperature of 100 °C. Under such temperature conditions, even if we assume blackbody radiation, where ϵ is equal to 1, the radiative heat transfer accounts for less than 2% of the total heat transfer. This is within an acceptable range to neglect in this work.

3.2.4 **Transient Heat Transfer**

In cartesian coordinates, the heat equation can be given as follows:

$$\frac{\partial T}{\partial t} = \alpha(\nabla^2 T) = \alpha\left(\frac{\partial^2 T}{dx^2} + \frac{\partial^2 T}{dy^2} + \frac{\partial^2 T}{dz^2}\right) \tag{3.2}$$

where temperature T is a function of time, t, and the three, dimensional variables, x, y, and z, (i.e. $T(x, y, z, t)$) and α is the thermal diffusivity given by the equation $\alpha = \frac{k}{\rho c_p}$. In the previous equation, k is the thermal conductivity, ρ is the density, and c_p is the specific heat. Solutions to the heat equation exist in many instances and for various applications.

The transient term in this equation serves as the energy storage term of a traditional energy balance equation, meaning that the term represents the amount of energy spent in heating up the heater itself. This energy storage can be isolated to the following form:

$$E_{storage} = \rho c_p \forall \frac{\partial T}{\partial t} \tag{3.3}$$

where ∀ is the volume of the system. Thus, we see that the thermal storage term is proportional to the derivative of the temperature. With this derivative comes numerical challenges as will be discussed in the following section.

3.3 Mathematical Processes for Numerical Calculations

Numerical methods exist for a wide array of applications useful in an engineering context. In terms of this specific work, some discussion on numerical differentiation is needed. A true derivative of a function, $\frac{df(x)}{dx}$, can be approximated with finite differences, $\frac{\Delta f(x)}{\Delta x}$. The definition of a true derivative tells us that as Δx becomes increasing small we approach the limit of the actual derivative. In an experimental context, this approach comes with a nontrivial flaw. The flaw is that experimental noise is amplified by a smaller time step.

Consider the case where a measured value includes noise, as shown in Figure 4. Here a function, $y = x^2$, is shown with random noise, which has a standard deviation of 1%, added to the function. The slight variation is hardly noticeable in the original lines shown in a). However, the changes become much more pronounced in the slope, b). The deviation becomes progressively more pronounced as the step size decreases, as marked by the number of points.

A method for numerical differentiation of noisy data is presented by J. Stickel [50]. This method involves smoothing the original data curve by regularization, employing a quadratic term for the regularization. This method is of particular note for numerical derivation as it introduces

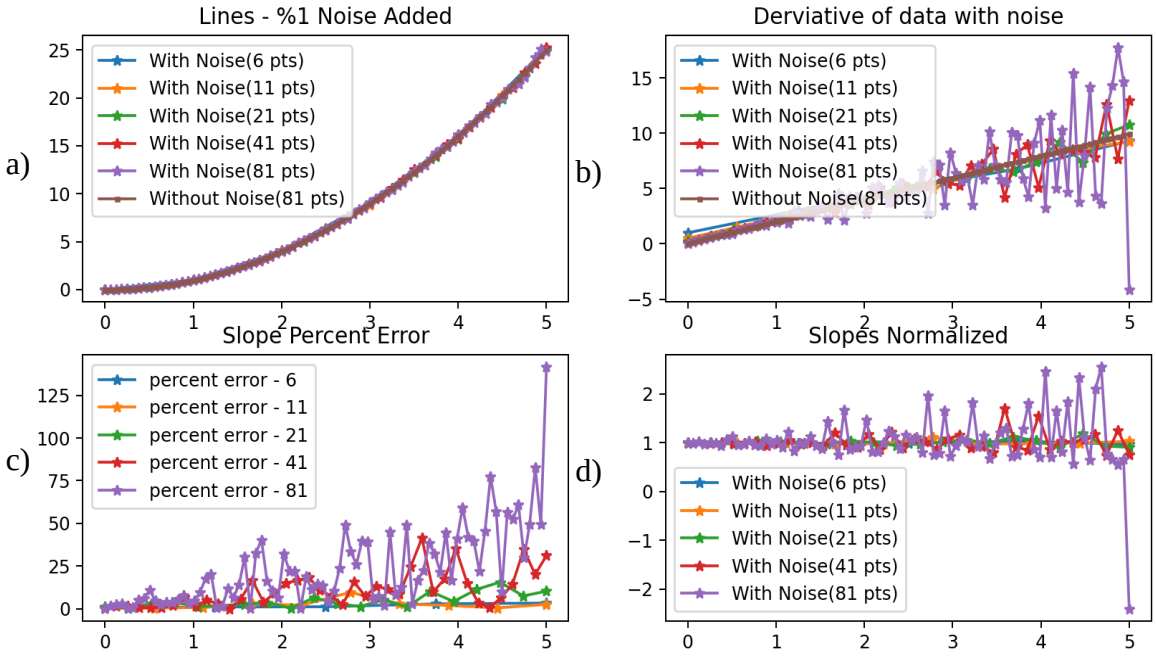

Figure 4: The percent error of a function increases as the step size of the derivative is reduced.

very little bias via the smoothing method. Ultimately, this method provides a mathematically rigorous way of creating a smooth curve that passes through the primary trend of the experimental data.

In order to do this a smoothed function, $\hat{y}$, is defined and the goodness of fit can be defined as follows:

$$\int_{x_1}^{x_N} |\hat{y}(x) - y(x)|^2 dx \tag{3.4}$$

where x_1 represents the first data point and x_N represents the final data point. A minimization of Equation 3.4, thus, would provide the best fit for the data. The "roughness" of the smoothed function $\hat{y}$ then can be defined as follows:

$$\int_{x_1}^{x_N} \left|\hat{y}^{(d)}(x)\right|^2 dx \tag{3.5}$$

where $\hat{y}^{(d)}(x)$ is defined as the following:

$$\hat{y}^{(d)\hat{y}}(x) = \frac{d^d \hat{y}}{dx^d}. \tag{3.6}$$

Stickel provides criteria for determining the appropriate order of this derivative and the interested reader is encouraged to review this [50]. A smooth curve with a good fit to the data will occur with the minimization of the term from equations 3.4 and 3.5. In order to minimize these two appropriately an objective function, $Q(\hat{y})$, can be defined as continues:

$$Q(\hat{y}) = \int_{x_1}^{x_N} |\hat{y}(x) - y(x)|^2 dx + \lambda \int_{x_1}^{x_N} \left|\hat{y}^{(d)}(x)\right|^2 dx \tag{3.7}$$

where λ is a weighting value. These equations and their numerical solutions are again presented by Stickel. This present work seeks to provide a background for the theoretical basis of this method without claiming the method and work presented by Stickel and as such further direction should be sought in the original draft. Figure 5 shows the application of this work in which the derivative of temperature is taken. It should be noted that the final, smoothed data still contains oscillations. This is not unexpected due to the nature of water vapor bubble formation and departure.

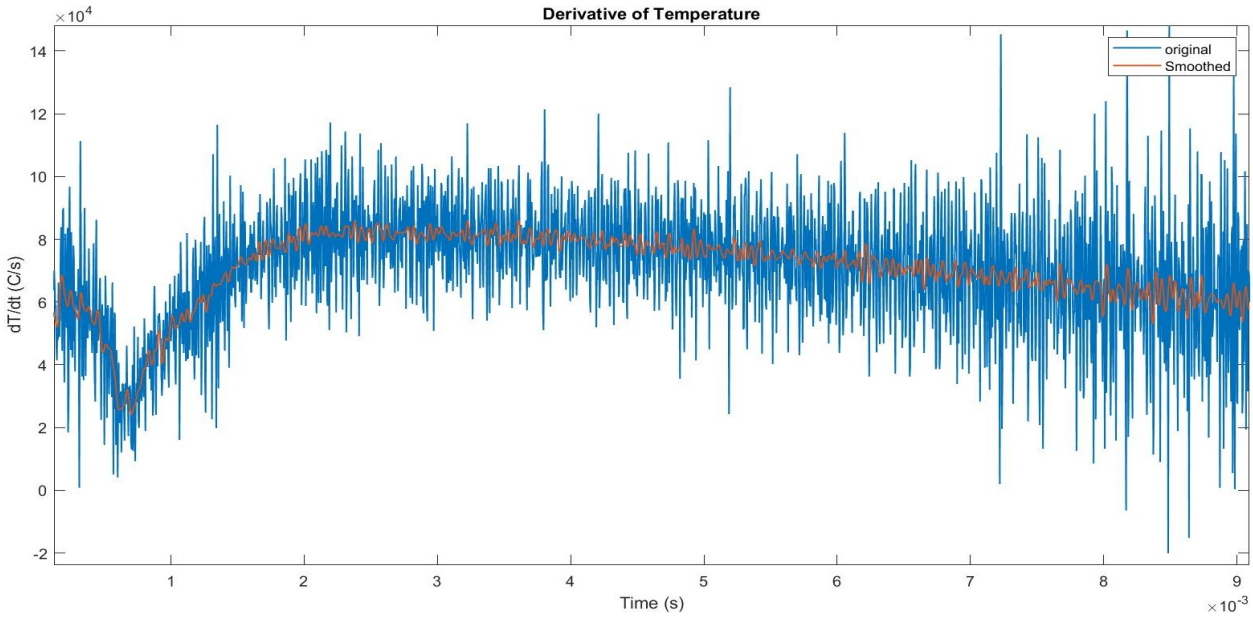

Figure 5: The derivative of temperature is shown, both smoothed and original.

4.0 Approach and Methodology

A description of the experimental setup and methodology is presented in this chapter. This will describe the bulk of the system. Slight variations and modifications were necessary to achieve certain measurements. These modifications are presented in the results chapters as needed to describe the appropriate system.

4.1 Experimental Setup

A new experimental system was required to complete this work at the University of Pittsburgh. In particular, the system needed to be able to withstand high pressure and temperature and the associated changes. System construction began with a stainless-steel pressure vessel with electrical feedthroughs and two windows (Parr Common Reactor 438M). In addition to the electrical feedthroughs, which supported 4 wires, other feedthroughs were used for pressure measurement, upper head pressure release (or water outlet), water inlet, and a rupture disc. The vessel temperature was monitored with a thermocouple placed in a sleeve and secured with thermal paste to ensure good thermal contact. A schematic of the vessel is provided in Figure 6. It should be noted that the figure does not include the opening for the rupture disc due to drawing constraints, but the configuration is identical to the upper head pressure relief labeled as water out.

System pressurization was achieved using only liquid water so as to prevent additional gases from dissolving in the water. The vessel was connected to a pressure generator (HiP model

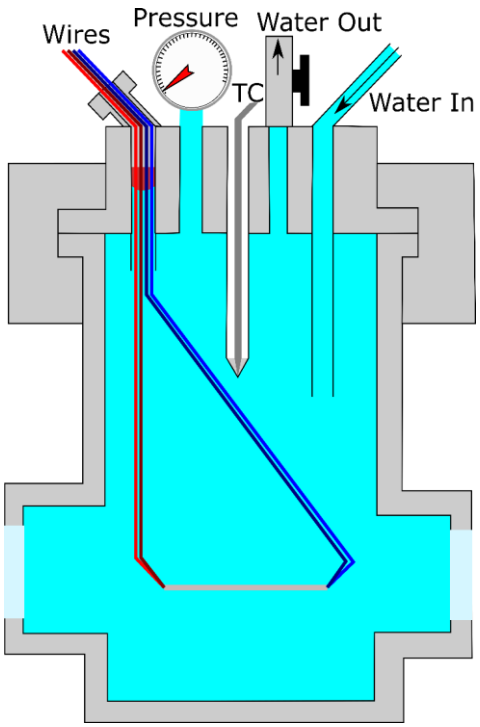

Figure 6: A schematic of the pressure vessel is provided.

62-6-10) at the water inlet port, which was used to control the operational pressure of the vessel from 1 atm to 150 atm. The pressure generator was used to relieve system pressure (over-pressurization caused by thermal expansion of the heated water is expected). The upper head pressure release (water out) was only used at low pressure for gas evacuation and water degassing as will be described later in this work.

The electrical circuit setup for the system is shown in Figure 7. For this setup, up to four identical power supplies connected in parallel (BK Precision 1696) are used to power the system. These supplies have a noise level at ±0.125 % at max power. To supply power pulses to the sample under test, a MOSFET diode (Onsemi RFP70N06) was included as a switch in the circuit. The diode is controlled by a voltage output from the NI DAQ (NI-USB-6281). When the diode is in a closed state, the current in the system passes through a Current Sense Resistor (CSR) (Riedon

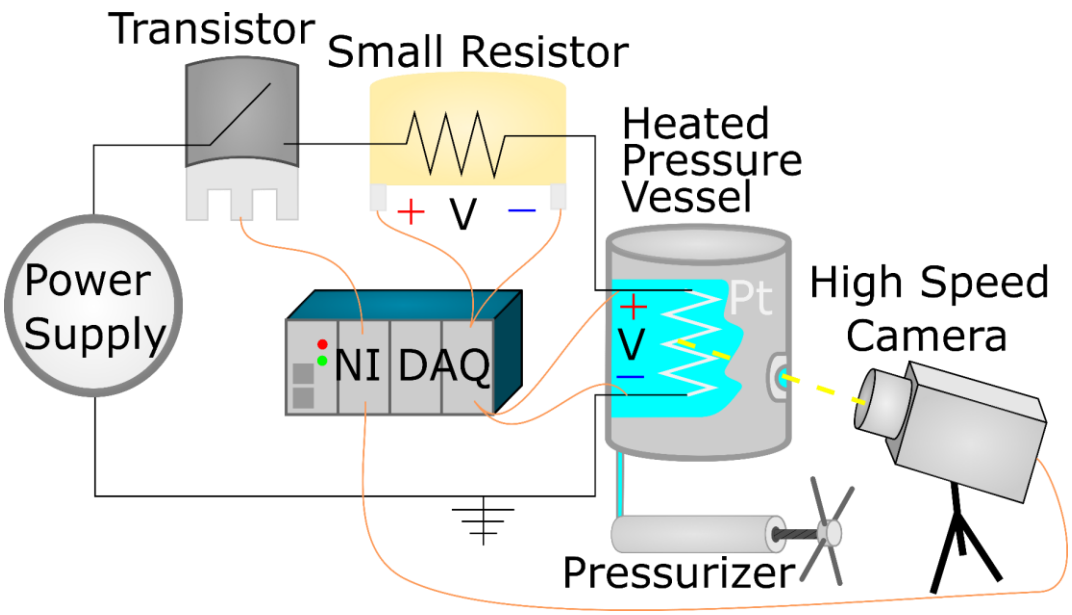

Figure 7: The experimental setup of the system circuit is shown.

FHR4V-0R1F1) with a known, precise resistance of 0.1Ω. The voltage across the CSR is measured with the NI DAQ. Next, two feedthrough wires carry the current into the pressure vessel and across the test sample of platinum wire (Surepure 99.95% pure Pt, P/N 1969)), or later zirconium wire (Eagle alloys Zirconium 702, 99.95% pure), with a fixed diameter of 0.005" (127 μm). The other two feedthrough wires measure the voltage drop across the platinum wire as it varies with time. The platinum wire is held in place with a test fixture made of large copper blocks serving as both heat sinks and electrodes. The resistances of these blocks are small enough that they do not heat up under the current pulses during testing.

In this system, there are many conductive components that are not intended to be part of the electrical circuit. Therefore, non-circuitry parts of the system are wrapped in Teflon to reduce the likeliness of accidental electrical losses or short circuits. An LED is wired in series with the transistor control and placed in the view of the high-speed camera to coordinate event timing between the high-speed imagery and the DAQ-collected data. Images are collected at 25,000 frames per second with a high-speed camera (Phantom 2511).

The vessel is heated with two separate PID controlled band heaters; one heater (Tempco MBH 20538) wrapped the main body of the vessel above the windows, and the other heater (Tempco MBH 20542) contacted the flange below the windows . The lower heater surface was only partially covered by the vessel flange; the remaining heated area was in contact with a super-conductive copper disc (McMaster-Carr 8312K75). This disc served both as a thermal sink to protect the heater integrity, and as a thermal mass to provide additional thermal stability to the vessel. This disc was maintained at a fixed temperature during the data collection phases thus allowing for a more uniform temperature across the vessel. Pictures of the experimental setup are shown Figure 8. While heating, the vessel is wrapped in two layers of insulation, first a rock wool for temperature integrity and then a layer of fiber glass insulation.

4.2 Measurement Theory and Approach

As mentioned previously, the TRT adaptation used in this work involves Joule heating of a thin wire sample. This means that the electrically conductive material is directly heated in a controllable, uniform manner by the passing of current through it. Here, a thin wire is one with a width to length ratio of less than 0.05. By employing this method, it is possible to obtain both the temperature of the wire and the heat transferred from the wire. Obtaining these data requires two simultaneous measurements, namely the current passing through the system and the voltage drop across the wire, from which the resistance can be calculated according to Ohm's law. The wire material resistivity (and therefore resistance) is a function of temperature, allowing this value to be calculated from the collected data. The heat transfer is calculated as a function of the power

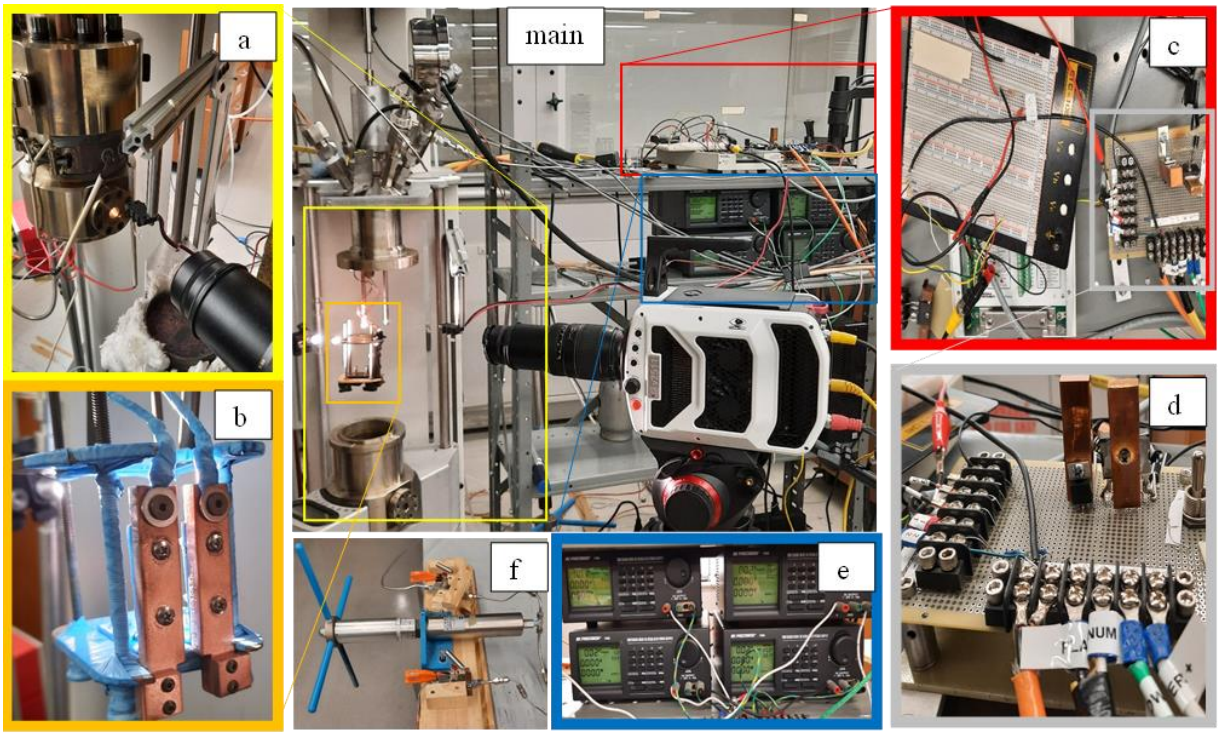

Figure 8: main) A photo of the experimental system with specific callouts for the following – a) the closed pressure vessel, heaters, LED and camera, b) pt wire fixture wrapped in teflon tape, c) NI DAQ and wiring boards, d) various cicuitry, the diode, CSR, each connected to a copper heat sink, e) power supplies, f) pressurizer (not shown in main).

dissipated across the wire. These measurements are presented in greater detail in the next two subsections.

4.2.1 **Wire Resistance Vs Temperature Measurement**

Two options for temperature measurement are presented here and both are employed at various stages of this work. The options are the Callandar-Van Dusen (CVD) equation and direct wire calibration of the temperature resistance thermometer (TRT). Both will be discussed below.

4.2.1.1 Callandar-Van Dusen (CVD) Equation

Platinum was selected for this work because it has a well-established correlation between temperature and resistance. This is described by the CVD equation [51]:

$$R(T) = R_0 \cdot (1 + A \cdot T + B \cdot T^2 \ - (T - 100) \cdot C \cdot T^3) \tag{4.1}$$

where: $R(T)$ is the resistance at temperature, T, R_0 is the resistance at 0° C, T is the temperature in °C, and $A, B, \& C$ are constants specified in DIN 43760

Table 1: The coefficients for the CVD equation as contained in DIN 43760 are presented.

Standard	**A (1/°C)**	**B (1/(°C)^2)**	**C (1/(°C)^4)**
DIN 43760	3.908 x 10^{-3}	-5.8019 x 10^{-7}	0 (if T > 0°C)

At low temperatures, it is often assumed that the temperature vs resistance curve for platinum is linear. However, as indicated by Figure 9, the linear approximation fails as the temperature increases. Since the quadratic form of this equation provides additional accuracy (but

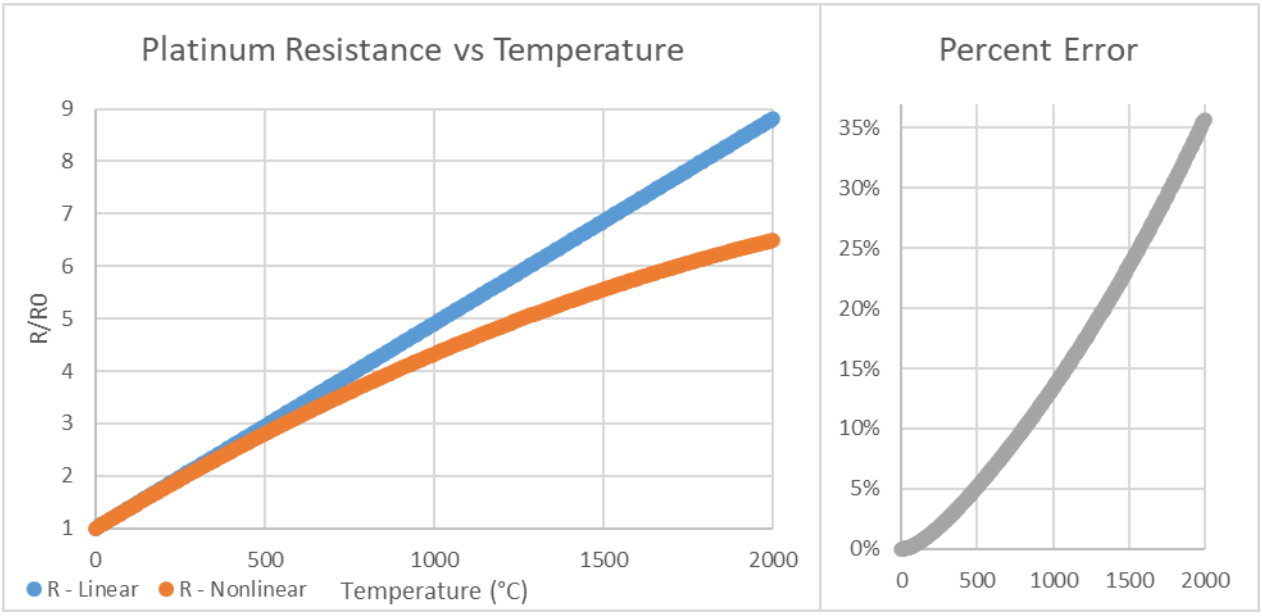

Figure 9: Resistance vs Temperature for platinum

not complexity) it is used in this work. Furthermore, some tests are run to high temperatures where the quadratic form is necessary in tests employing the CVD. This equation is used for the work that is presented in Chapter 6, where the platinum wire is heated until catastrophic failure occurs at a temperature above 1,700 °C. The CVD is particularly important in this range as a direct calibration at temperatures above 1,500 °C becomes tedious or impractical and extrapolation to such temperatures can create large uncertainties.

4.2.1.2 Direct Temperature Resistance Thermometer (TRT) Calibration

In Chapters 7-9, the resistance-temperature relationship is directly measured for each tested sample. An advantage of the experimental setup is that the samples are submerged in water that can be heated, thereby enabling direct calibration in the vessel. Direct sample calibration is also beneficial for the following reasons:

1) The wire diameter is half of the diameter employed in chapter 6. This reduced diameter creates more uncertainty in the reliability of the measured R_0 used in the CVD Equation. This uncertainty comes from the relative impact of small material or surface defects. Additionally, the thin wire is susceptible to bending, kinking, or other deformation which alters the resistance and can cause inaccuracies in the predicted temperature values.
2) The fixture employed in the pressure vessel supplies current to and measures voltage through large copper blocks (electrodes), as shown in Figure 8b. The electrical impacts of these blocks (added resistance, current leakage) are difficult to directly quantify and remove analytically. This is different from the previous setup in which the wire was secured and measured separately.

3) In addition to the unknown electrical impact of the copper blocks, it is difficult to determine if/how the sections of clamped wire affect the various calculations. All platinum wires were cut to 0.65” (15.54 mm), but the effective length could depend in part on the clamp force, location, and other factors relating to sample mounting. This also cannot be removed analytically.

To perform the resistance-temperature calibrations, the water temperature was controlled and a small current (sufficiently low as to not produce Joule heating) was passed through the system. The wire resistance under these conditions represents the resistance at the water temperature. A curve was then fit to this data and used for temperature calculations in place of the CVD equation. An example calibration curve is shown in Figure 10.

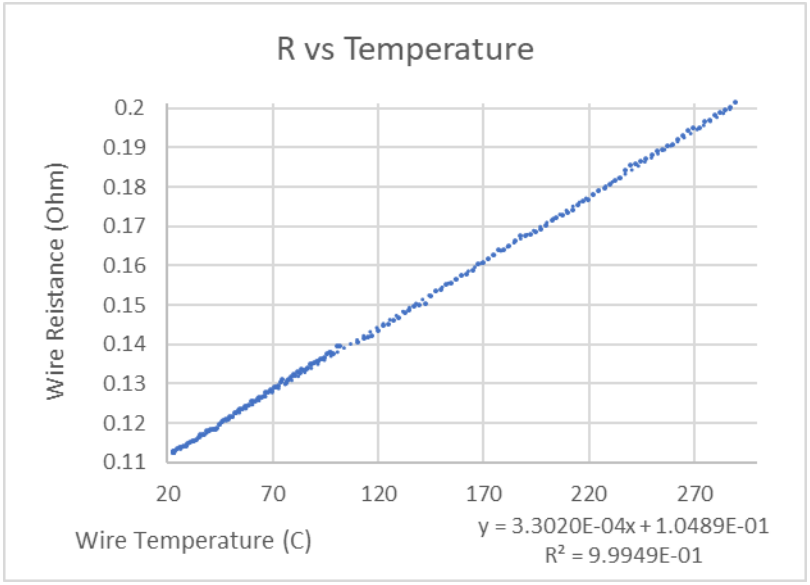

Figure 10: The calibration curve for the thin platinum wire is presented.

Throughout the tests, the system is filled with Deionized (DI) water and degassed directly in the test vessel by holding the water at 100 °C for approximately 1 hour before testing.

4.2.2 **Heat Transfer Measurement**

The local heat flux to the water from this system can be assumed to be:

$$q"_{water}(r,\theta,t) = q"_{tot}(t) - q"_{losses}(r,\theta,t) = \frac{I(t)\cdot V(t)}{A_s} - q"_{losses}(r,\theta,t)\,. \qquad (4.2)$$

The heat transfer losses will be addressed in the calibration section of this work. It is generally assumed that the thin wire acts as a uniform temperature body, but work will be presented showing this may not always be valid in the radial direction. The heat transfer of interest is at the boundary between the wire and water, which means the above equations can be written to be independent of r and θ.

To address the effective sample length uncertainty mentioned above, the equation, can be modified to be length independent by applying the fact the initial resistance value, R_0, is length dependent. This means that the length term will cancel out and the total heat transfer equation can be reduced as follows:

$$q"_{tot}(t) = \frac{I(t)\cdot V(t)}{A_s} = \frac{I(t)^2\cdot R(t)}{\pi\cdot d\cdot l} = \frac{I(t)^2\cdot R_o(1+A\cdot T(t)+B\cdot T(t)^2)}{\pi\cdot d\cdot l}$$

$$q"_{tot}(t) = \frac{I(t)^2\cdot\frac{4\cdot\rho_e\cdot l}{\pi\cdot d^2}\cdot(1+A\cdot T(t)+B\cdot T(t)^2)}{\pi\cdot d\cdot l}$$

$$q"_{tot}(t) = \frac{I(t)^2\cdot 4\cdot\rho_e\cdot(1+A\cdot T(t)+B\cdot T(t)^2)}{\pi^2\cdot d^3} \qquad (4.3)$$

where ρ_e is the resistivity of platinum and d is the wire diameter.

4.2.3 **Measurement Calibration**

There are two calibrations required for the successful operation of this system. These are the individual wire calibration, which is necessary in determining the initial resistance (method used in chapter 6), and a method for quantifying and removing the heat losses in the system.

4.2.3.1 Wire Calibration

The individual wire calibration is performed by passing a very small current through the system and measuring the wire resistance. It is imperative that the current is small enough to not heat the wire. This process is described above in Section 4.2.1.2 for the TRT case. When the CVD equation is used, a calculated resistance is used as a representative of the resistance at the known temperature in the system. With this information, the resistance at 0° C, R_0, can be directly calculated for each wire according to the equation in section 4.2.1.1. In practice, several measurements are made, and the resistance is averaged prior to calculating R_0.

4.2.3.2 Heat Loss Calibration

The heat loss in the system is assumed to be in the transient thermal storage of the wire as discussed above in transient heat transfer theory, section 3.2.4. The thermal storage in the wire can be directly calculated by the following equation:

$$q''_{st} = \rho \cdot c(T) \cdot \frac{V}{A_s} \cdot \frac{\Delta T}{\Delta t}$$

or

$$q"_{st} = \rho \cdot c(T) \cdot \frac{d}{4} \cdot \frac{\Delta T}{\Delta t} \tag{4.4}$$

where ρ is the density, $c(T)$ is the specific heat capacity of the wire at a given temperature, d is the wire diameter, ΔT is the change in temperature over each time step, Δt. The noise amplification of numerical differentiation is then treated through the smoothing described in section 3.3.

4.2.4 **Measurement Uncertainty**

Measurement uncertainty for the system performance and individual test repeatability was determined for this work. To calculate the measurement uncertainty, 30 tests were performed under identical conditions. 30 tests are a sufficiently large sample size so that standard confidence intervals can be applied, as opposed to Student's t-distribution intervals, which are employed for small sample sizes. The average and standard deviation of the voltage and current collected in repeated tests were calculated and are presented below in Figure 11. From this the uncertainty at a 95 % confidence interval was calculated and found to be under 7% after the initial rise with an average total uncertainty of 2.5% over the full pulse range.

In addition to the measurement uncertainty calculation, each experiment presented in later chapters was completed 3 times for repeatability. An example plot of the three tests is shown below in Figure 12, demonstrating the expected consistency in collected data.

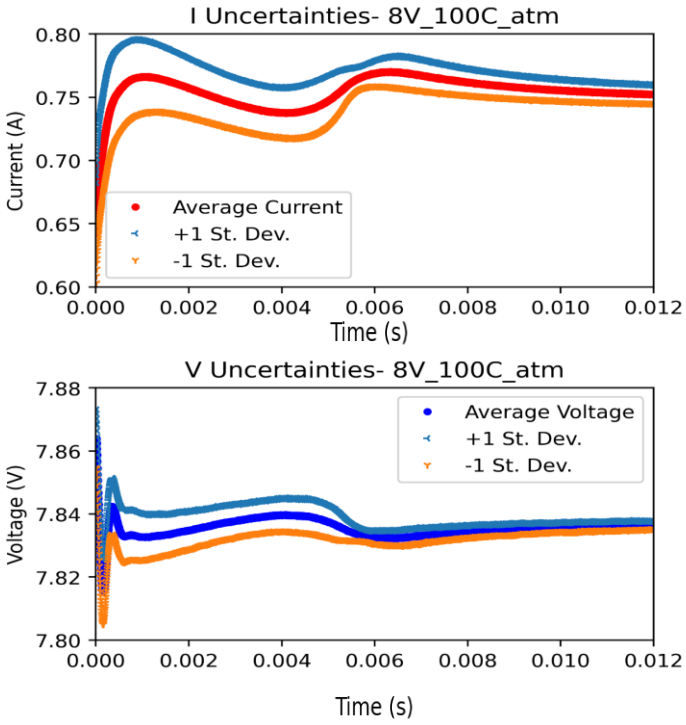

Figure 11: The average and 1 standard deviation for the voltages and currents after 30 repeat tests are shown.

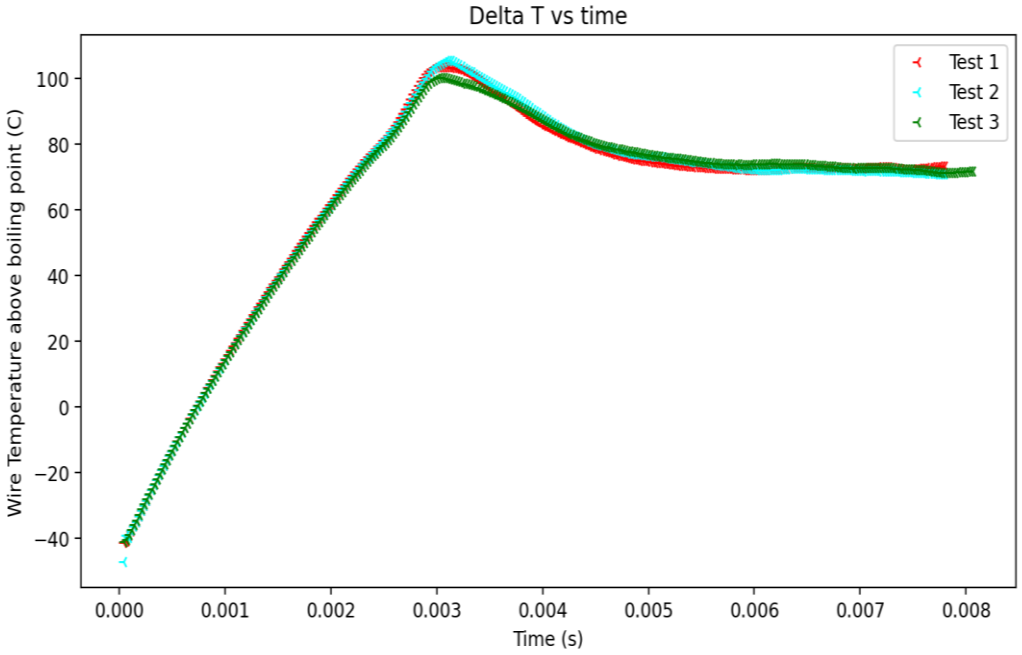

Figure 12: An example plot of the repeatability tests is shown.

4.3 Experimental Test Procedure

A test wire is cut to be 0.65” (15.54 mm) in length and then washed in acetone to remove any surface contamination. The wire is visually inspected for defects such as strictures or kinks that might affect the measurement. The wire is secured in the sample holder seen in Figure 8.b. The vessel is closed, and heaters are installed. The system is then filled until the vessel is “solid” with DI water as observed by water flowing out of the open upper head pressure relief valve. The water is heated just to the point of boiling, approximately 99.9 °C for mass conservation in the vessel and left to degas at elevated temperature for approximately 1 hour. Then the upper head gas relief valve is closed, and measurements are performed. As noted above, tests are repeated three times to verify system integrity and repeatability; high-speed imagery is saved for at least one of the test cases. The system operation and data collection are controlled by LabVIEW software. The front panel is shown in Figure 13. The block diagram and wiring are shown in Appendix B.

After data collection, the data file is reduced in the same LabVIEW code by operating a MATLAB script, which is also provided in Appendix B. This script takes the two collected voltages (one from the CSR and one from the test wire) and converts them into the system current and the test wire voltage together with a time stamp from the beginning of the heating pulse event.

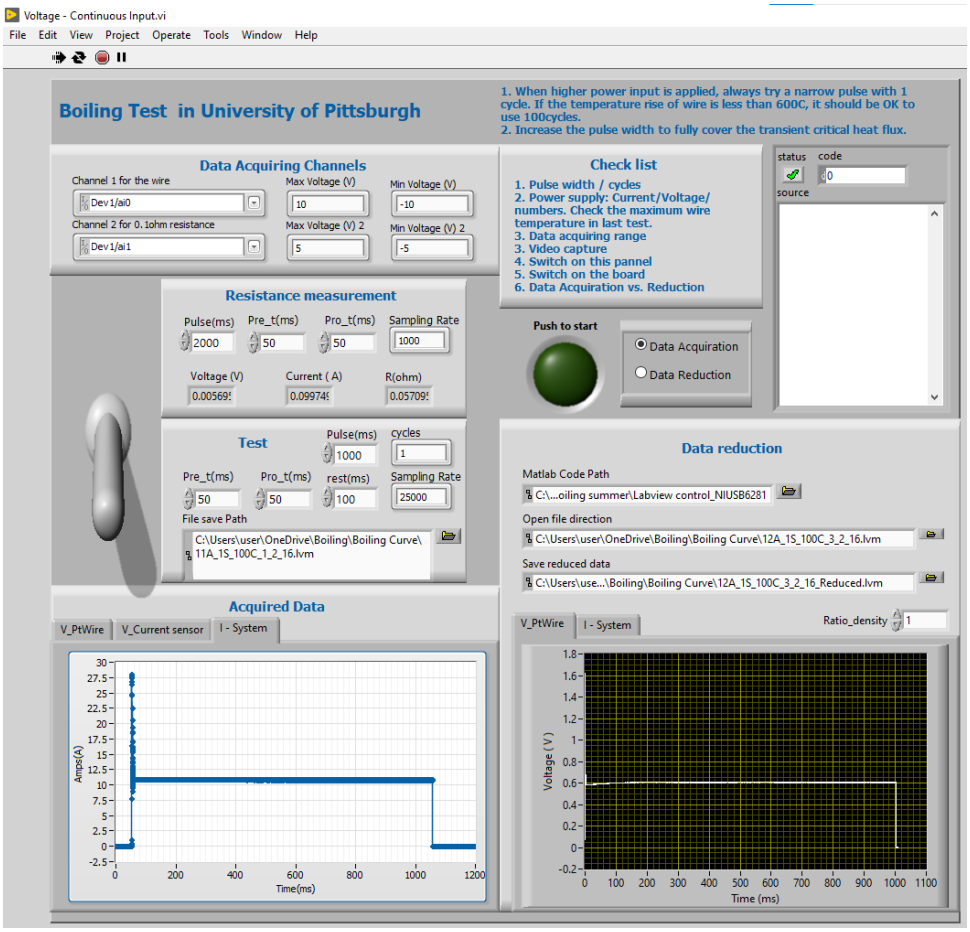

Figure 13: Front panel of the LabVIEW operational code is presented.

With these data, the temperature and heat transfer can be calculated for each experimental test condition. This is done according to equations presented in Sections 4.2.1 and 4.2.2 and performed using another MATLAB script. In addition to producing the raw temperature and heat transfer, the script also performs the necessary smoothing to calculate the numerical derivative according to the method presented in Section 3.3. This code is likewise presented in Appendix B.

4.4 2^k Factorial Design of Experiments

The 2^k factorial design of experiments method is used to determine the relative importance of various parameters on a desired output. The name of this method is descriptive of the number of experiments that must be performed, where k refers to the number of parameters of interest (e.g., a three-parameter system would require 2^3 tests). To employ this method, a high and low value spanning the entire experimental range is selected for each of the parameters of interest (e.g., in a test of a system where temperature can be varied, the maximum and minimum operating temperature for a system would be the appropriate high and low values for the temperature parameter). A combination of the various highs and lows of each parameter is tested. Table 2 presents an example of the combinations that need to be assessed in a test of three parameters.

A two-parameter test case is presented in Appendix C in order to more fully illustrate how the 2^k factorial method operates.

Table 2: The test matrix of a 2^k factorial study is presented.

Test Case	Parameter A	Parameter B	Parameter C
1	+	+	+
2	-	+	+
3	+	-	+
4	-	-	+
5	+	+	-
6	-	+	-
7	+	-	-
8	-	-	-

One benefit of the 2^k factorial method for quantifying the sensitivity of an output to the input parameters is the tests determination of "mixed parameter" sensitivities. This means that the

effect of moving any combination of the parameters is probed, and thus synergistic effects can be noted. To understand the meaning behind the "mixed parameter" test, it is first necessary to understand what is happening in the 2^kfactorial system. The variable changes are considered to move positively or negatively with the probed variable. In the case of a single variable (e.g., A, B, C, etc.) this is very simple. If the probed variable was increased for the observed test, the movement is positive, and the opposite is true for negative. In case of mixed parameter, the relative motion of the parameters is what is most important.

For example, a two-parameter variable (e.g., AB, BC, etc.) is considered to move in the positive direction if both sub-variables (A & B) are increased for the test or if both are decreased. In application each parameter change can be assigned a positive or negative movement and the overall effect then is a multiplication of the assigned movements to determine the overall variable movement.

In this work, 2^k factorial studies were performed for a variety of test conditions. These tests, and their results, provide a basis for design and heat transfer analysis and are meant to inform modification decisions of future analogous systems. The studies were performed in python with custom created code for solving 2^k factorial analyses. This code is robust and can be employed for cases including up to 26 independent test variables (as 2^{26} = 67,108,864, it was assumed not many people would seek to run more tests than this and the number of test variables in the code is sufficient for general application). This code is written in python and is believed to be broadly applicable to the design of experiments, and experimental community. It can be found in Appendix D as well as online in a code repository for public access and use.

In many instances, a computational sensitivity analysis would be performed to do the same work as the 2^k factorial study. However, such computations require a validated numerical model.

In this case, the complexity of the system does not permit an analytical or numerical model with which to calculate output sensitivity.

5.0 Experimental Parameters and Conditions

In order to accomplish the objectives of this research, a high pressure and temperature boiling apparatus was developed according to the specifications in the previous chapter. The experimental parameters and the variable parameter of interest are organized according to the following tables:

Table 3: Selected experemental parameters are shown.

Fixed Experimental Parameters	
Heating method	Joule Heating
Operating Fluid	Degassed, DI water
Heater Type	Platinum Wire
Heater Length	15.54 mm (0.65”)
Heater Diameter	127 µm

Table 4: Selected experemental parameters are shown.

Variable Experimental Parameters		
Water Subcooling	0 °C	50 °C
System Pressure	0 psig (1 Bar absolute) 54.4 psig (4.76 Bar absolute)	1109 psig (76.5 Bar absolute) 2161.1 psig (150 Bar absolute)
Power Level (pulse height)	Low power[1]	High power[1]
Power Pulse Step Increase	No initial Power	With Initial Power
Power Pulse Shapes	Exponential	With Initial spike
Wire Texture/Roughness	Smooth/Drawn Wire	Texturized Wire

[1]The values of the power level depend upon the pulse shape and the presence of a step increase. Typical values are 5 & 8 volts for constant voltage cases and the corresponding values of 9 and 15 amps for constant amperage cases.

The experimental results are broken into several smaller groups that will be discussed in the next several chapters. In addition to these focused parameters, a study on the mechanism of the platinum wire failure under high loading was performed and will be included in this work. The work breakdown and outline of the coming chapters is presented as follows:

- Chapter 6 – Platinum wire failure mechanism and considerations
    - This chapter is performed under atmospheric conditions, for rapid wire replacement, and with focus on the failure mechanism of the wire.
    - Various subcooling states and power levels are considered.
- Chapter 7 – The effect of pressure and water subcooling on transient boiling phenomena
    - This chapter explores the impact of system pressure, subcooling levels, and power levels on various aspects of transient boiling.
    - This chapter additionally presents relevant considerations of the experimental system.
- Chapter 8 – The effect of power shape and heating behavior on transient boiling phenomena
    - This chapter explores the impact of pulse shape and initial power with a step increase, together with the impact of pressure, subcooling, and power level, on transient boiling.

- Chapter 9 – Impact of surface condition and material change on transient boiling phenomena
    - This chapter explores the impact of wire texture, and brief comparison of wire material, along with the impact of pressure subcooling, and power level on transient boiling.

Together these chapters will highlight the results of the ultra-fast transient boiling regime and push the fundamental understanding of fastest end of transient boiling under a variety of operating conditions including those similar to a PWR. In the concluding chapter of this work, comparisons between the results will be made and conclusions on the work will be presented.

6.0 Catastrophic Failure of Platinum Wire under Exponentially Increasing, Extreme Heat Inputs

6.1 Introduction

Boiling has been an active field of research ever since the publishing of boiling characterization in 1934 [1]. Since that time, extensive research has been done in the characterization of boiling in many different scenarios. One particular field of interest is the characterization of the transient heat transfer of a cylindrical heating source experiencing exponentially increasing heat inputs. This is of particular interest as it is can accurately describe the physics that can occur on a nuclear fuel rod during a RIA.

A RIA occurs when a sudden, unwanted increase in fission rate happens, and results in a near instantaneous increase in reactor power [2-3]. One cause of such an accident is the sudden ejection of a control rod. This accident is characterized by a peak in the power put out by the core which occurs over a very short time period, usually on the order of 100 ms or less. This energy is transmitted to the primary coolant which can be vaporized. The vaporization, in effect, insulates the nuclear fuel leading to increased temperatures. This insulation reduces the heat transfer between fluid and fuel and can weaken the cladding material [52-57]. In severe cases, it can shatter the fuel and can lead to rupture of the pressurized, reactor containment vessel.

As noted throughout this work, a vast amount of research has been done to characterize a multitude of transient boiling phenomena and mechanisms. The transient boiling mechanism is described [34, 58], some trends have been highlighted [24, 26], and with a variety of techniques

and fluids, as emphasized in the theoretical backgrounds and considerations of this dissertation.. A recent review article published by the author of this work, with many collaborators, provides an in depth look into many of these papers [10]. Of particular note to this work, Glod et al [59] studied the microscale explosive vaporization of water on ultrathin platinum wires. They heated platinum at extreme rates for a matter of microseconds and observed the vaporization of the surrounding water. Their work focused on the nucleation temperature, and they noted that the bubble nucleation temperature increases with heating rate. This work is limited to a maximum temperature of approximately 550 °C, which means no observation or presentation on wire failure is presented. In addition, the work provides no analysis of the heat transferred from the wire as their focus was primarily on bubble nucleation temperature.

A. Sakurai performed a study on the mechanism of transition to film boiling from critical heat flux of various fluids [60]. This work presents the idea that sufficiently fast heating leads to heterogenous spontaneous nucleation of vapor, in which originally flooded cavities along the surface of a wire explosively produce vapor bubbles. This contrasts with vapor bubbles formed from active cavities entraining vapor to form bubbles gradually. This is examined under many subcooling and pressure states with the related heat transfer and temperature behavior. However, the temperature rise is limited to below 200 °C, again unable to provide failure mechanism information. In addition, the heating rates employed are on the order of hundreds of milliseconds and larger.

While these studies and many others set the background for this research, none of them address the failure behavior and resultant transient heat transfer from a thin platinum wire experiencing ultra-fast heating to total wire failure. This failure mechanism is important as it

highlights not only the water behavior under rapid, high-temperature excursions, but also the failures that may occur on the heating surface if left unresolved.

6.2 Measurement Theory and Approach

The general theory and approach for this work, namely a joule heated platinum wire for heating and measurement, are presented in section 4.2 of this work. The alterations specific to this work will be presented below.

6.2.1 **Experimental Setup**

A schematic of the experimental configuration for this work is presented in Figure 14. The setup is the same as that shown in Figure 7 of chapter 4 except that the data is collected on an NI RIO and the water is boiled in a glass vessel not suited for high pressure. As specified in chapter 4, the CVD equation (Equation 4.1) was employed for analysis of the temperature of the wire.

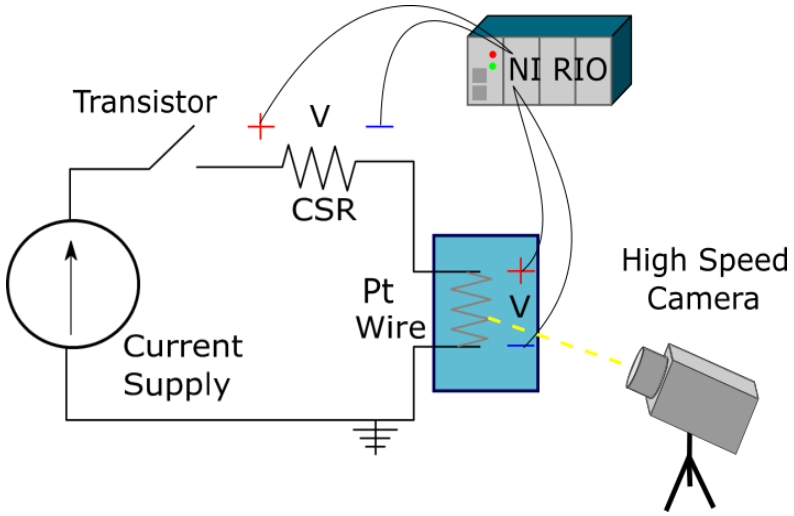

Figure 14: Schematic of the experimental setup.

A fixed height, floating width power pulse was passed from the current supplies to the platinum wire until the wire failed (i.e., melts and pulls apart to break the path of the current). This experiment was repeated for various water temperatures and pulse heights. The pulse heights tested were 20, 30 and 40 Amps, and the water temperatures ranging from 70 °C to saturated in increments of 10 °C. Temperature and heat transfer data, and high-speed images were collected and analyzed to understand the heating and failure mechanism of the thin wire.

6.3 Results

6.3.1 **Floating Pulse Width Test Results**

It was immediately noted, and should be stated upfront, that the power supplies uniformly generated an initial spike in the power when the pulse was initiated. This spike was found to peak with an average value of 94.8 A at 0.2 ms and lasted 0.7 ms total. This is believed to occur due to a large power buildup then sudden capacitor discharge when the diode gate is closed. A numerical simulation of this phenomenon was performed using Ansys software in order to determine the effect this spike would have on the measurement. It was determined to have repeatable effect on the overall results in that it provided the average equivalent of 1 ms extra run time to the front of the test. What is most noteworthy is the rapid bubble layer formation that occurred during this power spike. It was seen that film boiling could occur nearly instantaneously with the spike depending on the water subcooling and pulse height. The power spike is seen in the recorded power pulses seen in Figure 15.

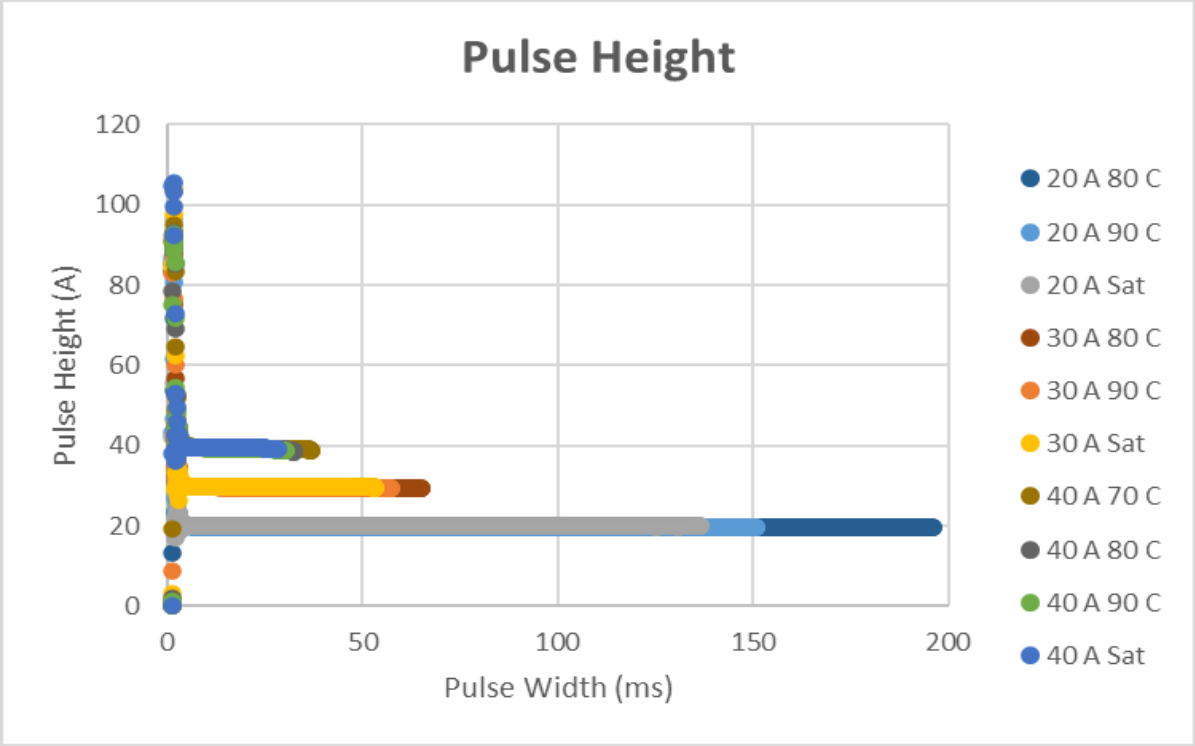

Figure 15: An initial spike in the recorded power is seen to occur in each test case.

6.3.2 **Heating Rate**

The heating of the wire was found to be exponential. This behavior is to be expected due to the positive feedback phenomenon that occurs as a heated cylinder is completely encased in vapor. The temperature will naturally increase driving up the resistance, and thus, the heating rate. However, the heating rates can be simplified to a strictly linear approximation in order to better compare with the heating rates demonstrated in previous works. The results of this approximation can be seen in Table 5.

Table 5: The linearized heating rate for each experimental case is shown.

Test Case	**Linearized Heating Rate** (K/**s**)
20 A 80C	9,756.39
20 A 90C	13,226.98
20 A Sat	13,732.23
30 A 80C	34,043.79
30 A 90C	37,664.88
30 A Sat	38,100.23
40 A 80C	58,999.40
40 A 90C	67,772.19
40 A Sat	71,097.04

6.3.3 **Wire Failure**

At the point of wire failure, an interesting phenomenon was captured with the high-speed camera. It was observed that the wire would explode at some initial point. Figure 16 shows the point of explosion in every test case. It can be seen that the wire failed by the same mechanism in every case, regardless of pulse height or subcooling. The exact location where the explosion occurred along each wire varied. In each wire, the wire was seen to give off a flash at the point of failure. With this flash, pieces of the wire were observed to fly off into the water. The pieces were small and so their exact state at the point of failure is difficult to ascertain.

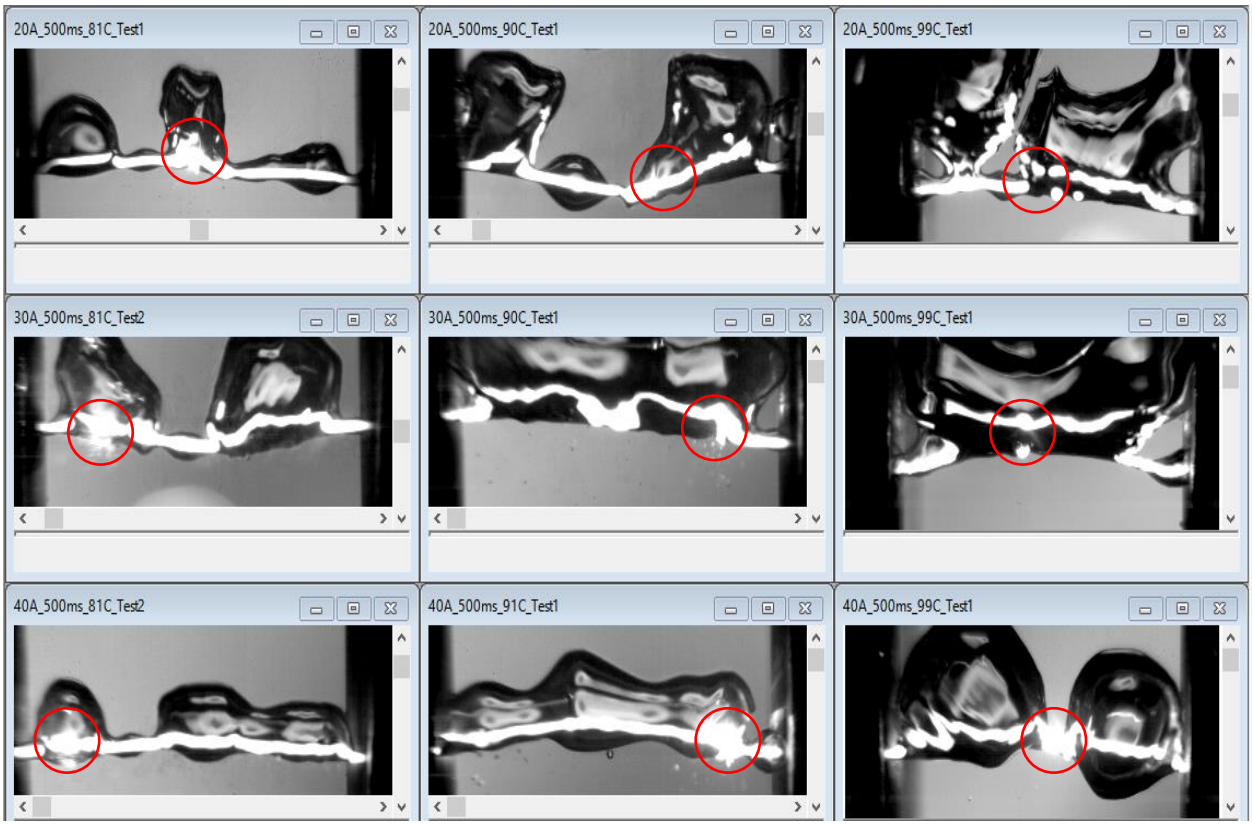

Figure 16: The point of explosion for each wire is shown.

Two modes of wire failure were observed: total wire melt and partial wire melt. In each case, some amount of platinum would recede or fall away, breaking the electrical connection and causing a very sharp increase in the measured voltage while the current measurement would plummet. This was used as the indication of wire failure. Discussion of the failure mechanism will be saved for the conclusion and discussion section of this chapter, Section 6.4. The total wire melt of the 40 A 80 °C case is seen below in Figure 17.

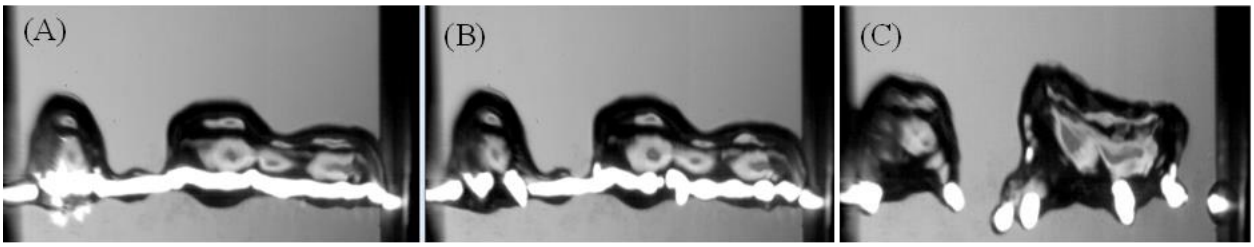

Figure 17: The coalescence of the wire is seen (A) 0ms, (B) 1 ms and (C) 6.5 ms after the explosion.

6.3.4 **Temperature and Heat Flux Analysis**

The temperature and heat transfer data are not the primary goal of the work in this chapter, the emphasis of which is on the failure mechanisms. However, these data can provide some insight into the phenomena which are occurring. The temperature and total heat transfer data tell a uniform story. The two increase together as seen in Figures 18-20. Figures 18 and 19 show locations where a slight decrease occurs in the temperature and heat transfer. These dips appear to be caused by bubbles coalescing or shifting and causing the vapor layer around the wire to locally shrink allowing colder water to approach the wire surface. This progression is shown in Figure 21. What is interesting in this behavior is that the dips are not seen in Figure 20 where the heat transfer is plotted as a function of temperature. This indicates that the dips on each curve occur simultaneously, and that the regression lies along the same path previously traveled. This means no hysteresis is seen and could be useful in the case where a desired temperature is sought.

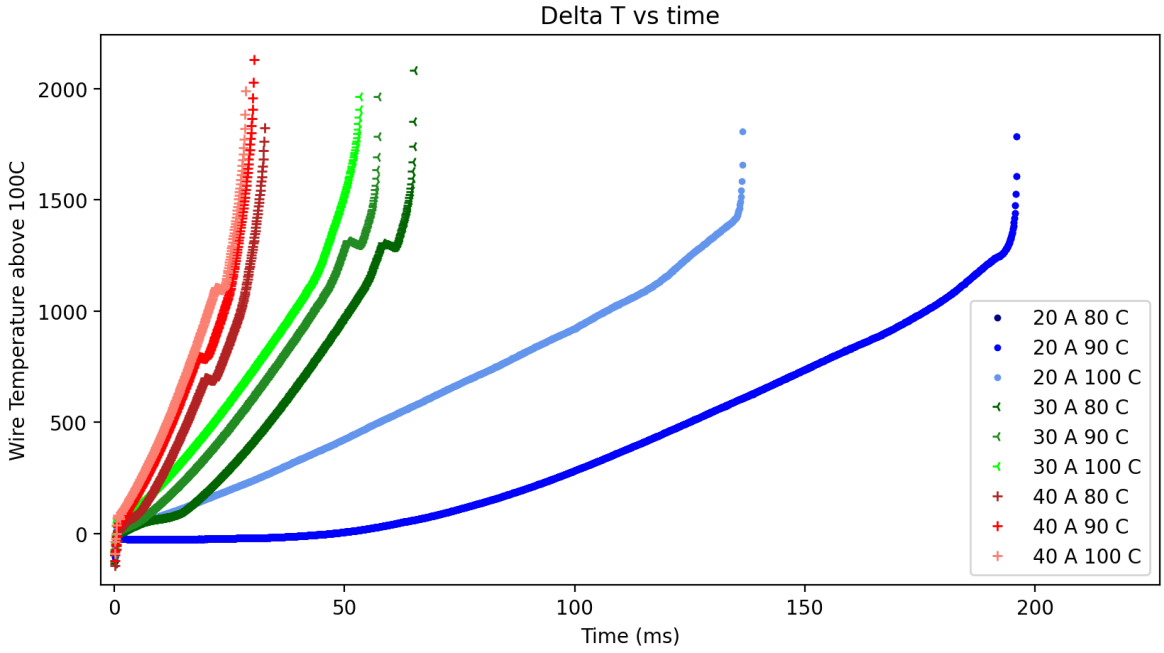

Figure 18: The temperatures vs time for the wires are shown.

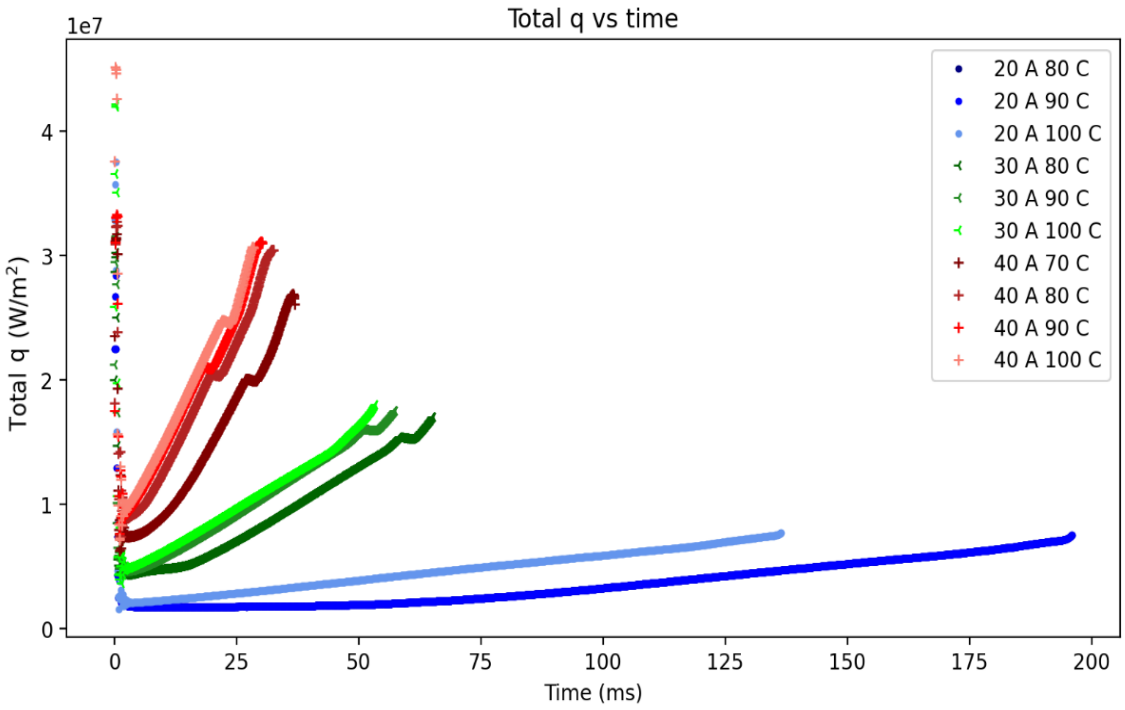

Figure 19: The total heat transfers vs time are shown.

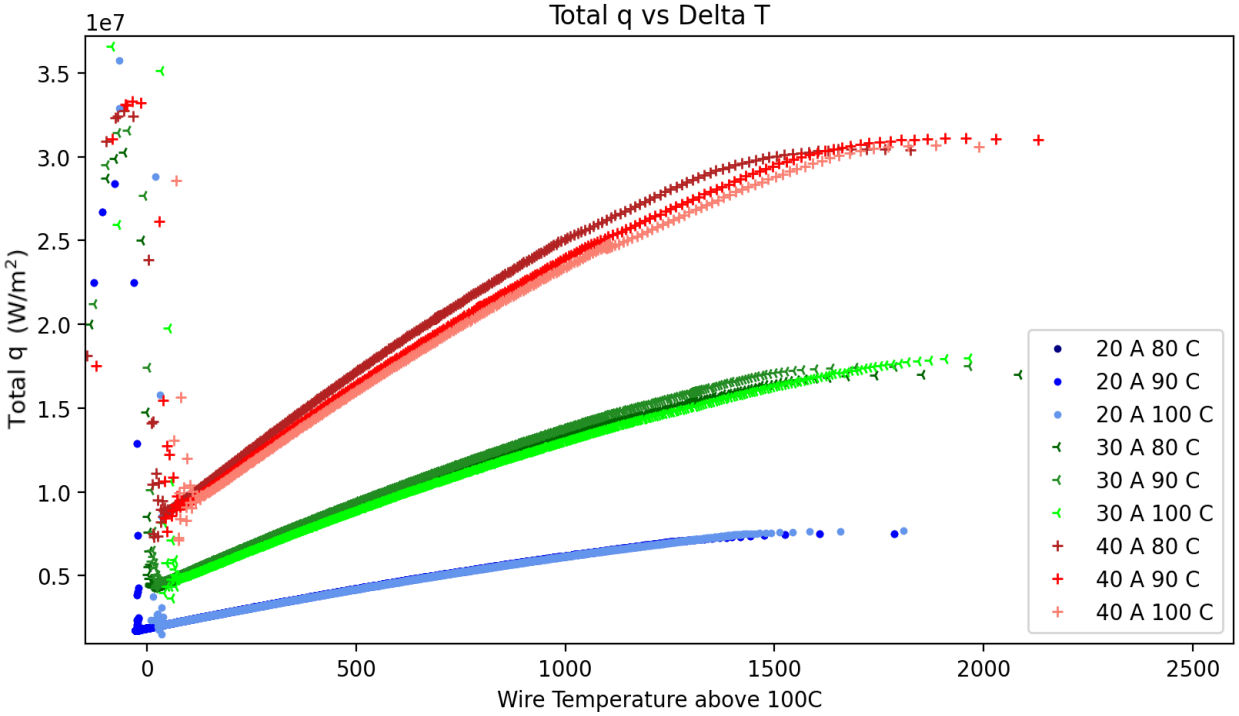

Figure 20: The total heat transfer vs temperature is shown for each wire.

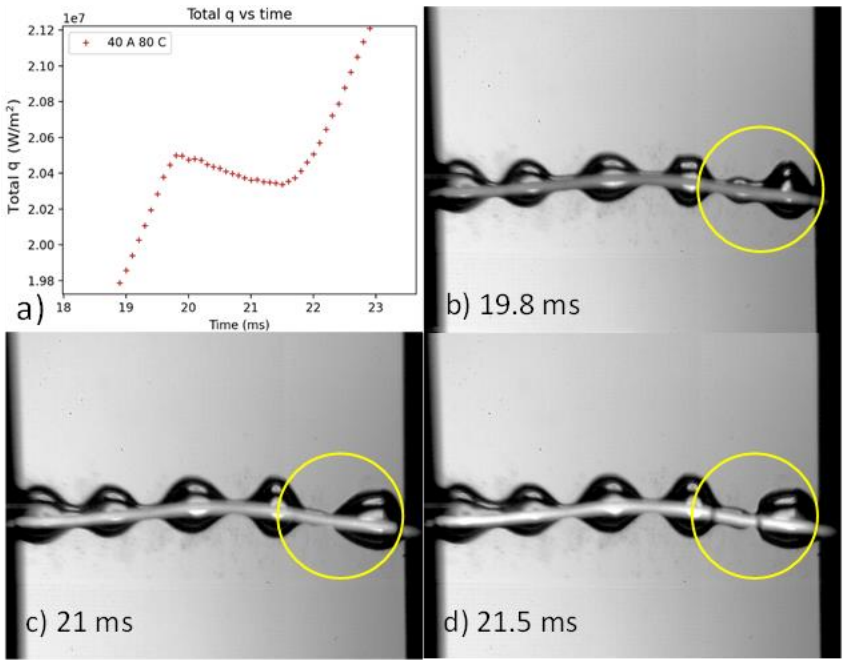

Figure 21: Bubble coalescence is seen at the point when the dip occurs in the temperature and heat transfer graphs for the 40 A 80 °C case.

The previous graphs represent the total heat transferred to the system. Interesting trends are observed when considering the heat transfer to the water. As noted in chapter 4, the heat generated in the system is presumed to go to either the water or is used to increase the heat of the wire (thermal storage). As this is a fast transient, it is assumed that the wire thermal storage will represent a nontrivial percentage of the heat transfer. The graph of the heat transfer to the water can be seen in Figure 22. Two main characteristics of note will be discussed here with further discussion occurring later.

First, large peaks occur at various times in the heat transfer to water for several experiments. These spikes coincide with the dips seen in the total heat transfer and temperature. This observation is explained by the behavior of the transient. In the case where the wire temperature briefly decreases, the transient loss due to wire heating suddenly becomes a transient

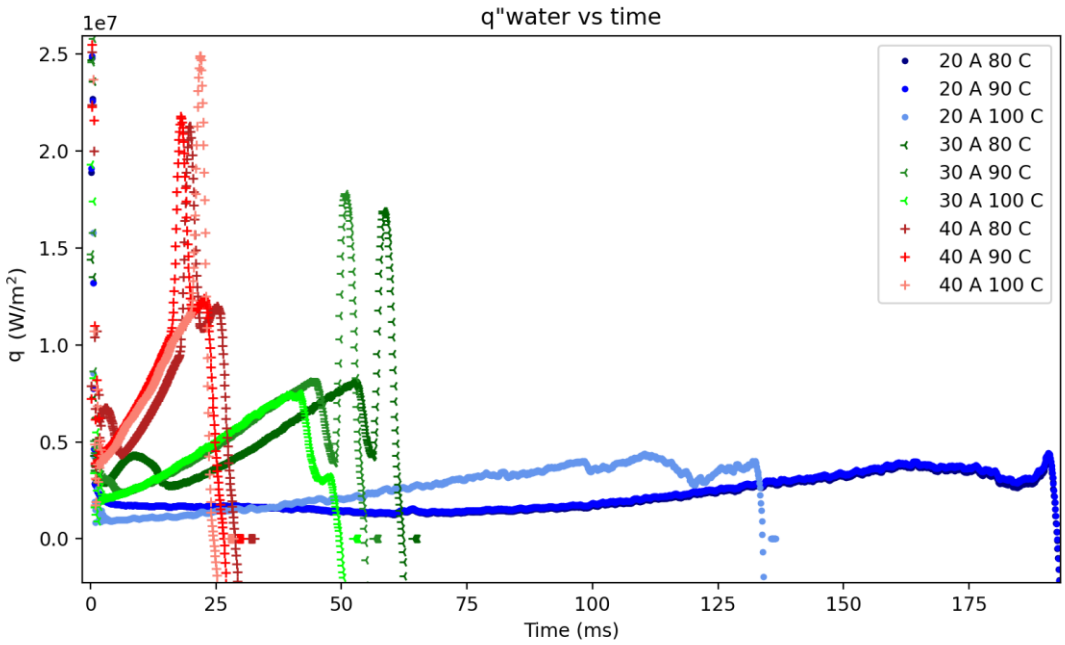

Figure 22: The heat transfered to the water is shown.

again. Thus, it is logical that the water would experience additional heat transfer which drives the cooling of the wire.

Second, there comes a point where the heat transfer to the water stops increasing, and then begins to decrease until it becomes negative. This occurs when the wire heating rate increases to a point where it is so fast that more than the total amount of supplied power would be required to continue to heat the full wire at this rate. In this case, this would indicate that the water, which is colder than the wire, suddenly transfers its heat back into the wire, which is at a higher temperature. However, this breaks the second law of thermodynamics and cannot be accurate. The proposed phenomenon occurring will be presented in the conclusion and discussion section immediately following.

6.4 Conclusion and Discussion

6.4.1 **Platinum Wire Failure Behavior and Mechanism**

The platinum wire employed in this work was heated at very high heating rates until the point of material failure. Three key observations from the collected data and images are the following: 1) the temperature recorded by the CVD equation on the platinum wire is higher than the melting point of the platinum (1,768 °C), 2) the heat transfer to the water appears to reach a plateau then goes negative in order to maintain the measured wire heating rate, and 3) the wires are seen to physically explode under high-speed imagery, then drop as balls into the water as all or most of the wire has simultaneously melted. Together, these major phenomena form the basis of the proposed driving mechanism of the wire failure. One proposed solution has been identified that could lead to these simultaneous effects.

The hypothesized solution is that the wire experiences melting and, ultimately, vaporization in the center without melting the outer wall. This begins with centerline melting of the platinum wire. As the wire melts a change in resistance will ensue creating two competing effects. If a second resistor of equal or larger value is added in parallel to a given resistance, the overall resistance will decrease. This is the first effect. The second is that the volume of platinum that has melted reduces the cross-sectional area of the solid resistor, which will in turn increase the resistance of that electrical path. A study was performed on the competing effects, and it was found that so long as the melted material has a higher resistivity than the solid material, the loss of cross-sectional area will ensure a net increase in the overall resistance of the mix. This directly accounts for the first phenomenon seen. The temperature overshoot can be viewed two ways, either

as an artificially high resistance leading to a high temperature measurement or as a potentially semi-accurate temperature measurement with a high thermal gradient inside the wire.

The second phenomenon can be caused by the same mechanism. As the platinum melts the resistivity of liquid platinum is upwards ten times larger than the value of the solid depending on the relative temperatures [61-62] This higher resistance, molten platinum diverts a larger percentage of the current to pass through a smaller volume of increased-resistance solid. This leads to a higher volumetric heat generation than would have originally been possible with the fully solid wire. This will in turn lead to more wire melt and a further increase in the heating of the solid platinum. Thus, the thermal storage term would need to account for the amount of the change in the volume that is being heated to not overpredict the needed power, and ultimately, underpredict the heat transfer to the water.

The third phenomenon, namely the explosion, is of particular interest in this work because of its ubiquitousness in the tests. Because the wire explodes and is seen to eject platinum fragments through the water, it is assumed that some small amount of platinum vapor must have formed at the centerline, where temperature is highest, in order to propel the explosion. This would lead to a further increase in the resistance and heating effects previously described and would likely correspond with the highest local heating rate seen right before wire failure. In order to assess the validity of this assumption a numerical model of the temperature of a joule heated wire was made. The equation for the temperature distribution is shown as follows:

$$T(r,t) - T_\infty = \frac{q''' r_o^2}{4\,k}\left(1 - \frac{r^2}{r_o^2} + \frac{2}{Bi}\right) + \sum_{k=1}^{\infty} a_k\, e^{-\lambda_k^2 \alpha t}\, J_o(\lambda_k r) \tag{6.1}$$

$$a_k = \frac{q'''\left(h\, r_o - \frac{Bi}{2} - r_o - \frac{4h}{r_o} + 2\lambda_k\right)}{\lambda_k^3\, k\, J_o(\lambda_k r_0)}$$

and λ_k can be found as the roots to the following equation:

$$Bi\, J_0(\lambda_k r_o) = (\lambda_k r_o) J_1(\lambda_k r_o)$$

where q''' is the heat generation, k is the thermal conductivity, r_o is the wire radius, Bi is the Biot number, α is the thermal diffusivity, h us the convective heat transfer coefficient, and J is the Bessel function of the first kind. By filling in the appropriate values for material and experimental properties, it was determined that the centerline temperature could be 4,000 °C while the wall temperature was still solid at 1,000 °C. While this model does not account for the latent heats of melting and vaporization, it does suggest that even in a thin wire, the tested heating rates could lead to a sufficiently large temperature gradient as to allow for plausible vaporization.

Thus, the catastrophic failure of platinum wire under exponentially increasing, extreme heat inputs was found to be localized wire explosion and melting plausibly caused by wire centerline melting and vaporization. This is a never-before-described phenomenon. The phenomenon occurred at every heating rate and every water temperature level tested in this work, and additional work could be pursued to understand the limits of this result. Two additional results relating to the boiling and heat transfer behaviors show in this work are presented below.

6.4.2 **Boiling and Heat Transfer Behavior and Observations**

An interesting result of this work is the boiling behavior occurring in each test. In all of the 30-amp and 40-amp heat pulse cases, bubble lift off never occurs on the wire. The classical boiling regimes (i.e., natural convection, nucleate boiling, transition boiling, and film boiling) are not observed to occur. Instead, combinations of the following phenomena are observed:

- spontaneous nucleation – bubbles suddenly for in localized spots or across the entire wire; the nucleation either continues to rapid bubble movement or turns directly into film growth.
- rapid bubble movement – this is similar to nucleation in classical boiling except the bubble continuously erupt and then shrink back down to nothing with small bubbles appearing to move all around the wire; if they progress bubbles either go through partial bubble collapse or total bubble collapse, though this can be a localized phenomenon.
- partial bubble collapse – the bubbles in rapid bubble movement condense on the wire leaving some visible film on the wire; this progresses to microbubbling.
- Microbubbling – the film around the wire produces very small "microbubbles" (smaller than 20μm in diameter) across its entire surface. These bubbles are expelled from the wire, but to not coalesce and turn back to liquid prior to departing; if they progress bubbles next go to total bubble collapse.
- total bubble collapse – the film around the wire shrinks even smaller to where it is barely distinguishable from the wire; bubbles then progress to film growth.
- film growth – the tiny film around the wire (~14μm or less) begins to grow and vapor beads form along the surface.

In general, the bubbles never leave the surface to rise through the liquid as is seen in classical boiling. In the cases where bubbles are ejected, the condense prior to visibly leaving the wire.

Of particular note here is that the boiling behavior described here is seen for the 30 A and 40 A heating cases, but not in the 20 A cases. In the 20 A case, classical film boiling is achieved

with bubble liftoff. The bubbles depart the surface after 29.4 ms, 87.6 ms, and 145.1 ms for the three subcooling levels respectively (where the hotter water led to quicker bubble liftoff). This is interesting because bubble liftoff is not seen to occur in any of the 30 A or 40A cases even when they were seen to be in similar film boiling at and beyond 29.4 ms. This suggests that there is a sufficiently fast transient heating rate at which point the boiling behavior fundamentally changes. This behavior has not been previously described in literature.

6.4.3 **Heat Transfer Results**

Figure 23 below shows the heat transfer vs temperature in a log-log plot. This figure appears to show an apparent lack of CHF behavior prior to the wire failure. As noted previously, when CHF is achieved the heater will undergo a temperature transient at a relatively stable heat transfer value. Such behavior is not seen in these results until the point of failure. Rather, a consistent increase in the heat transfer and temperature is seen. This would indicate the CHF value is the final heat transfer value seen in each case. However, Figure 23 represents the total heat transfer to the system, and it is possible that a temperature excursion is occurring at the point when the heat transfer to the water begins to decrease as seen in Figure 22. At this point the values of the CHF range from 4 to 12.5 times the value of CHF in steady state. This indicates that the fast-heating transient leads to a substantial heat transfer increase, with the amount of increase rising with higher heating rates.

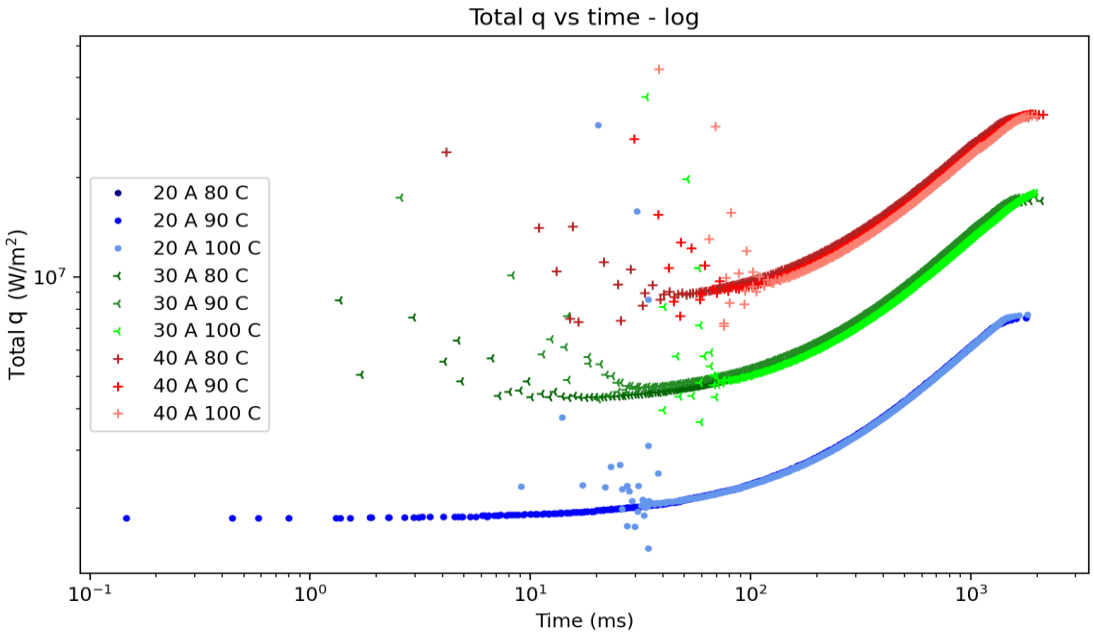

Figure 23: A log-log graph of the heat transfer vs temperature is presented.

The final result that will be presented here is shown most clearly in Figure 23 above. The heat transfer vs temperature behavior was most directly dependent on the power pulse height. Each test followed the same curve for a given power regardless of its subcooling level. The duration of the test before failure, but the relative behavior remained unchanged.

Together these results highlight the mechanism and effect on heat transfer of catastrophic platinum failure. Further work could be done to relate this failure mechanism to other materials, geometries, and power shapes.

6.4.4 **Summary**

A transient boiling experiment was conducted on a thin platinum wire under exponential heating until wire failure occurred. The temperature, heat transfer data, and boiling images were

collected. It was observed that the wires would flash at the point of failure and explode. After the explosion, the wire would fall apart, either partially or completely, into molten, platinum beads. High-speed images, the collected data, and a theoretical model were used to determine a plausible platinum failure mechanism of partial wire vaporization and melt. This is a never-before-described phenomenon. Other cylindrical heat sources could undergo similar failure under comparable volumetric heating rates. Additional discussion occurs in this chapter on boiling without bubble liftoff and the factors impacting the heat transfer of the ultra-fast transient used.

7.0 Experimental Determination of Pressure and Subcooling Impact on Fast Transient Boiling using thin Platinum Wires

7.1 Introduction

Boiling heat transfer has been an active field of research for nearly the last century [1]. Despite significant progress in this field, there remain interesting aspects of transient boiling behavior that are not fully understood [10, 32-34, 47, 63]. Applications and interest in transient boiling range from nuclear accident prediction and safety (including accident tolerant configurations) to cooling electronics, to a variety of other industries including chemical, automotive, aerospace and aeronautics, and marine [10, 23, 34, 47, 63].

Recent work focused on characterizing the transient boiling response of water to a nuclear accident condition, namely a RIA, in which a sudden and large energy spike can occur rapidly vaporizing the water around the fuel. While such accidents are well within the safety specifications of modern nuclear reactors, and inherent feedback mechanisms exist to prevent full-scale failure, localized damage can occur; numerous attempts have been made to characterize and mitigate such effects [64-72]. This work has highlighted unknown fundamental areas of boiling research. The recent work directly describing what is known and offering the highlight of unknown areas can be found in previous chapters of this dissertation. Despite the research that has been performed, the region of ultra-fast heating (heating rates above 9,000°C/s), with the associated heat transfer has not been explored at high temperature and pressure. This represents a fundamental knowledge gap

in the field of transient boiling that, when filled, will provide baseline understanding for fast transient systems.

The high-pressure transient boiling system described in Section 4.1 was built for this and the following chapters (Chapters 8 and 9). A repeat of the description will not be provided in this dissertation but should be reviewed in Chapter 4 above.

7.2 Experimental Setup and Measurement Theory

The operational theory of the work presented in this chapter is identical to that presented in Chapter 4. The work is performed with a direct wire calibration for a TRT measurement. The calibrated resistance-temperature curve for the wire under test is given in Figure 24. The wire resistance was calculated from voltage and current data collected as the water in the vessel was heated using a small enough current to ensure the wire remained at the water temperature.

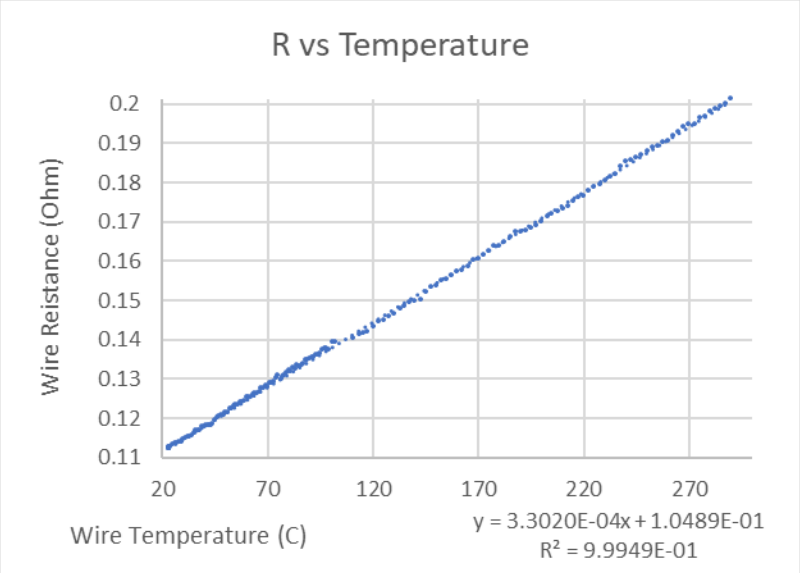

Figure 24: The calibration curve for the thin platinum wire is presented.

7.3 Test Scope and Parameters, and Experimental Procedures

DI water was boiled using a thin platinum wire (D/L = 0.0082) under pool boiling conditions and the following additional conditions:

Table 6: Test parameters for platinum wire undre fundemental conditions are laid forth.

PARAMETER	LOW VALUE	HIGH VALUE
WATER SUBCOOLING	0°C Subcooled	50°C Subcooled
PRESSURE	Low Pressure $\sigma(1\ \text{Bar})$	High Pressure $\sigma(150\ \text{Bar})$
POWER PULSE HEIGHT	5 V (floating current)	8 V (floating current)

To create these experimental conditions, the system is first heated to 100°C at atmospheric pressure, 1 Bar, and data is collected at both power pulse levels. The pressure is then increased to such a point where 100 °C becomes 50 °C subcooled (i.e., the pressure is increased to 4.76 Bar, which has a saturated temperature of 150 °C). Measurements of both pulse heights are taken in this condition. The system is then heated to 292 °C, at saturated pressure (77.9 Bar), where again measurements at both pulse conditions are taken. Finally, the system is pressurized to 150 Bar at constant temperature, 292 °C (which is 50 °C subcooled); measurements at each pulse condition are obtained. Each of the eight conditions presented above is measured three times in quick succession for repeatability and uncertainty quantification as described in Section 4.2.4. The heating rates, measured as the rate of temperature increase before a steady temperature is reached, ranged from approximately 15,000 °C/s and 85,000 °C/s.

7.4 Results

7.4.1 **Heat Transfer and Temperature**

The data plotting convention is uniform throughout the results of the next three chapters. The subcooling is represented by the color of the line (red for saturated, blue for 50 °C subcooled), pressure is represented by the value of the line (dark red/blue for low pressure, light red/blue for high pressure), and the power level in represented by the direction on the indicator (left arrow for high power, right arrow for low power). This is presented on the legend of each figure.

The graphical results will be presented in this section. These include combinations of temperature, heat transfer, time, and Heat Transfer Coefficient (HTC). The HTC is defined by the following equation:

$$HTC = \frac{q''_{water}}{\Delta T}. \tag{7.1}$$

This provides a proportionality between the heat flux of the system and the thermodynamic driving force of the heat, namely the ΔT. In practical terms the HTC can help determine whether two systems are in an equivalent "heat trajectory" even if they are in a locally different place (relative to the heat transfer level or temperature value). This is noted by having similar HTCs regardless of the exact heat transfer and temperature.

The data is collected at a high rate (250k sample/s), which can make the markers difficult to distinguish on a graph. In order to mitigate this on graphs with multiple lines, the markers are placed only on every 20th sample collected. This spacing improves marker visualization without

obscuring important information such as major fluctuations in the data. On graphs with a single line present, every data point is shown as no confusion exists between lines.

The temperature, heat transfer, and HTC are presented in various forms below in Figures 25 -28. The temperatures in Figure 25 indicate that the initial wire temperature had equilibrated with the water subcooling temperature and begin to increase with the heating pulse. Most tests reach a steady plateau, but the low-pressure saturated cases are outliers in their behavior. In these tests, the temperature continues to increase throughout the pulse. This increase is less pronounced, if seen at all, in heat transfer over the full pulse duration.

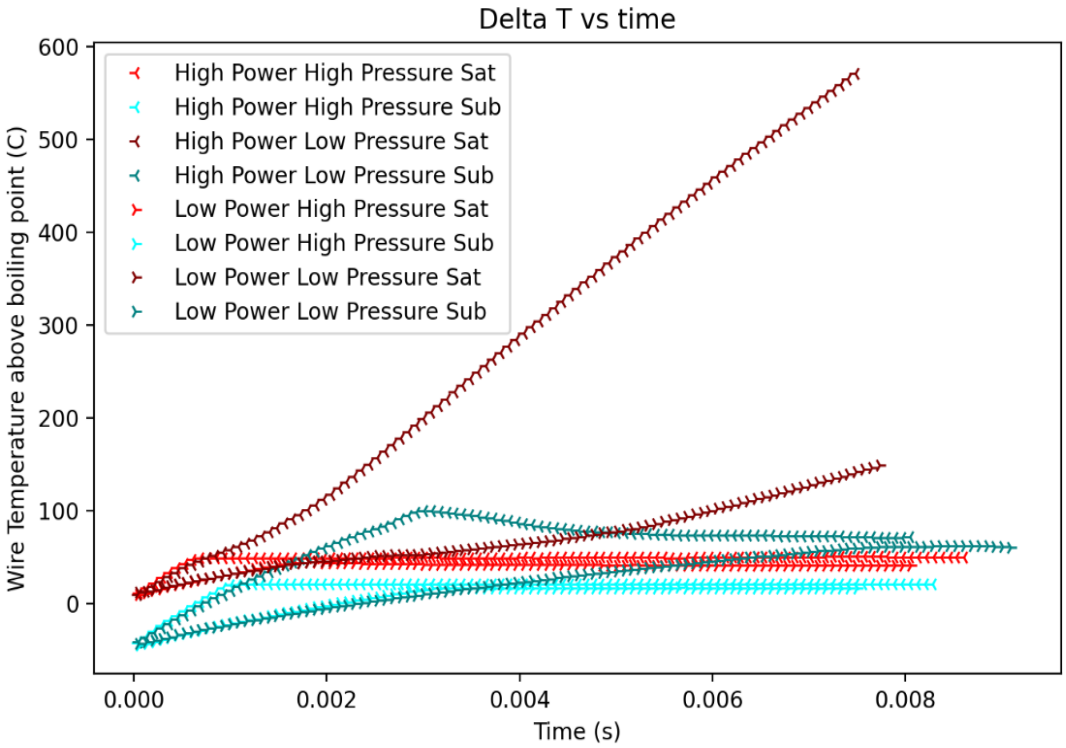

Figure 25: The temperature vs time for each case is presented.

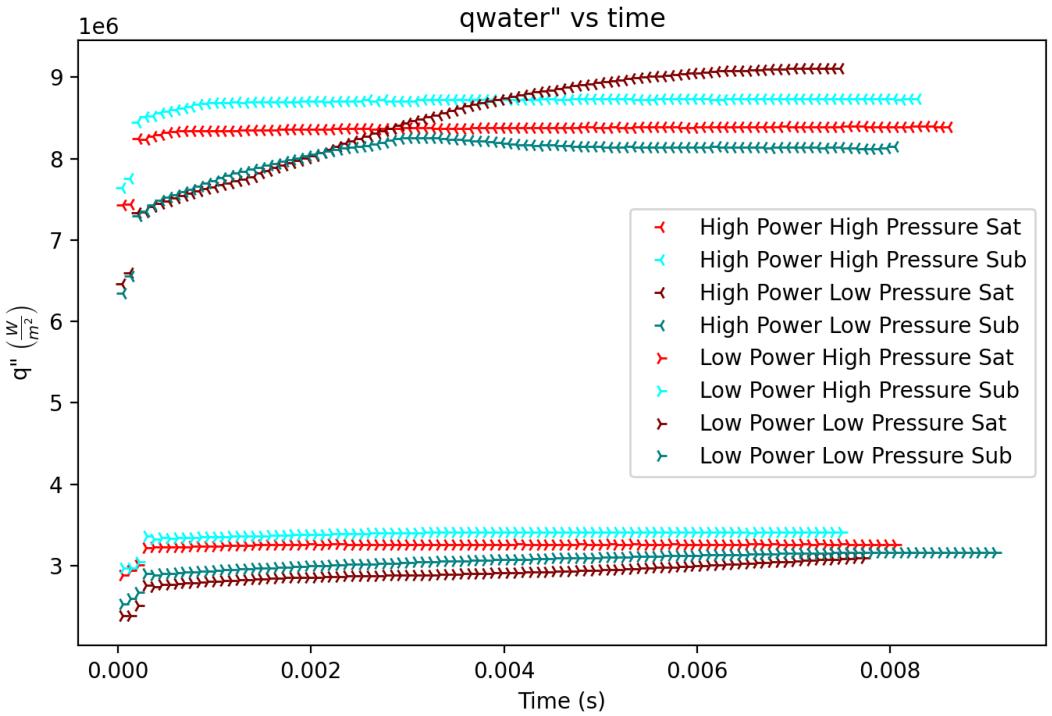

Figure 26: The heat transfer vs time for each case is presented.

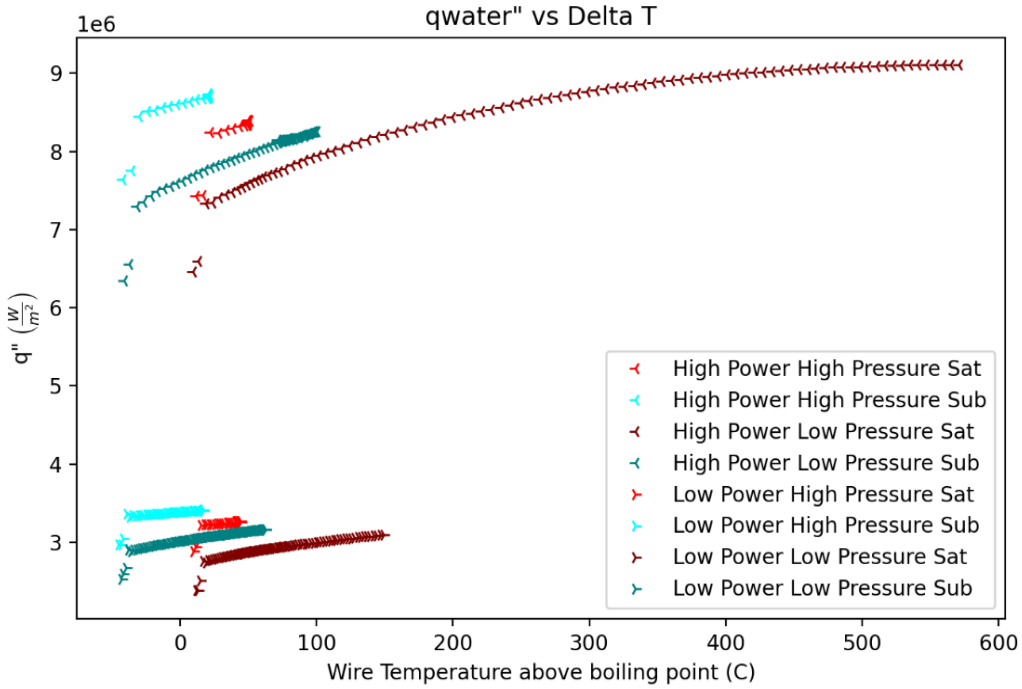

Figure 27: The heat transfer vs temperature is shown.

Figure 27 shows that for both high and low power pulses, the heat transfer versus temperature curves exhibit the same trends depending on pressure and subcooling level. The high-pressure, subcooled case performs best in terms of maximum heat transfer and minimum temperature rise.

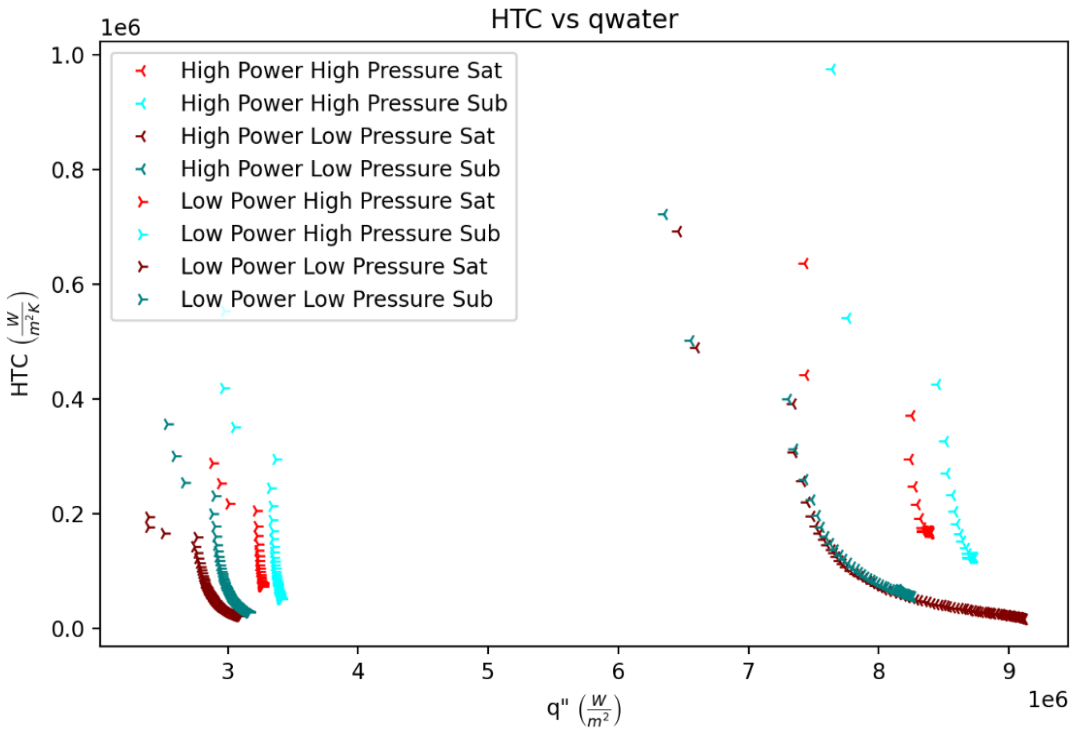

Figure 28: The heat transfer coefficient (HTC) vs water heat transfer is presented.

While the combined plots above nicely present a comparison of the various tests, some minor details are obscured. For instance, in each test, an initial overshoot and settling occurs in the heat transfer data. This phenomenon is more clearly seen in a magnified plot of the lower temperature region (Figure 29), but the clearest picture is provided by the results from a single wire (Figure 30). Figure 30 presents the analogous conditions to an operating PWR, namely high pressure subcooled. After a brief transient, a quasi-steady-state condition is reached. This is not

the same behavior of steady state boiling as the heat transfer remains elevated, but fluctuations and additional changes to the temperature and heat transfer stop after the initial heating.

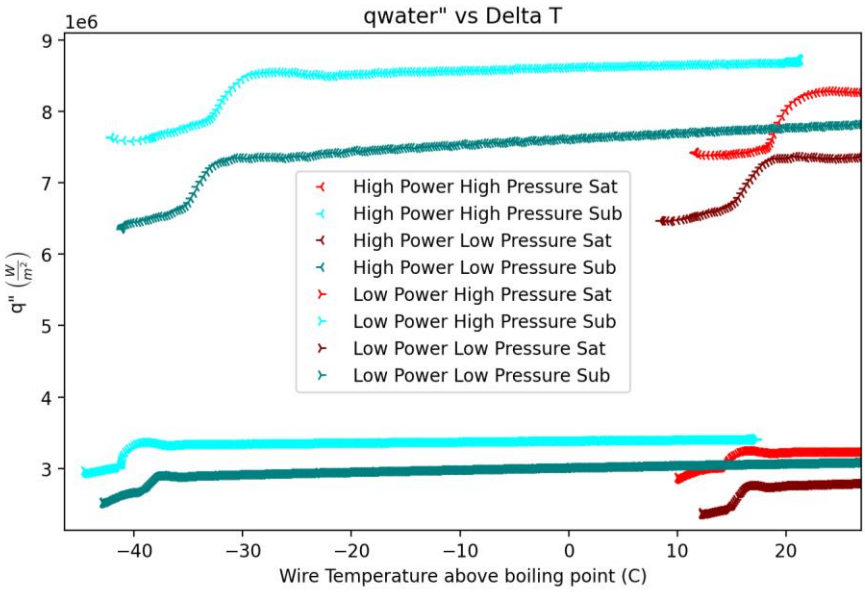

Figure 29: A zoomed in view of the heat transer vs temperature shows an initial overshoot in the heat transfer.

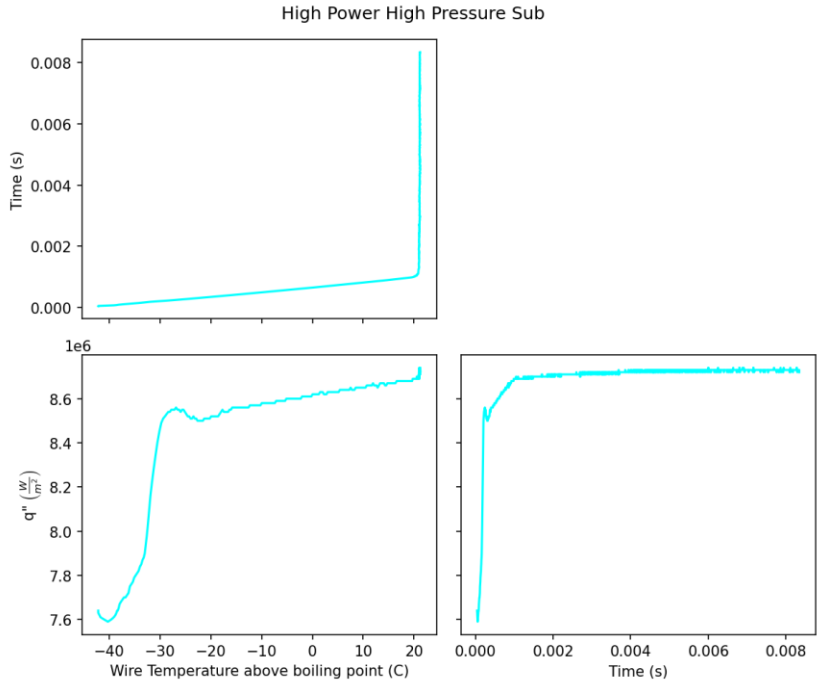

Figure 30: The various graphs of a single wire are presented offering a clearer view of the initial overshoot as well and the relationship between heat transfer and temperature.

7.4.2 **Boiling Behavior and Regime**

The boiling behavior and regime are defined by the high-speed imagery. For brevity, representative tests are selected and shown in this section. These representative tests are the high-powered pulse cases. The same general boiling behavior is seen in the low-power tests, but the overall quantity of bubbles produced tends to be less. The complete sets of both power pulses can be found in Appendix E. The images collected along with the associated time stamp are presented. The times selected represent the beginning, the initial heat transfer overshoot, the first frame of initiation of nucleate boiling, and 5 ms, by which time a steady state condition has been reached if one is going to be reached by the conclusion of the test.

Figures 31 and 33 represent the saturated temperature cases, while 32 and 34 are subcooled. These images illustrate that a smaller vapor layer is formed in the subcooled water and that smaller bubbles are formed at high pressure. While neither of these results are startling, they are striking in appearance. The bubble behavior (i.e., bubble to bubble interactions and coalescence in particular) shows a strong connection to changes in system pressure, where the high-pressure system had small bubbles that do not readily coalesce to form larger bubbles.

Another interesting observation is presented in the 240 μs time stamp image in each set in Figures 31-34. Shortly after the pulse begins, a shiny film forms around the wire. The layer measures approximately 14μm thick based on image processing calculations. This layer is assumed to be a micro-vapor layer surrounding the wire; alternatively, the visual change may result from a change in the water's index of refraction due to localized heating. This layer shows up every test and every experimental condition with proper illumination on the wire.

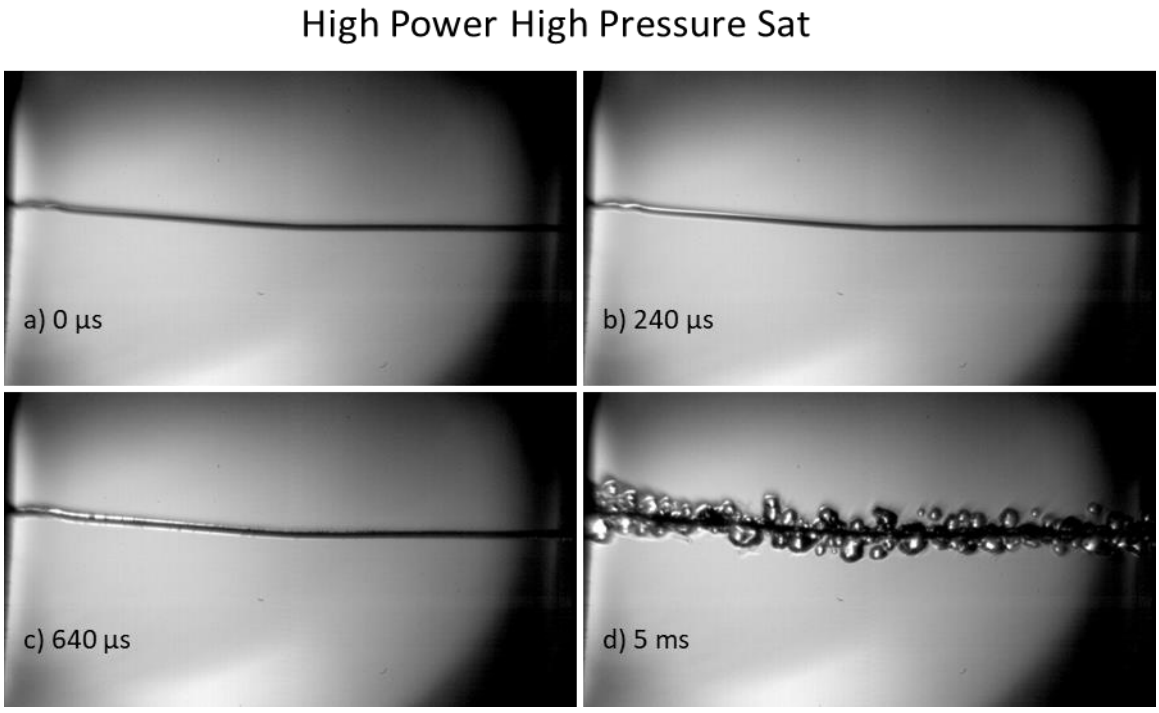

Figure 31: A progression of boiling is seen for the case of high power, high pressure water at saturated temperature (77.9 Bar and 292 °C).

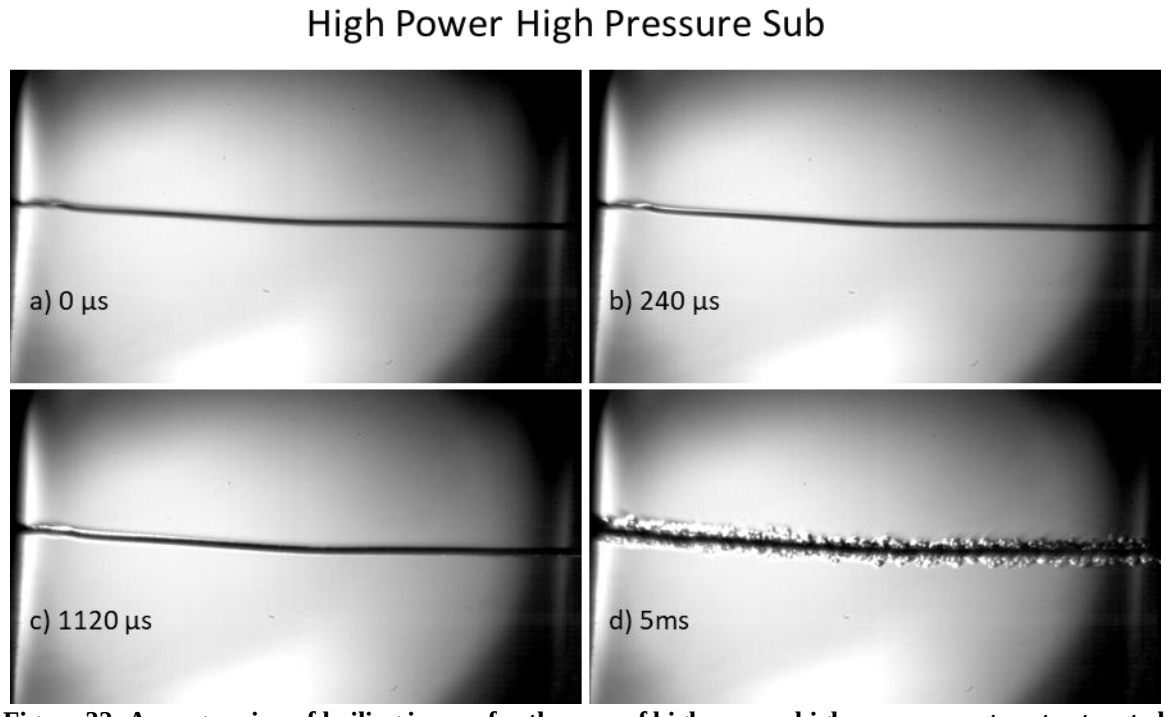

Figure 32: A progression of boiling is seen for the case of high power, high pressure water at saturated temperature (150 Bar and 292 °C).

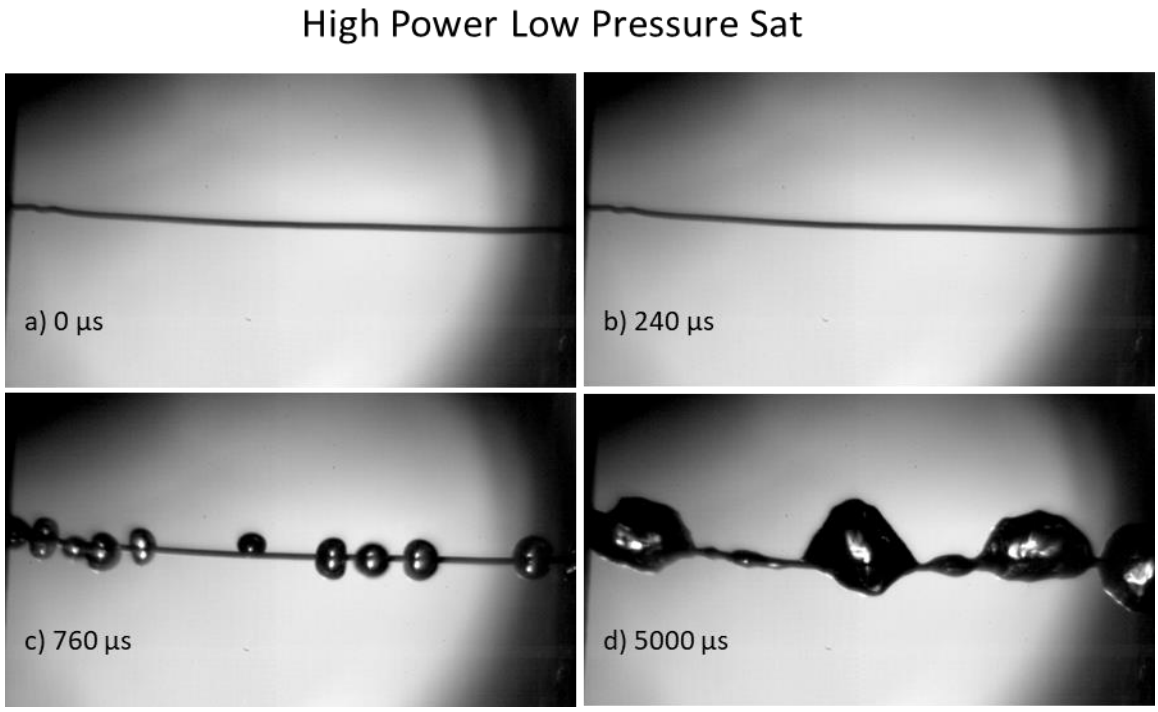

Figure 33: A progression of boiling is seen for the case of high power, low pressure water at saturated temperature (1 Bar and 100 °C).

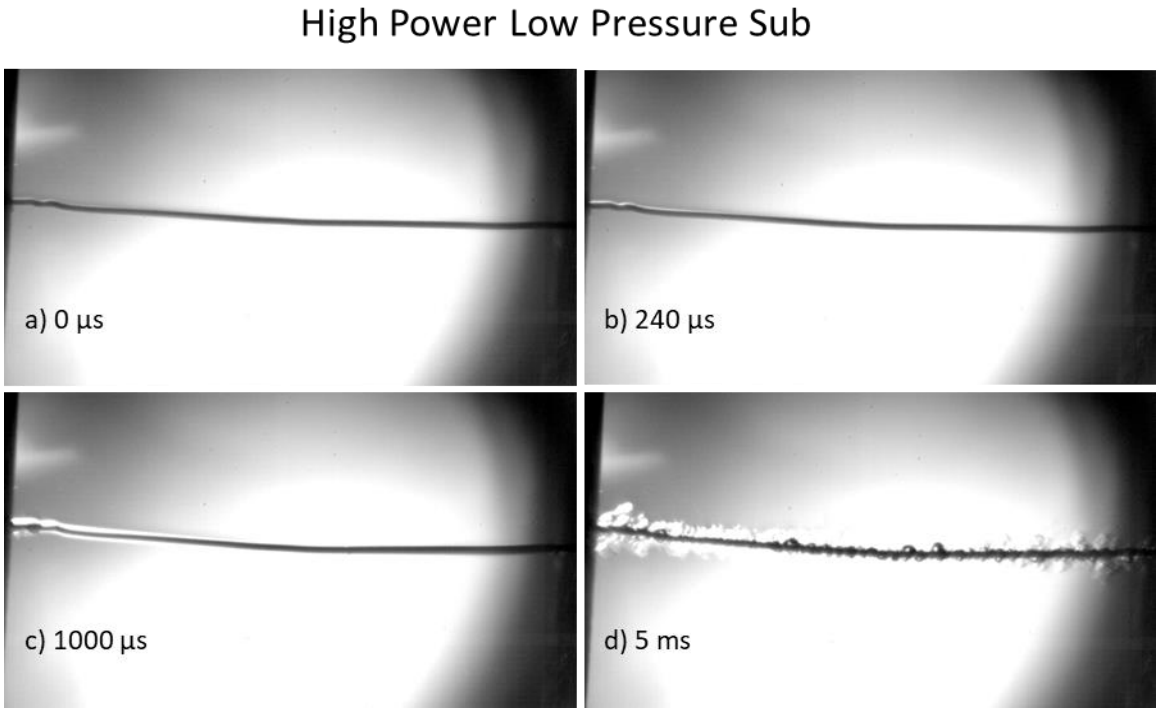

Figure 34: A progression of boiling is seen for the case of high power, high pressure water at saturated temperature (4.76 Bar and 100 °C).

While only the high-powered cases are shown directly in the chapter (all figures are found in Appendix E), the low powered cases demonstrated similar phenomena.

7.4.3 2^k Factorial Comparison

The 2k Factorial design of experiments method was used to evaluate the relative impact of subcooling level, system pressure, and power pulse height on various experimental results (e.g., max temperature, temperature after a prescribed time, etc.). However, the discussion becomes long and repetitive to review the impact of the variable parameters on 14 different experimental results. For the purposes of this work the influence on maximum temperature, maximum heat transfer, and maximum HTC are selected for full presentation and review. These parameters describe the most severe consequences of boiling runaway and highlight impacts on the fundamental boiling behavior. Furthermore, the other trends largely align with these three and none contradict the conclusions drawn in this chapter. The full result set is found in Appendix E and includes the impact on minima, average values, and specific experimental time stamps. The full list of the chosen outputs, together with their definitions are defined in the appendix.

Table 7: The results of the study for maximum temperature, heat transfer, and heat transfer coefficient are seen.

	Max Temp	Q Max	h Max
Subcooling (A)	-154.7	-7.78E+04	5.13E+05
Pressure (B)	-188.5	4.13E+04	1.96E+06
Pulse Height (C)	117.6	5.39E+06	-1.33E+05
AB	126.3	3.21E+05	4.88E+05
AC	-96.9	-1.81E+05	-1.62E+06
BC	-112.5	-1.62E+05	-6.80E+05
ABC	95.7	2.76E+05	-1.48E+06

To interpret the results of these studies, comparison of the given numerical values is only accurate and beneficial across cases where the output variable is identical (e.g., the numerical values between max and min temperatures could be compared because both relate a temperature change). As mentioned above, it is accurate to compare values across the row, as indicated by the color scheme, where red indicates and decrease in the output and blue an increase. Reading down a column is useful to assess trends in one control parameter, but the relative values are not necessarily indicative of overall importance. For example, the change across the entire range of pulse height in this work was found to have a positive impact on the maximum heat transfer raising the average maximum value by $5\,\frac{MW}{m^2}$ across otherwise identical cases.

7.5 Conclusion and Discussion

Several conclusions can be drawn from the presented data. The first is that the amount of heat transferred was most directly related to the pulse power level. This is most clearly seen in Figure 26 and the 2^k factorial study, which indicates an order or magnitude greater influence from

that factor over any other. In contrast, the same trend is not seen in the wall temperature. Figure 25 indicates that the final temperature between each power level at any given temperature and pressure combination was nearly identical, with the noted exception of the low pressure, saturation case. Temperature runaway appears in both power cases under the low-pressure, saturated condition. The mechanism for this run away is most readily seen in Figure 33, and in Appendix E for the low power case. In these figures irreversible wire dryout or Departure from Nucleate Boiling (DNB), indicative of CHF and film boiling transition, is seen as the wire is fully encased in bubbles that do not immediately depart from the surface. Under this condition the temperature will continue to rise, even as a plateau forms in the heat transfer. This finding is noteworthy because it indicates that DNB is tied to multiple parameters as opposed to one single control, and the power levels probed do not cause DNB. An increase in power level cause larger temperatures and increased heat rates but not DNB.

An unusual occurrence is seen to happen in Figures 25, 26, and 30. In these figures, the temperature and heat transfer are seen to rise immediately for between 1 and 3 ms for each test case where DNB does not occur. After this rise time a quasi-steady state is achieved, where the values do not increase. The temperature and heat transfer data remain elevated over steady state values but are no longer increasing at the ultra-fast rate. This quasi-steady state is seen to coincide with the rapid bubble movement or microbubbling phases described above in Section 6.4.2.

In the case of the maximum temperature overheat, meaning the amount to which the wire temperature is above the water boiling point, the single largest impact comes from the pressure of the water. As the pressure increases the wire temperature decreases. There are several simultaneous effects at play in this result. The specific heat, C_p, of the water increases with increased temperature. This means that more energy is required to heat the surrounding water, which is at a

higher pressure with an associated higher absolute temperature defining an equivalent subcooling space. The latent heat of vaporization, however, is known to decrease with an increase in pressure, meaning that it will require less energy to transition from liquid to vapor. Finally, the increased pressure results in a decrease in the diameter of any given mass of water that vaporizes. This allows for more liquid contact on the wire surface, which reduces the insulative effect of the bubble. Together, these effects result in more water vaporization without necessarily creating additional insulation through wire dryout and as seen in Figures 31-34. While this does not inherently remove more heat from the wire, it causes the amount of heat that is removed at a given temperature to be greater; in other words, a lower wire temperature is able to remove a given amount of heat. Ultimately, this leads pressure to be the largest contributor to the HTC as more heat is removed at a given temperature value, which is confirmed in the results of Table 7.

The subcooling of the water has a unique impact on the experimental results. Overall, its effect is muted but never trivial, as shown down the column in Table 7. An increase in the subcooling level leads to a logical decrease in maximum temperature because increased subcooling represents a lower absolute temperature. Compared to saturated water, the lower temperature water will require additional heat to form the same bubbles and insolation layers. The effect of the subcooling on the heat transfer value is, at first glance, counterintuitive. It would be expected that cooler water would be able to absorb more heat without producing insulative bubbles, meaning that the anticipated result would be in the positive direction with increased subcooling. This is true in 7 of the 8 cases presented in Figure 27, and is true of all temperature vs heat transfer pairs, or x-y coordinates, seen in the same figure (i,e. the heat transfer value at any given temperature). However, since the output metric is the maximum temperature value achieved in all 8 cases, the temperature runaway in the low pressure saturated case skews the 2k factorial results. While the

curve is presumably lower than the other curves would have been in such conditions, no other condition leads to the same heat transfer progression as that seen under this condition. Thus, under these sampling circumstances, the excursion does result in the highest value. Because this saturated case is so much larger than the other values, its influence is still felt over the other tests. This effect is non-spurious and therefore should not be neglected from the consideration. The full story indicates an area of improved behavior, but across the full range negative changes can occur. It is seen that DNB can lead to vastly different dynamics and overall effects even at the short time-scales of this work.

7.5.1 **Discussion**

The transient boiling response to ultra-fast heating at the pressures and subcoolings described here indicates that the event power level is the major factor in determining the amount of heat transferred from the system in any given condition. Under accident conditions, it is usually not possible to control the amount of power coming from the accident. Therefore, it is important to design the other parameters, namely pressure and subcooling to mitigate unwanted effects, such as DNB. This work demonstrates that it is possible to aim for maximization of heat transfer and simultaneous minimization of the temperature at which the heat transfer will occur.

As in the previous chapter the boiling observed on the wires is not identical to boiling under standard steady state, or even transient, conditions. Once again, the bubbles are seen to remain on the wire and not lift off. The boiling regimes once again align with the ultra-fast boiling regimes presented in chapter 6. This is confirmed for elevated pressure as well.

7.5.2 **Summary**

In summary, ultra-fast heating (with heating rates between 15,000 and 85,000 °C/s) transient boiling was performed using a thin platinum wire at elevated and standard pressures and water subcoolings. The temperature and heat transfer were calculated and correlated with boiling images. It was observed that the thin wire's ability to transfer heat to water was most directly tied to the heating rate or amount of power being produced by the wire. The associated temperature, however, was most strongly influenced by the system pressure. The separation of these two effects is interesting in that it permits the design of a transient boiling system which can maximize heat transfer and minimize component heat. This is a promising result in terms of accident safety and future design for the next generation of nuclear reactors. In terms of the conditions of a present LWR experiencing a RIA, which is demonstrated by the light blue line/lines in each graph, Figures 25-30, the system is found to heat up rapidly and then maintain the elevated temperature throughout the duration of the pulse, forming an elevated quasi-steady state. The heat transfer values seen under this heat pulse and condition are more than 8 times larger than the steady-state heat transfer value for the noted wire temperature. This represents an advantageous position for maintaining the safety and integrity of the core.

8.0 Experimental Study on the Effect of Power Shape and Heating Behavior on Transient Boiling Phenomena

8.1 Introduction

As noted in previous chapters, there remain aspects of boiling to be plumbed for understanding and completeness in the transient boiling phenomenology. Among the recent fields of study is the impact of heating pulse shape on the transient boiling behavior [10, 25, 47-48]. The power shape is interesting due to the hydrodynamic instability of boiling. This instability indicates that a variety in bubble formation and behavior will lead to more drastically varied results than may be expected in other systems. For example, the power excursion of a nuclear reactor under RIA accident conditions is expected to behave differently from an exponential power generation due to natural, inherent reactor kinetics.

When a large amount of reactivity is suddenly inserted into a nuclear core, the fission rate at that location will instantaneously respond driving up the local fuel and moderator temperature. However, as the water moderator becomes hotter and less dense its efficacy decreases. Doppler broadening of the fuel makes neutron capture for additional fission less likely, essentially reducing the local reactivity to compensate for the previous addition. The feedback process is what leads some to postulate that other models may more accurately predict the nuclear core behavior than the exponential source [2-3, 10, 47].

While research studies investigate various heating shapes, the impact of the heating shape in combination with other experimental parameters (e.g. pressure, and subcooling) remains

unknown. In addition, recent consideration of power step increases, where the baseline power before the pulse is non-zero, has shown an impact on boiling inside of a pipe under ambient, flow conditions, but has not been explored at other pressures or for transient pool boiling.

Two main conditions of interest are presented in this chapter. The first is a front-loaded pulse, in which the initial power at time $t = 0$ is higher than the average pulse height for a short duration. This represents the pre-dampening spike from the power supplies that may trip initial boiling behavior sooner than would occur otherwise. This is achieved naturally with the power supplies when put in constant current mode with a free-floating voltage and will be referred to as constant current mode. While the fast neutron response to a RIA is faster than can be replicated in this work, the impact of the dynamics will be studied to see how a front loaded (constant current) pulse ultimately impacts transient pool boiling. This has an unknown effect on fundamental boiling. This pulse shape has not been explicitly explored previously, so the impact of the initial spike remains fully unknown. The second power condition is a power step increase up from a non-zero initial power condition. This represents a core, or other heat source, that was operating under safe power levels then then suddenly increases to boiling power levels. This mode will be referred to as power step increase. As noted above, recent research shows that power step increases impact flow boiling through a tubular geometry at ambient pressure. Additional studies are needed to extend the understanding to pool boiling and to changes in pressure. In order to achieve this power shape in this work, circuitry changes are required and will be described in the following section.

8.2 Experimental Setup and Measurement Theory

8.2.1 System Setup and Modifications

Both of these power shapes operate under the same calibration mode as the previous chapter, namely TRT. As noted in the introduction, the power step increase will require hardware changes to achieve the desire power outputs; however, the constant current mode does not require hardware changes, just programming the power supply to the correct mode. The circuit for the power step increase is shown below in Figure 35. In this configuration, a solid-state relay (Crydom D1D80) was used in place of the transistor used in other configurations. Under a biased current condition, the transistor will always be in an open state, negating its switching capabilities.. The solid-state relay was controlled identically to the transistor and no other system modifications were necessary to operate in the power step increase mode.

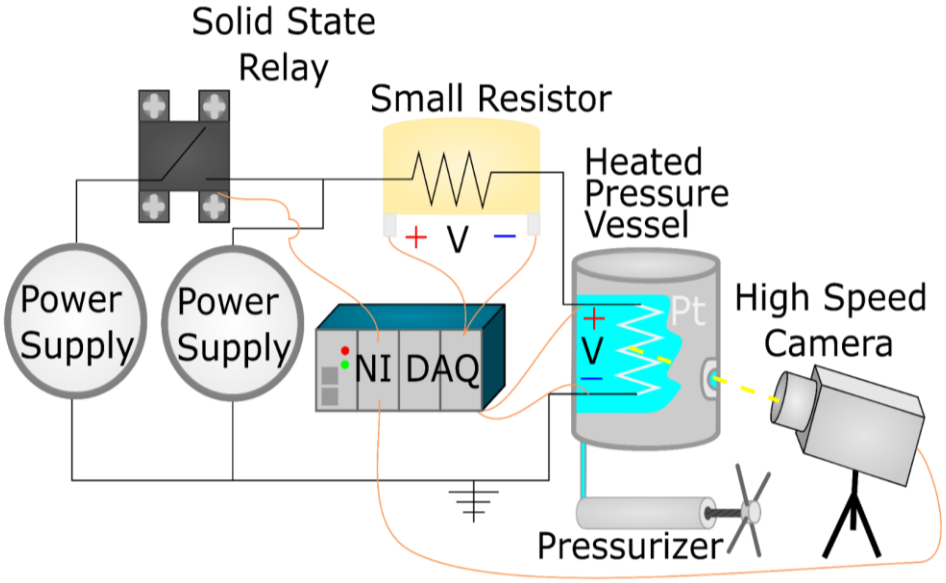

Figure 35: The modified circuitry for a power step increase is shown.

8.2.2 **Sample Calibration**

The calibration curve for the constant current mode is identical to the calibration presented in Figure 24 in Chapter 7 for the primary experiment; the two experiments were run concurrently on the same wire and under fully identical conditions. The calibration curve for the power step increase is presented below in Figure 36.

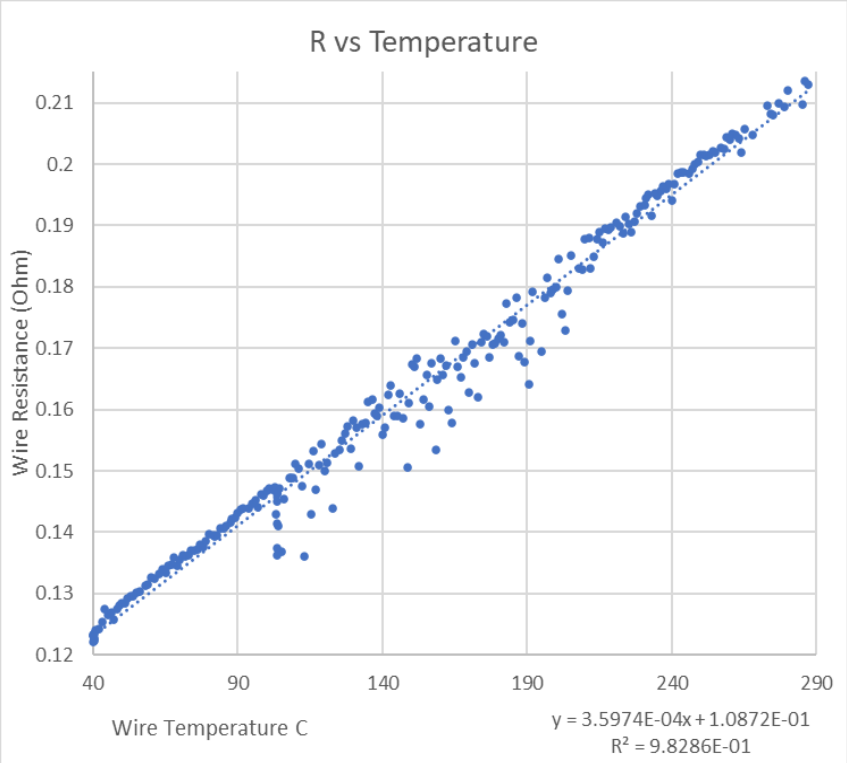

Figure 36: The calibration curve for the power step increase test is presented.

8.3 Test Scope and Parameters

The experimental procedures in these cases match those set forth in Section 7.3. In order to compare the overall effect of the power pulse shape change, each test set is compared with

another test. In the case of the constant current, the tests are compared with the constant voltage tests presented in Chapter 7. The test parameters for this test and comparison are laid out in Table 8.

Table 8: Test parameters for platinum wire under constant current heating are presented.

PARAMETER	LOW VALUE	HIGH VALUE
WATER SUBCOOLING	0°C Subcooled	50°C Subcooled
PRESSURE	Low Pressure σ(1 Bar)	High Pressure σ(150 Bar)
POWER PULSE HEIGHT	5 V (floating current) Or ~ 10 A (floating voltage)	8 V (floating current) Or ~ 15 A (floating voltage
POWER PULSE SHAPE	Constant Voltage (no initial spike)	Constant Current (with initial spike)

As in Chapter 7, the exact pressure is determined by the subcooling temperature condition. At low pressure and 0 °C subcooling, the pressure is atmospheric, while at low pressure and 50 °C subcooling, the pressure is 4.76 Bar absolute. In both cases the water is physically 100 °C, but the saturation state is altered by pressure. In addition, the values of the current chosen for the high and low were selected to be the average current drawn from the floating current in constant voltage mode. This makes the two tests as analogous as possible. Heating rates under the constant current mode, defined identically to the heating rates described in Section 7.3, range from 23,000°C/s to 250,000 °C/s.

The power step change test is inherently a constant current test as well, and as such, is compared with the values from the constant current test as its baseline. The test parameters for this

comparison are show below in Table 9. The heating rates of the pulse step increase range from 23,000 °C/s to 45,000 °C/s.

Table 9: Test parameters for platinum wire under pulse step increase heating are laid out.

PARAMETER	LOW VALUE	HIGH VALUE
WATER SUBCOOLING	0°C Subcooled	50°C Subcooled
PRESSURE	Low Pressure $\mathcal{O}(1\ \text{Bar})$	High Pressure $\mathcal{O}(150\ \text{Bar})$
POWER PULSE HEIGHT	3 A increased to 9 A or ~ 10 A (floating voltage)	3 A increased to 12 A Or ~ 15 A (floating voltage
POWER PULSE SHAPE	Pulse Step Increase (increased from baseline heating)	Constant Current (with initial spike)

The two tables presented here, represent the breakdown and separation of the results that will follow. Due to the complexity of the various power shape variations, a direct 2^k factorial analysis using all the variables present in this chapter is infeasible. Thus, two separate, but similar analyses are presented.

8.4 Results

As before, a full discussion of the results presented is saved for the following section, Section 8.5.

8.4.1 **Heat Transfer and Temperature**

Graphical representations of the collected data are presented. Collection information as well as the coloring convention were previously presented in Section 7.4.1.

8.4.1.1 Constant Current

The power supply exhibits significantly different behavior in constant current mode as compared to constant voltage mode. The current shows an initial spike as opposed to the square pulse of the constant voltage heating. In addition to the initial pulse, the constant current mode causes a phase delay between the current and voltage over the driven, upward pulse. Both this delay and the pulse shape are seen in Figure 37. The current delay appears in each case that is operated in constant current mode. This is not an uncommon occurrence and can be explained by the power supply having an inherent inductance that induces delay, overshoot, and ringing under fast transients [73]. This delay causes nontrivial issues in calculating the resistance of the wire. By

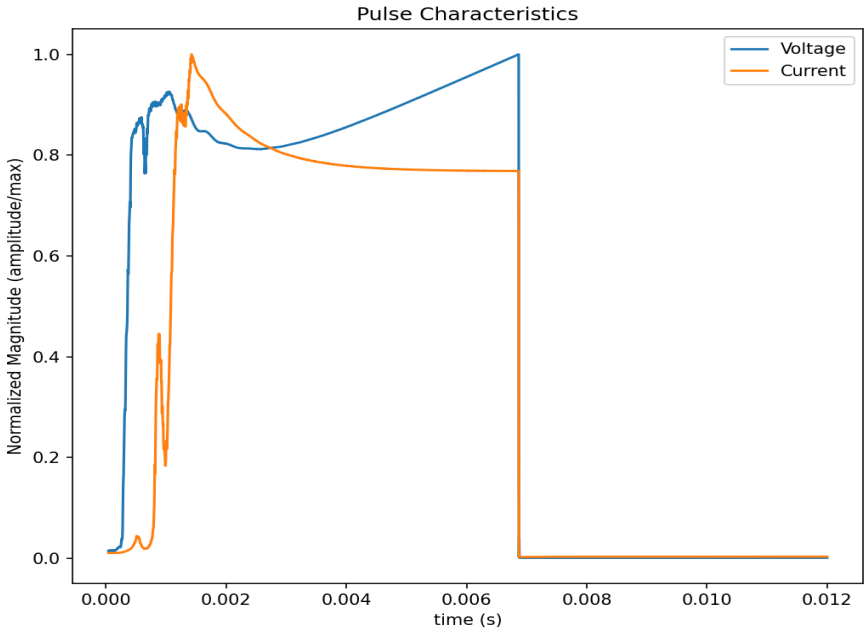

Figure 37: Constant current pulse is seen.

Ohm's law if the voltage is elevated, but the current remains near zero, the resistance, or more accurately impedance, must be very large. As this measurement, and its calibration, are performed under non electrically transient condition, it is not possible to calculate the temperature and heat transfer while the transient lag is happening. An alignment point is found in each test case to mark where calculations become valid. This coincides with the voltage and current curves moving in unison again.

As before, the temperature, heat transfer, and HTC are presented in Figures 38 – 42. The coincidence point spoken of is shown by the figures beginning after 1 ms of heating has occurred. The temperature profiles in Figure 38 indicate that the low-power, low pressure subcooled case cooled after the initial power spike. This indicates that the initial heating rate could lead to different boiling and thermal behavior.

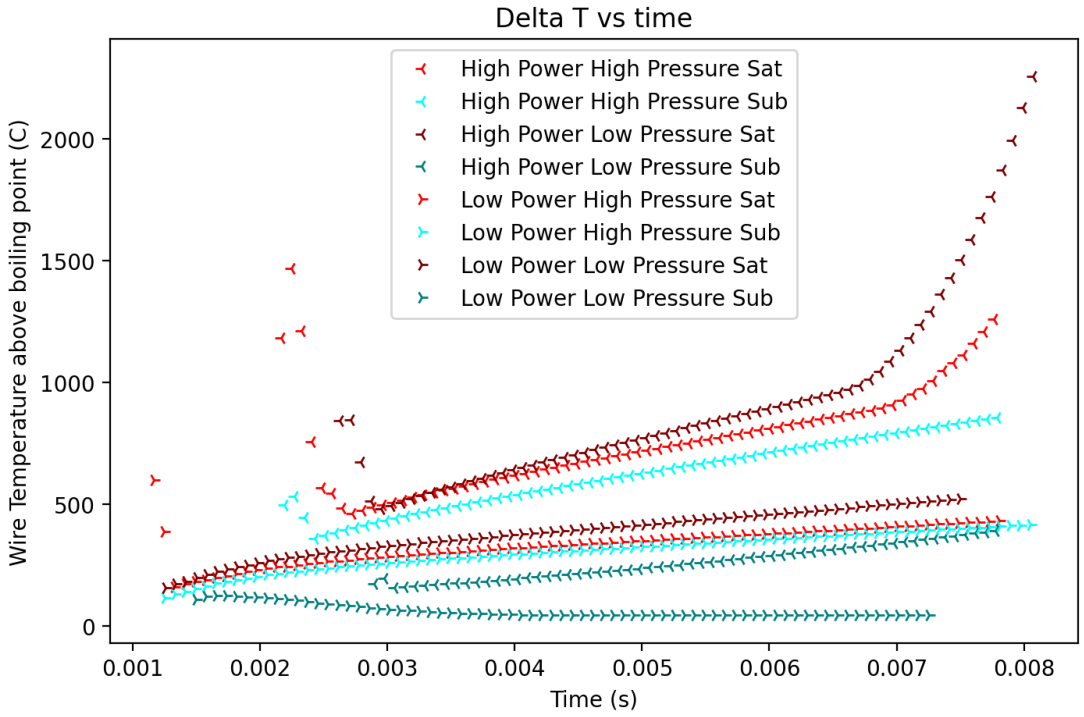

Figure 38: Temperature vs time for the constant current pulse.

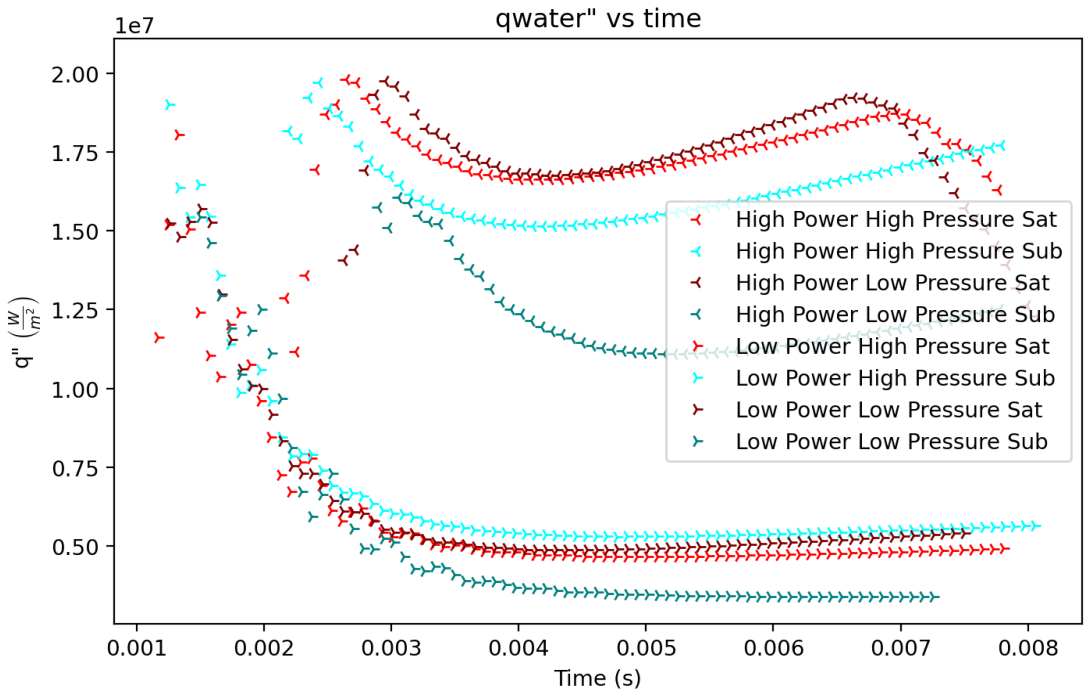

Figure 39: Heat transfer vs time for the constant current pulse.

An inflection point is seen in Figure 39 for the two highest cases which may indicate the same behavior as the wire show prior to material failing wire as discussed in Chapter 6.

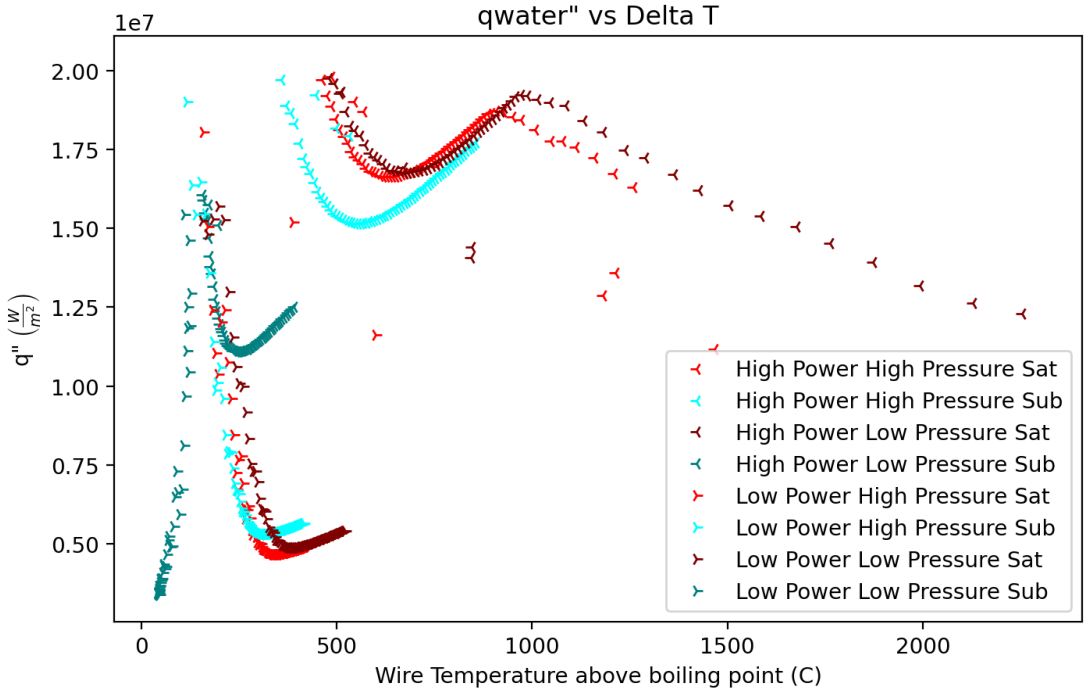

Figure 40: Heat transfer vs temperature for the constant current case is presented.

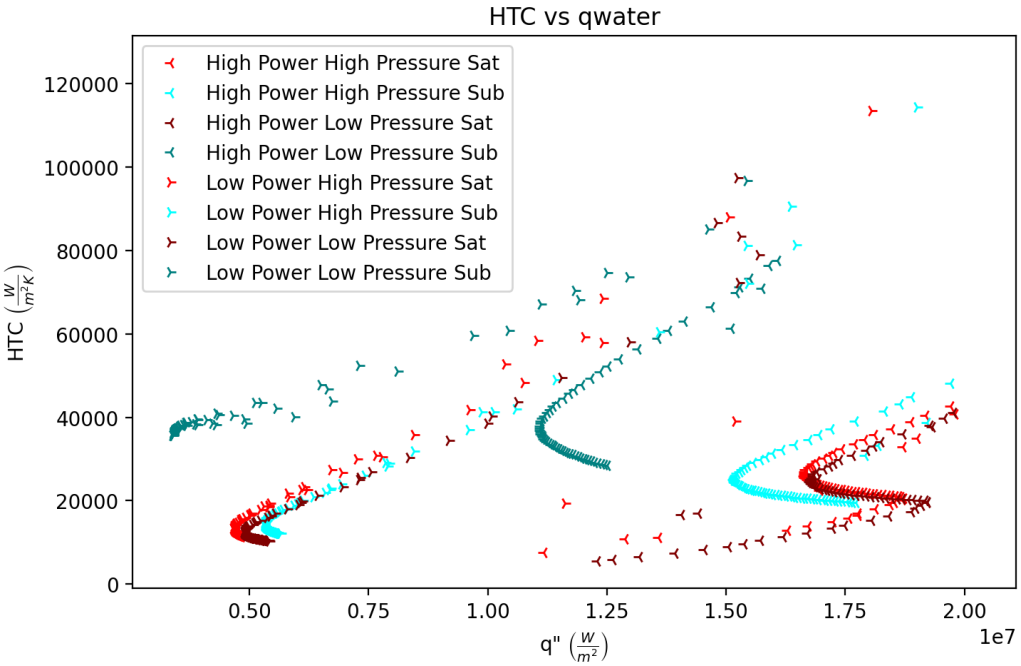

Figure 41: The heat transfer coefficient vs heat transfer for the constant current pulse is shown.

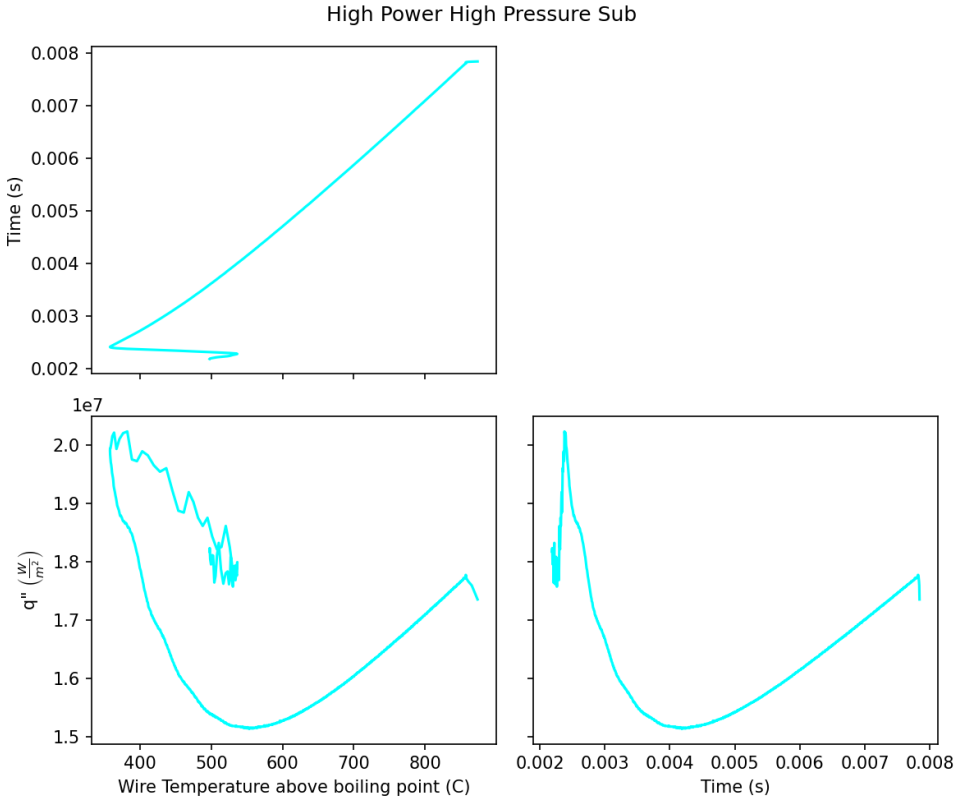

Figure 42: The individual curves for the high power, high pressure, subcooled case (analogous to a LWR) are presented.

The temperatures seen in Figure 35, particularly for both high-powered saturated temperature tests, are rather high. This is very similar to the results seen in Chapter 6, where constant current was also employed. It is assumed that the same resistance increases explained in that chapter are occurring in these cases but that the tests are halted prior to material failure.

8.4.1.2 Pulse Power Step

The pulse power step is also a constant current mode, but the size of the step increment is smaller leading to smaller lag between the voltage and current. This can be seen in Figure 43. This figure also shows that a greater amount of system noise occurs over the duration of the pulse. This is most likely caused by the difference in components needed to operate in the desired configuration. More detailed explanation and diagrams of this configuration can be found in Section 8.2.1.

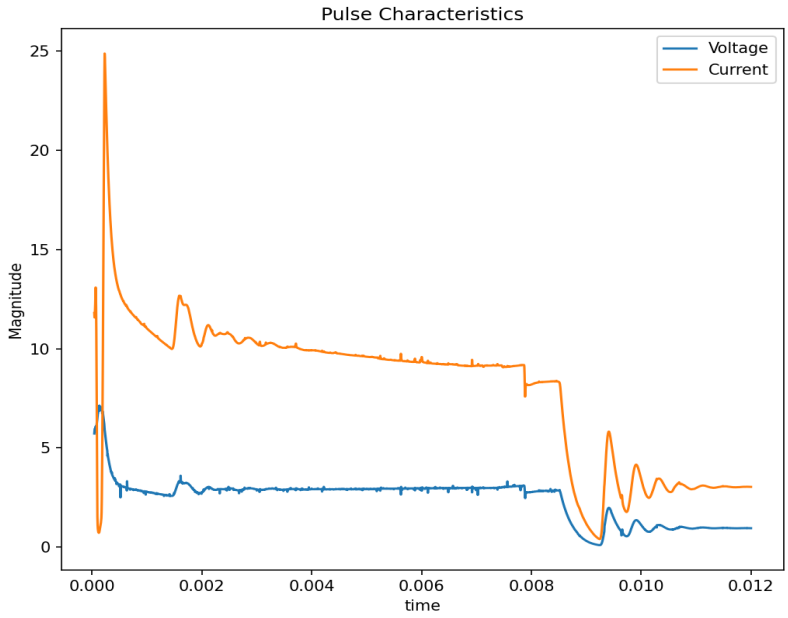

Figure 43: The power pulse for the power step increase is shown.

There are two additional points to call out from the power pulse seen in Figure 43. The first is, as before with a constant current pulse, the calculated results of measurement are not valid where the voltage and current are out of phase. Thus, an alignment point is employed again for where calculated values are valid. The second point is that the system ringing is seen when the pulse ends in this test case, which was not seen previously. This agrees well with the proposed assumption of a small transient inductance in the power supply [73] because the power transient will depend on the new power level, which is non-zero at shutoff in this case.

Figures 44- 48 present the same data layout as seen for previous tests. As noted for the power pulse, the calculated data tend to be noisier, particularly during changes in the power state, than other data collected and presented in this work. Figure 44 shows that more uniform grouping of identical pressure and subcooling groups begins to occur. This means that many tests behave similarly at high or low power. These similarities are also seen among the presented HTCs. Indeed, some of the HTCs are so similar as to be indistinguishable from one another. Figure 44 also shows that after the elevated pulse ends and the original power level is restored the temperature does not fall away at a uniform pace. Similarities exist between various cases, but no there is no guaranteed consensus among the cooling rates after the pules ends.

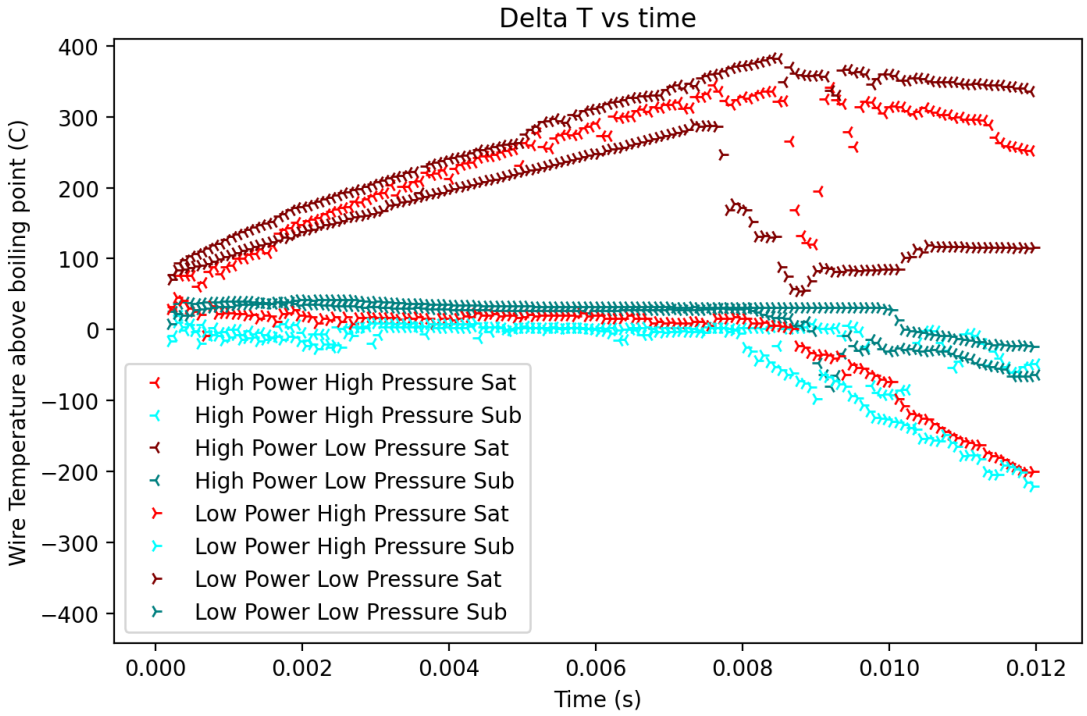

Figure 44: Temperature vs time for the pulse power step is shown.

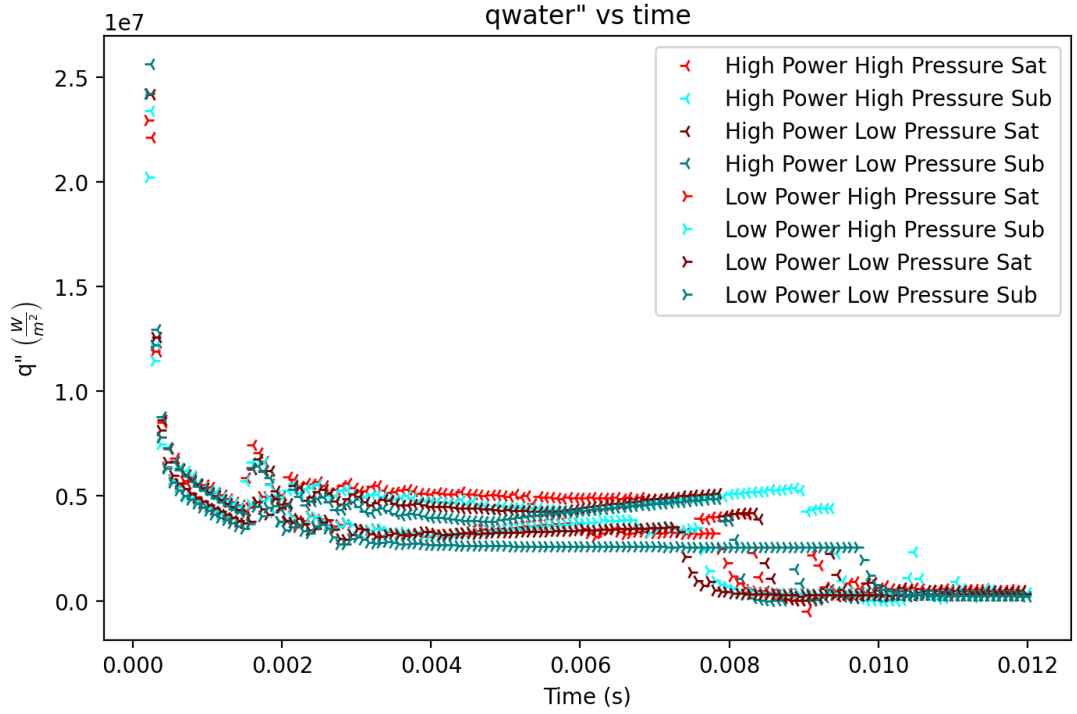

Figure 45: Heat transfer vs time for the pulse power step is shown.

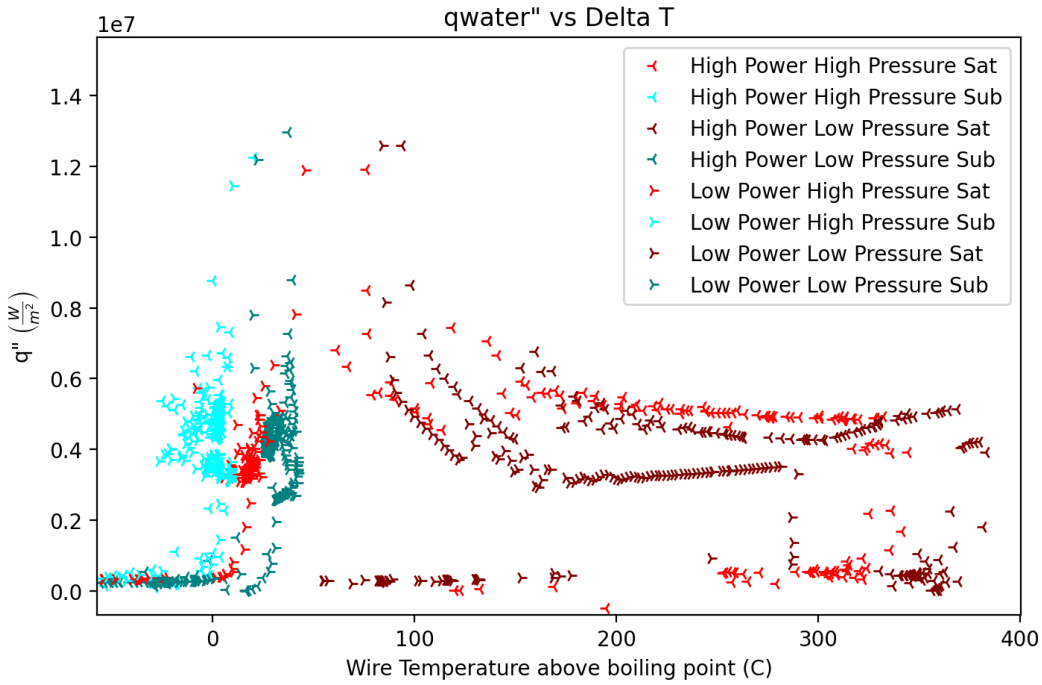

Figure 46: The constant current heat transfer vs temperature is seen.

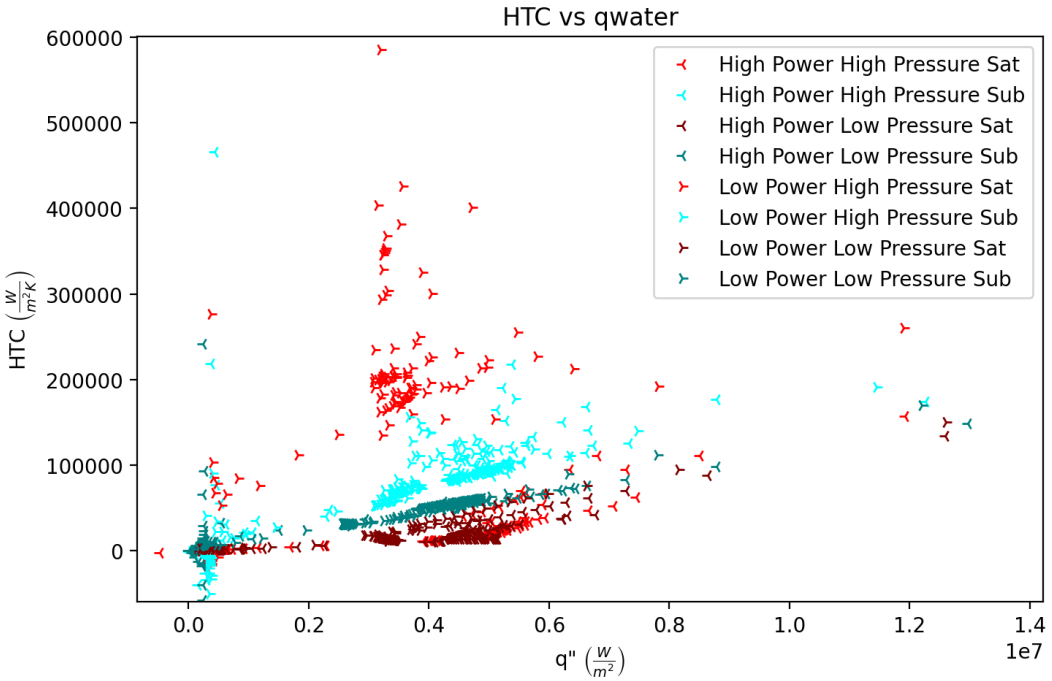

Figure 47: The heat transfer coefficient vs heat transfer is seen.

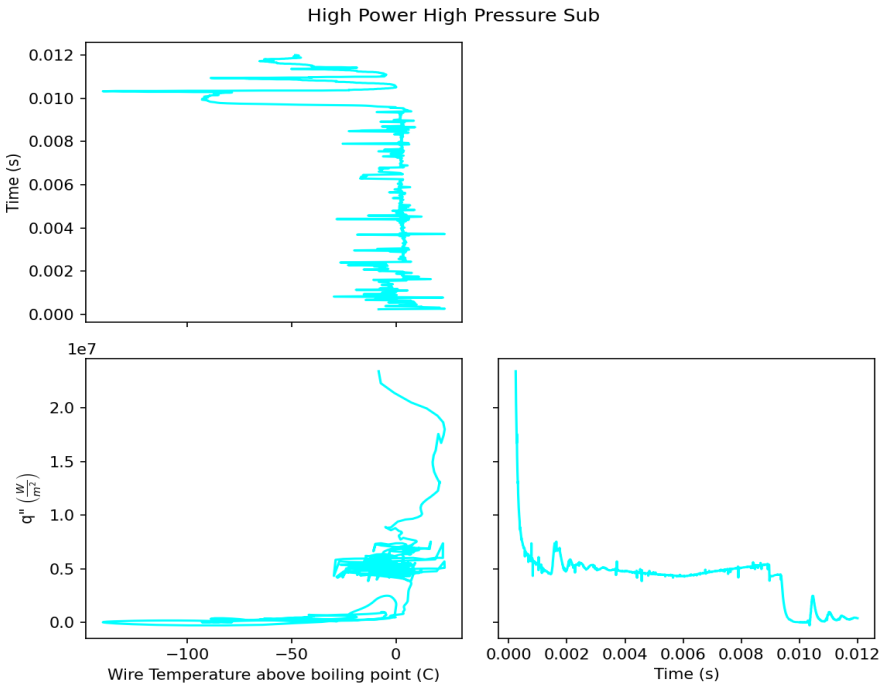

Figure 48: The various heat transfer, temperature, and time plots are shown for the case of high power, high pressure, subcooled boiling.

8.4.2 **Boiling Behavior and Regime**

Under the conditions presented in this chapter, event timing and alignment become more critical as the initial phase delay between the current and voltage render calculated values inaccurate. Under constant current, timing events are aligned from the end of the pulse to prevent any uncertainty from the initial delay. It should be noted that the lack of clarity is always in the electronic data, not the high-speed imagery, and alignment between the two is what is of interest.

8.4.2.1 Constant Current

In the previous chapter, four images were selected for each condition presented as this was found to be sufficient. In the case of the constant current pulse, however, many of the datasets lose most if not all of the first millisecond of information due to the aforementioned phase issues. Thus, under these circumstances, six images are presented to allow for some insight to be drawn from the boiling behavior in regions where there is less immediate data.

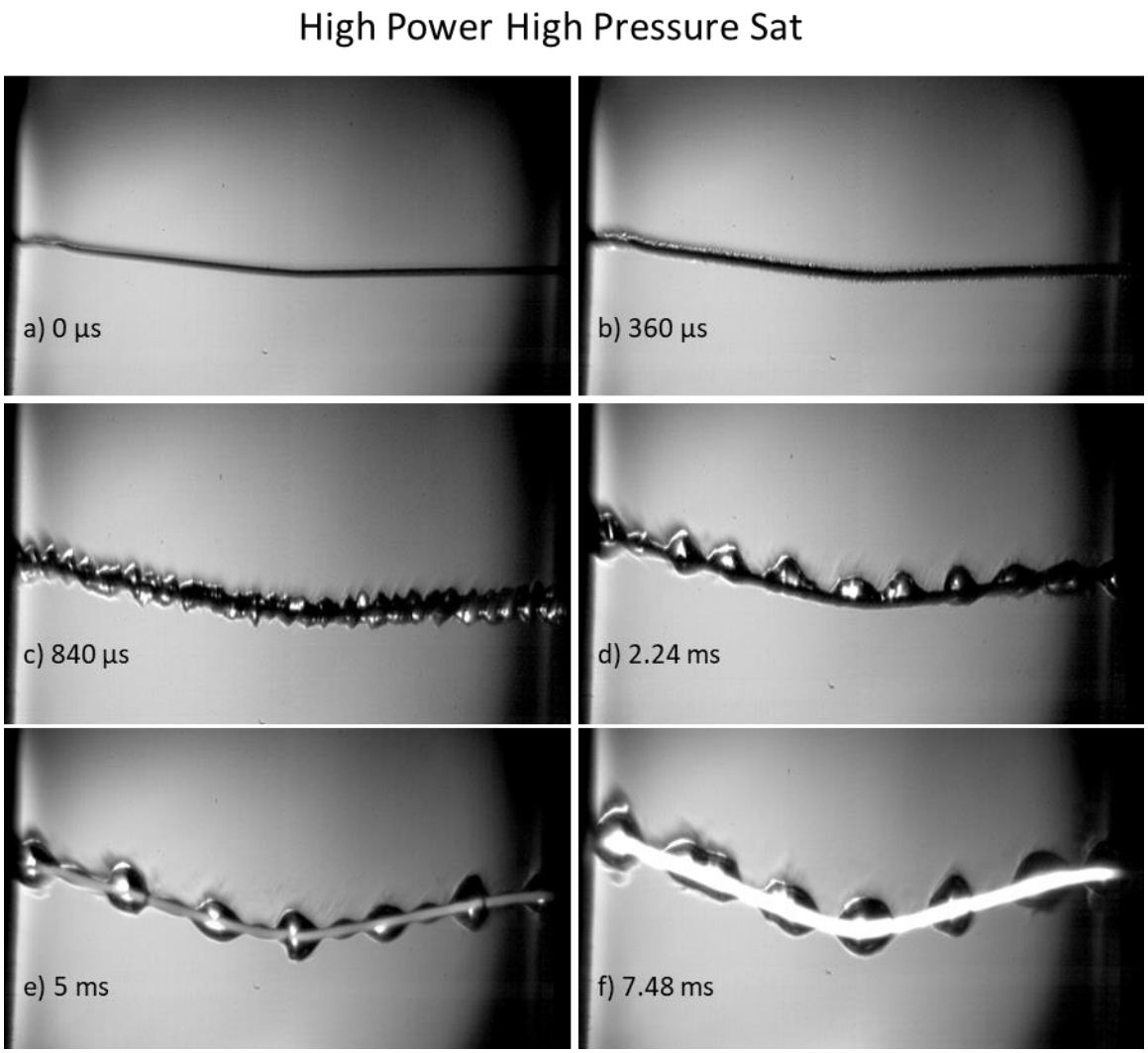

Figure 49: Boiling images for the high power, high pressure saturated condition with a constant current pulse are shown.

Figure 49 shows that the final state of the wire does look very similar to the wire failure cases presented in chapter 6 of this work in the glow and flexure of the wire.

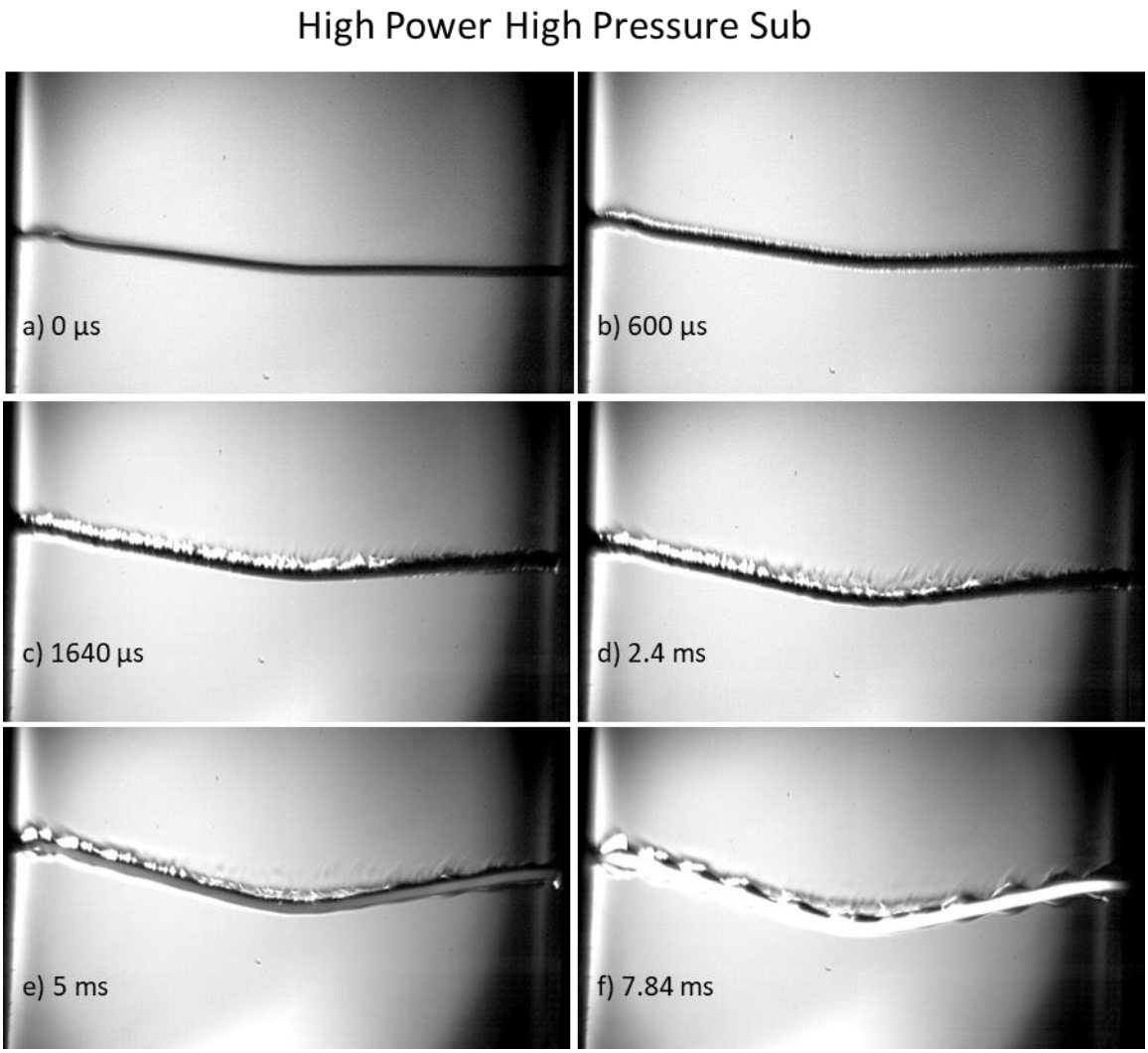

Figure 50: Boiling images for the high power, high pressure subcooled condition with a constant current pulse are shown.

As in Figure 49, Figure 51 also shows a similar final state to the wire failure cases presented in Chapter 6. The formation of the vapor layer is interesting here, where nucleation occurs at the end points seen in image b and the bubble simultaneously erupts inward to the middle of the wire.

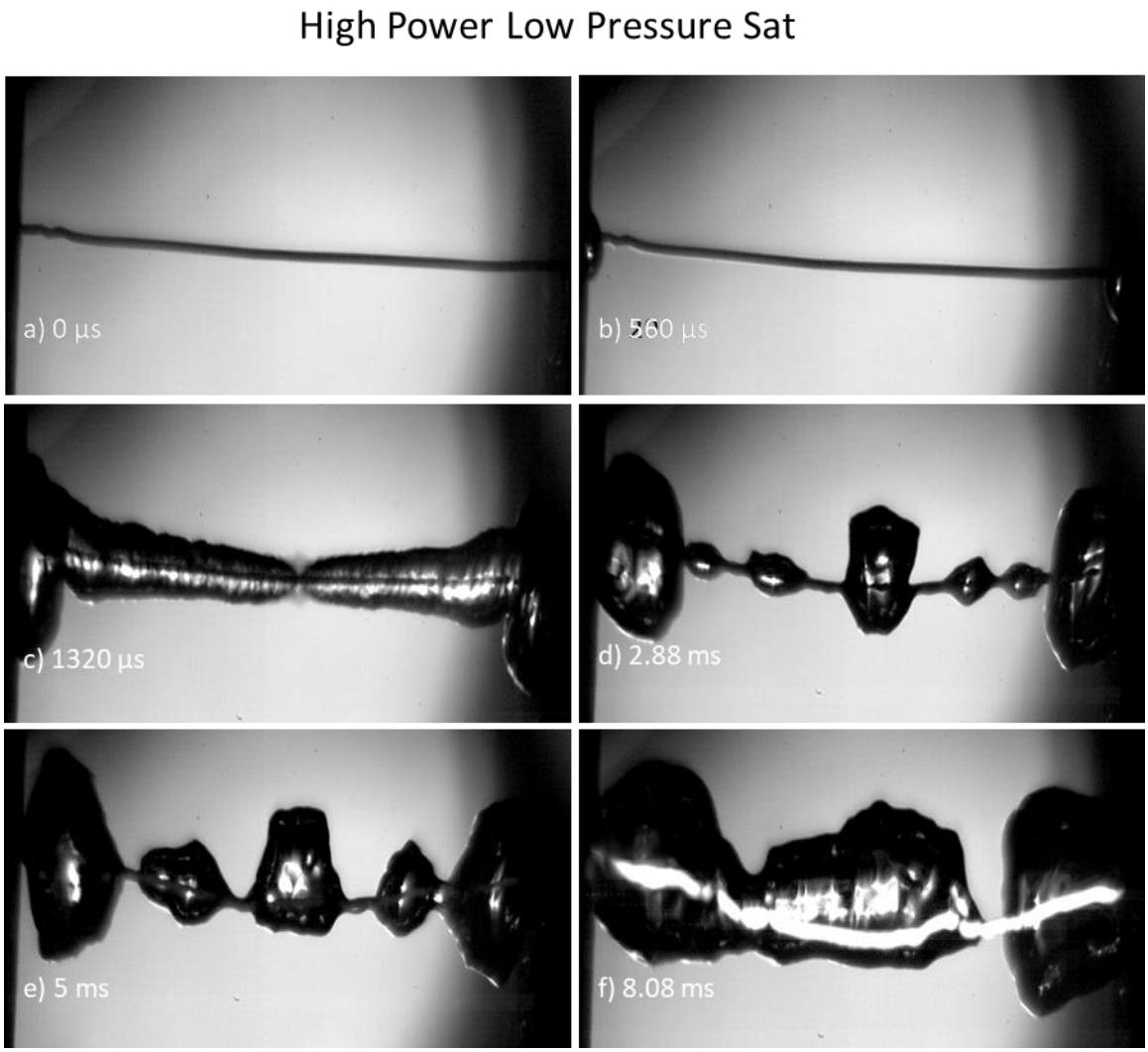

Figure 51: Boiling images for the high power, low pressure saturated condition with a constant current pulse are shown.

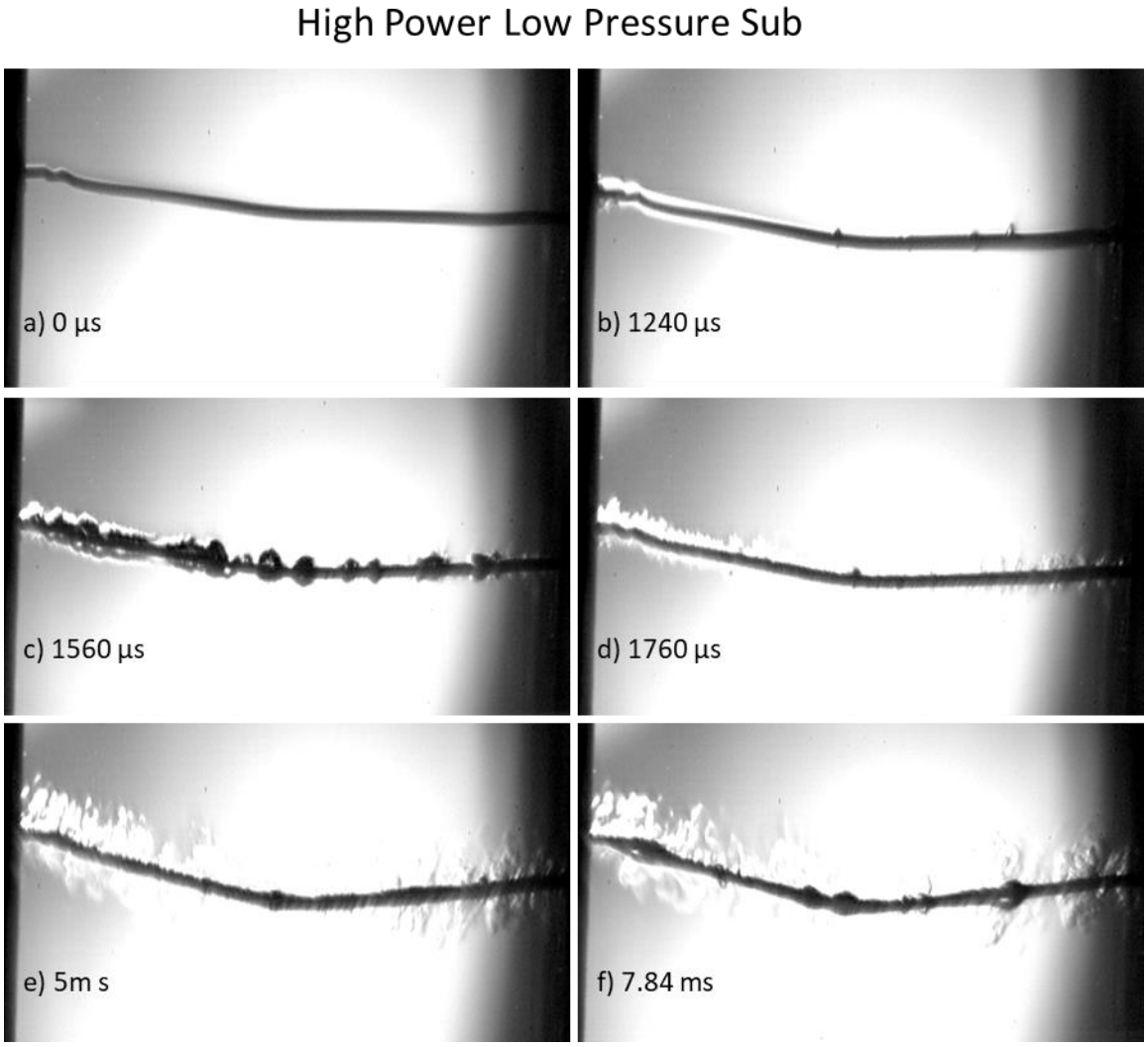

Figure 52: Boiling images for the high power, low pressure subcooled condition with a constant current pulse are shown.

8.4.2.2 Pulse Power Step

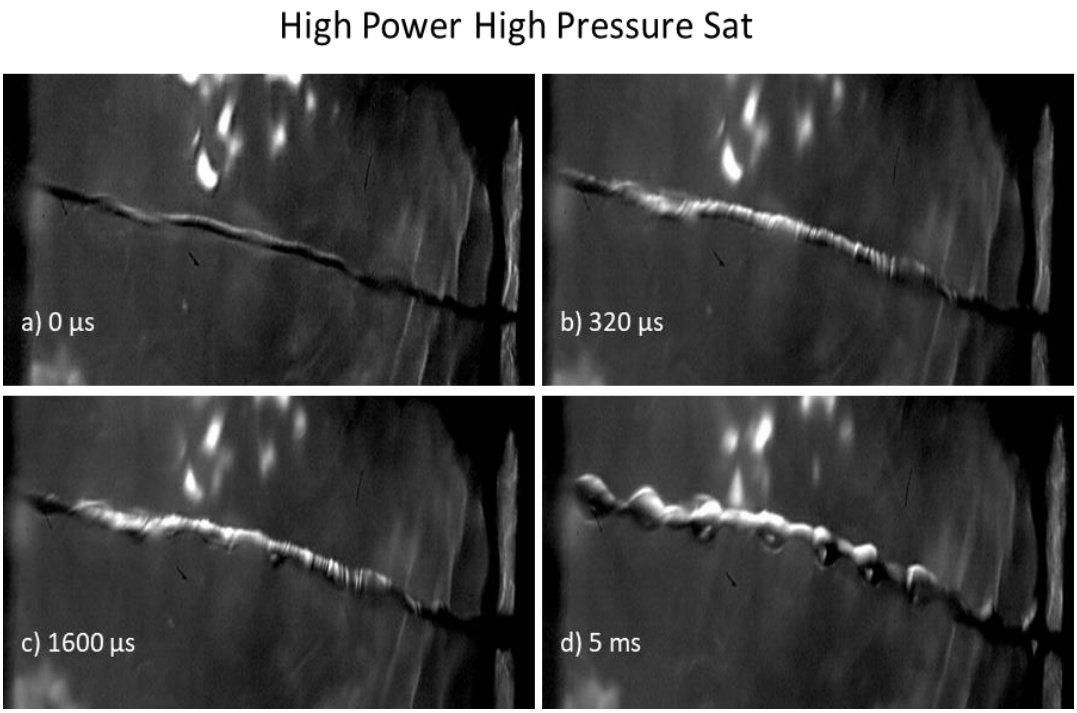

Figure 53: Boiling images for the high power, high pressure saturated condition with a step power increase pulse are shown.

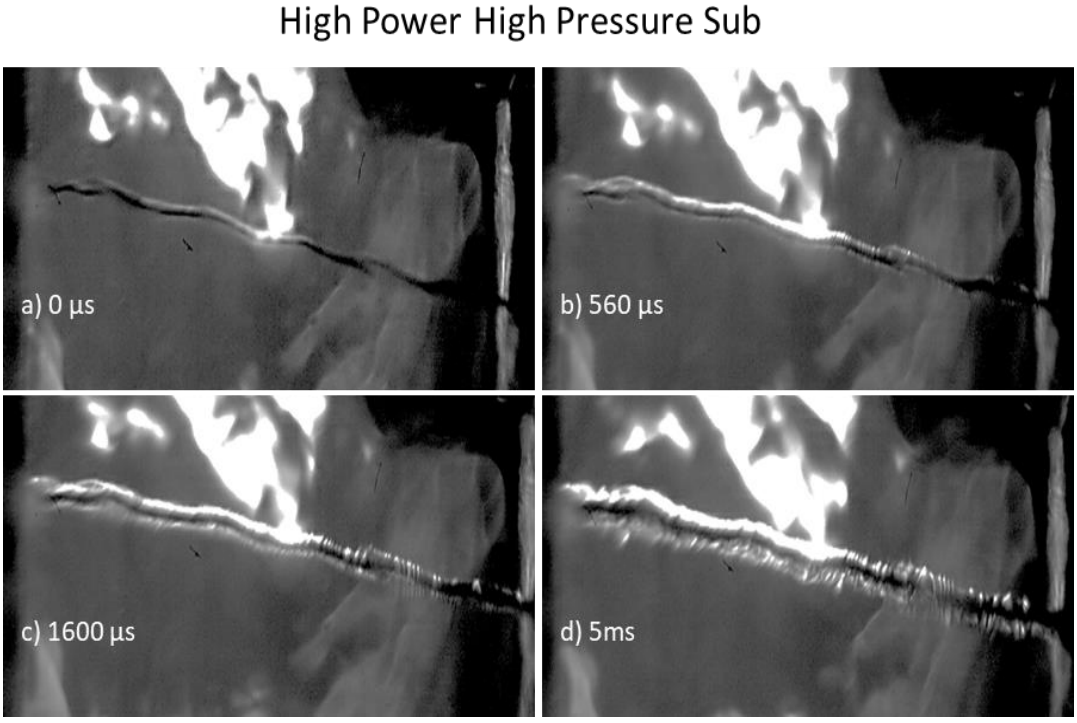

Figure 54: Boiling images for the high power, high pressure subcooled condition with a step power increase pulse are shown.

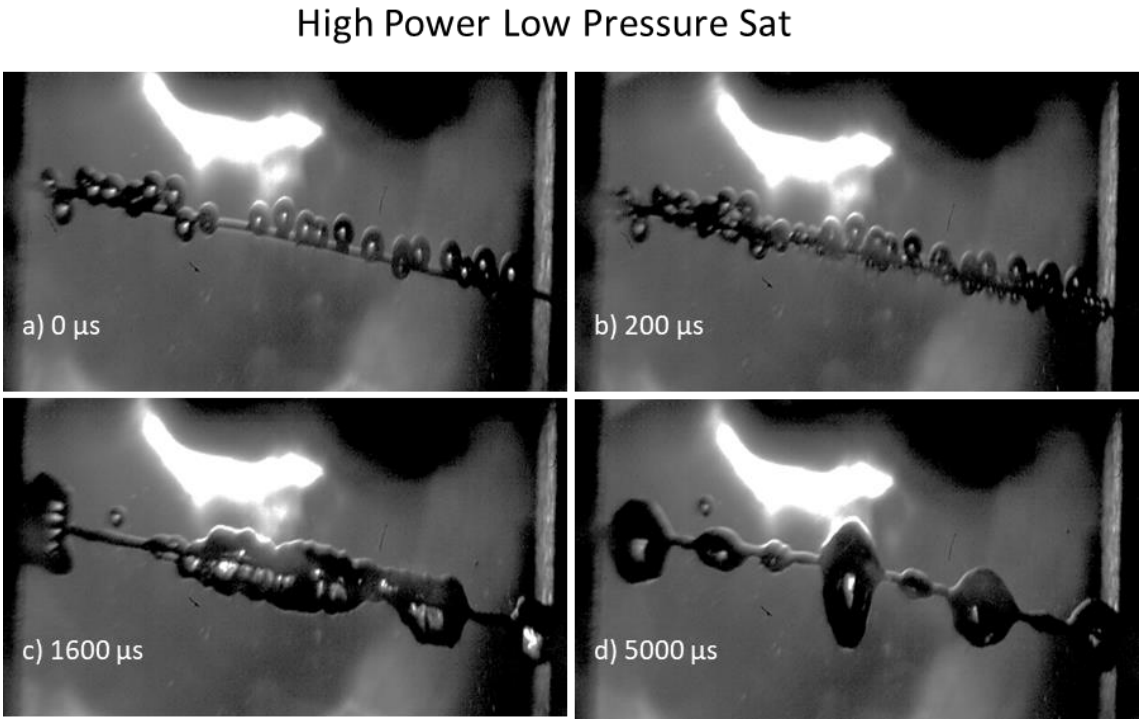

Figure 55: Boiling images for the high power, low pressure saturated condition with a step power increase pulse are shown.

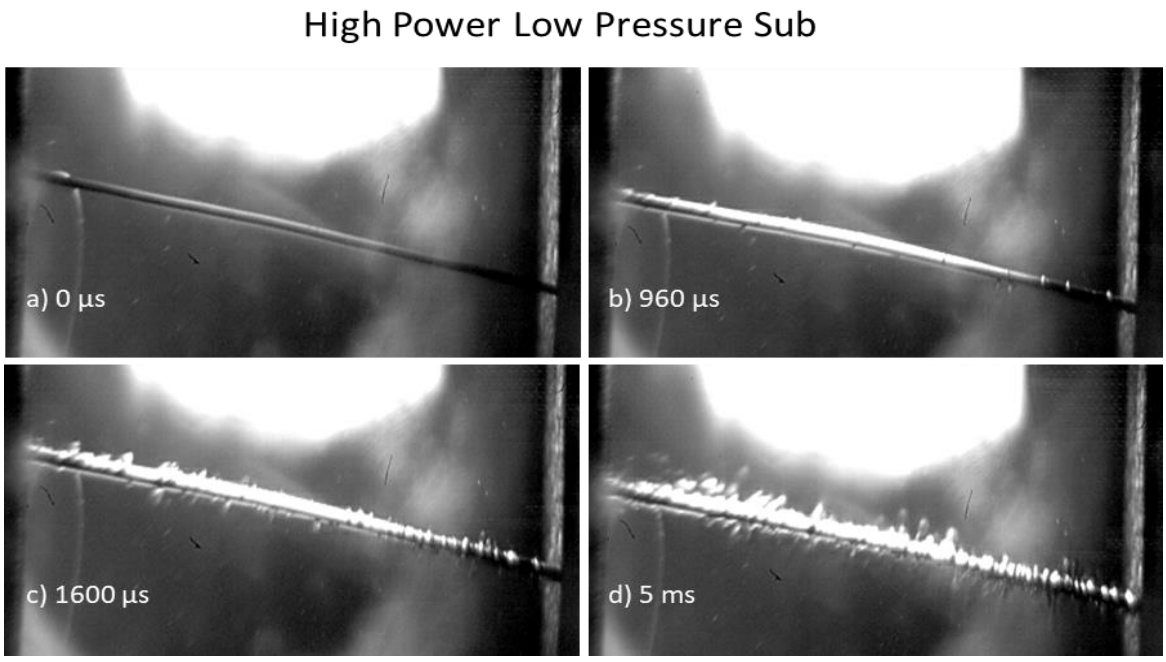

Figure 56: Boiling images for the high power, low pressure subcooled condition with a step power increase pulse are shown.

8.4.3 2^k Factorial Comparison

A full comparison and 2^k factorial test between the data sets collected in this chapter is not possible. This is because, under the present configuration, there is no ability to perform a constant voltage power step increase, rending no direct comparison for this variable. For this purpose, two studies are performed and presented. The first, seen in Table 10, compares the constant current mode to the constant voltage results of the previous chapter. Table 11 presents the comparison of results between the constant current and the pulse power step increase, which is a constant current heating mode. Some inference may be achievable between the two tables.

Table 10: The results of the 2^k facotrial study between the constant current and pusle step pulse are presented.

	Max Temp	Q Max	h Max
Subcooling (A)	-241.2	-4.98E+05	2.60E+05
Pressure (B)	-312.8	1.39E+06	9.81E+05
Pulse Height (C)	703.8	3.59E+06	-9.44E+04
Pulse Shape (D)	892.5	1.22E+07	-1.45E+06
AB	70.9	6.99E+05	2.39E+05
AC	-108.7	-4.99E+05	-8.02E+05
AD	-86.5	-4.20E+05	-2.52E+05
BC	-324.3	-4.20E+05	-3.49E+05
BD	-124.3	1.35E+06	-9.77E+05
CD	586.2	-1.80E+06	3.90E+04
ABC	-40.4	6.02E+05	-7.43E+05
ABD	-55.4	3.78E+05	-2.49E+05
ACD	-11.8	-3.18E+05	8.16E+05
BCD	-211.8	-2.58E+05	3.31E+05
ABCD	-136.2	3.26E+05	7.38E+05

Where the pulse shape variable, D, Compares Constant Voltage (no initial spike – seen in Chapter 7) to the Constant Current (with initial spike – seen in this chapter).

Table 11: The results for the 2^k factorial study between constant current and the pulse step are presented.

	Max Temp	Q Max	h Max
Subcooling (A)	-283.5	-3.30E+05	-5.68E+05
Pressure (B)	-257.0	5.18E+05	1.78E+06
Pulse Height (C)	696.1	1.24E+06	-1.56E+06
Pulse Shape (D)	-868.7	5.79E+06	2.77E+06
AB	36.6	5.43E+05	-1.31E+06
AC	-111.3	-3.13E+05	1.35E+06
AD	44.2	5.88E+05	-5.76E+05
BC	-240.8	-5.90E+05	-2.23E+06
BD	180.1	-2.23E+06	1.77E+06
CD	-593.8	-5.55E+05	-1.50E+06
ABC	-114.5	4.45E+05	6.45E+05
ABD	21.0	-5.35E+05	-1.30E+06
ACD	9.2	5.05E+05	1.34E+06
BCD	295.3	8.75E+04	-2.21E+06
ABCD	62.1	-4.83E+05	6.50E+05

Where the pulse shape, D, compares a Pulse Step Increase (increased from baseline heating) to a Constant Current heating mode (with initial spike).

8.5 Conclusion and Discussion

8.5.1 **Constant Current Conclusions**

The results presented in this chapter are noisier and more variable than the previous chapter. Perhaps the experimental variability has contributed to the lack these studies in the literature. As before, cases which undergo DNB experience higher temperatures. Surprisingly, DNB occurs much more frequently in these tests compared to the constant voltage cases. As noted above, the current values of the constant current tests were selected to be analogous to the current drawn during the constant voltage cases, and the experiments were performed successively on the same wire, under identical vessel conditions. This impact is indicated as variable D in Table 10 and is seen throughout the boiling regimes given in Figures 49-52. The initial pulse immediately

induces film boiling in the high-powered, low pressure saturated case, without nucleation over the whole wire. Bubble nucleation on either side of the wire leads to full film coverage of the wire.

Both Table 10 and Table 11 indicate that the power pulse shape is the single largest factor affecting maximum temperature, heat transfer, and the heat transfer coefficient. This is true of nearly every result probed in Appendix Tables 3-6. Importantly, the power shape has such a profound impact on a wide variety of metrics. Under ultra-fast heating rate transients, the results of any test, simulation, or proposed equation will be largely influenced by the heating pulse shape applied to the system. Although general trends can be gleaned from the transient boiling of one pulse shape on another, exact data and predicted behavior will likely only align as well as the power shapes align. Therefore, substantial care should be given to align the power shapes of any experiments seeking to be an analog or provide insight into another. This result has not been thoroughly addressed in the previous literature to establish proper analog.

The overall heat transfer values increased under the constant current pulse. This is unusual since DNB occurs. Despite this increase, the heat transfer coefficient still decreased since this increase in heat transfer occurred at substantially higher temperatures. During DNB, heat can still be drawn out through vaporization of the surrounding water, but the wire temperature will increase as well, and the process will be less efficient.

8.5.2 **Power Step Increase Conclusion**

Another interesting conclusion of this work is demonstrated by the temperature behavior of the power pulse step increase tests. The subcooling of the water has a larger effect on the maximum wire temperature than the pressure does. Except for the high pressure, saturated cases,

where the power level increase induced DNB, the temperature results seem to align well based most directly on the water subcooling. This is not altogether unexpected. In this probed configuration, the wire was already producing heat when the pulse occurred. Though never actively boiling prior to the pulse onset, the surrounding water is heated and more ready to form a film in DNB. This film would then insulate the wire leading to expectedly similar results.

Comparison of the power step increase with the baseline constant voltage case presented in Chapter 7 is reserved for Chapter 10 of this work.

8.5.3 **Discussion**

Ultimately, these tests indicate that the pulse shape is critically important in the prediction of transient boiling behavior. Additionally, the maximum temperature will increase, and the HTC will decrease as DNB occurs. By studying the boiling mechanisms with high-speed imagery, it was identified that the initial pulse present in the constant current heating modes would often lead to DNB directly after nucleation. This is clearly seen in Figure 51, where nucleation begins on the left and right extrema and a film crashes into the middle. However, the initial DNB state does not guarantee that the boiling will remain in this regime. Figure 52 indicates that film boiling occurred but collapsed back down to nucleate boiling.

It is essential to accurately model the supplied power profile in order to predictably model the response of general heat transfer systems (or more specifically nuclear reactors) [74-79].

The boiling characteristics of these tests, like those seen in Chapter 7, match the ultrafast behavior described in Section 6.4.2. Yet again, a quasi-steady state behavior (where temperature

and heat transfer stop changing but are found to be at an elevated state compared with steady state boiling values) is found to exist for each in each test case that does not experience DNB.

8.5.4 **Summary**

In summary, a transient pool boiling experiment was performed on thin platinum wires under a variety of heat pulse shapes. The shapes include a classical square pulse (presented alone in Chapter 7, names constant voltage), a square pulse with an initial power spike at the beginning (named above as constant current) and a square pulse added onto a non-zero initial background heating (named above as pulse power step). The power shape was found to have the most profound impact on the maximum temperature, heat transfer, and HTC. The initial power spike in constant current was seen to induce substantial changes to the boiling behavior (specifically tripping DNB to occur) that did not uniformly go away after the spike ended. In addition to the power shape, the relative impact of several other parameters is given in the results. DNB was found to be the primary driving factor in the behavioral differences observed under different power shapes. The pulse shape with the initial power spike, constant current, was found to induce DNB more readily than the other heating conditions. This led to substantially higher temperatures along the wire and was also accompanied by an increase in the associated heat transfer over the other studied power shapes, which is somewhat counterintuitive to the insulation layer formed. General boiling behavior and quasi-steady state behavior, as described in Chapters 6 and 7 were again observed.

The initial power spike was sufficiently energetic to induce rapid DNB even in conditions that would otherwise not have experienced DNB. Most cases would remain in DNB after the spike since large enough heating occurred in the film layer to maintain film boiling temperatures. This

phenomenon has not been previously identified. Additional work investigating the importance of the spike and its occurrence in operating reactors is for use in RIA accident simulations warranted.

9.0 Experimental Study on the Effect of Heater Material and Surface on Transient Boiling Phenomena

9.1 Introduction

While much boiling work has been done in the more distant past, a substantial amount of the present focus on boiling relates to surface or material boiling enhancements [10, 32, 34, 42-46]. As new fabrication techniques and new materials become viable options for numerous conditions, it is critical to understand the impact that these materials will have on the full range of behaviors where they are applied. It is possible that a process which maximizes a property or benefit in one area will simultaneously reduce a benefit in another area. For example, recent work has been performed by Wen et al to increase bulk material strength and protection against irradiation damage [80-82] by drastically reducing the grain boundary size down to the nanoscale. This is novel research and shows tremendous promise for increased strength and irradiation protection, but the effect is likely to be catastrophic to the heat transfer properties of the material. The grain boundaries pose a reduction to the effectiveness of heat carriers along the lattice. This impact will need to be studied in conjunction with the strength if the ultimate application is a situation where both strength and thermal properties are of importance. The relative changes to all parameters that matter can then effectively be compared.

Specifically related to this chapter, research on the influence of fluid changes (e.g., the introduction of nano particles in the fluid), controlled microscale surface modifications, heater surface condition at ambient pressure, and heater coatings to induce surface wettability changes

have been performed. These works do not establish the impact of ultra-fast transient heating with wire surface changes at high pressure and temperature or with changes in heating wire material. The final independent tests run in this work set forth the relative impact and boiling mechanistic behavior changes from changes on of heating surfaces at high temperature and pressure, and the impact of wire material change at low pressure. This will be done by comparing the behavior of scratched wire with a smooth, drawn wire of each material. The focus of this work is on a platinum heating surface. However, low pressure comparison will also be extended to a zirconium (zirconium 702) wire.

It is important to be able to relate future work for modeling and simulation or initial design criteria to existing data. Thus, an understanding of how changes in the surface affect other areas is of crucial importance. This will also provide insight into comparative benefits, where, as in the example above, some material and experimental properties increase while other decrease.

9.2 Experimental Setup and Measurement Theory

9.2.1 **Sample Preparation**

The experimental setup and measurement theory match the TRT method and general vessel description provided in chapter 4 of this work. For the cases in which a scratched wire was employed, a protocol for wire scratching was followed to maximize uniformity in the outcome. Each wire was rubbed with 120 grit sandpaper axially 20 times with a ~ 45 ° rotation between each pass of the sandpaper. The wire was then radially scratched by rolling the wire between the

sandpaper and a soft, wooden surface. The location of the wire axially relative to sandpaper was adjusted after approximately 10 rotations. This radial treatment was repeated 3 times. Microscope images of each wire were collected and are shown in Figure 57. No significant change to the diameter of each was made; the hypothesized impact of the wire roughening is in the formation of nucleation sites for ready bubble formation as well as potential lift-off enhancement.

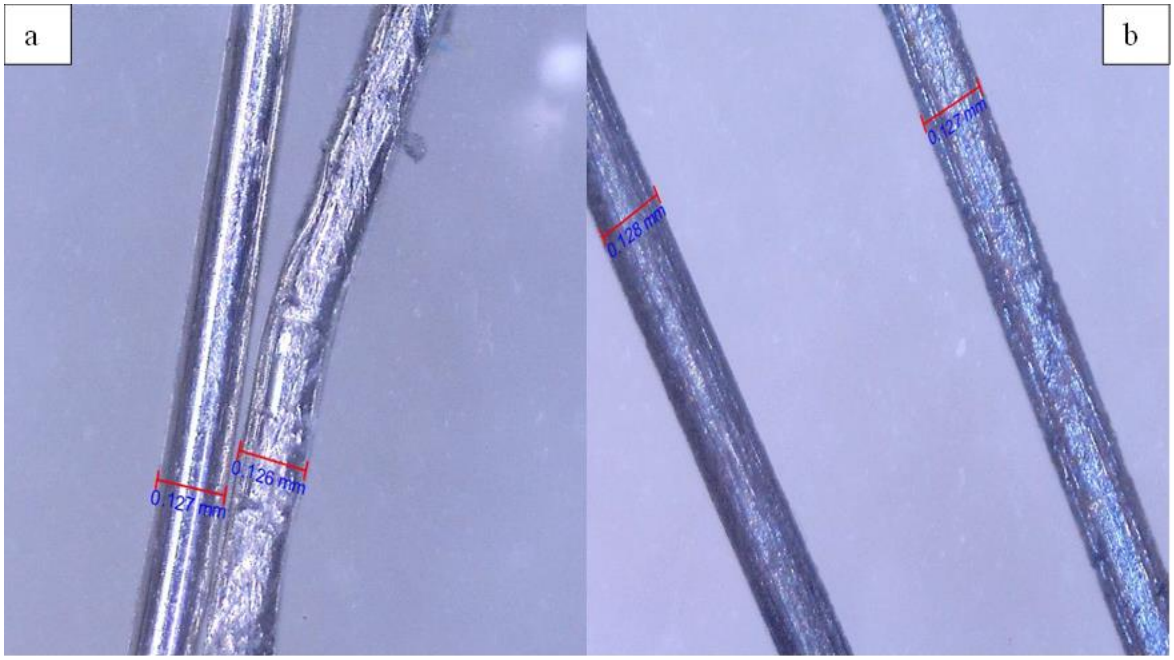

Figure 57: Microscopy images of the wires are shown with a) showing platinum wire, and b) showing zirconium wire.

9.2.2 **Sample Calibration**

As noted above, all of the wires of this study are calibrated with a TRT curve. Zirconium is a higher resistivity material than platinum. While the initial prediction was that a high resistance wire would lead to more accurate measurement, as the larger value is more centered in the measurement range of the DAQ, it was quickly discovered that the zirconium showed inconsistencies with temperature, particularly in repeatability.

As the zirconium wire was cycled in calibration, the values that were measure for the resistance showed large variations, unlike the platinum case which showed great repeatability particularly in the high temperature range. Observation showed that the variations in the calibration eventually diminished with each repeat. This is shown in Figure 58. However, occasional large fluctuation would still occur above an ambient temperature of approximately 170 °C. In order to have an accurate measurement on the zirconium wire, a restriction to low-pressure operation was necessary. To best collect consistent measurements at low temperature, a length of wire, long enough to run many iterations of each experiment, was placed in the pressure vessel and allowed to sit at elevated pressure and temperature sufficiently long that the variations were diminished.

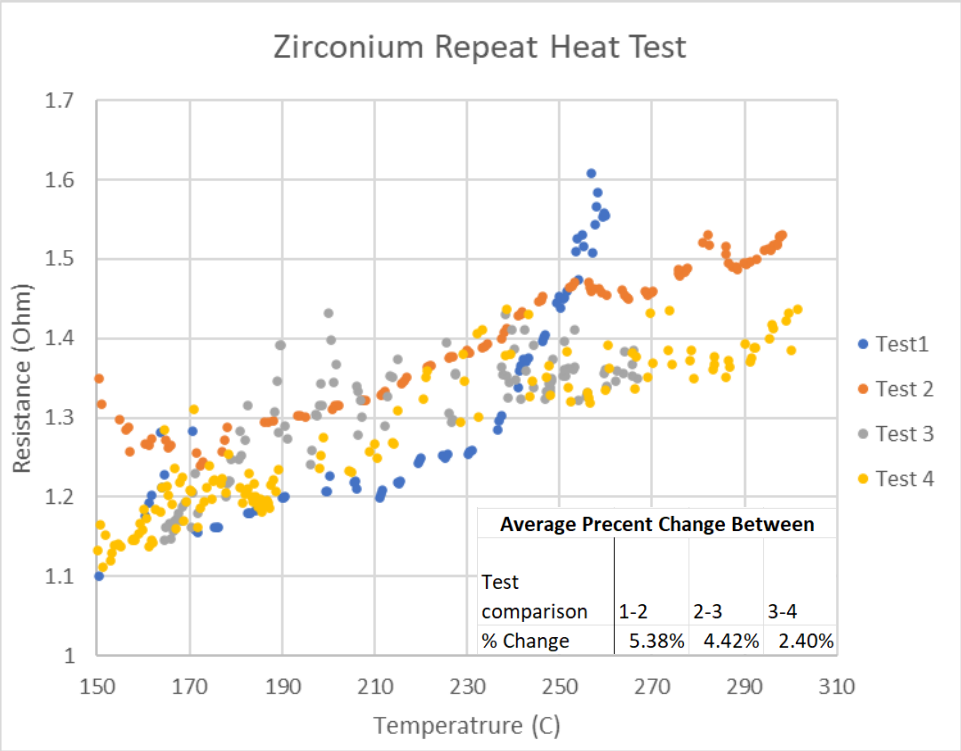

Figure 58: The repeat tests on the calibration of a single zirconium wire show that variation occurs, but diminishes with repeated testing.

Once the wire had been “cooked” it was calibrated according to the same TRT method used in previous tests. The various calibration curves can be seen as follows in Figure 59 line. Multiple tests of the zirconium wire indicated that the accurate TRT calibration would be best achieved by using a quadratic fit to the calibration data collected. In addition, the zirconium resistance calibration, shown in Figure 59 showed a spurious drop in resistance between performed tests at 100 °C. This drop is accounted for by a correction performed in the temperature calculation of this test case. The change in resistance was shown to go away after the heating calibration resumed.

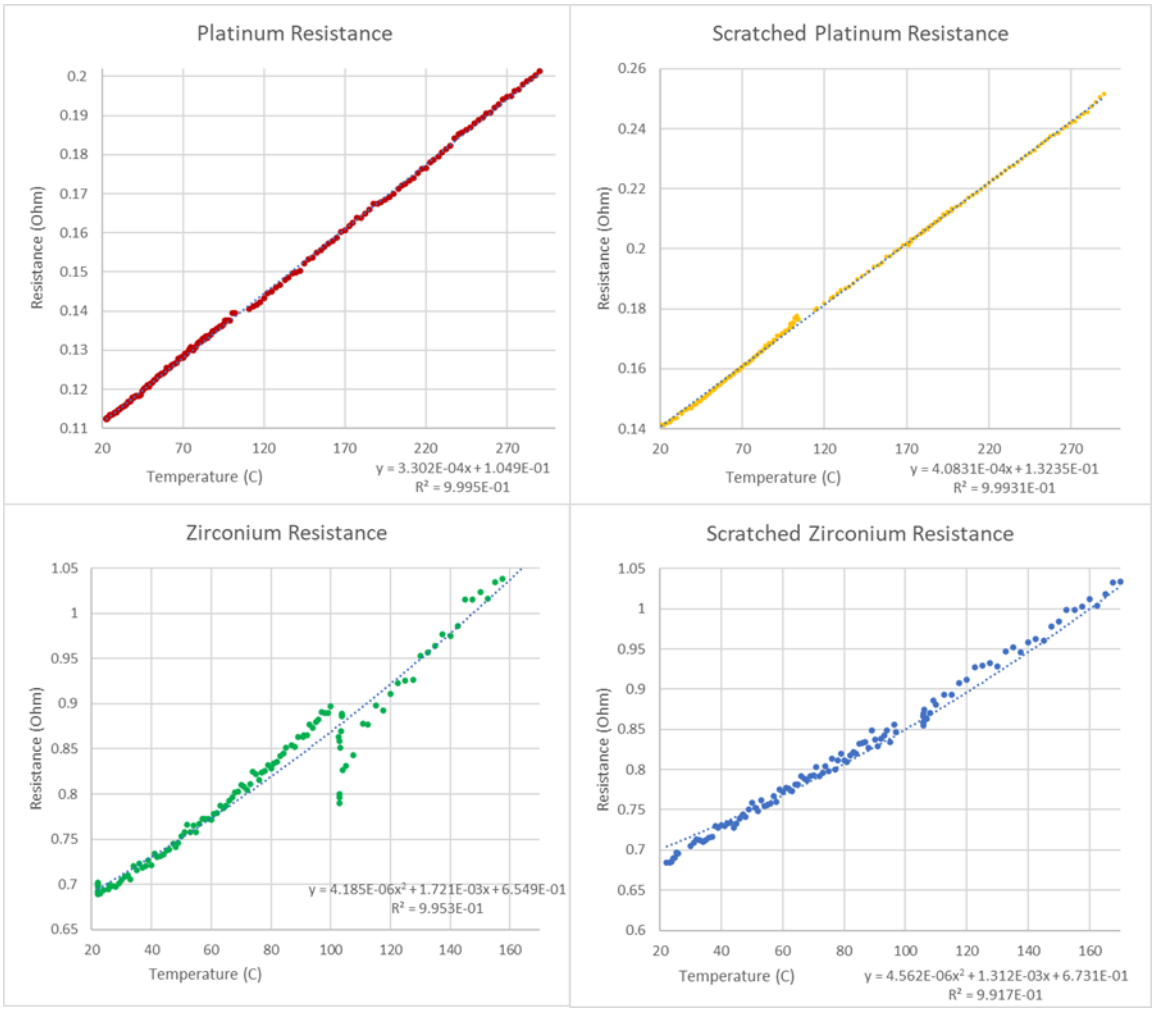

Figure 59: Calibration curves for the 4 wires are shown.

9.3 Test Scope and Parameters

The experimental procedures of this work again match the previous work. The baseline platinum comparison for these tests comes from the results of chapter 7. In order to effectively assess the tests that are performed, two testing groups are made. The test parameters of these groups are presented in Tables 12 and 13.

Table 12: Test parameters for tests with elevated pressure wire are presented.

PARAMETER	LOW VALUE	HIGH VALUE
WATER SUBCOOLING	0°C Subcooled	50°C Subcooled
PRESSURE	Low Pressure σ(1 Bar)	High Pressure σ(150 Bar)
POWER PULSE HEIGHT	5 V (floating current)	8 V (floating current)
MATERIAL	Platinum	
SURFACE CONDITION	Smooth, Drawn Wire	Scratched Wire

Table 13: Test parameters for platinum wire are presented.

PARAMETER	LOW VALUE	HIGH VALUE
WATER SUBCOOLING	0°C Subcooled	50°C Subcooled
PRESSURE	Low Pressure σ(1 Bar)	
POWER PULSE HEIGHT	5 V (floating current)	8 V (floating current)
MATERIAL	Platinum	Zirconium
SURFACE CONDITION	Smooth, Drawn Wire	Scratched Wire

It should be noted that the nomenclature of a “low value” and “high value” are maintained even in the case of material and surface. Though this has little direct significance, the distinction will be of importance in the 2^k factorial study as the prescribed valuations will be employed for such comparison.

9.4 Results

As in previous chapters, the data is presented initially with minimal discussion. Full discussion will occur after the data is presented.

9.4.1 **Heat Transfer and Temperature**

9.4.1.1 Scratched Platinum

The temperature, heat transfer and HTC data for scratched platinum wire are shown in Figures 60 – 64. The general trends shown by these tests align with the trends seen for platinum in Chapter 7.

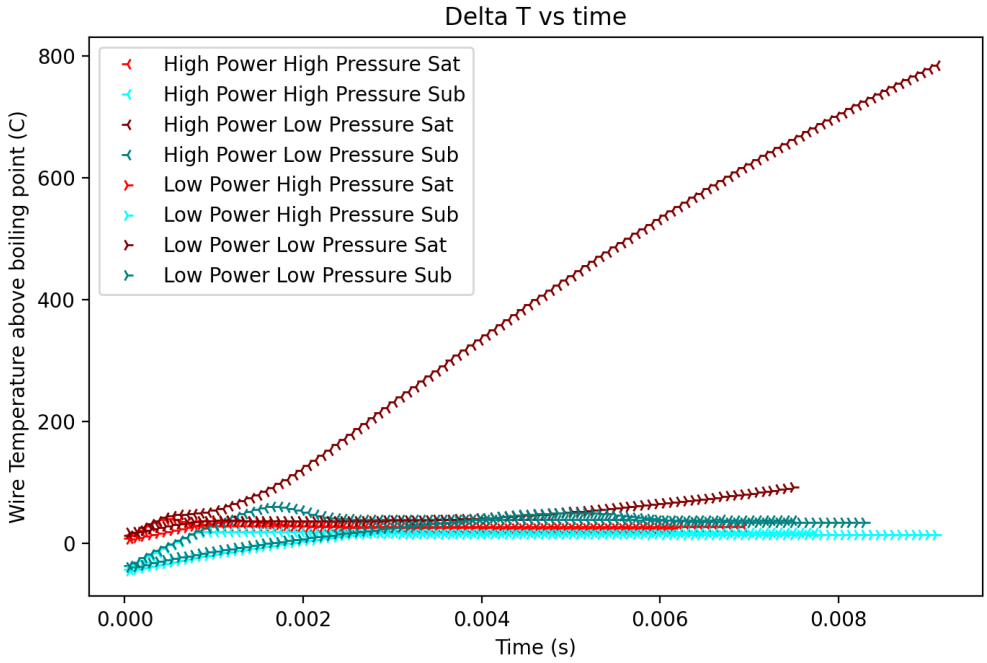

Figure 60: The scratched platinum temperature vs time is shown.

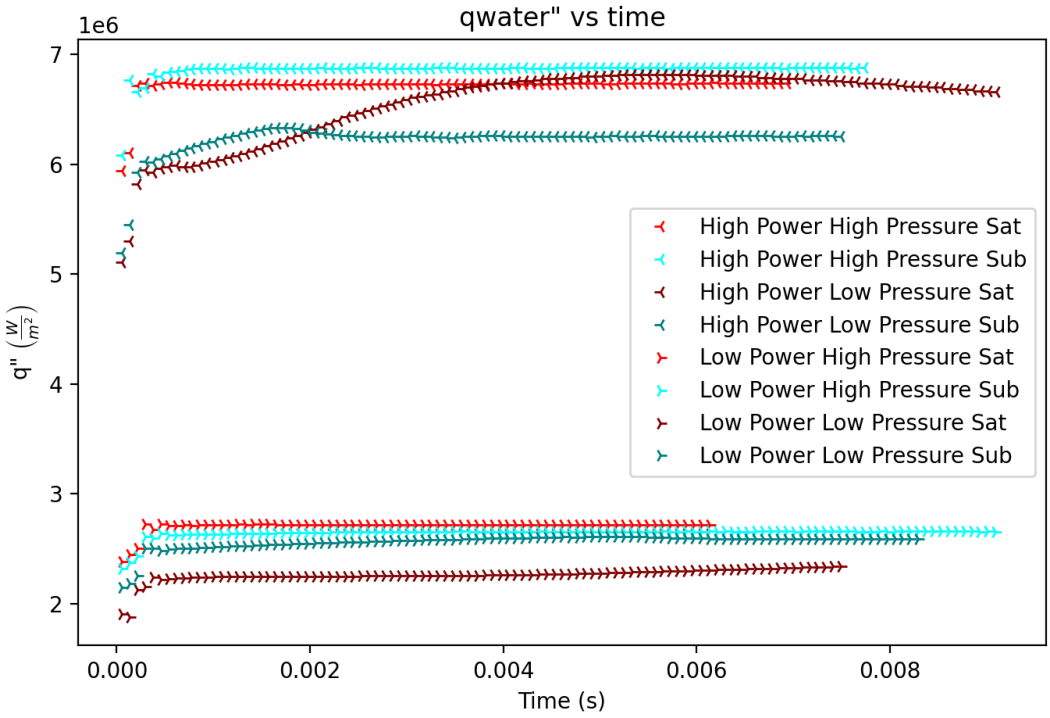

Figure 61: The scratched platinum heat transfer vs time is shown.

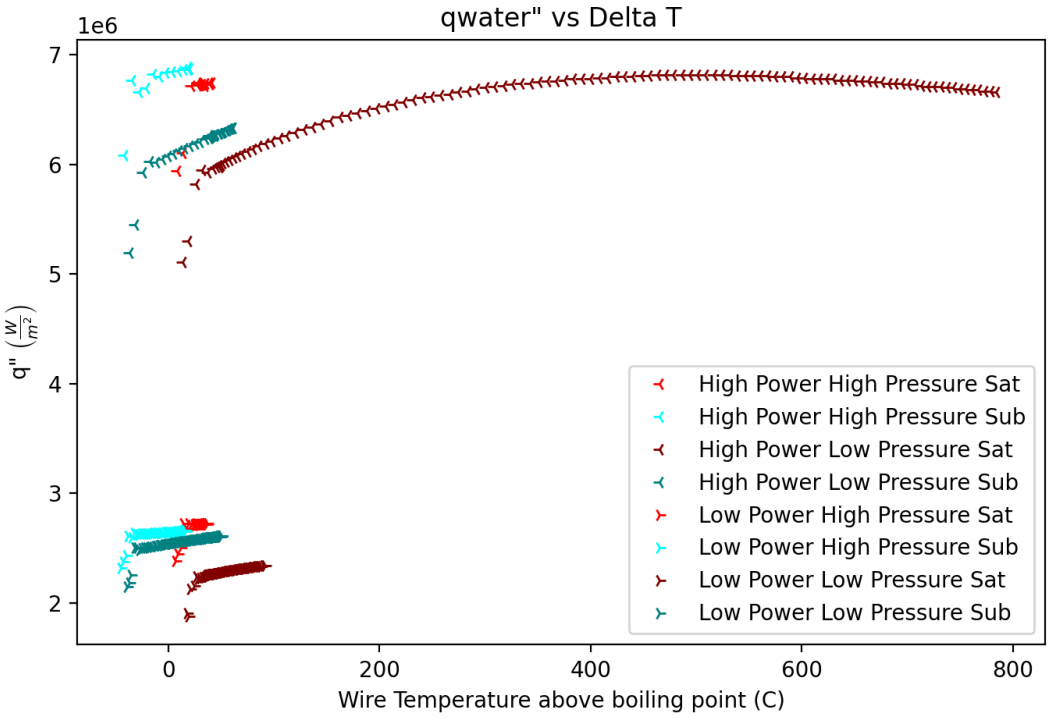

Figure 62: The scratched platinum heat transfer vs temperature is shown.

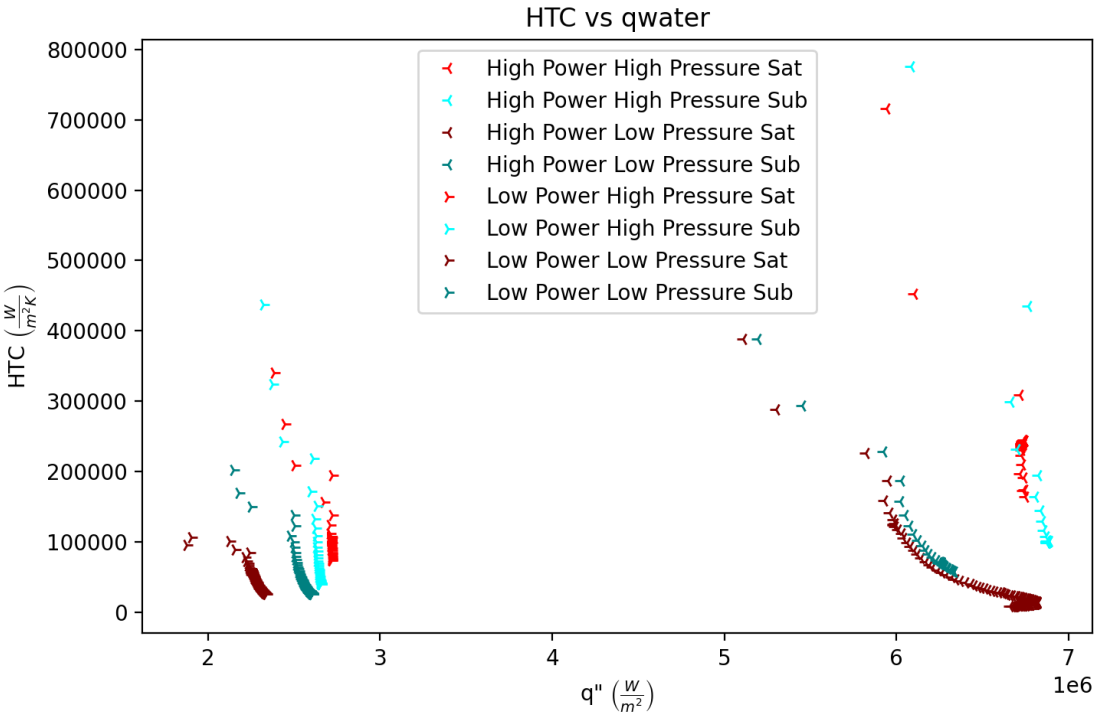

Figure 63: The scratched platinum HTC vs heat transfer is shown.

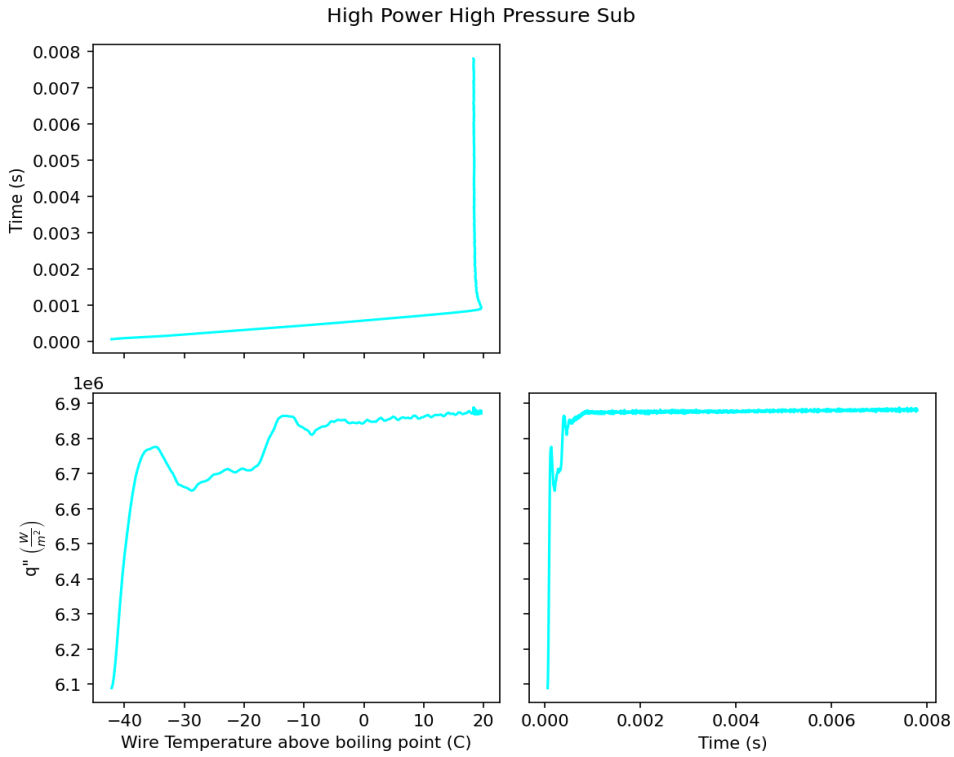

Figure 64: The comparative values for temperature, heat transfer, and time for the case under PWR conditions is presented.

9.4.1.2 Zirconium (commercial, as drawn)

The temperature, heat transfer and HTC figures are seen below for smooth Zirconium in Figures 65-69. The selected figure for representative data, seen as the final figure in each graph seen throughout this work, cannot be the PWR conditions for the Zirconium cases as the high-pressure test is not performed. The High-powered, low pressure subcooled case is shown instead.

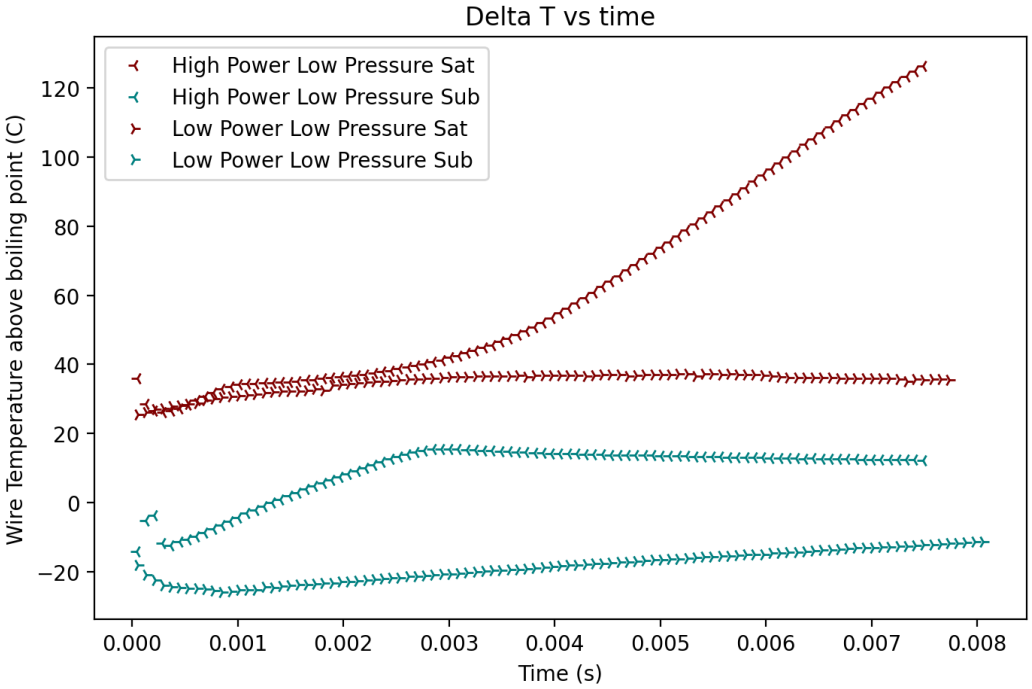

Figure 65: The smooth (drawn) zirconium temperature vs time is shown.

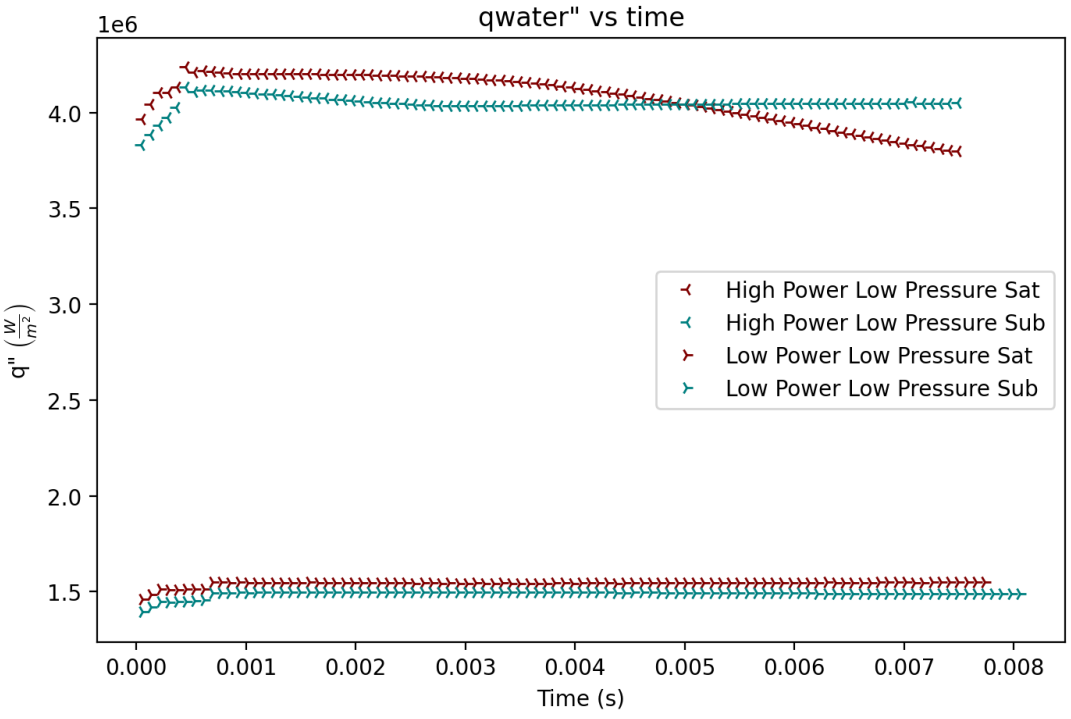

Figure 66: The smooth (drawn) zirconium heat transfer vs time is shown.

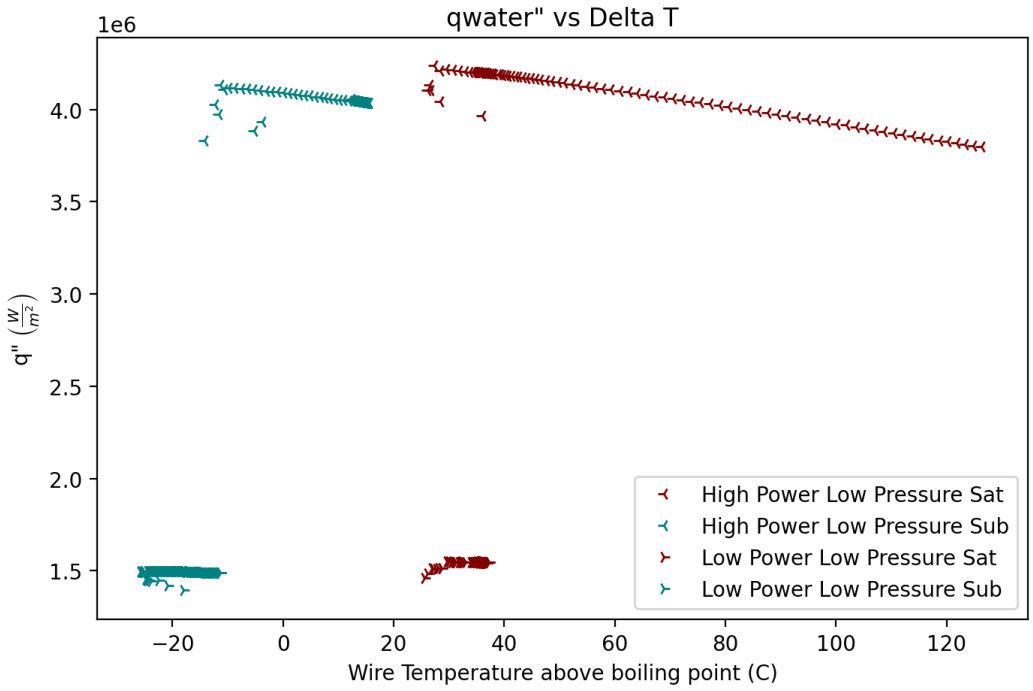

Figure 67: The smooth (drawn) zirconium heat transfer vs temperature is shown.

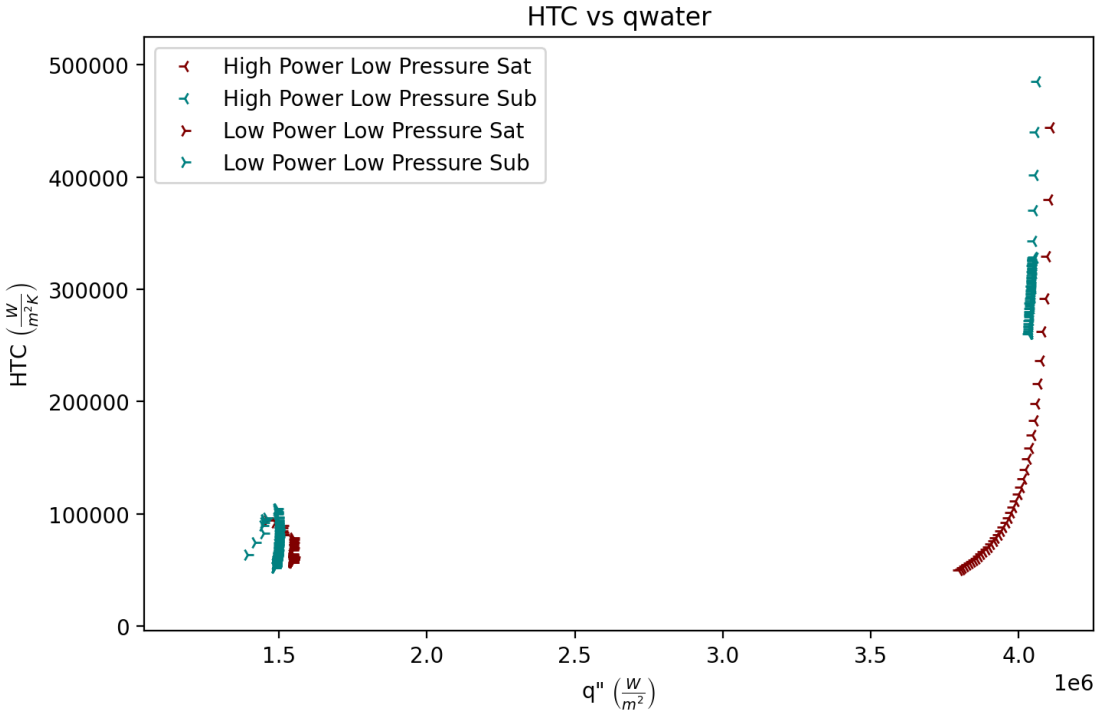

Figure 68: The smooth (drawn) zirconium HTC vs heat transfer is shown.

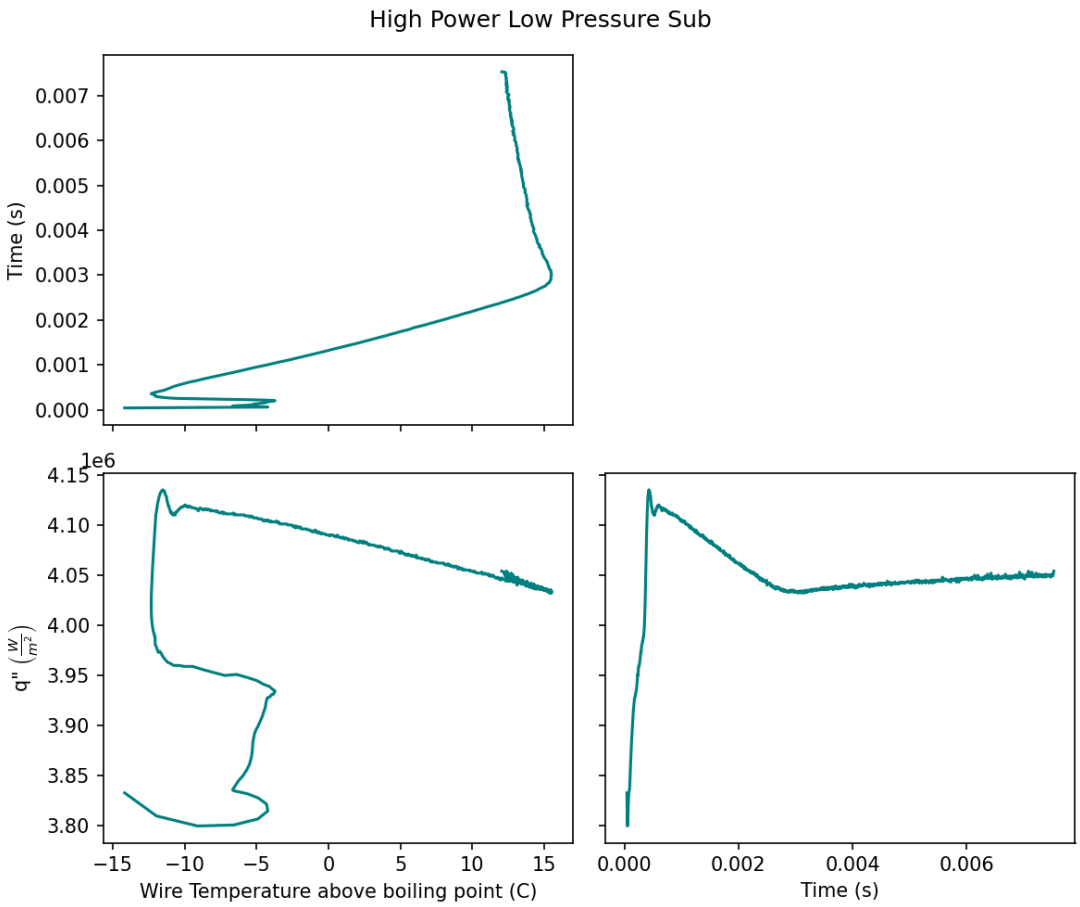

Figure 69: A representative test for the smooth (drawn) zirconium heat transfer, temperature, and time variables is presented.

9.4.1.3 Scratched Zirconium

Finally, the temperature, heat transfer and HTC figures are seen below for scratched Zirconium in Figures 70-74. As in the smooth Zirconium, the selected figure for representative data, seen as the final figure in each graph seen throughout this work, cannot be the PWR conditions for the Zirconium cases as the high-pressure test is not performed. The high-powered, low pressure subcooled case is shown instead.

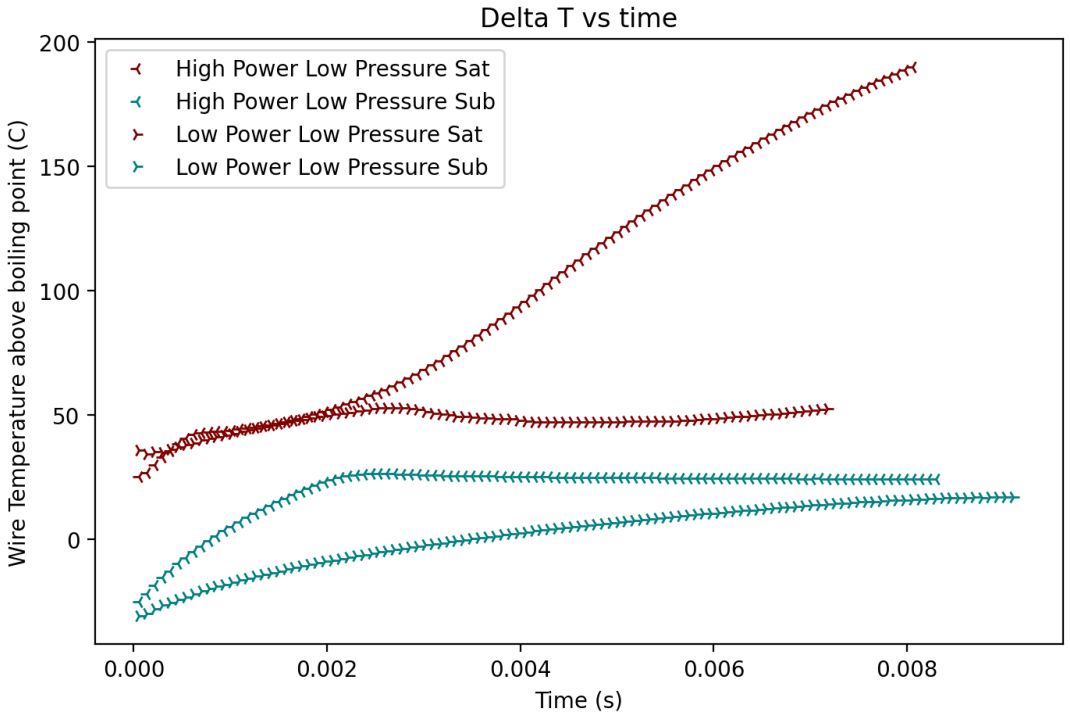

Figure 70: The scratched zirconium temperature vs time is shown.

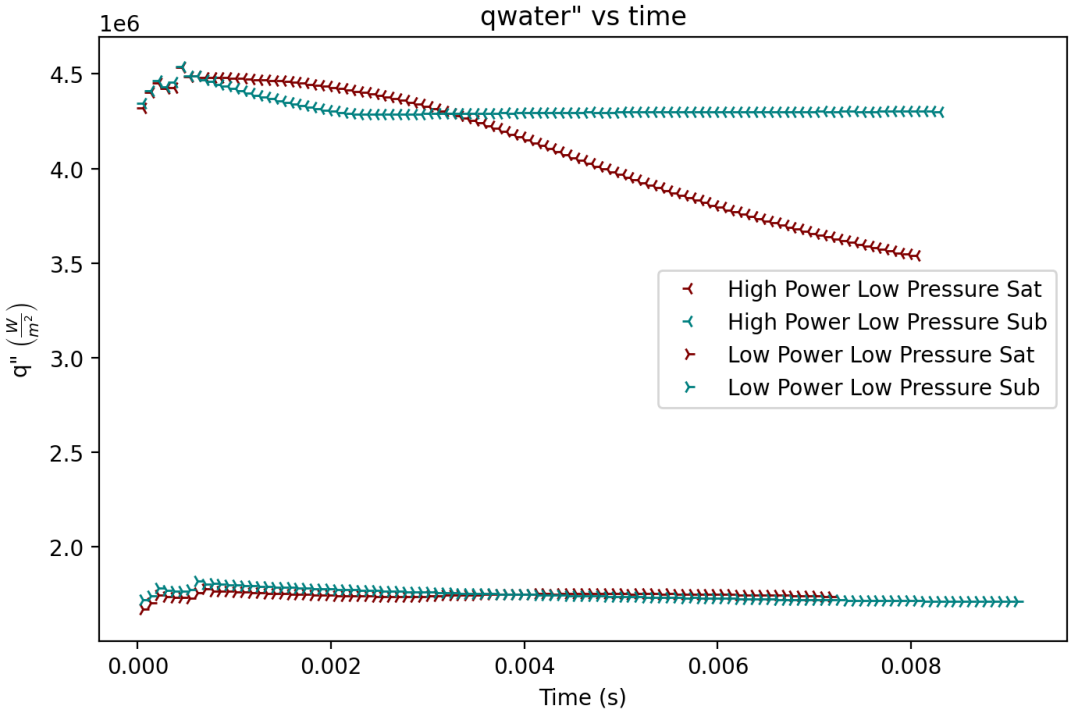

Figure 71: The scratched zirconium heat transfer vs time is shown.

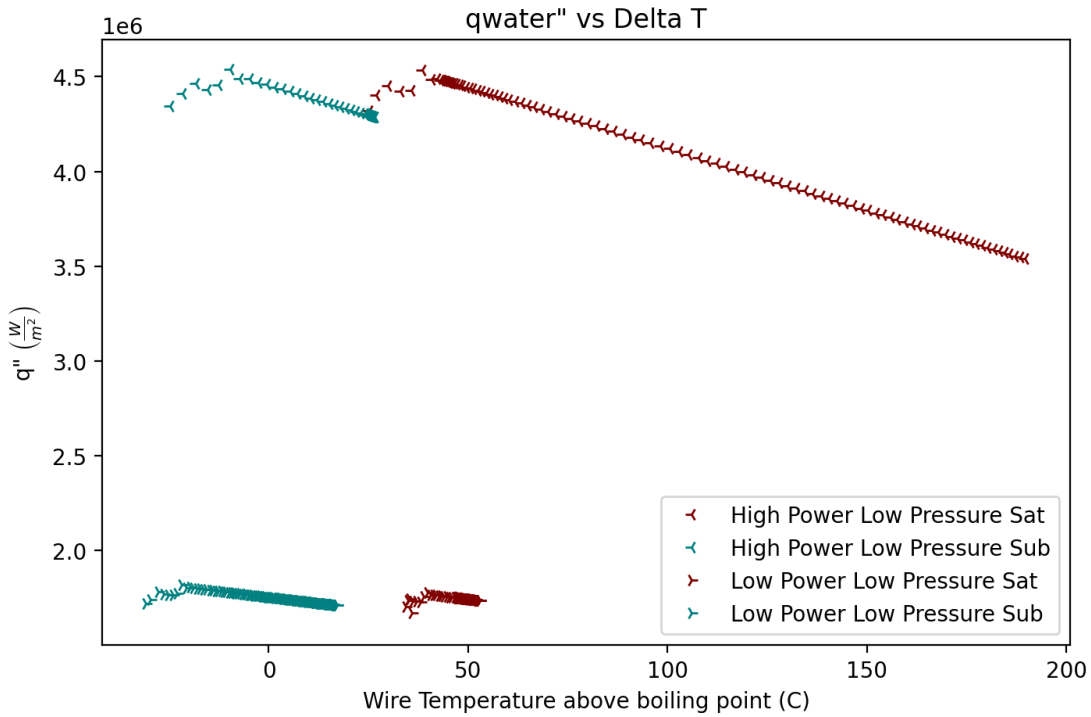

Figure 72: The scratched zirconium heat transfer vs temperature is shown.

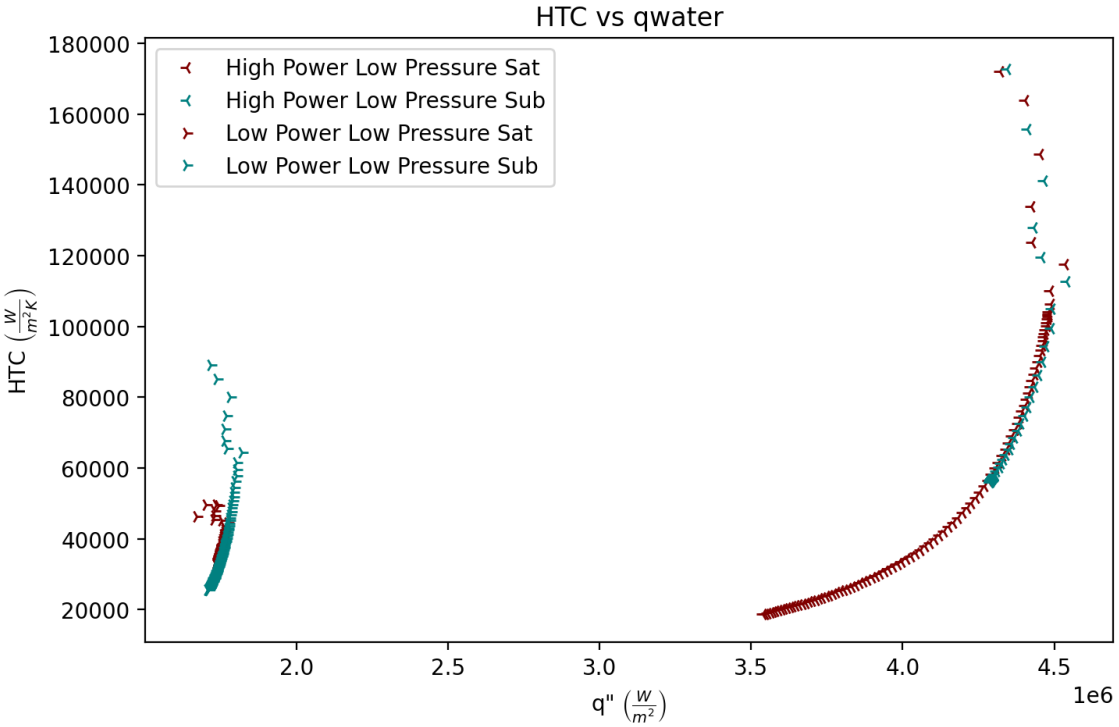

Figure 73: The scratched zirconium HTC vs heat transfer is shown.

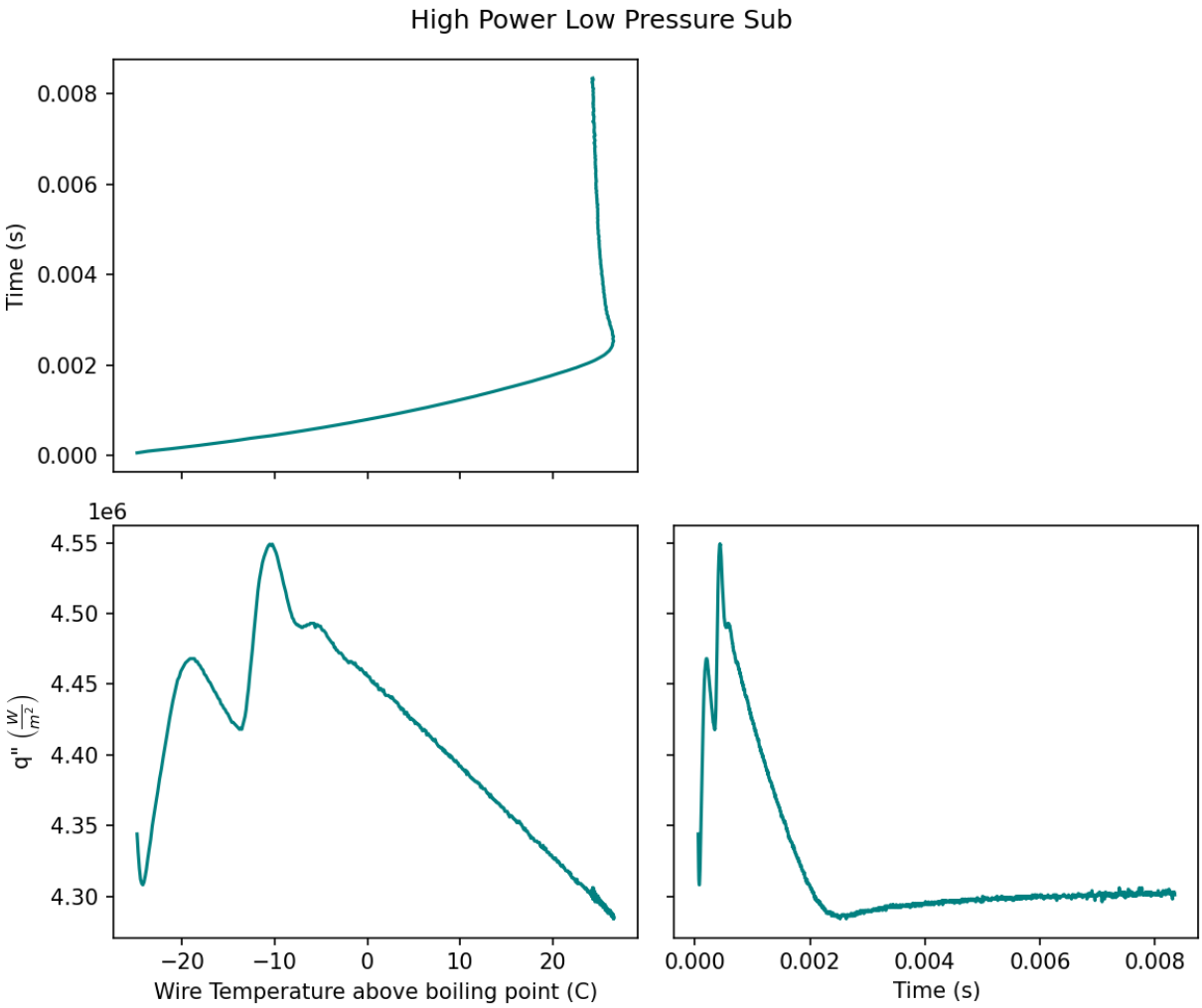

Figure 74: The scratched zirconium representative test is shown.

9.4.2 **Boiling Behavior and Regime**

The scratched platinum will follow the same presentation as previous chapters, meaning the high-powered tests will be presented. In the zirconium tests, the four low pressure tests are presented for comparison.

9.4.2.1 Scratched Platinum

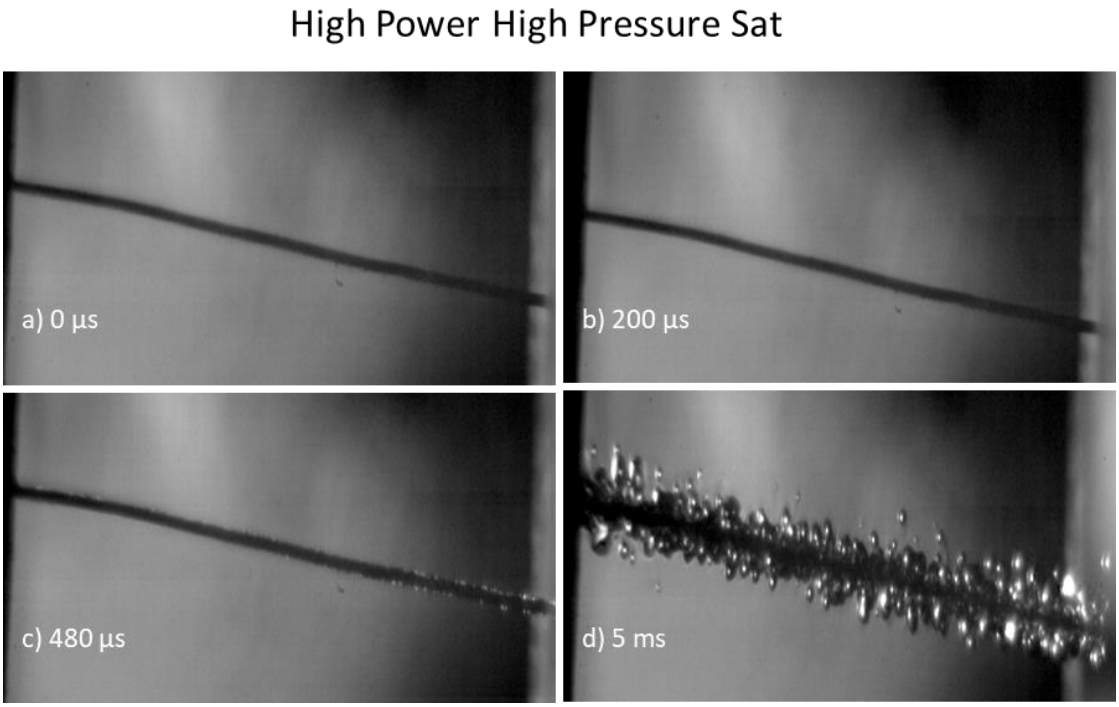

Figure 75: Boiling images for the high power, high pressure, saturated case on scratched platinum wire.

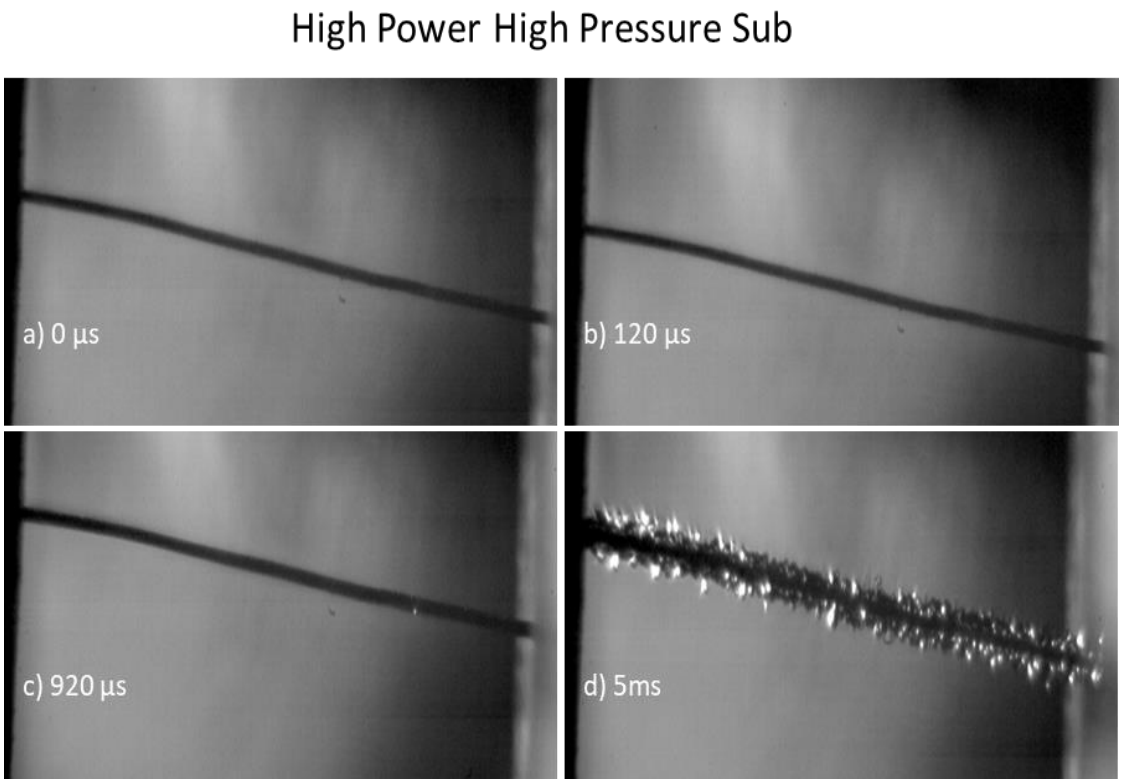

Figure 76: Boiling images for the high power, high pressure, subcooled case on scratched platinum wire.

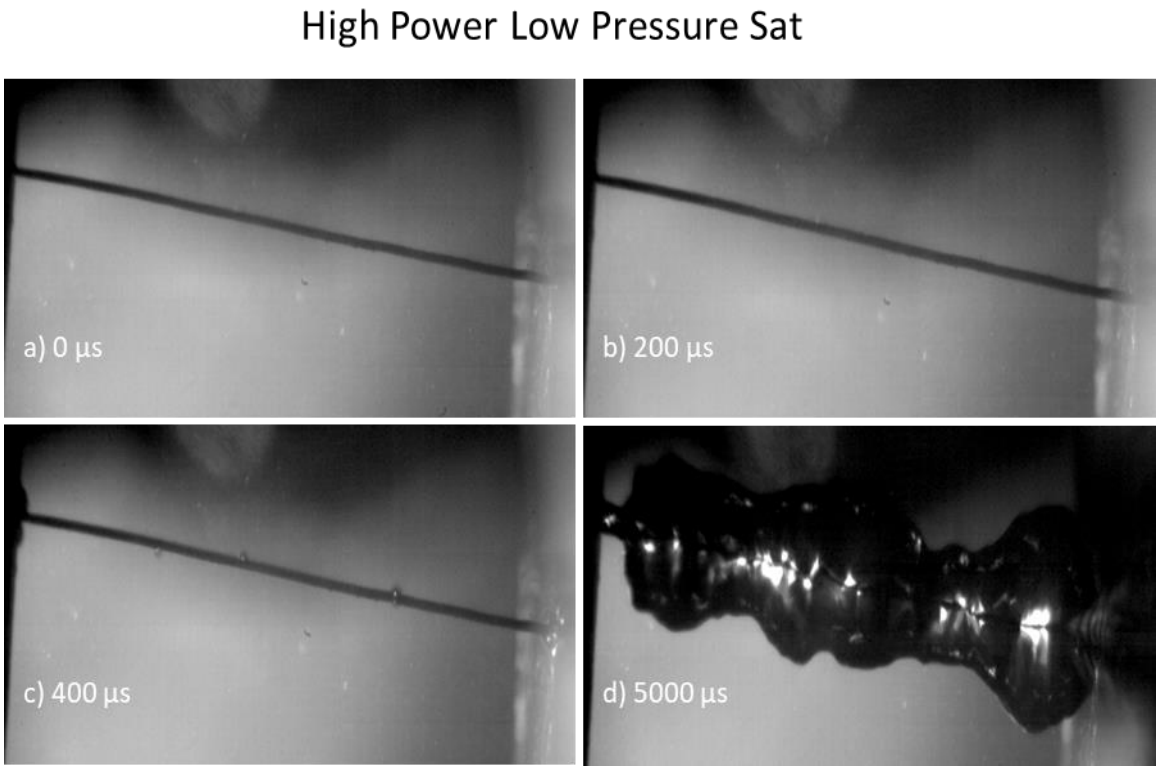

Figure 77: Boiling images for the high power, low pressure, saturated case on scratched platinum wire.

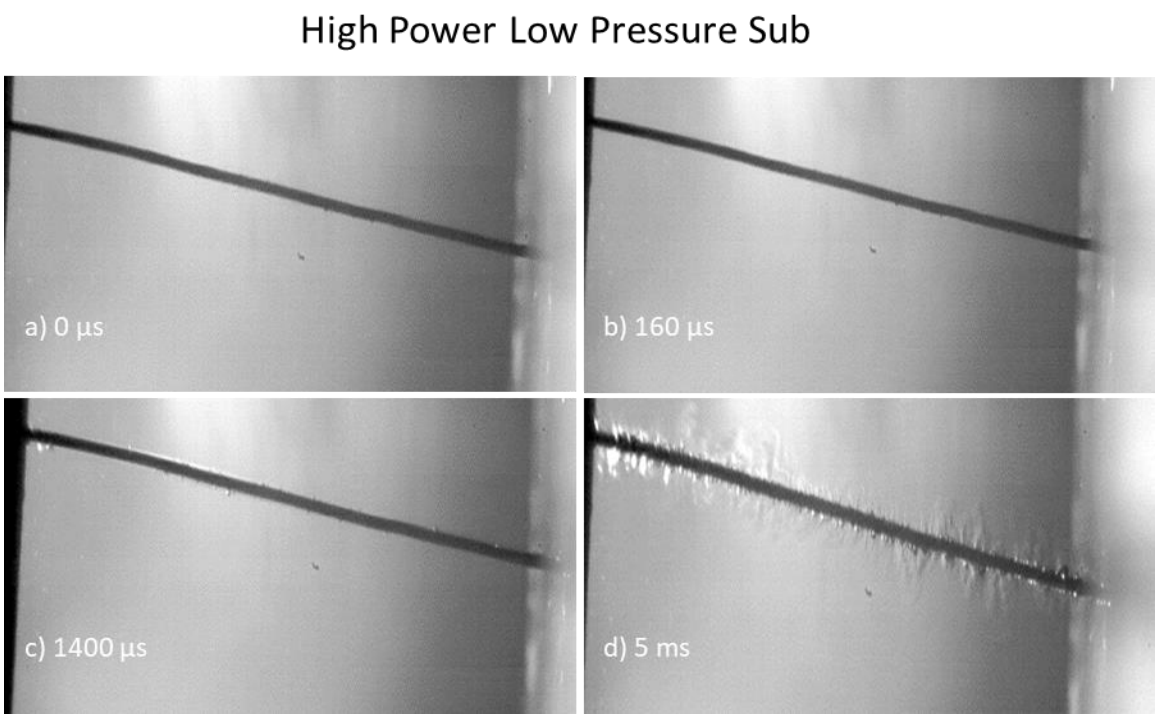

Figure 78: Boiling images for the high power, low pressure, subcooled case on scratched platinum wire.

9.4.2.2 Zirconium (commercial, as drawn)

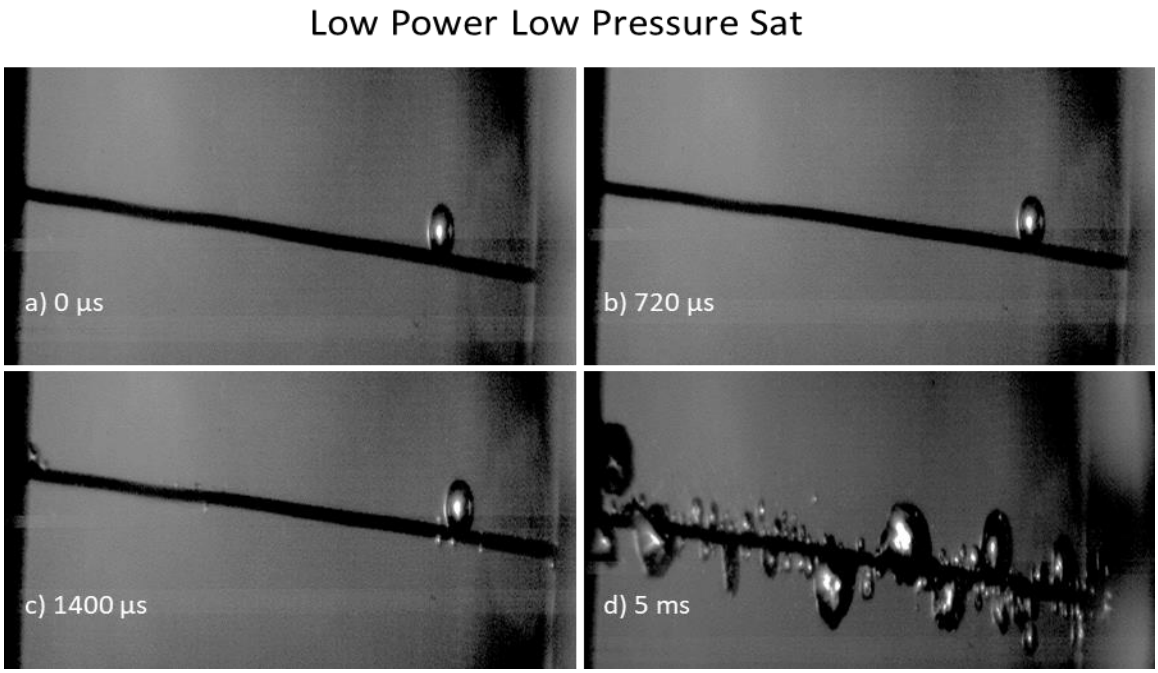

Figure 79: Boiling images for the low power, low pressure, saturated case on smooth (drawn) zirconium wire.

Figure 80: Boiling images for the low power, low pressure, subcooled case on smooth (drawn) zirconium wire.

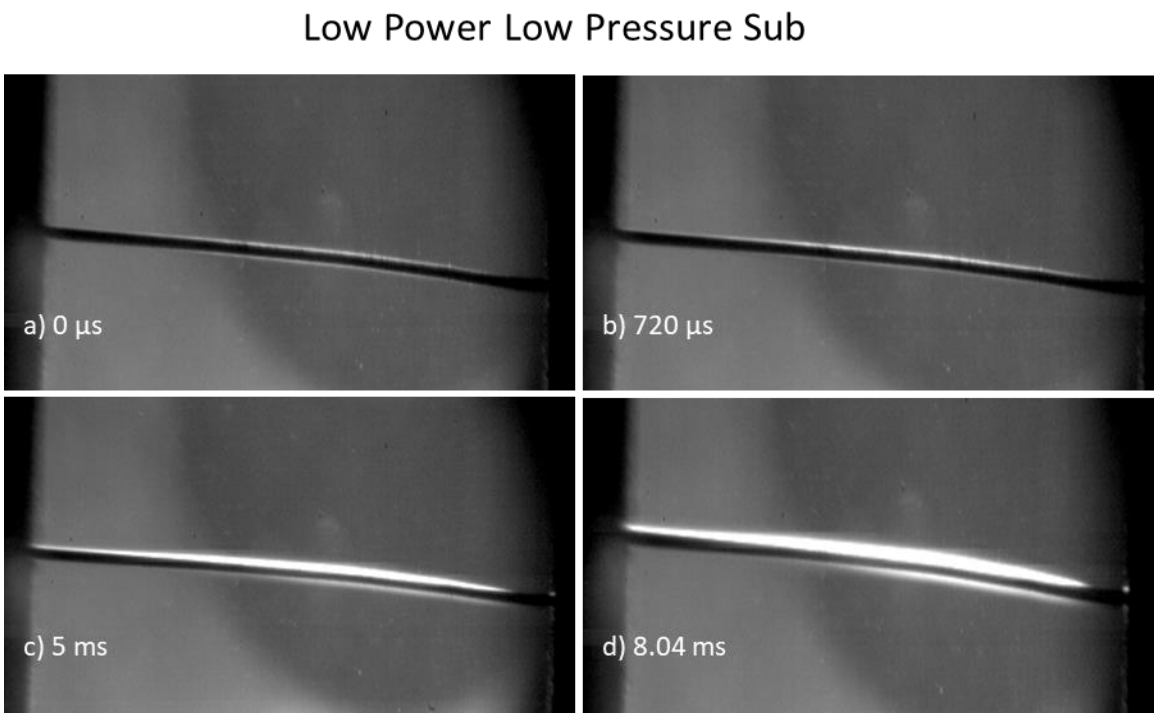

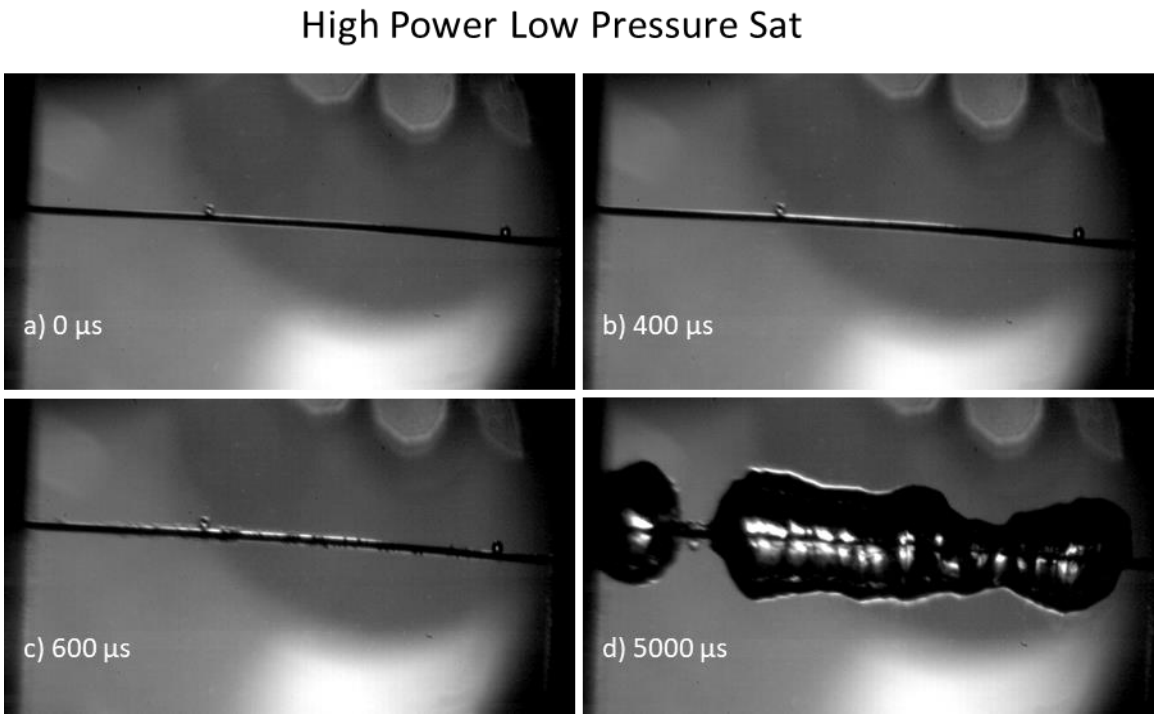

Figure 81: Boiling images for the high power, low pressure, saturated case on smooth (drawn) zirconium wire.

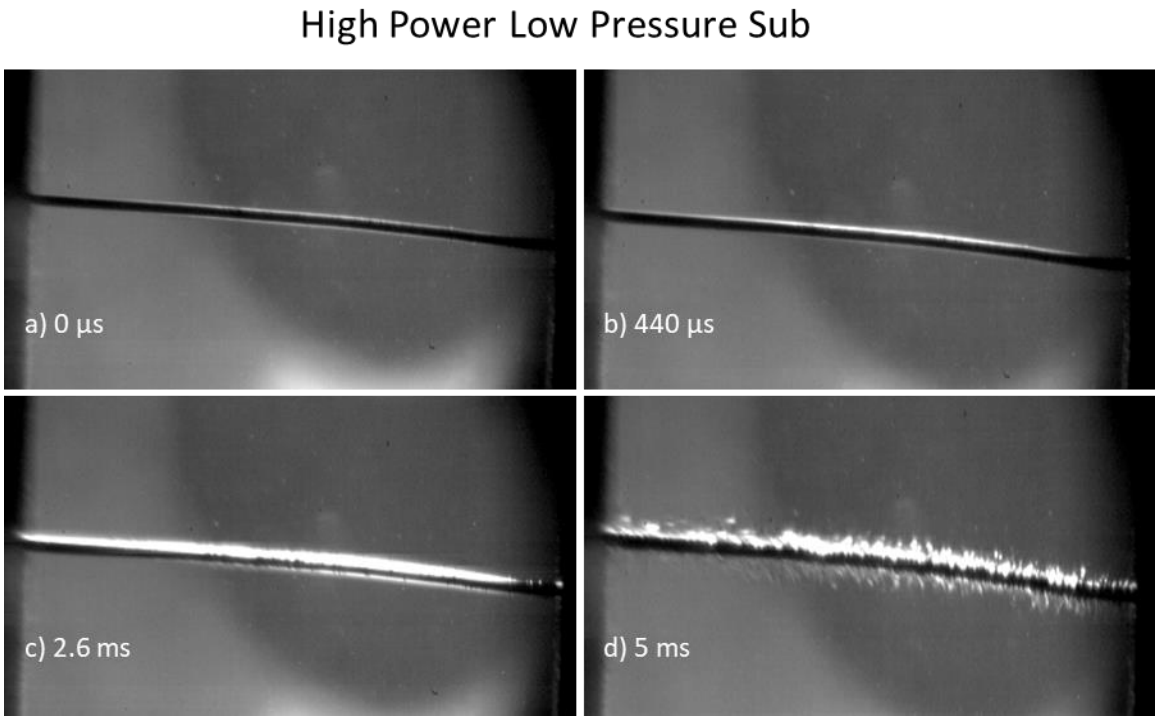

Figure 82: Boiling images for the high power, low pressure, subcooled case on smooth (drawn) zirconium wire.

9.4.2.3 Scratched Zirconium

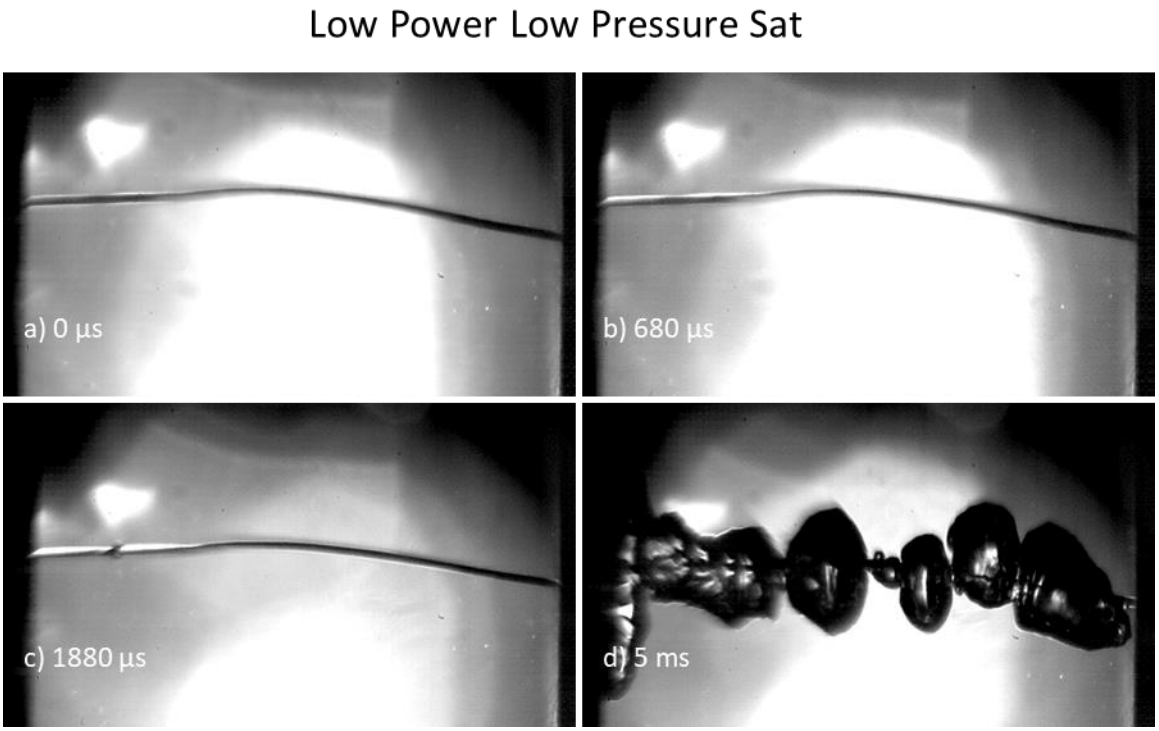

Figure 83: Boiling images for the low power, low pressure, saturated case on scratched zirconium wire.

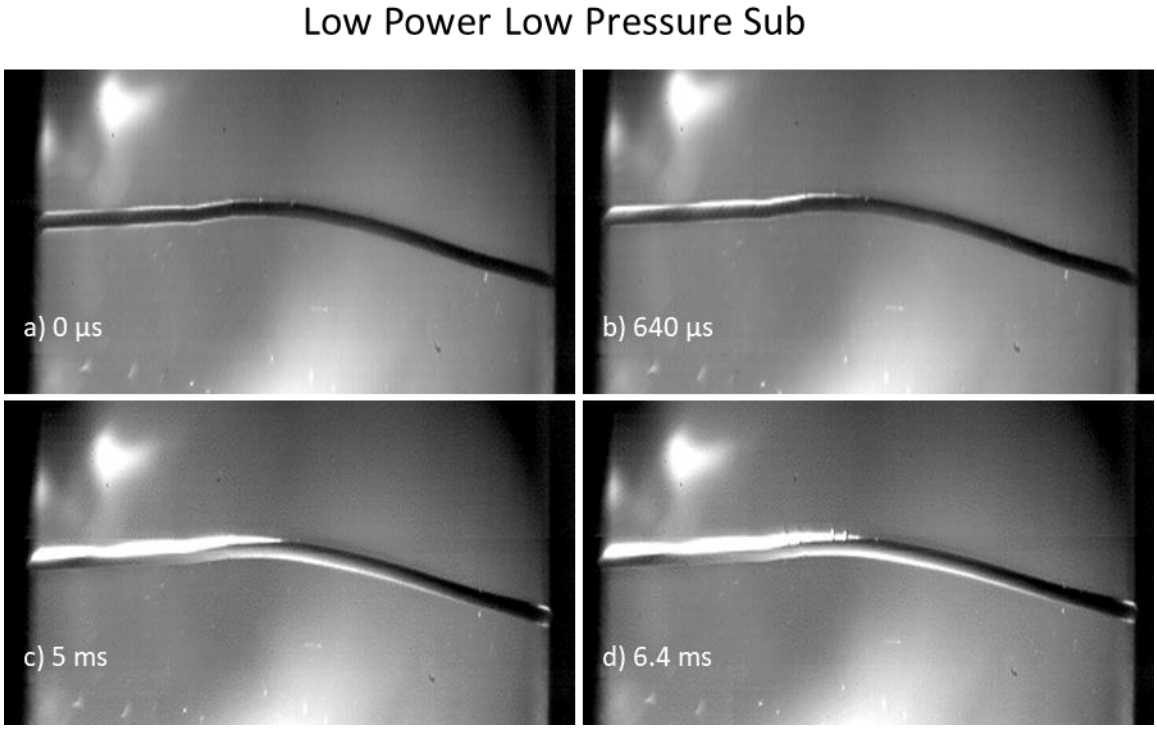

Figure 84: Boiling images for the low power, low pressure, subcooled case on scratched zirconium wire.

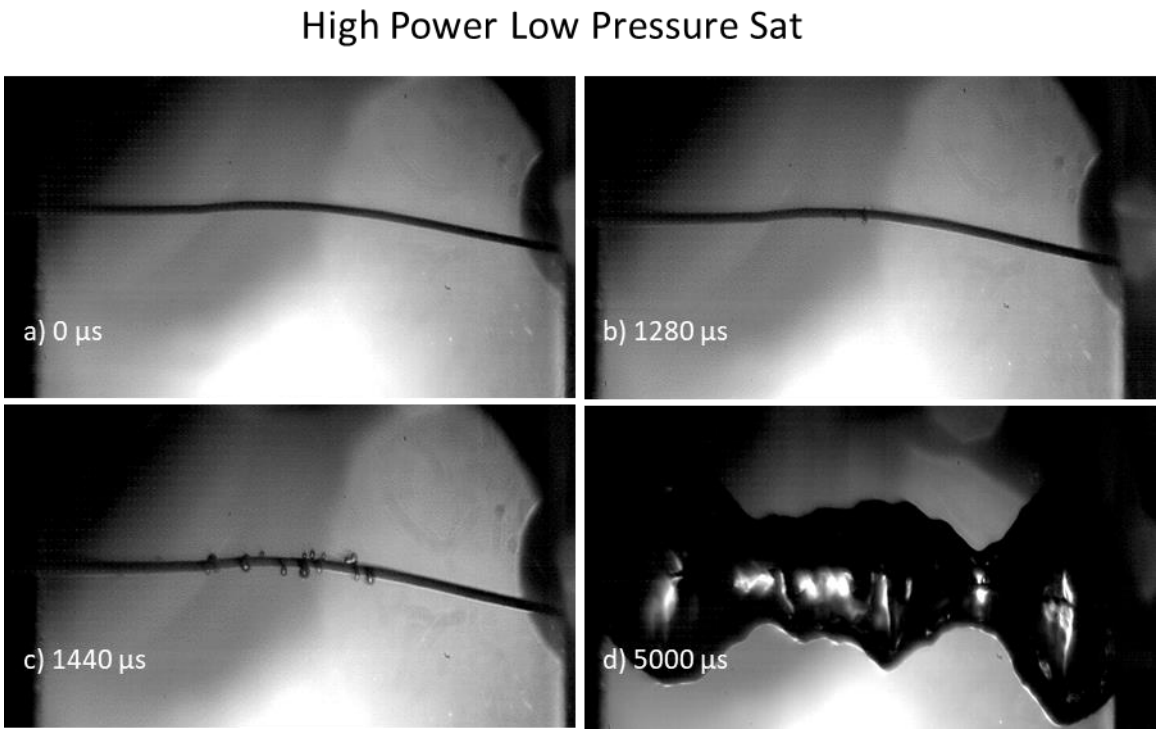

Figure 85: Boiling images for the high power, low pressure, saturated case on scratched zirconium wire.

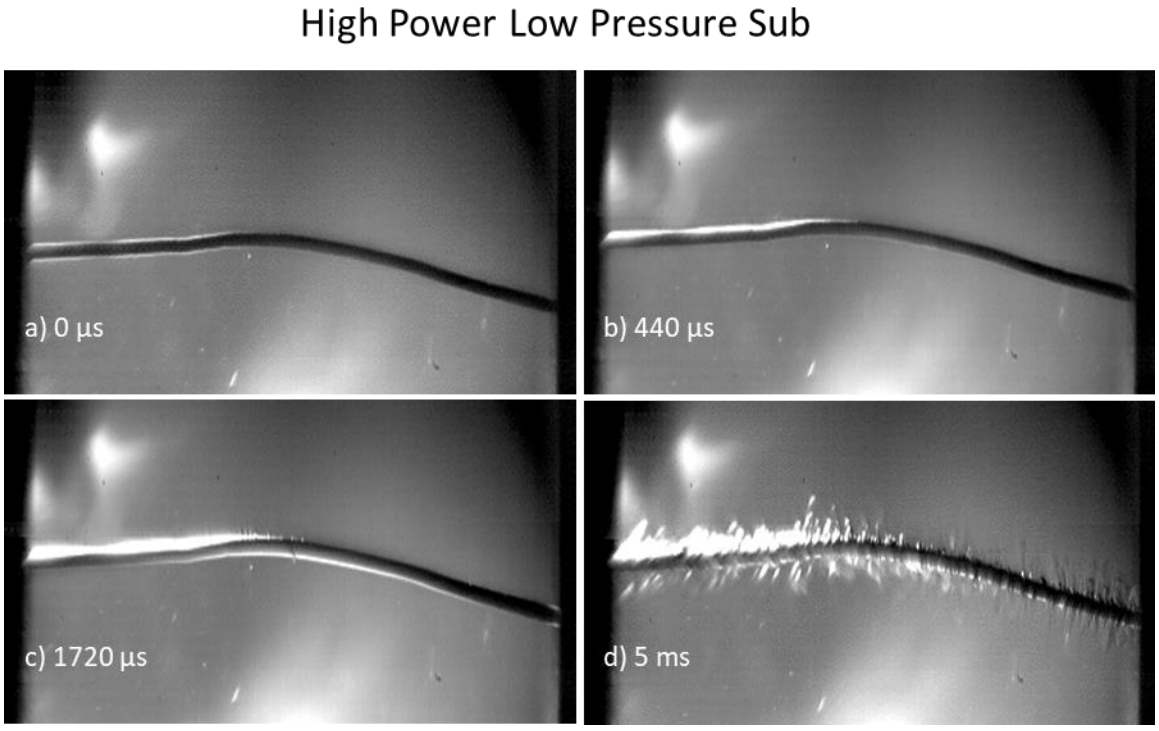

Figure 86: Boiling images for the high power, low pressure, subcooled case on scratched zirconium wire.

9.4.3 2^k Factorial Comparison

Two separate studies were performed according to the configurations outlined in Tables 12 and 13. The full factor tests performed on additional output variables are presented in Appendix E.

9.4.3.1 2^k Factorial Study on Scratched/Smooth Platinum

Table 14: A 2k factorial study was performed between the scratched and smooth platinum wires over the full range of temperatures, pressures, and pusle heights.

	Max Temp	Q Max	h Max
Subcooling (A)	-178.8	-6.34E+04	2.80E+05
Pressure (B)	-204.0	1.41E+05	1.68E+06
Pulse Height (C)	148.0	4.75E+06	2.76E+05
Roughness (D)	10.7	-1.29E+06	-4.61E+05
AB	154.2	1.91E+05	3.05E+05
AC	-134.3	-1.57E+05	-7.49E+05
AD	-24.1	1.44E+04	-2.33E+05
BC	-143.7	-7.79E+04	-2.00E+05
BD	-15.6	1.00E+05	-2.73E+05
CD	30.4	-6.40E+05	4.10E+05
ABC	133.5	2.60E+05	-5.94E+05
ABD	27.8	-1.31E+05	-1.83E+05
ACD	-37.4	2.36E+04	8.69E+05
BCD	-31.2	8.39E+04	4.80E+05
ABCD	37.8	-1.64E+04	8.87E+05

9.4.3.2 2^k Factorial Study on Low Pressure Scratched/Smooth Zirconium and Platinum

Table 15: A 2k factorial study was performed between the scratched and smooth platinum wires over the full range of temperatures, pressures, and pusle heights.

	Max Temp	Q Max	h Max
Subcooling (A)	-211.4	-1.41E+05	-4.40E+06
Pulse Height (B)	178.7	3.77E+06	3.02E+07
Roughness (C)	27.9	-5.37E+05	-3.00E+07
Material (D)	-178.1	-2.21E+06	2.96E+07
AB	-157.7	-2.19E+05	-4.48E+06
AC	-30.9	9.98E+04	4.39E+06
AD	121.6	1.14E+05	-4.38E+06
BC	34.5	-3.41E+05	-3.00E+07
BD	-113.0	-1.06E+06	2.97E+07
CD	1.6	8.49E+05	-2.98E+07
ABC	-45.6	2.33E+04	4.39E+06
ABD	110.0	1.98E+05	-4.33E+06
ACD	21.1	-4.53E+04	4.44E+06
BCD	-27.1	3.82E+05	-2.99E+07
ABCD	29.5	-1.68E+04	4.40E+06

9.5 Conclusion and Discussion

As was seen in the results of Chapters 7 and 8 of this work, the largest gains in the maximum heat transfer came from the power pulse height. This also led to an increase in the maximum wire temperature, as seen previously. This reiterates the consistent findings of this work, that pool boiling under ultra-fast power transients are critically, and inseparably, connected to the pulse power behavior, both height and shape.

It can be seen that the roughened wire surface led to a modest increase in maximum wire temperature and a decrease in the maximum heat transfer value, with the zirconium offering a

slightly muter reduction in heat transfer. The initial hypothesis for these experiments was that the roughened surface would lead to quick bubble nucleation and a smaller holding surface for the bubble leading to more efficient bubble lift-off from the wire. This hypothesis, however, can be seen to be incorrect. In the case of the full temperature-pressure range platinum tests, the wire roughness was seen to be the single largest negative factor on maximum heat transfer. While the images of the boiling regime do indicate that bubbles form more readily on the roughened surface, the bubbles do not more readily depart the surface. Instead, they serve to insulate the wire as is seen in classical boiling experiments. Thus, the roughened surface does facilitate bubble generation, but at the cost of a decrease in the heat transfer.

It is noteworthy to state that the wire material did play a large role in the maximum heat that was transferred. The zirconium performed less well in its ability to transfer heat than the platinum. In every case, when viewed side by side, the bubbles around the zirconium wire were smaller and closer to the wire than those of the analogous platinum case. Deeper analysis of this result, included in Appendix E found that the driving mechanism for this change was the zirconium produced a lower power heating pulse from the same voltage pulse. This shows that the material change was driving a pulse height effect.

9.5.1 **Discussion**

Change in the pulse height was once again a dominant factor in temperature and heat transfer response. In addition, both the change in wire finish and the change of material impacted various facets of fast-transient pool boiling, most notably by reducing the maximum heat transfer value. Observation of the bubble images indicate that the zirconium, in general, tended to produce

a larger quantity of bubbles in each configuration as compared with the platinum. Once again, the non-standard bubbles dynamics, lack of lift off, and quasi-steady state behavior described in Chapter, 6, 7 and 8 are observed. The boiling behavior does not match classical theory.

9.5.2 **Summary**

In summary, transient boiling experiments were performed on platinum and zirconium wires, both smooth (drawn) and roughened, and with a variety of other experimental parameters. Temperature, heat transfer data, and high-speed images were collected, as has been done throughout this work. Similar to previous results, the heating pulse height is the dominant mechanism driving the heat transfer behavior. The increase in surface roughness led to bubble nucleation and retention, increasing the wire temperature and decreasing heat transfer. An effect is seen in the change of wire material, but the results are limited to low pressure for the zirconium wire. Ultra-fast boiling dynamics and the noted quasi-steady state are again seen to occur.

10.0 General Conclusions and Perspectives

In summary, a transient boiling system was created to study the ultra-fast heating, pool boiling heat transfer under elevated pressure and subcooling (analogous conditions to operating nuclear PWRs). This was achieved through Joule heating of a thin wire of which the resistance was calculated by measuring the current and voltage drop across the wire. The system was operated to conduct experiments studying wire failure mechanisms and transient boiling behavior changes in response to numerous parameters. These parameters are combinations of pressures and subcooling levels, the wire material, the heating shape, including heating from a baseline, non-zero heating, the heating level, and the wire surface condition. Temperature and heat transfer information was derived from the voltage and current data and coupled with high-speed imagery to elucidate the various behaviors of transient boiling. Several 2^k factorial design of experiment analyses were performed on the data to highlight trends and parameter sensitivities. Complete sets of all this information are found in Appendix E.

A case was made for the material failure by explosive vaporization of the wire (Chapter 6). The trends across the experiments consistently indicate the critical importance of power shape and heating level in the resultant transient behavior (Chapters 7-9). DNB played a large factor in runaway heating (Chapters 7-9). Roughened surfaces led to increased bubble production and retention, lowering heat transfer, and increasing wire temperature (Chapter 9). The wire material impacted the overall heat transfer, but results are limited to low pressure test cases (Chapter 9).

The high-pressure, subcooled test condition, which is at the standard operating condition of a PWR, was found to consistently have a lower temperature, relative to the other tests, and

typically high heat transfer response to the accident-similar power pulses. The various tests under this condition are presented as a full comparison case study of this work in section 10.1.

10.1 High Pressure, Subcooled Testing

As noted throughout this work PWRs operate at approximately 150 Bar pressure (2161.1 psig) and 50 °C subcooled (292 °C). This condition is ideal for transferring heat from the nuclear reactor core to a secondary loop at lower pressure, generating high temperature steam to drive a turbine. This condition also provides a safer operating space in the case of an accident, such as a RIA, where local temperatures at locations in the core can increase. This case is being presented as semi-representative of the whole, and of particular interest due to the direct applicability in the nuclear industry.

Figure 87 presents the temperature vs pulse time for each of the high-powered cases studied in this work. The temperature behavior is seen to be experimentally very similar for the smooth and rough platinum under constant voltage heating and the power step increase case after approximately 1 ms. (Further discussion the power step increase behavior will be saved for the following section, 10.2) The major outlier in the data seen in this figure is the constant current pulse on the smooth platinum wire. This test quickly reaches elevated temperatures and continues to rise. The high-speed images collected showed DNB and the wire glows white with substantial flexing due to thermal expansion at the end of the pulse heating.

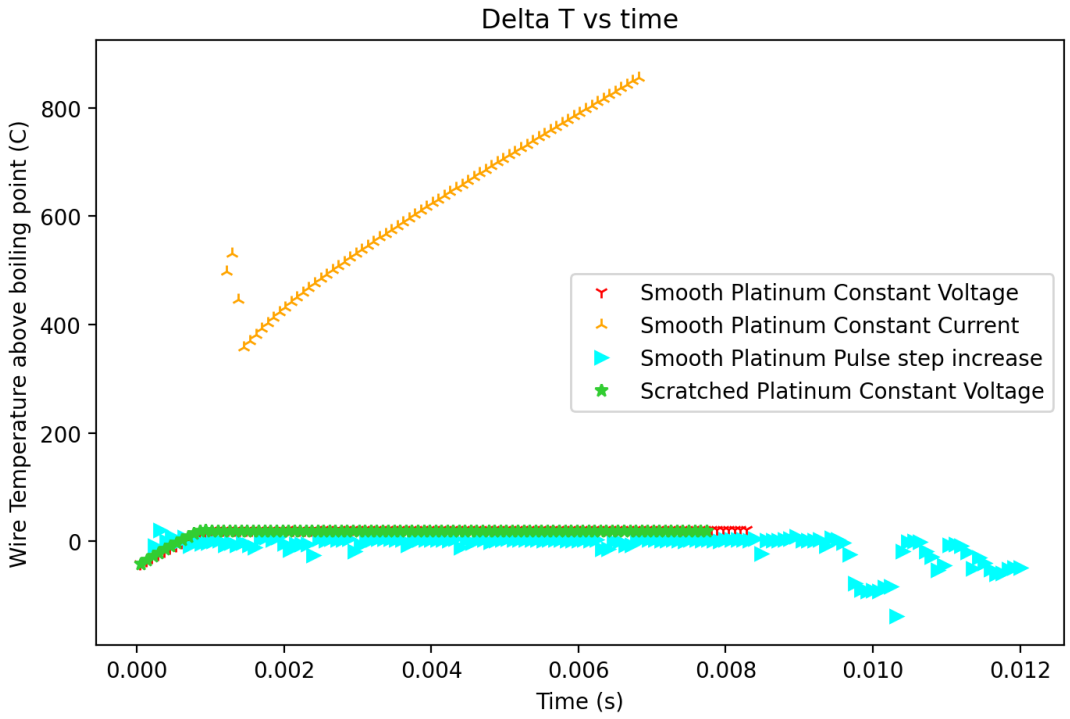

Figure 87: The temperature vs time plots for all high-powered, high-pressure, subcooled cases are presented for comparison.

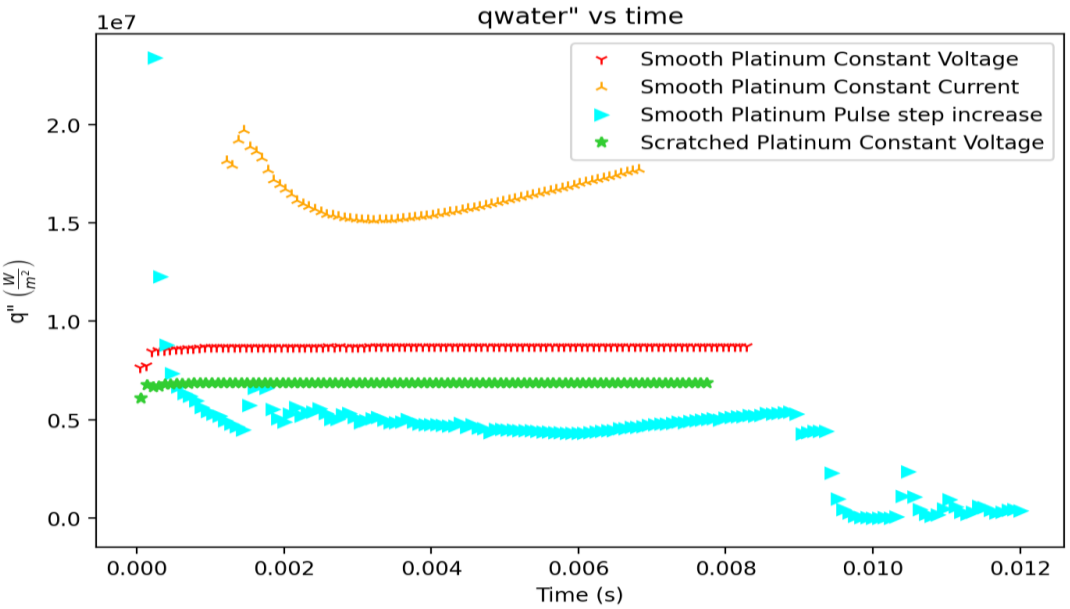

Figure 88: The heat transfer vs time plots for all high-powered, high-pressure, subcooled cases are presented for comparison.

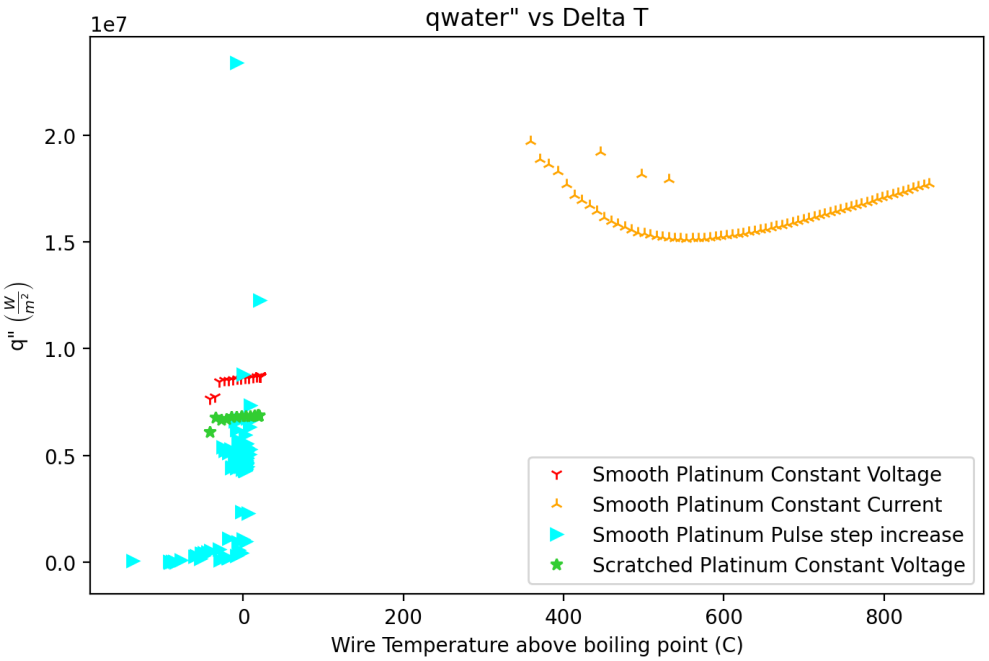

Figure 89: The heat transfer vs temperature for each case at PWR conditions is shown.

Figure 88 shows the heat transfer behavior as a function of time. The data sets no longer align as they did for the temperature curve. This indicates that in response to the fast transients applied in this work, the heat transfer under some set ambient condition cannot be a function of only heater temperature. Indeed, the heat transfer value spans a range of triple the lowest case based on heat pulse form. The surface condition corresponds to a heat transfer reduction of nearly 25%. This is further emphasized by the variation of the heat transfer vs temperature curve seen in Figure 89, and the HTC seen in figure 90. In all of the cases presented, the heat transfer value is elevated above the steady state values. The CHF value for water at steady state is approximately 1 $\frac{MW}{m^2}$.

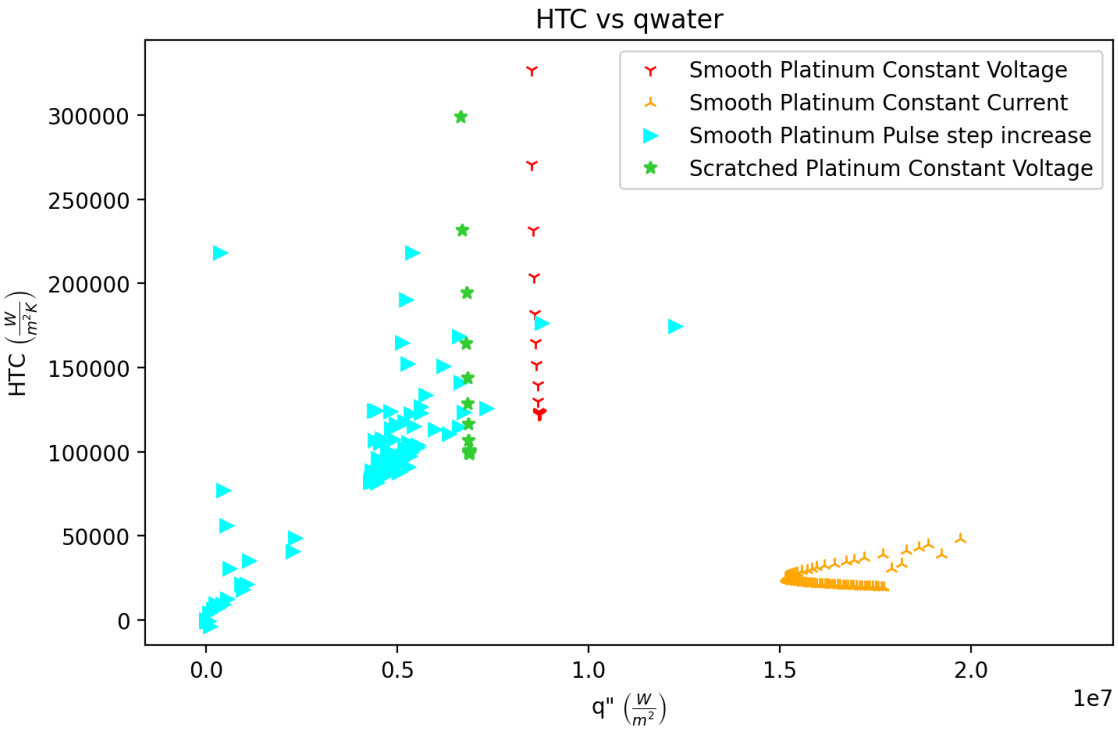

Figure 90: The HTC vs heat transfer for each case at PWR conditions is shown.

Ultimately, these graphs indicate that an elevated heat transfer over steady state CHF is achieved and maintained. Over the duration of the pulses employed, a quasi-steady state was achieved for all cases, except the constant current heating, where DNB has occurred, as seen in Figure 50. The largest impact on temperature and heat transfer behavior is caused by the heating shape that is employed.

10.2 Pulse Power Step Increase Behavior

A brief comparison between the behavior of the power step increases and the constant voltage platinum is instructive in understanding the changes and values seen in Chapter 8. The

plotted results allow for the observation of trends and are therefore employed despite inherent difficulties in determining specific values.

Figure 91 shows the temperature vs time for all of the cases. Under saturated conditions a temperature excursion is seen to occur in all but one case for the power step increase. This indicate that DNB occurred more readily for the cases with preheating. This is discussed above in Chapter 8. The subcooled case, along with the one saturated case that did not experience DNB, are grouped together. It appears that the pulse step increase has a dampening effect on the dynamics observed in the various cases of the constant voltage tests.

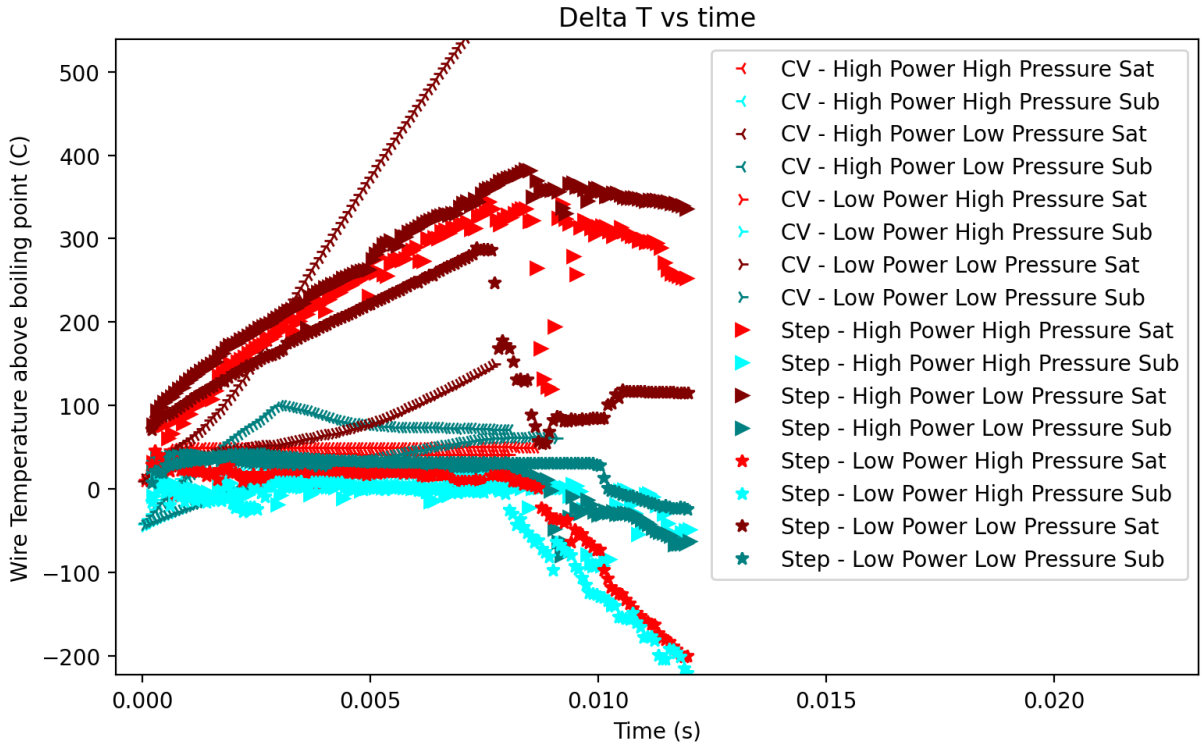

Figure 91: The various temperature vs time curves are seen for the constant voltage, and power step increase cases.

Figures 92 and 93 show the heat transfer vs time and temperature respectively. It is interesting to note that these figures also show a dampening effect on the impact of changes to other variables. In addition, the heat transfer values tend to begin at an elevated level seen with the

higher-powered constant voltage curves, and then fall toward the lower levels seen at lower power heating.

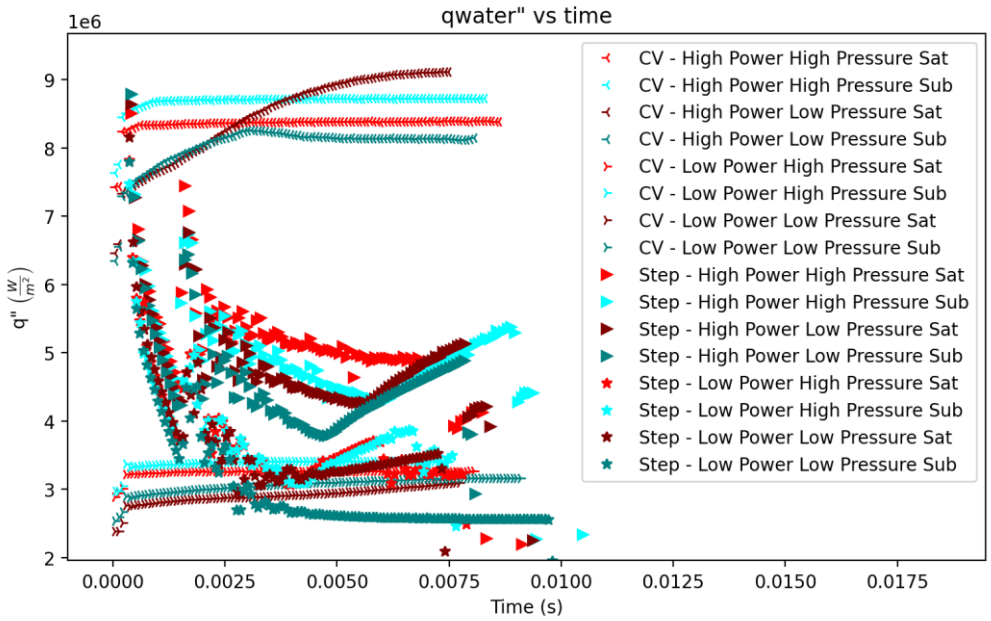

Figure 92: The heat transfer as a function of time for the constant voltage, and power step increase cases are seen.

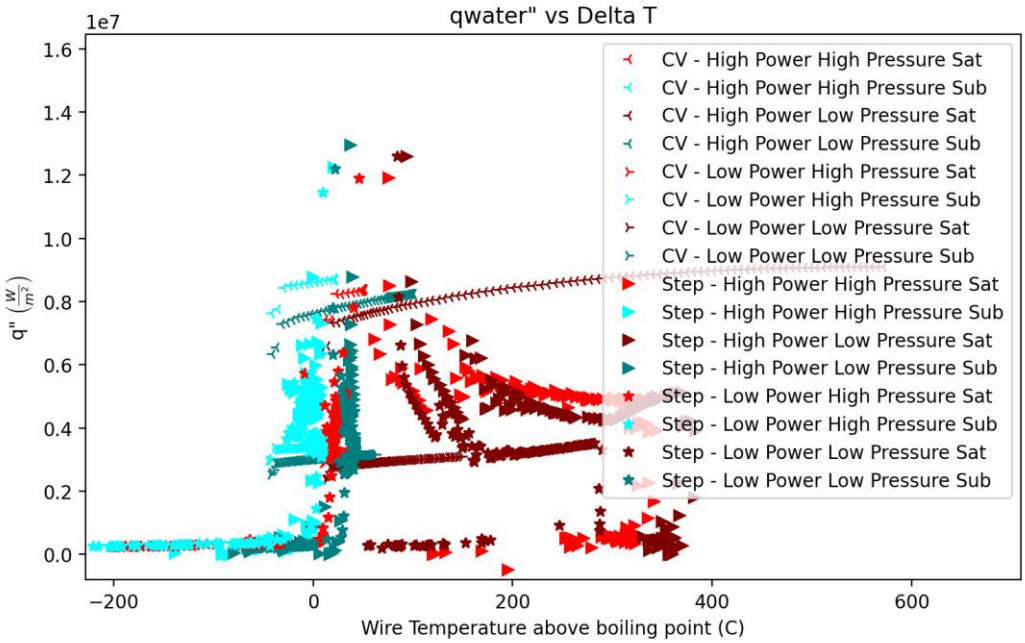

Figure 93: The heat transfer as a function of temperature for the constant voltage, and power step increase cases are seen.

10.3 Dissertation Conclusion

A first of its kind study of the fundamental heat transfer and temperature behavior of ultra-fast transient pool boiling under high pressure and subcoolings was successfully completed. The major findings are summarized into the following points:

- The single biggest factor impacting the boiling behavior, temperature, and heat transfer behavior under these ultra-fast transients is the power shape.
- An elevated heat transfer, quasi steady state can be achieved for non-DNB cases in under 3 ms, with many reaching the quasi-steady state within 1 ms.
- Traditional boiling behavior with bubbles departing the wire surface generally does not occur, even in cases with timescales sufficiently long for buoyancy effects to remove the bubble.
- Extremely high thermal gradients are seen with vapor layers under 50μm in size separating water from wires glowing white at temperatures over 1000 °C.
- Platinum is perceived to physically explode upon full wire melting, and centerline vaporization is presumed to occur.

These summarized points represent a small, but important fraction of the full work present herein. Ultimately these results establish the behavior of heating pulses at timescales even shorter than the full timescale of most nuclear accidents. This knowledge provides insight into the extreme end and, together with previously achieved research, establishes the dynamics seen in pool boiling as the heating rate increases to ultra-fast levels.

10.4 Broader Impact and Future Work

The US Department of Energy's (DOE) mission is "to ensure America's security and prosperity by addressing its energy, environmental and nuclear challenges through transformative science and technology solutions." [83] In order to accomplish this mission, the DOE needs data and instruments that indicate the current state of affairs. This is precisely hopes to allow. Specifically, this research addresses gaps in the fundamental understanding of fast-transient boiling that must be understood to overcome the nuclear challenges that face the nation.

One specific nuclear challenge that this work hopes to enable future research of is the RIA. As mentioned earlier in this proposal, a RIA occurs when a large pulse of energy is unexpectedly released from a nuclear reactor in a very short amount of time. This is the kind of accident that caused the nuclear disaster at Chernobyl. This work serves to provide fundamental physics of an unknown boiling regime of pool boiling in nuclear-like conditions to guide and inform future tests on flow boiling, which can ultimately inform modeling and simulations. In addition, this work highlights the parameters that are of highest significance on the boiling regime and can be used in boiling system design and accident simulations for future mitigation of accident effects.

Furthermore, this work has broader impact to the heat transfer industry. Pool boiling heat transfer has been studied for potential use in areas ranging from power generation to chemical and food processing, and microelectronics and cooling devices to space applications [40]. This work will provide a means for informing development of better pool boiling heat transfer systems for these, and still other, applications. By understanding the changes in pool boiling heat transfer that accompany variations in the studied parameters of this work, scientists and researchers have a guide for developing characteristics of interest in numerous applications. This adds to the present

body of knowledge and provides potential industry-wide application. An example application could be heat dissipation through repeated, ultra-fast, high energy pulses, which would allow for elevated pool boiling heat transfer.

As a whole, the research has an impact on the Department of Energy's mission of addressing nuclear challenges and safety as well as impacting the industry application of pool boiling heat transfer. This work provides fundamental knowledge to better understand the phenomena present in a RIA, predict the possible accident behavior of various new, accident-tolerant nuclear fuels through informed modeling, and quantify the impact of varying experimental parameters. Together these impacts have the potential to increase the safety of nuclear power plants and reduce operation costs by increasing the reasonable lifespan of the fuel.

While great care was taken throughout this work to ensure completeness, additional work can build upon what is presented here. Testing the impact of repeated short duration pulses (e.g., a 5 ms pulse followed by a 10 ms pause, repeated over a given time) would be of potential interest in the cooling of high-powered electronics and other similar applications. Zirconium 702 was selected as the test wire in this work because zircaloy-4 wires are not available in the tested size. Zircaloy-4 would represent a more interesting material as this is what is used as actual fuel cladding. In addition, extending the zirconium or zircaloy testing to high pressure would be of relevant interest. A study on the impact of wire diameter would also be of interest to provide a means of extrapolating this work out to thick wires or ultimately other annular geometries. Additional power shapes and a full comparison of all parameters (material and pulse) under every condition would allow for a more full 2^k factorial comparison to be undertaken. Other materials including ceramics as well as coated fibers would be additionally interesting in this work. Controlled surface modification could also be performed on these materials, though this field is

presently very active in research. Finally, the impact of flow boiling on these results would be useful.

Appendix A Curriculum Vitae

www.linkedin.com/in/zeke1
Pittsburgh, PA 15207

435.764.1549
zeke.vlr@gmail.com

Ezekiel (Zeke) T. Villarreal

EDUCATION

University of Pittsburgh (Pitt), Pittsburgh, PA **GPA: 4.0**
PhD, Mechanical Engineering Emphasis: Heat Transfer & Measurement May 2023
MS, Mechanical Engineering May 2022
Graduate Certificate in Nuclear Energy and Technology May 2022

Utah State University (USU), Logan, UT **GPA: 3.81**
BS, Mechanical Engineering Minor: Mathematics May 2016
Passed the FE Exam, February 2016

Consortium for Advanced Simulation of Light Water Reactors (CASL), Raleigh, NC
CASL Institute Certificate August 2018
This certificate covers the theory and application of advanced nuclear reactor (LWR) simulation codes.

TECHNICAL SKILLS

- Bilingual: English/Spanish
- LabVIEW
- Vibrational Spectroscopy (Raman & FTIR)
- Atomic Force Microscopy (AFM)
- Laser Flash Apparatus (LFA)
- Radiation Detection Methods
- Frequency Domain ThermoReflectance (FDTR)
- Scanning Electron Microscopy (SEM & EBSD)
- Vera, Cobra CTF, & Bison Modeling Software
- Thermomechanical Analysis (TMA)
- Photothermal Radiometry (PTR)
- COMSOL Multiphysics
- X-Ray Diffraction (XRD)
- Working knowledge: Finite Element Analysis, MATLAB, C++, Python, CAD & other characterization techniques

INTERNSHIP EXPERIENCE

Sandia National Laboratories –

Nuclear Forensics R&D, Albuquerque, NM May 2019 – August 2019

- Created a custom Raman spectroscopy system to measure the presence of radiation in air at long-range distances
- Modeled and fit captured data to know equations for verification and validation of results

Idaho National Laboratory –

High Temperature Test Lab, Idaho Falls, ID June 2017 – August 2017

- Developed a boiling detector capable of being placed in a nuclear reactor for use in the INL Transient Reactor (TREAT)
- Modeled boiling detector behavior using COMSOL Multiphysics software
- Designed and ran parameter sensitivity experiments to characterize the detector's response to changes in parameters

Orbital ATK –

R&D Division (Aerospace Structures: Composites), Clearfield, UT May 2015 – August 2015

RESEARCH SKILLS & EXPERIENCE

Pitt/USU Multi-Scale Thermophysics Laboratory Research,

Pittsburgh, PA February 2016 – Present

- Design, and run experiments with high intensity lasers, visible and IR, to measure variations in thermal properties
- Measure direct electron heat transfer contribution using frequency domain thermoreflectance on custom Schottky diode
- Lead an international research team performing preliminary research on transient boiling phenomena with application in nuclear modeling and safety, including tests at high temperature and high pressure
- Capture heat transfer and boiling regime information in the explosion of platinum wire with extreme heat rates
- Perform tests on transient boiling detection capabilities
- Characterized an unknown superconductor, including material composition, using XRD and SEM techniques

URCA Institut de Thermique, Mécanique, Matériaux,

Reims, France January 2020 – July 2021

- Designed and ran Photothermal Radiometry experiments with high power lasers for thermal property measurement
- Modified and streamlined automation of optothermal system (lock-in amplifier and function generator) using Python
- Developed a direct, theoretical transfer function for modulated laser heat input using Hankel transforms
- Devised techniques to heterodyne Photothermal Radiometry systems for high-speed operation (>10 MHz)

USU Advanced Composites Laboratory Research,

Logan, UT March 2014 – July 2016

- Conducted research on the uses of kenaf fibers and spider silk in the creation of composite materials
- Performed preliminary tensile strength tests on synthetic spider silk strands
- Led a team of students on the study of the critical length of kenaf fibers
- Created test specimen of spider silk with varying matrices for Dynamic Mechanical Analysis (DMA)

PUBLICATIONS & PRESENTATIONS

Experimental Investigations to Power Transient Flow Boiling … - December 2022

- Authors: Mingfu He, Minghui Chen, **Ezekiel Villarreal**, Heng Ban, Raul B. Rebak
- Paper in process with The International Journal of Heat and Mass Transfer

Direct Measurement of Thermal Boundary Resistance Reduction Due to Electron Carriers by PTR - January 2022

- Authors: **Ezekiel Villarreal**, Nicolas Horny, Heng Ban
- 2021 IMECE Conference Paper

The Influence of Rapid Transient Heating in Critical Heat Flux of Boiling Heat Transfer - January 2022

- Authors: Yuan Gao, Zhuorui Song, **Ezekiel Villarreal**, Heng Ban
- 2021 IMECE Conference Paper

Boiling Heat Transfer under Power Transients: A Review Study - November 2021

- Authors: Mingfu He, **Ezekiel Villarreal**, Heng Ban, Minghui Chen
- Journal: Progress in Nuclear Energy

Spatially localized measurement of isotropic and anisotropic thermophysical properties by PTR… - November 2020

- Authors: Georges Hamaoui, **Ezekiel Villarreal**, Heng Ban, Mihai Chirtoc, Nicolas Horny
- Journal: Journal of Applied Physics

Fast atom effect on helium gas/graphite interfacial energy transfer - May 2020

- Authors: Lin Zhang, Zhuorui Song, Binxing Zhao, **Ezekiel Villarreal**, Heng Ban
- Journal: Carbon

Transient Boiling Heat Transfer on Platinum Wire with Extreme Heating Rates - November 2019

- Authors: **Ezekiel Villarreal**, Heng Ban
- Poster and presentation at the 2019 ANS Winter Meeting

Development of In-Water, Transient Boiling Detector - April 2019

- Authors: **Ezekiel Villarreal**, Austin Fleming, Eric Larsen, Colby Jensen, Heng Ban
- Awarded Best Presentation at the 2019 ANS Student Meeting – Human Factor, Instrumentation & Controls track

Development of In-Water, Transient Boiling Detector - November 2018

- Authors: **Ezekiel Villarreal**, Austin Fleming, Eric Larsen, Colby Jensen, Heng Ban
- Presentation at the 2018 International Mechanical Engineering Congress and Exposition (IMECE)

Thermal Characterization of Alkali Treated Kenaf Fibers and Composites - February 2018

- Authors: Levi Gardner, Troy Munro, **Ezekiel Villarreal**, Kurt Harris, Thomas Fronk, Heng Ban
- Journal: Fibers and Polymers

In-Pile Boiling Detector - August 2017

- Poster and presentation at the 2017 Idaho National Laboratory Intern Exposition
- 1st place entry in World Nuclear Energy Future

Laser Flash Measurements on Thermal Conductivity of Bio-Fiber (Kenaf) Reinforced Composites - May 2017

- Authors: Levi Gardner, Troy Munro, **Ezekiel Villarreal**, Kurt Harris, Thomas Fronk, Heng Ban
- International Thermal Conductivity Conference Paper

USU Bio-Composites: A Composite Future for Kenaf and Spider Silk - May 2016

- Authors: **Ezekiel Villarreal**, Thomas Fronk
- Plenary presentation at the SAMPE Utah Chapter Conference

LEADERSHIP & SERVICE

Frontiers in Energy Research, Journal Editor, Pittsburgh, PA - June 2022 – Present

University of Pittsburgh Design Expo, Judge, Pittsburgh, PA - April 2022

Ingenium Journal of Undergraduate Research, Journal Editor, Pittsburgh, PA - September 2021 – January 2022

Graduate and Professional Student Governing Board, Assembly Board Member, Pittsburgh, PA - August 2021 – May 2022

University Council on Graduate Study, College of Engineering Appointee, Pittsburgh, PA - August 2021 – July 2022

Engineering Graduate Student Organization, Communications Officer, Pittsburgh, PA - July 2021 – June 2022

Pittsburgh Regional Science Fair, Judge, Pittsburgh, PA - March 2019

Pittsburgh Quantum Institute, Member, Pittsburgh, PA - May 2018 - Present

American Nuclear Society (ANS), Graduate Student Representative, Logan, UT - August 2016 – May 2017

USU Tutor (Thermodynamics & Math), Logan, UT - September 2013 – May 2017

Engineering Council, Vice President, Logan, UT - February 2015 – May 2016

ASME Human Powered Vehicle Competition, Project Manager, Logan, UT - August 2015 – May 2016

Tau Beta Pi, Engineering Honor Society - May 2015 – Present

SAMPE Club (Composites), Vice President, Logan, UT - August 2015 – May 2016

Full-Time Humanitarian Service (Spanish Speaking), Tulsa, OK - December 2010 – December 2012

AWARDS & FUNDING

2022-2023 ANS Pittsburgh Local Section Graduate Scholarship - August 2022

US NRC Fellowship - December 2020-Present

2020-2021 STEM Chateaubriand Fellowship - September 2020 – June 2021

ANS Student Best Paper/Presentation Award, Human Factor, Instrumentation, & Controls - April 2019

Roy G Post Foundation Graduate Scholarship - March 2019

2018 CASL Poster Competition Award - August 2018

1st Place Poster, World Nuclear Energy Future, 2017 INL Intern Exposition - August 2017

NEUP Fellowship - August 2017 – July 2020

$150,000 awarded over the length of the fellowship
1 of 31 people nationally to receive this fellowship (2017)

Dean's List - January 2013 – May 2016

Presidential Scholarship - August 2010 – December 2010, January 2013 – May 2016
Full Tuition and Fees

Richard and Moonyeen Anderson Scholarship - August 2010 – December 2010, January 2013 – May 2016
$1000 Stipend for engineering excellence
1 of 2 people nationally to receive this scholarship (2010)

Eagle Scout Award - May 2007

Appendix B Data Collection and Reduction Resources

The various code, LabVIEW and MATLAB used in data collection and post-processing is presented here.

Appendix B.1 LabVIEW Code Diagrams

The LabVIEW block diagram is presented in a group of images due to the code length and paneling.

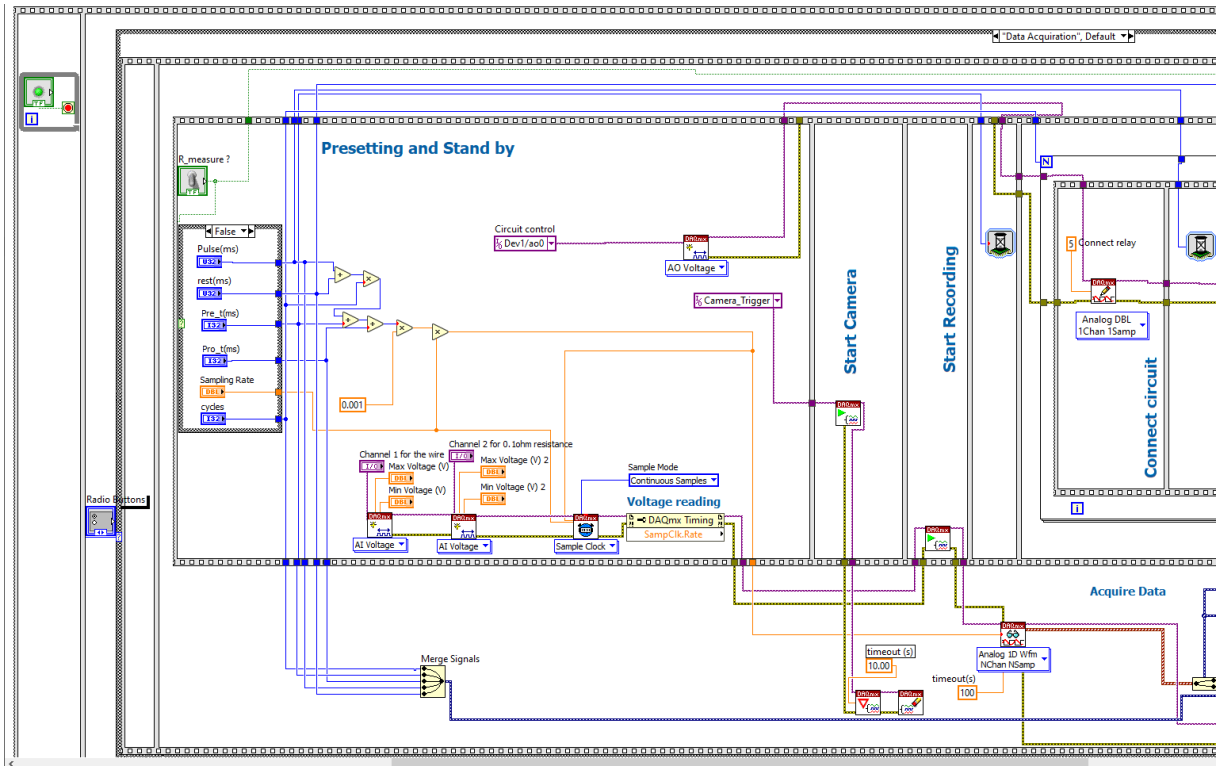

Appendix Figure 1: The left side of the LabVIEW collection code is shown.

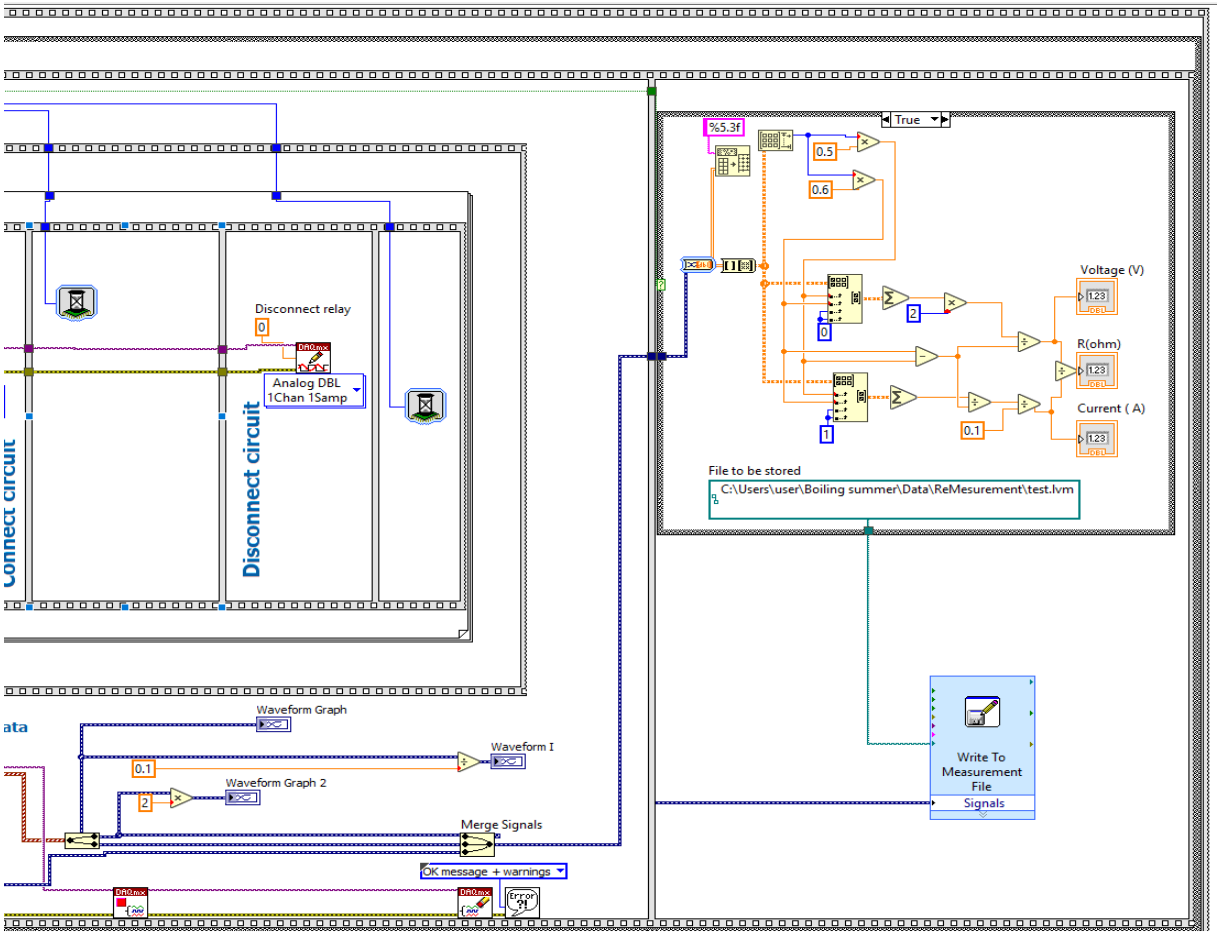

Appendix Figure 2: The right side of the LabVIEW collection code is shown.

Together Appendix Figures 1 & 2 present the code employed for the general collection of data employed in this work. The front panel of this code can be seen in Chapter 4 as Figure 14. The data reduction block diagram is presented next as Appendix Figure 3. It will be quick to observe that the bulk of the data reduction occurs outside of LabVIEW in an integrated MATLAB file.

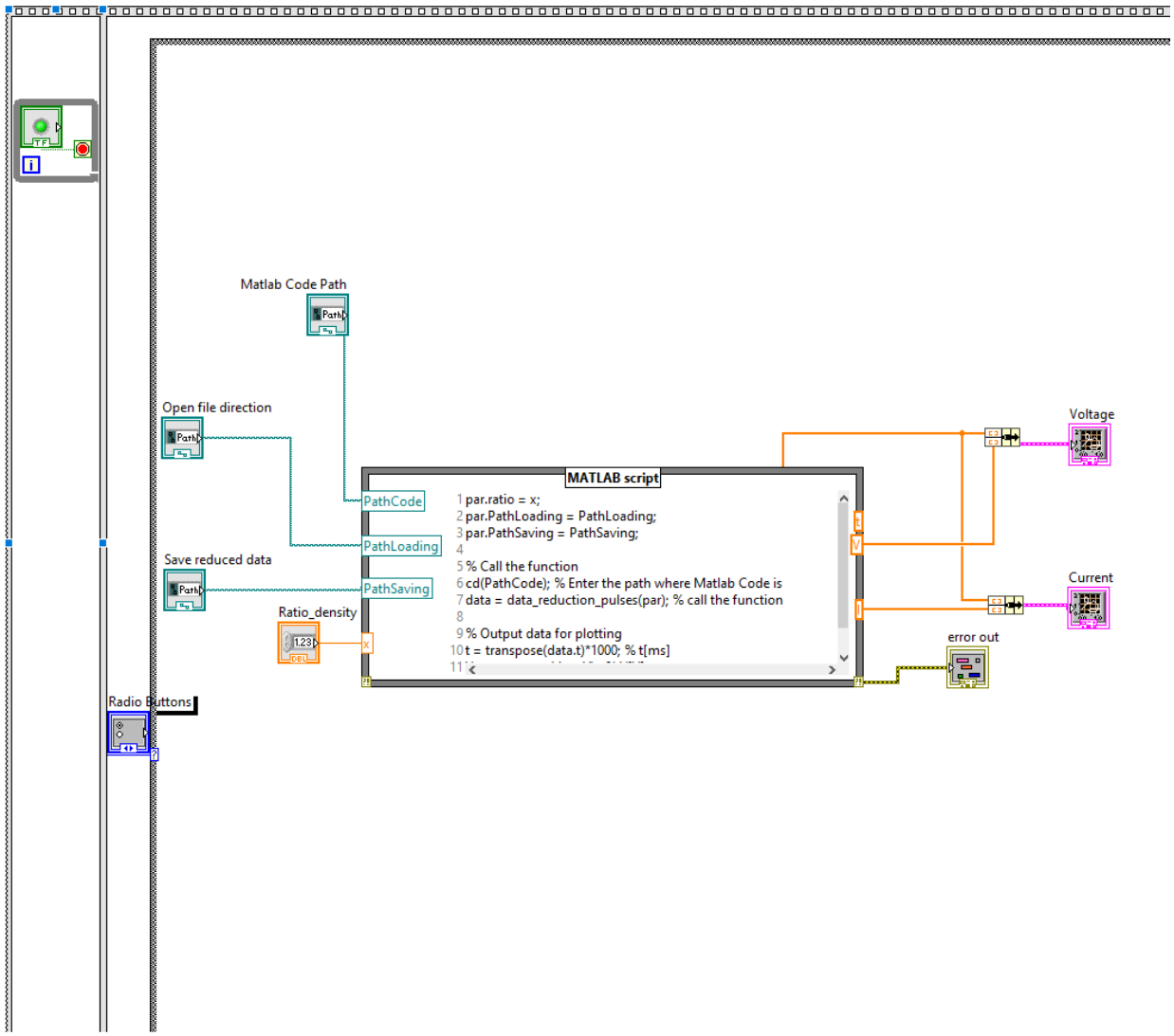

Appendix Figure 3 The LabVIEW data reduction code is shown.

Appendix B.2 MATLAB File Reduction

```
function data = data_reduction_pulses(par)
% This function is used for data reduction of pulsed heating in the boiling project

%par.ratio = 10; %used in debugging
par.relax_eachcyle = 10; %[ms]

% [FileName, PathName]=uigetfile('*csv;*lvm'); %pop up a window to choose data file,
used in debugging
```

```
% if PathName~=0 % In case that the user cancel.
%     par.PathLoading=fullfile(PathName, FileName);
% end
data_origin = load(par);% Load data acquired by NI-6821

data_processed = func_processing(data_origin,par); %convert the data into groups,
chopped, and loosed.

if ndims(data_processed)>=3
    data_processed(:,:,end) = []; % If there is more than one group, delete the last
one
end

data_averaged = mean(data_processed,3); % Average all data points

data.t= data_averaged(:,1); data.V= data_averaged(:,2); data.I= data_averaged(:,3);

% [FileName, PathName] = uiputfile('*.txt', 'Save As'); % pop up a window to choose
path and define file name, used for debugging
% if PathName~=0
%     par.PathSaving = fullfile(PathName,FileName);
% end
func_save(data,par.PathSaving); %save data
end
%% Load and save files
function data = load(par)
ratio_V = 2; %[V] convert acquired voltage to the real value
ReSen = 0.1;%[ohm] Resistance of the Resistance sensor
% ReSen2 = 100; %[ohm] Resistance in serial connection with the battery. For future
use.

fullFileName = par.PathLoading;
if fullFileName ~=0

    delimiterIn = ',';
    headerlinesIn = 24; % depends on the format of Netzsch file
    original_data = importdata(fullFileName,delimiterIn,headerlinesIn);
    data.M(:,1) = original_data.data(:,1);
    data.M(:,2) = original_data.data(:,2)*ratio_V;
    data.M(:,3) = original_data.data(:,3)/ReSen;
    %             data.I2 = original_data.data(:,4)/ReSen2;
    %             data.V2 = original_data.data(:,5);
    data.groupNo = original_data.data(1,4);
    data.pre = original_data.data(1,5);
    data.pro = original_data.data(1,6);
    data.pulsewidth = original_data.data(1,7);
    data.relax = original_data.data(1,8);
else
    disp('No file will be loaded!');
    return;
end
end
function func_save(data,Name)
```

```
if Name~=0
    fileID = fopen(Name,'w'); fclose(fileID); % clear the content of the file
    fileID = fopen(Name,'wt');
    fprintf(fileID,'%12s%12s%12s\n','t(s)','V(V)','I(A)');
    fprintf(fileID,'%12.8f%12.8f%12.8f\n',transpose([data.t,data.V,data.I]));

    fclose(fileID);
else
    disp('Cannot find the file to save')
    return;
end
end
%% functions used to break the data into groups, chop, and loose.
function data_processed = func_processing(data,par)

[datachopped,data] = func_chopdata(data,par);
dataloosed = func_loose(datachopped,par);
data_processed = zeros([size(dataloosed),data.groupNo]);
data_processed(:,:,1) = dataloosed;
for i = 2:data.groupNo
    [datachopped,data] = func_chopdata(data,par);
    if isempty(datachopped)
        data_processed(:,:,i:end) = [];
        return
    else
        dataloosed = func_loose(datachopped,par);
        data_processed(:,:,i) = dataloosed;
    end
end
end
function [datachopped,data] = func_chopdata(data,par)
% Identify the start point of heating as V rises upto V_jump.
V_jump = 0.1; %[V]
t_baseline = 30e-3+data.M(1,1); %[s]
V =abs( data.M(:,2) - mean(data.M(data.M(:,1) <= t_baseline,2)));
idx = find(V >= V_jump );
if isempty(idx)     % If less groups were recorded, the idx would be empty.
    datachopped = [];
else
    idx_startpoint = idx(1)-1;

    % Define the last point for the cycle.
    Timestamp = data.M(2,1) - data.M(1,1);
    idx_endpoint = idx_startpoint +
round((data.pulsewidth+par.relax_eachcyle)/1000/Timestamp) ;

    % chop the data.
    if idx_endpoint < length(data.M(:,1))
    datachopped(:,1) = data.M(idx_startpoint:idx_endpoint,1) -
data.M(idx_startpoint,1);
    datachopped(:,2:3) = data.M(idx_startpoint:idx_endpoint,2:3);

    data.M(1:idx_endpoint,:) =[];
```

```
    %         datachopped.I2 = data.I2(origin_t:end);
    %         datachopped.V2 = data.V2(origin_t:end);
    else
        datachopped = [];
    end
end
end
function data = func_loose(datachopped,par)
% Reduce data density
if (par.ratio > 1)
    Points_average=ceil(par.ratio); % the number of points used to calculate one
average number.
    t = transpose(mean(transpose(vec2mat(datachopped(2:end,1),Points_average))));
    V = transpose(mean(transpose(vec2mat(datachopped(2:end,2),Points_average))));
    I = transpose(mean(transpose(vec2mat(datachopped(2:end,3),Points_average))));
    %             V2 =
transpose(mean(transpose(vec2mat(datachopped.V2(2:end),Points_average))));
    %             I2 =
transpose(mean(transpose(vec2mat(datachopped.I2(2:end),Points_average))));

    data(:,1) = [datachopped(1,1);t(1:end-1)]; % Add zero, and delete the last point
    data(:,2) = [datachopped(1,2);V(1:end-1)];
    data(:,3) = [datachopped(1,3);I(1:end-1)];
    %             data.V2 = [datachopped.V2(1);V2(1:end-1)];
    %             data.I2 = [datachopped.I2(1);I2(1:end-1)];

else
    data = datachopped;
end
end
% function data = func_loose(datachopped,par)
% % Reduce data density
% if (par.ratio > 1)
%     Points_average=ceil(par.ratio); % the number of points used to calculate one
average number.
%     t = transpose(mean(transpose(vec2mat(datachopped(2:end,1),Points_average))));
%     V = transpose(mean(transpose(vec2mat(datachopped(2:end,2),Points_average))));
%     I = transpose(mean(transpose(vec2mat(datachopped(2:end,3),Points_average))));
%     %             V2 =
transpose(mean(transpose(vec2mat(datachopped.V2(2:end),Points_average))));
%     %             I2 =
transpose(mean(transpose(vec2mat(datachopped.I2(2:end),Points_average))));
%
%     data(:,1) = [datachopped(1,1);t(1:end-1)]; % Add zero, and delete the last
point
%     data(:,2) = [datachopped(1,2);V(1:end-1)];
%     data(:,3) = [datachopped(1,3);I(1:end-1)];
%     %             data.V2 = [datachopped.V2(1);V2(1:end-1)];
%     %             data.I2 = [datachopped.I2(1);I2(1:end-1)];
%
% else
%     data = datachopped;
% end
```

```
% end
```

Appendix B.3 MATLAB Data Processing

```
close all
clear all
clc
%%  Material Properties
Diam = 127e-6;
rho = 21450;   %density of Pt*******************************
% rho = 6500;    %density of Zr*******************************
tsat = 100;    %Boiling point of water at tested condition*******************************
%% File Info
fname = "Pt_CV_8V_101-0C_1psig_5ms_1_reduced"; %*******************************
pname = "1\";        %*******************************
name2 = pname+fname + ".xlsx";
X = xlsread(name2);
index1 = 2;       %************************************************************
index2 = 2292; % choose/change for each data set *******************************
tIV = X(:,1); % time vector from saved (reduced) data
Vsamp = X(:,2); % Voltage signal across sample
Iapp = X(:,3); % Supplied current
```

```
Rref = 0.1; % Reference resistance
Vtot = Vsamp + Iapp*Rref; % Calculated total voltage drop across reference and sample
figure;
plot(tIV,Vsamp,tIV,Iapp,'LineWidth',1)
%% Pt Calculations
RsampH = Vsamp./Iapp; % Vector of sample resistance values (over time)
%This is the linear function for Platinum**************************************
Ro = 1.0872e-1; % from particular calibration curve for the sample
Ralpha = 3.5974e-4;
Tcalcabs = (RsampH-Ro)/Ralpha;
Rrho = 9.85e-8;  %Pt resistivity ohm*m   ********************************
QappB = 4*(Iapp.^2)*Rrho.*(1 + (Ralpha/Ro)*Tcalcabs)/(pi^2*Diam^3);
%********************************
% %%This is the quadratic function for Zirconium*******************************
% Ro = 6.5352e-1; % from particular calibration curve for the sample
% Ralpha = 1.7524e-3; %this is the coefficient for the linear term
% Rbeta = 4.0885e-6;  %this is the coefficient for the squared term
% Tcalcabs = (-1*Ralpha +(Ralpha.^2-4*Rbeta*(Ro-RsampH)).^0.5)/(2*Rbeta);
% Rrho = 3.97e-7;  %Zr resistivity ohm*m   ********************************
% QappB = 4*(Iapp.^2)*Rrho.*(1 +
(Ralpha/Ro)*Tcalcabs+(Rbeta/Ro)*Tcalcabs.^2)/(pi^2*Diam^3);
%********************************
Qappsub = QappB(index1:index2);
```

```
Ttest = Tcalcabs(index1:index2); % Subset of the absolute temperature calculated above that corresponds to pulse length seen in the data set
ttest = tIV(index1:index2); % Time vector for subset
figure;
plot(ttest,Ttest)
m = length(Ttest); % Number of points in the data set to be smoothed
E = eye(m); % Square identity matrix of size m x m
D1 = diff(E); % Differentiation operator - 1st order
D2 = diff(D1); % Differentiation operator - 2nd order
D3 = diff(D2); % Differentiation operator - 3rd order
D4 = diff(D3); % Differentiation operator - 4th order
lambda = 100; % Choice of regularization factor
z1 = (E + lambda*D1'*D1)\Ttest; % Smoothed data - 1st order
z2 = (E + lambda*D2'*D2)\Ttest; % Smoothed data - 2nd order
z3 = (E + lambda*D3'*D3)\Ttest; % Smoothed data - 3rd order
z4 = (E + lambda*D4'*D4)\Ttest; % Smoothed data - 4th order
delz4= z4-tsat;
%% Cp Values with temperature
%%These are the values for Platinum Cp  ****************************************
% a = 0.000000006761;
% b = 0.00001664;
% c = 0.1274;
%%These are the values for Zirconium Cp ****************************************
```

```
a = -1.1027E-7;

b = 1.7777E-4;

c = 0.23839;

Cpvar0 = a*Ttest.^2+b*Ttest+c;

Cpvar4 = a*z4.^2+b*z4+c;

%% Comparison of the Various Operators

figure;

plot(ttest,Ttest,ttest,z1,ttest,z2,ttest,z3,ttest,z4,'LineWidth',1)

hold on;

xlabel('Time (s)')

ylabel('Temperature (C)')

legend("original","1st","2nd","3rd","4th")

%QappSM = 4*(Iapp(1:index).^2)*9.85e-8.*(1 + B*z + A*z.^2)/(pi^2*(127e-6)^3); % still noisy

because of Iapp data set

%% Take the derivative of the smoothed data to use in heat storage term

h = ttest(2)-ttest(1); % time step

% original data set (for comparison)

dz0 = [];

dz0(1) = (Ttest(2)-Ttest(1))/h;

for i = 2:length(Ttest)-1 % Central differences for middle data points

    dz0(i) = (Ttest(i+1)-Ttest(i-1))/(2*h);

end

dz0(length(Ttest)) = (Ttest(end)-Ttest(end-1))/h;
```

```
% 1st-order
dz1 = []; % empty matrix for derivative values
dz1(1) = (z1(2)-z1(1))/h; % Forward difference for first data point
for i = 2:length(z1)-1 % Central differences for middle data points
    dz1(i) = (z1(i+1)-z1(i-1))/(2*h);
end
dz1(length(z1)) = (z1(end)-z1(end-1))/h; % Backward difference for end data point
% 2nd-order
dz2 = []; % empty matrix for derivative values
dz2(1) = (z2(2)-z2(1))/h; % Forward difference for first data point
for i = 2:length(z2)-1 % Central differences for middle data points
    dz2(i) = (z2(i+1)-z2(i-1))/(2*h);
end
dz2(length(z2)) = (z2(end)-z2(end-1))/h; % Backward difference for end data point
% 3rd-order
dz3 = []; % empty matrix for derivative values
dz3(1) = (z3(2)-z3(1))/h; % Forward difference for first data point
for i = 2:length(z3)-1 % Central differences for middle data points
    dz3(i) = (z3(i+1)-z3(i-1))/(2*h);
end
dz3(length(z3)) = (z3(end)-z3(end-1))/h; % Backward difference for end data point
% 4th-order
dz4 = []; % empty matrix for derivative values
```

```
dz4(1) = (z4(2)-z4(1))/h; % Forward difference for first data point
for i = 2:length(z4)-1 % Central differences for middle data points
    dz4(i) = (z4(i+1)-z4(i-1))/(2*h);
end
dz4(length(z4)) = (z4(end)-z4(end-1))/h; % Backward difference for end data point
figure;
% plot(ttest,dz0,ttest,dz1,ttest,dz2,ttest,dz3,'LineWidth',1)
plot(ttest,dz0,ttest,dz4,'LineWidth',1)
hold on;
xlabel('Time (s)')
ylabel('dT/dt (C/s)')
legend("original","Smoothed")
title("Derivative of Temperature")
%% Calculate the Q values with Cp
Qstor = dz0.*Cpvar0'*Diam*rho/4;
QstorB = (dz4.*Cpvar4'*Diam*rho/4)';
Qwater = Qappsub - QstorB;
data = [ttest';delz4';Qappsub';QstorB';Qwater']; % variable created for file writing
figure;
plot(ttest,Qstor,ttest,QstorB,'LineWidth',1)
%% Print out a file of time, temp, and q's
fileID = fopen(pname+fname+"_TQ.txt",'w'); %Change the file name to correspond to data file
above
```

fprintf(fileID,'%6s %6s %6s %6s %6s \n','t (s)','DeltaT_abs (C)','Q_app','Q_stor','Q_water'); % Creates the column headings

fprintf(fileID,'%6.4e %6.4e %6.4e %6.4e %6.4e \n',data) % Adds the data to the file in the appropriate columns in exponential notation

Appendix C 2k Factorial 2 Parameter Example Study

The various sensitivities of two parameters, here named A and B, are desired. These parameters will be probed using the 2k factorial method. Thus 2^2 tests are required to determine the relative importance of the parameters. The accordant tests and parameters can be visualized in the following manner:

The results, Y, of the four tests will be referred to numerically as indicated by the numbers present in the various corners of the image above. The resultant values are then combined to determine the relative sensitivity or parameter importance according to the following equations:

$$a = \overline{Y_{A+}} - \overline{Y_{A-}}$$

$$a = \frac{Y_2 + Y_3}{2} - \frac{Y_4 + Y_1}{2}$$

$$b = \overline{Y_{B+}} - \overline{Y_{B-}}$$

$$b = \frac{Y_3 + Y_4}{2} - \frac{Y_2 + Y_1}{2}$$

$$ab = \overline{Y_{AB+}} - \overline{Y_{AB-}}$$

$$ab = \frac{Y_3 + Y_1}{2} - \frac{Y_4 + Y_2}{2}$$

As a full example, imagine that the following table has the results of the parameter tests:

Appendix Table 1: Experimental Test Matrix Setup

Test Case	Parameter A	Parameter B	Results, Y
1	+	+	50
2	-	+	10
3	+	-	90
4	+	+	60

According to the previous equations, this yields the following sensitivity parameters:

$$a = (50 + 90)/2 - (10 + 60)/2 = 35$$

$$b = (50 + 10)/2 - (90 + 60)/2 = -45$$

$$ab = (50 + 60)/2 - (10 + 90)/2 = 5$$

This indicates that, over the chosen range, the experiment is most sensitive to a change in parameter B, and that an increase in this parameter leads to a decrease in the measured result. Parameter A is of a similar, though slightly reduced magnitude, and there is negligible effect seen in the interaction between parameters A and B.

Appendix D 2k Factorial Design of Experiments Code (Python)

The code is provided below in section B.1. It can also be found on GitHub under "2kFactorial" and at https://github.com/Zeke-Vlr/2kFactorial. The specific libraries and versions install on the machine that ran the code are included in section B.2.

Appendix D.1 - Code

```
#Start=============================================================

    #%% Libraries used in the program. (Globally defined, though not strictly necessary)
    import numpy as np
    import math
    import codecs
    import itertools
    from pyDOE2 import *

    #%%Functions created for the program
    #This function is used to iteratively create letters from its hexidecimal number
    def var_name(i):
       if(i<9):
```

```
        stri = 41+i          #"42434445464748494a4b4c4d4e4f505152535455565758595a" =
```
Hex alphabet A-Z (capitalized)
```
    elif(i==9):
        stri = "4a"
    elif(i==10):
        stri = "4b"
    elif(i==11):
        stri = "4c"
    elif(i==12):
        stri = "4d"
    elif(i==13):
        stri = "4e"
    elif(i==14):
        stri = "4f"
    elif((i>14) and (i<25)):
        stri = 41+i-6
    elif(i==25):
        stri = "5a"
    else:
        stri = "343034"     #If, somehow, a wrong number is used, or more than
    string = str(stri)      #26 elements are called, the variable is named "404"
    b_str =codecs.decode(string, "hex")
    a_str = str(b_str, encoding = "ascii", errors ="ignore")
```

```
    key = (a_str)
    return key

#This is where the DOE test values are created
def twok(test,tm,n,i,o):
    A = 0
    B=1
    for j in range(2**n):
        if(o==1):
            A +=test[j]*tm[j][i]/(2**(n-1))
        else:
            for k in range (o):
                B*=tm[j][i[k]]
            A+=test[j]*B/(2**(n-1))
            B=1
    return (A)

#This is used to import the data from a file
def readfile(filename):
    data = np.loadtxt(filename + '.txt')
    return data

#This is used to write the results to a file
```

```
def writefile(filename,lib,n,i,savefile):
    fn = filename+".txt"
    file=open(fn,'a')
    with open(fn,'a') as fi:
        if (i==0):
            fi.write('A 2k factorial study was performed using '+str(n)+' variables\n')
            fi.write('The results come from the file named "'+str(savefile)+'"\n')
        fi.write(str(lib)+'\n')
        if (i==(n-1)):
            fi.write('\n')
    file.close()
    return

#%%This is the area to manipulate/ load data
#*********************************************************
#Test values - ***Comment out which ever method you are not using***
    ###Handtyped values
# test = [1154/2,1319/2,1234/2,1277/2,2089/2,1617/2,2178/2,1589/2]

    ###Read values from .txt - The other option is to load a txt file with the
    ###data saved in the proper order
filename = "test_example"  #without the .txt file extension, just the saved name
test = readfile(filename)
```

```
#^^^ This is where the results of the experiments should be placed,
#^^^ ie the function value being evaluated for changes do to experimental
#^^^ parameters. The order in which these are placed is crucial. The tests
#^^^ should match what is produced in the test matrix "tm". "tm" starts with
#^^^ the all low value cases. Uncomment out the print below "tm" to verify that
#^^^ your test order matches.



#************************************************************
#Do you want to save the 2k factorial results to a .txt file?
savefile = 'y'          #Use 'y' to save a file
filewrite =' Results'   #If you do not change the file name it will append the
                        #next results to the same file. I would recommend naming
                        #this file the type of test/parameters being explored
#************************************************************
k = int(math.log2(len(test))) # the k value is calculated based on the number of test results
tm = ff2n(k)
# print(tm)
#^^^ This is the test matrix to compare your testing order. "-1" is a low value
#^^^ and "1" is high. You need to make sure the order of the results placed in
#^^^ "test" match the matrix "tm". In general "tm" follows the following pattern:
```

```
#[-1,-1,-1]   #The pattern is that the first column alternates by ones,
#[ 1,-1,-1]   #the second column alternates by twos, and the third  column
#[-1, 1,-1]   #alternates by fours, etc, all beginning with the low values.
#[ 1, 1,-1]
#[-1,-1, 1]
#[ 1,-1, 1]
#[-1, 1, 1]
#[ 1, 1, 1]


#%% The running part of the code. This is where the work is done. No changes
#are needed here to run the study.
g = []
combin = []
te = ''
for i in range(k):
    exec(f"dict{i+1} = "+"{}")


for i in range(k):
    key1 = var_name(i)
    for j in range(k-1-i):
        key2 = var_name(i)+var_name(j+1+i)
        p = [i,j+1+i]
```

```
        exec("dict2[key2]=twok(test,tm,k,p,2)")
    exec("dict1[key1]=twok(test,tm,k,i,1)")
    combin.append(i)


if 'filename' in locals():
    check = 1
else:
    filename = "Unnamed - data entered by hand"


for z in range (k-2):
    o = z+3
    y3 = set(list(itertools.combinations(combin,o)))
    for i in range(1):
      for id,val in enumerate(y3):
          for j in range(o):
              g.append(val[j])
          for l in range(o):
              te+=var_name(g[l])
          exec(f"key{o} = te")
          exec(f"dict{o}[key{o}]=twok(test,tm,k,g,o)")
          g = []
          te = ''
for i in range(k):
```

```
        exec(f"print(dict{i+1})")
        if savefile=='y':
            exec(f"writefile(filewrite, dict{i+1},k,i,filename)")
#End=============================================================
```

Appendix D.2 Libraries and versions employed

The most important libraries are called out on top, but all libraries are presented for reference if needed.

Python	3.8.8
pyDOE2	1.3.0
spyder	5.3.3

Python	3.8.8	asttokens	2.0.5	backports.weakref	
alabaster	0.7.12	atomicwrites	1.4.0	1.0.post1	
anaconda-client	1.11.0	attrs	22.1.0	bcrypt	3.2.0
anaconda-navigator	2.1.0	autopep8	1.6.0	beautifulsoup4	4.11.1
anyio	3.5.0	Babel	2.11.0	binaryornot	0.4.4
argon2-cffi	21.3.0	backcall	0.2.0	black	22.6.0
argon2-cffi-bindings	21.2.0	backports.functools-lru-		bleach	4.1.0
arrow	1.2.3	cache 1.6.4		Bottleneck	1.3.5
astroid	2.11.7	backports.tempfile	1.0	brotlipy	0.7.0

certifi	2022.12.7	dill	0.3.6	isort	5.9.3
cffi	1.15.1	docutils	0.18.1	jedi	0.18.1
chardet	4.0.0	entrypoints	0.4	jellyfish	0.9.0
charset-normalizer	2.0.4	executing	0.8.3	Jinja2	2.11.3
click	8.0.4	fastjsonschema	2.16.2	jinja2-time	0.2.0
cloudpickle	2.0.0	filelock	3.9.0	json5	0.9.6
clyent	1.2.2	flake8	4.0.1	jsonschema	4.16.0
colorama	0.4.6	flit_core	3.6.0	jupyter_client	7.4.8
conda	22.11.1	fonttools	4.25.0	jupyter_core	5.1.1
conda-build	3.23.3	future	0.18.2	jupyter-server	1.23.4
conda-content-trust	0.1.3	glob2	0.7	jupyterlab	3.5.2
conda-package-handling	1.9.0	hankel	1.1.0	jupyterlab-pygments	0.1.2
		idna	3.4	jupyterlab-server	2.10.3
conda-repo-cli	1.0.24	imagesize	1.4.1	jupyterlab-widgets	1.0.0
conda-token	0.4.0	importlib-metadata	4.11.3	keyring	23.4.0
conda-verify	3.4.2	importlib-resources	5.2.0	kiwisolver	1.4.4
cookiecutter	1.7.3	inflection	0.5.1	lazy-object-proxy	1.6.0
cryptography	38.0.1	intervaltree	3.1.0	libarchive-c	2.9
cycler	0.11.0	ipykernel	6.15.2	MarkupSafe	2.0.1
debugpy	1.5.1	ipython	7.31.1	matplotlib	3.4.3
decorator	5.1.1	ipython-genutils	0.2.0	matplotlib-inline	0.1.6
defusedxml	0.7.1	ipywidgets	7.6.5	mccabe	0.7.0
diff-match-patch	20200713	iso8601	0.1.16	menuinst	1.4.18

mistune	0.8.4	parso	0.8.3	pyDOE	0.3.8
mkl-fft	1.3.1	pathlib	1.0.1	pyDOE2	1.3.0
mkl-random	1.2.2	pathspec	0.9.0	pyflakes	2.4.0
mkl-service	2.4.0	pexpect	4.8.0	Pygments	2.11.2
mpmath	1.2.1	pickleshare	0.7.5	pyhank	2.2.1
munkres	1.1.4	Pillow	9.3.0	PyJWT	2.4.0
mypy-extensions	0.4.3	pip	22.3.1	pylint	2.14.5
navigator-updater	0.2.1	pkginfo	1.8.3	pyls-spyder	0.4.0
nbclassic	0.4.8	pkgutil_resolve_name		PyNaCl	1.5.0
nbclient	0.5.13	1.3.10		pyOpenSSL	22.0.0
nbconvert	6.4.4	platformdirs	2.5.2	pyparsing	3.0.9
nbformat	5.7.0	pluggy	1.0.0	PyQt5	5.15.7
nest-asyncio	1.5.6	ply	3.11	PyQt5-sip	12.11.0
notebook	6.5.2	poyo	0.5.0	PyQtWebEngine	5.15.4
notebook_shim	0.2.2	prometheus-client	0.14.1	pyrsistent	0.18.0
numexpr	2.8.4	prompt-toolkit	3.0.36	pyserial	3.5
numpy	1.21.5	psutil	5.9.0	PySocks	1.7.1
numpydoc	1.5.0	ptyprocess	0.7.0	python-dateutil	2.8.2
packaging	22.0	pure-eval	0.2.2	python-lsp-black	1.2.1
panda	0.3.1	pycodestyle	2.8.0	python-lsp-jsonrpc	1.0.0
pandas	1.4.1	pycosat	0.6.4	python-lsp-server	1.5.0
pandocfilters	1.5.0	pycparser	2.21	python-slugify	5.0.2
paramiko	2.8.1	pydocstyle	6.1.1	pythonnet	2.5.2

pytz	2022.7	sniffio	1.2.0	textdistance	4.2.1
PyVISA	1.11.3	snowballstemmer	2.2.0	three-merge	0.1.1
pywin32	305.1	sortedcontainers	2.4.0	tinycss	0.4
pywin32-ctypes	0.2.0	soupsieve	2.3.2.post1	toml	0.10.2
pywinpty	2.0.2	spark-parser	1.8.9	tomli	2.0.1
PyYAML	6.0	Sphinx	5.0.2	tomlkit	0.11.1
pyzmq	23.2.0	sphinxcontrib-applehelp		toolz	0.12.0
QDarkStyle	3.0.2	1.0.2		tornado	6.2
qstylizer	0.1.10	sphinxcontrib-devhelp		tqdm	4.64.1
QtAwesome	1.0.3	1.0.2		traitlets	5.7.1
qtconsole	5.3.2	sphinxcontrib-htmlhelp		typing_extensions	4.4.0
QtPy	2.2.0	2.0.0		ujson	5.4.0
requests	2.28.1	sphinxcontrib-jsmath	1.0.1	uncompyle6	3.8.0
rope	0.22.0	sphinxcontrib-qthelp	1.0.3	Unidecode	1.2.0
Rtree	0.9.7	sphinxcontrib-serializinghtml	1.1.5	urllib3	1.26.13
ruamel.yaml	0.17.21	spyder	5.3.3	watchdog	2.1.6
ruamel.yaml.clib	0.2.6	spyder-kernels	2.3.3	wcwidth	0.2.5
scipy	1.9.3	stack-data	0.2.0	webencodings	0.5.1
Send2Trash	1.8.0	sympy	1.9	websocket-client	0.58.0
serial	0.0.97	terminado	0.17.1	whatthepatch	1.0.2
setuptools	65.5.0	testpath	0.6.0	wheel	0.37.1
sip	6.6.2	text-unidecode	1.3	widgetsnbextension	3.5.2
six	1.16.0			win-inet-pton	1.1.0

wincertstore	0.2	xdis	6.0.3	yapf	0.31.0
wrapt	1.14.1	xmltodict	0.12.0	zipp	3.11.0

Appendix E Full Data Sets

Appendix E.1 High-Speed Image Sets

Appendix E.1.1 Smooth Platinum Under Constant Voltage Heating (exponential, no initial pulse)

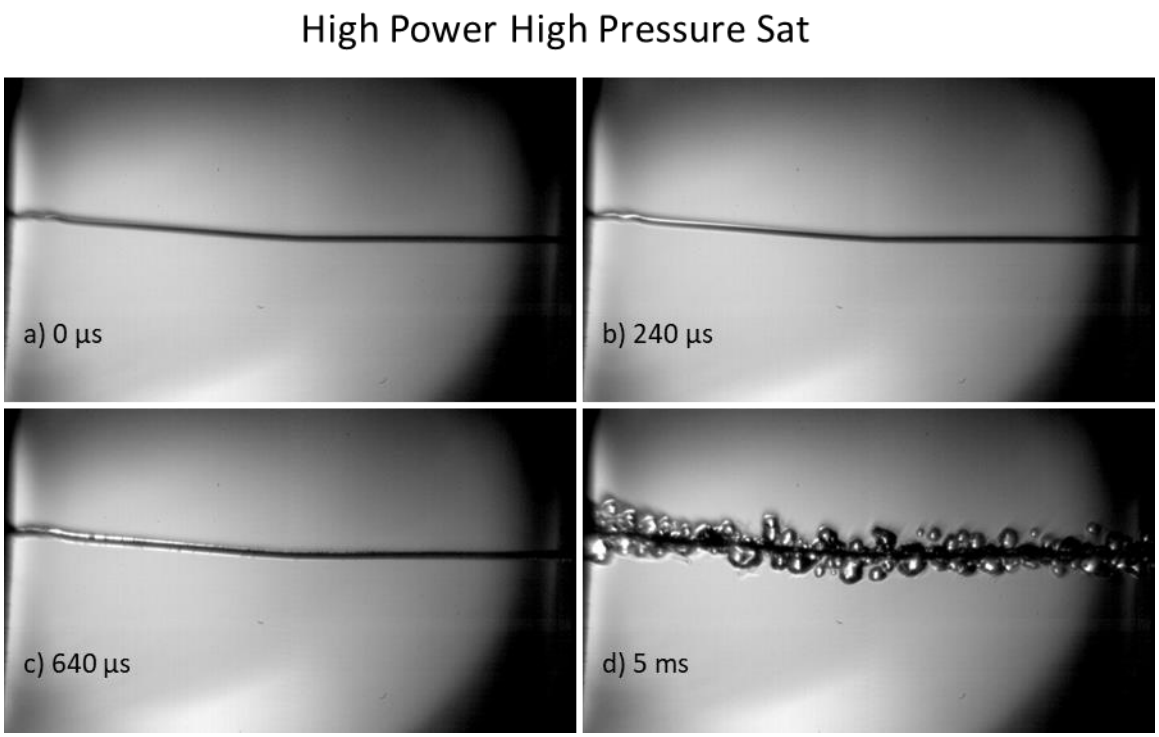

Appendix Figure 4: Smooth platinum under high power, high pressure, saturated condition with constant voltage heating bubbles is shown.

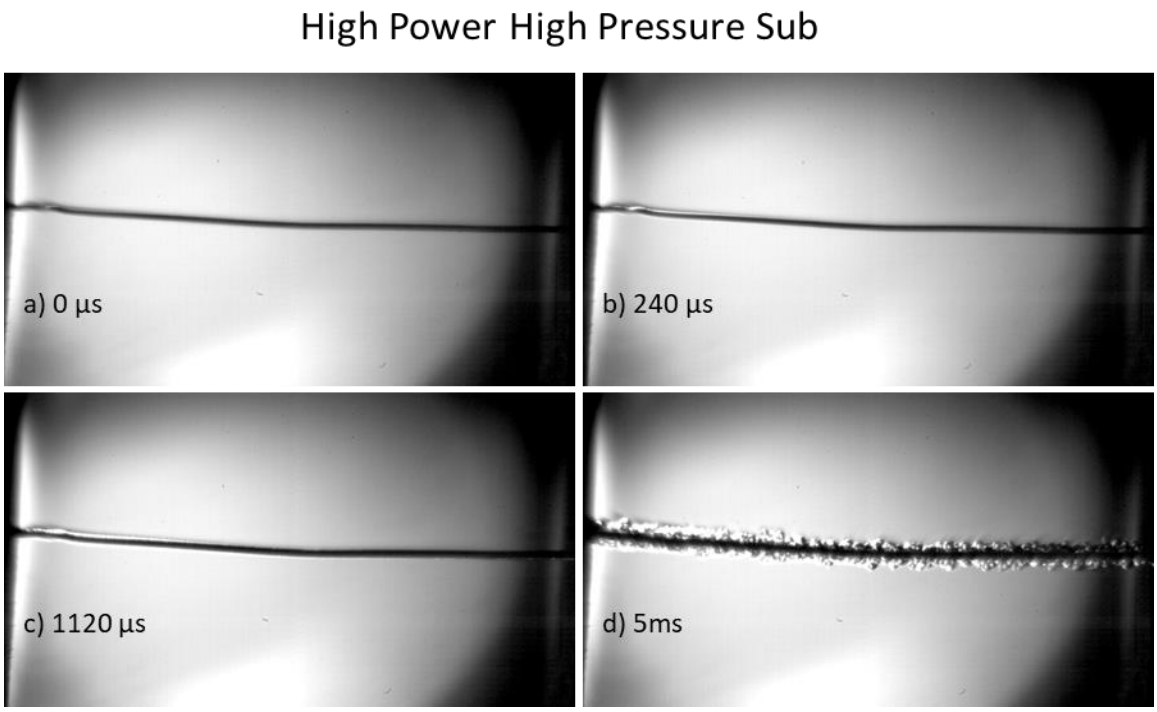

Appendix Figure 5: Smooth platinum under under high power, high pressure, subcooled condition with constant voltage heating bubbles is shown.

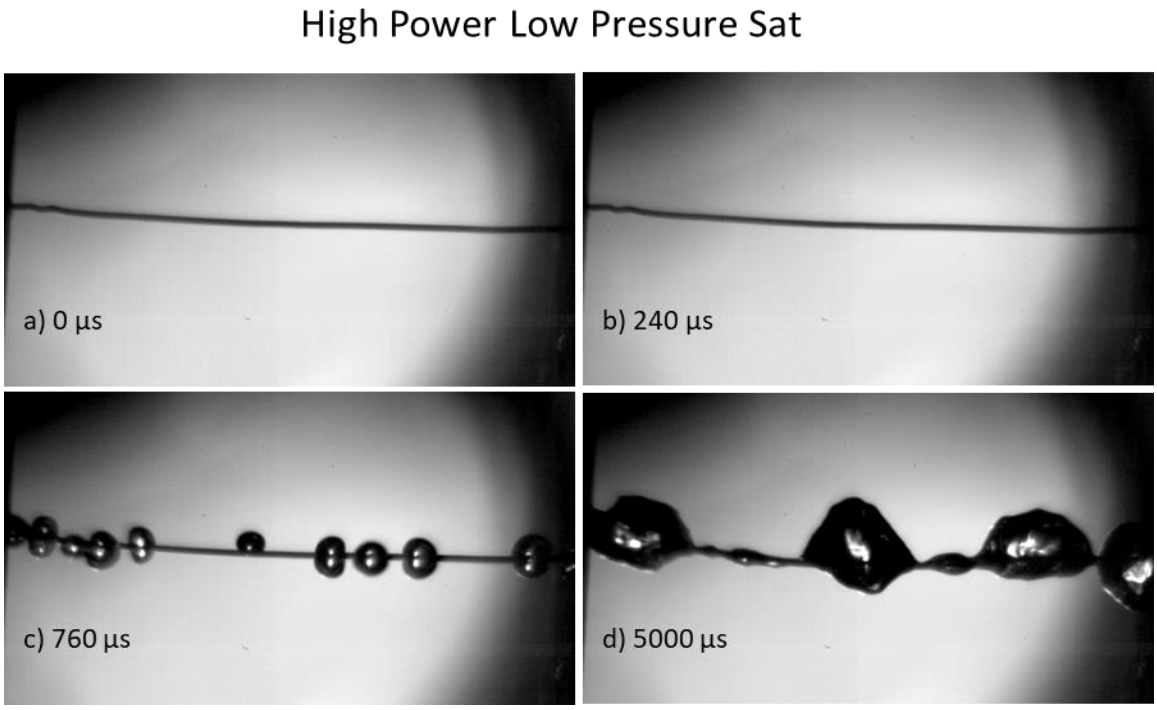

Appendix Figure 6: Smooth platinum under high power, low pressure, saturated condition with constant voltage heating bubbles is shown.

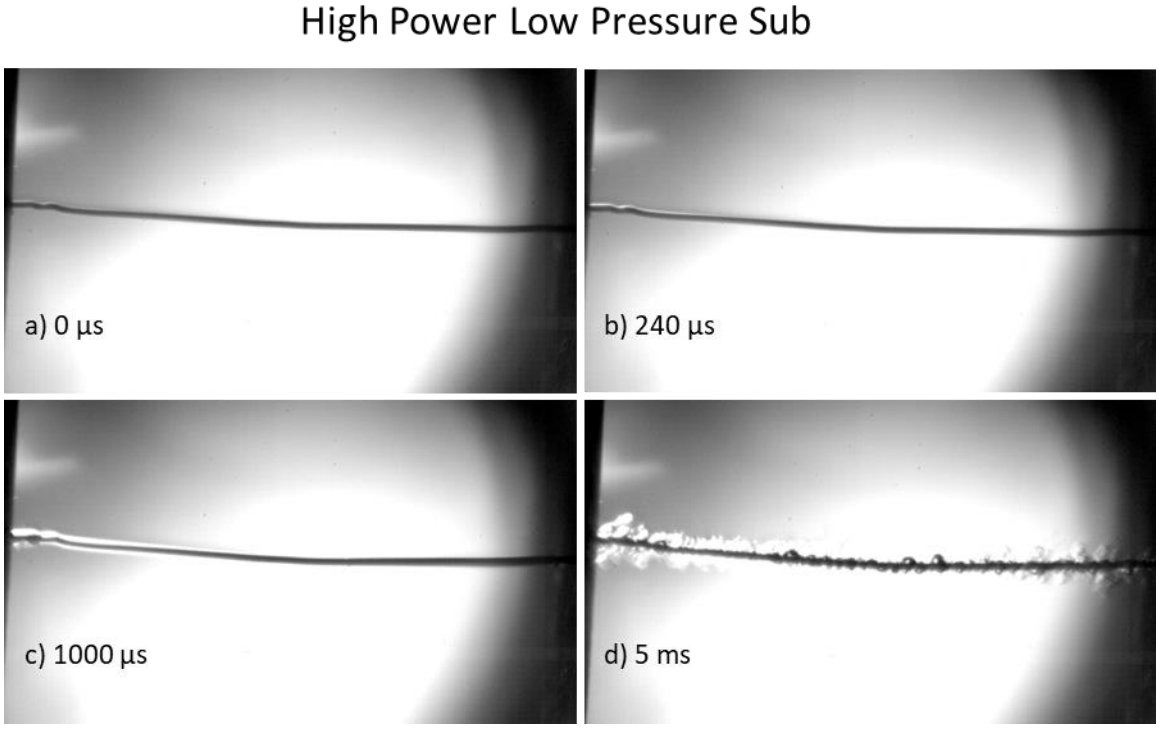

Appendix Figure 7: Smooth platinum under under high power, low pressure, subcooled condition with constant voltage heating bubbles is shown.

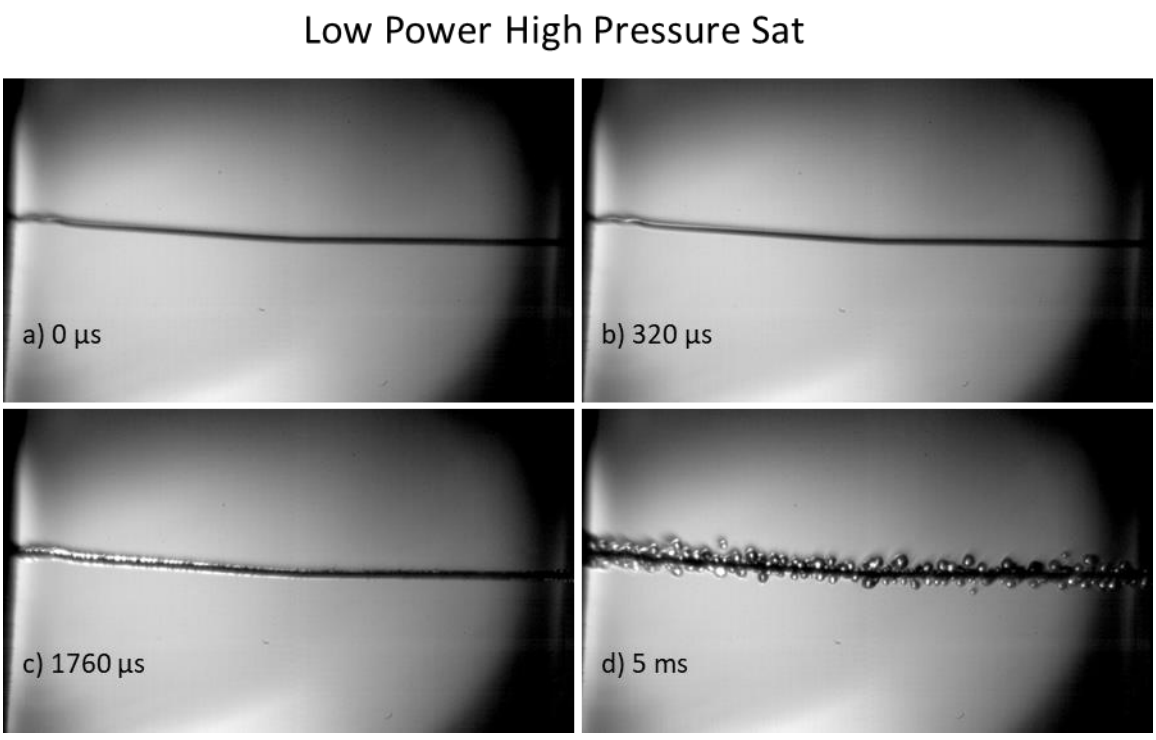

Appendix Figure 8: Smooth platinum under low power, high pressure, saturated condition with constant voltage heating bubbles is shown.

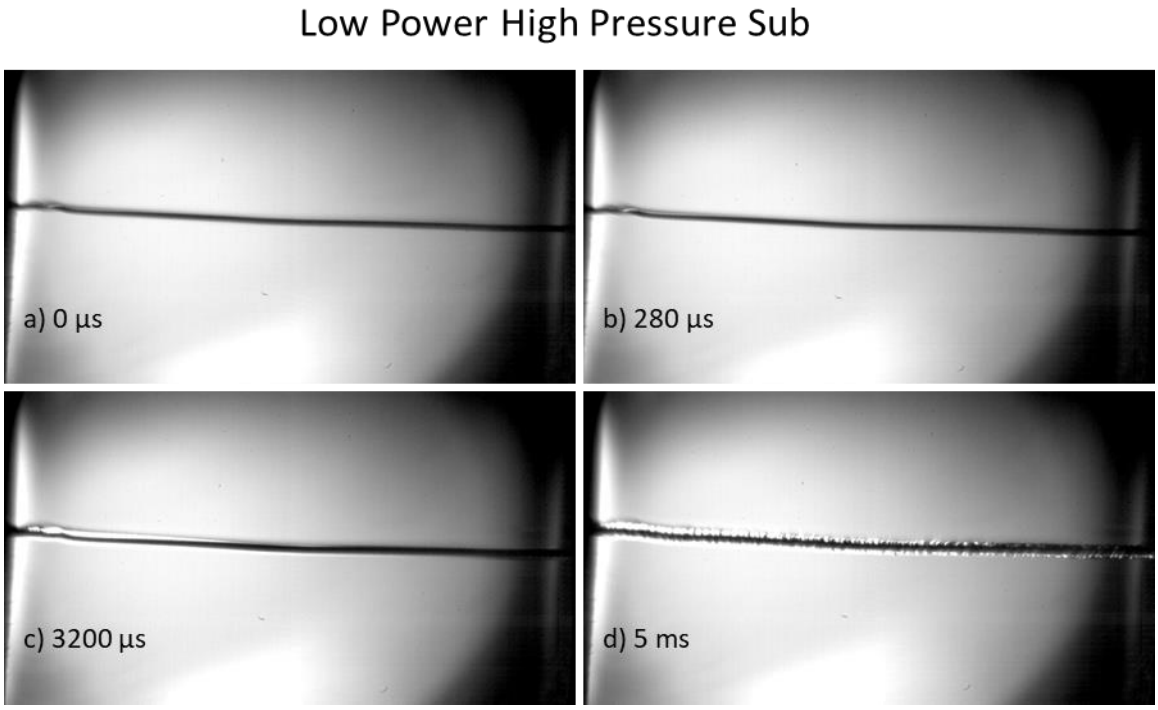

Appendix Figure 9: Smooth platinum under low power, high pressure, subcooled condition with constant voltage heating bubbles is shown.

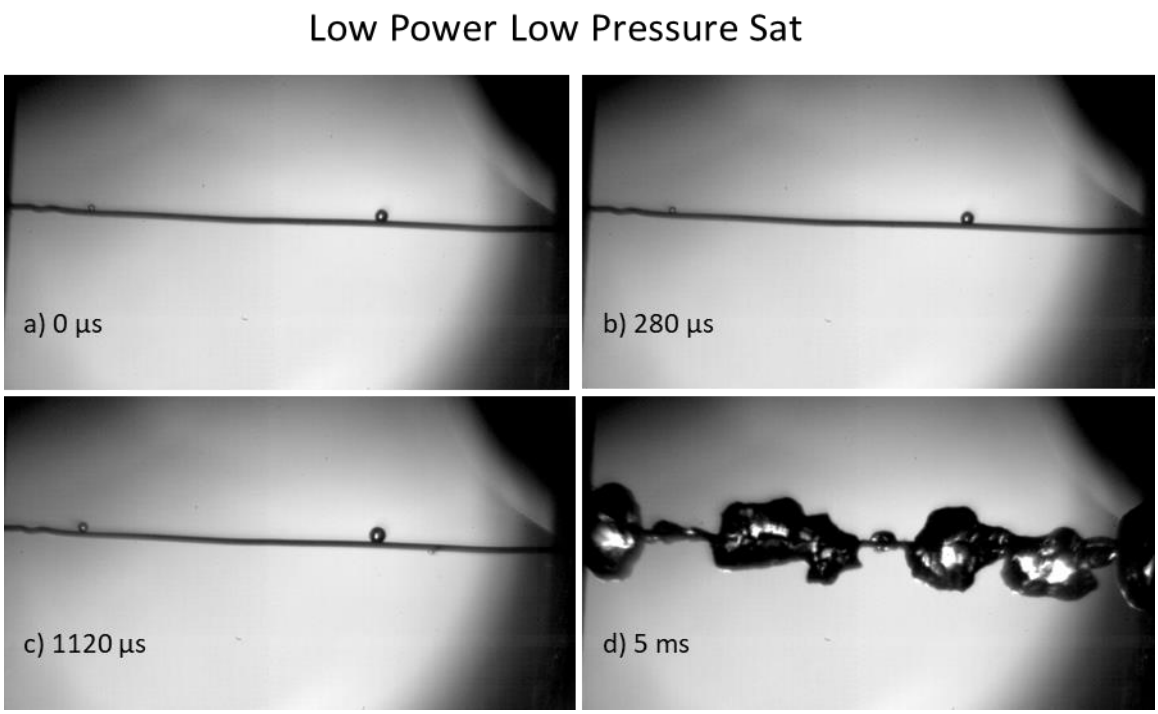

Appendix Figure 10: Smooth platinum under low power, low pressure, saturated condition with constant voltage heating bubbles is shown.

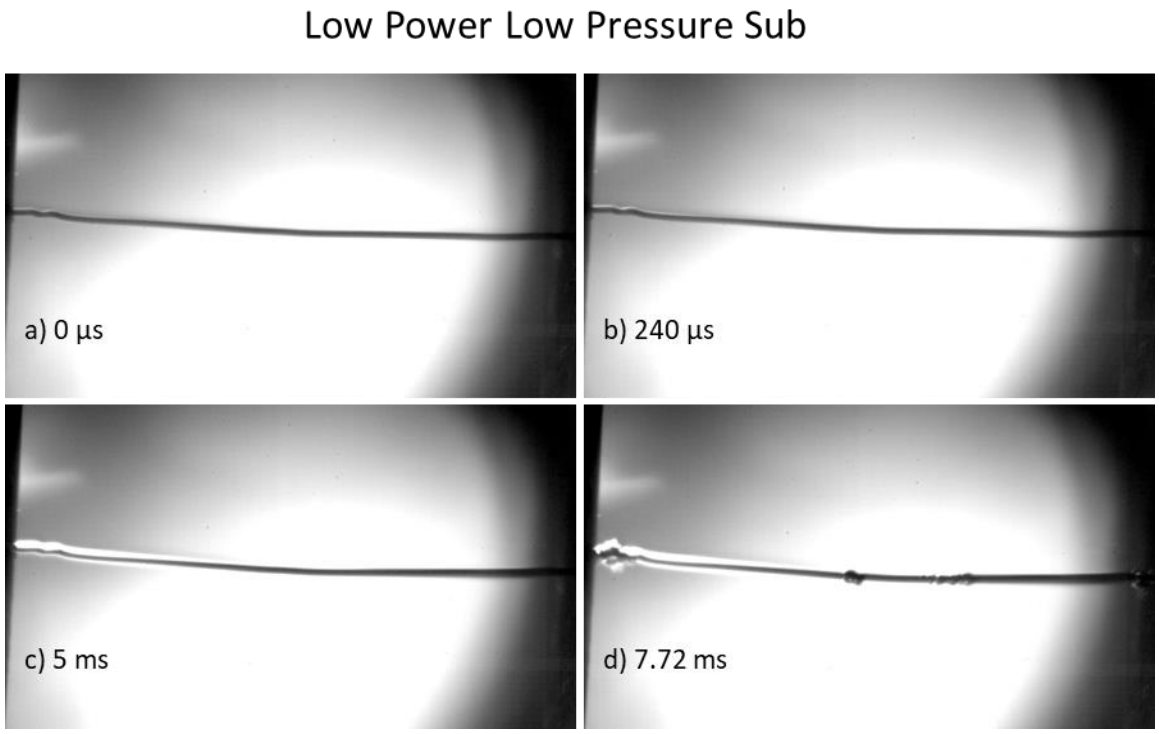

Appendix Figure 11: Smooth platinum under low power, low pressure, subcooled condition with constant voltage heating bubbles is shown.

Appendix E.1.2 Smooth Platinum Under Constant Current Heating (semi-exponential with large initial pulse)

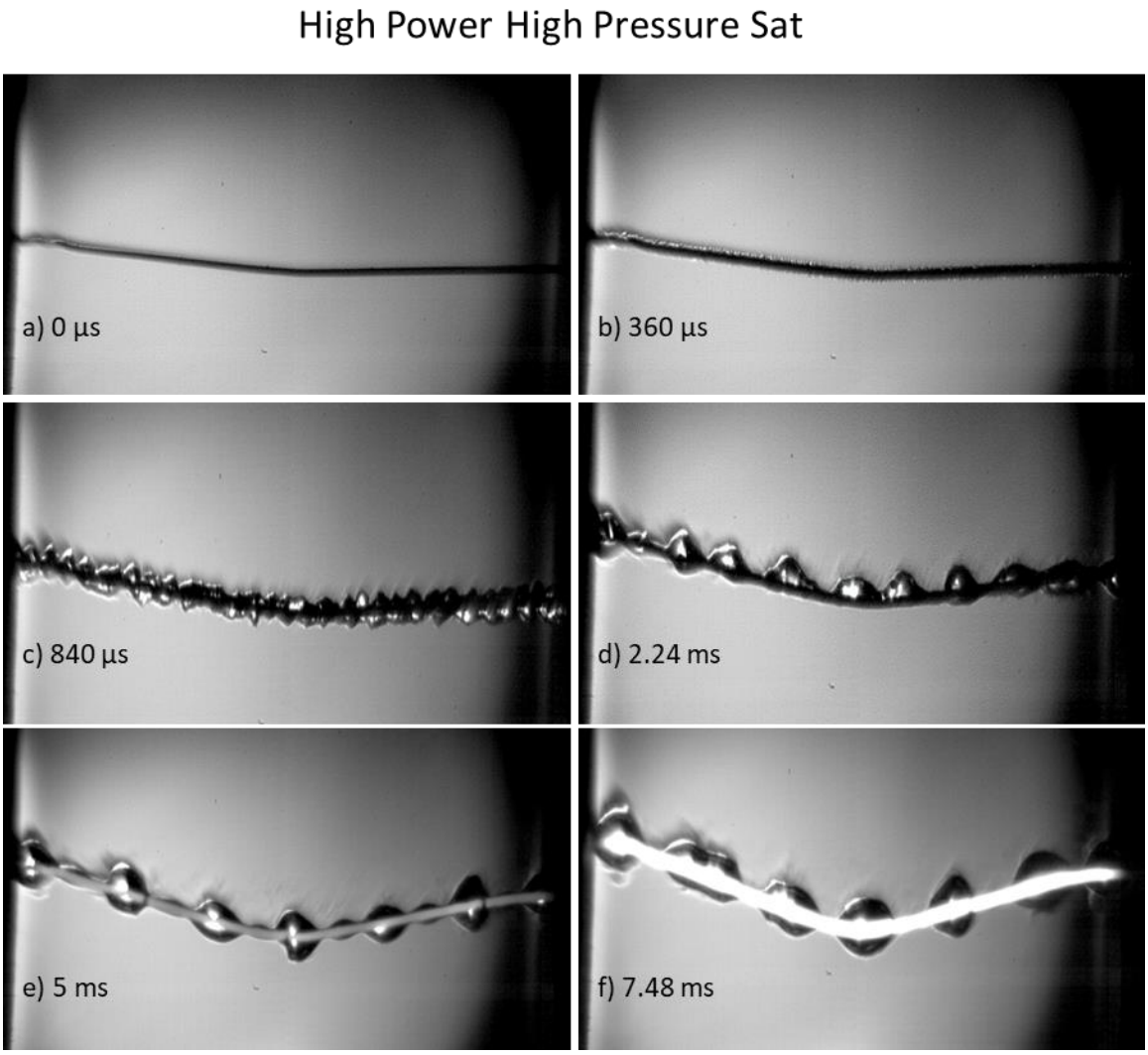

Appendix Figure 12: Smooth platinum under high power, high pressure, saturated condition with constant current heating bubbles is shown.

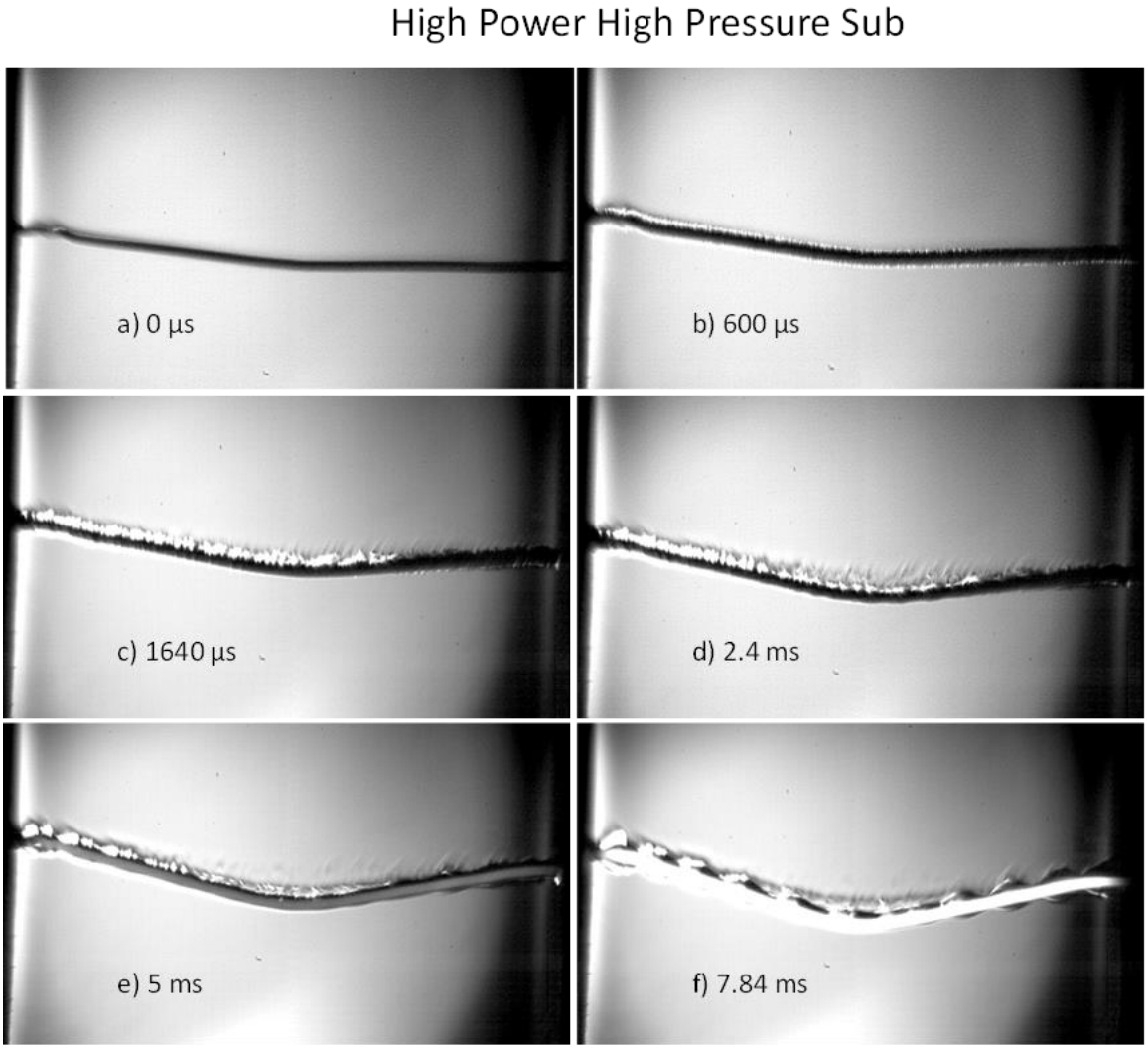

Appendix Figure 13: Smooth platinum under high power, high pressure, subcooled condition with constant current heating bubbles is shown.

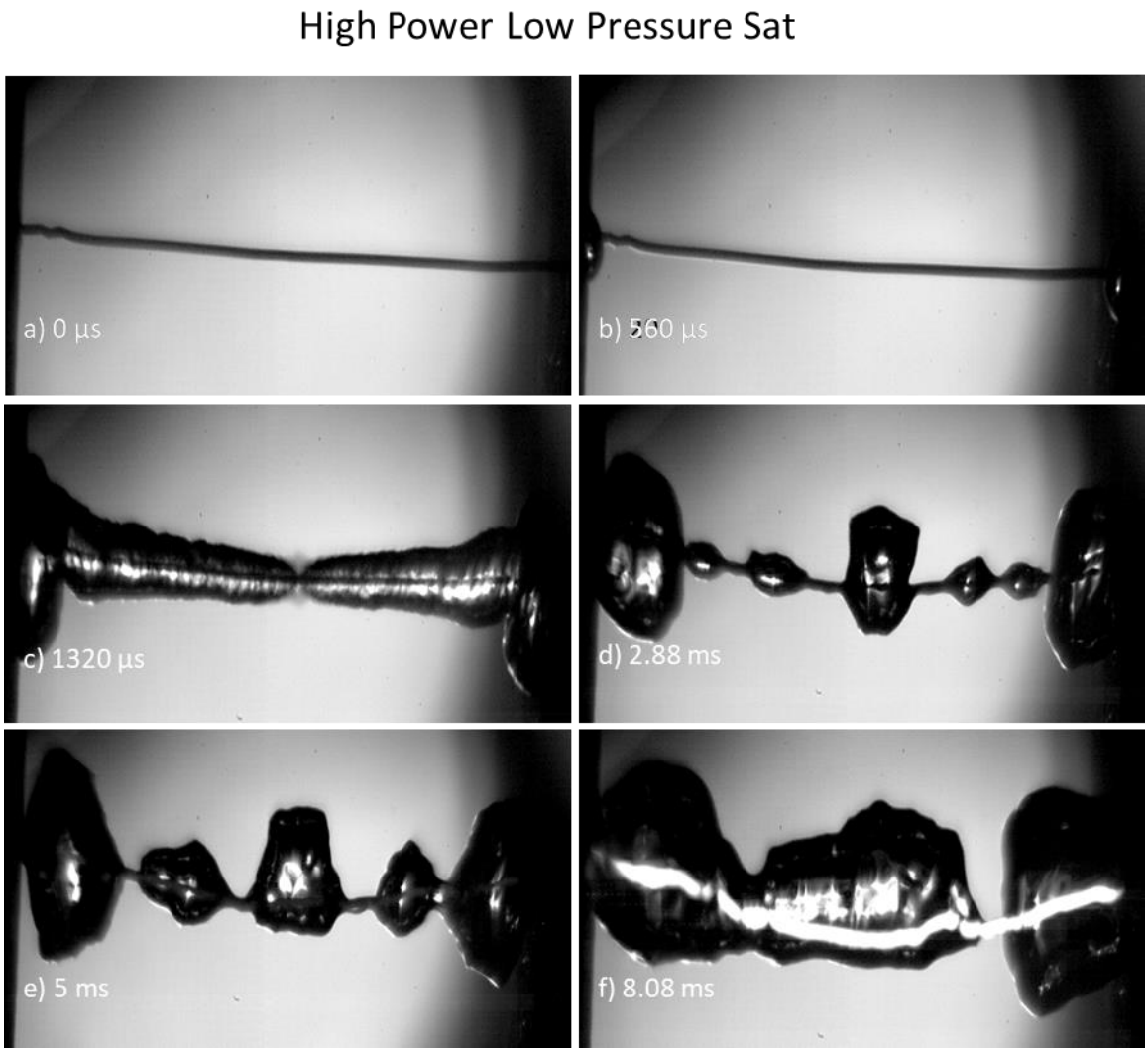

Appendix Figure 14: Smooth platinum under high power, low pressure, saturated condition with constant current heating bubbles is shown.

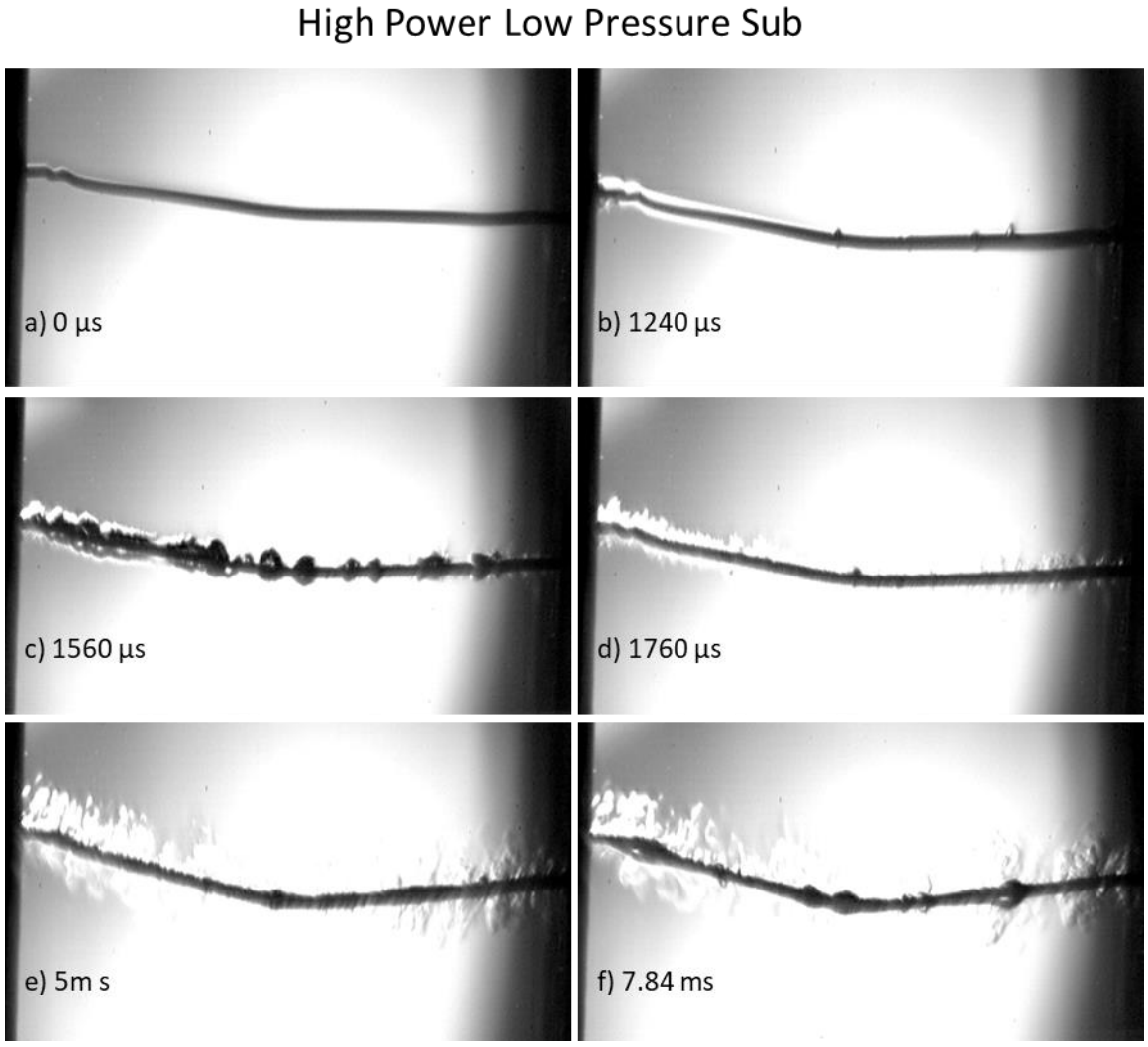

Appendix Figure 15: Smooth platinum under high power, low pressure, subcooled condition with constant current heating bubbles is shown.

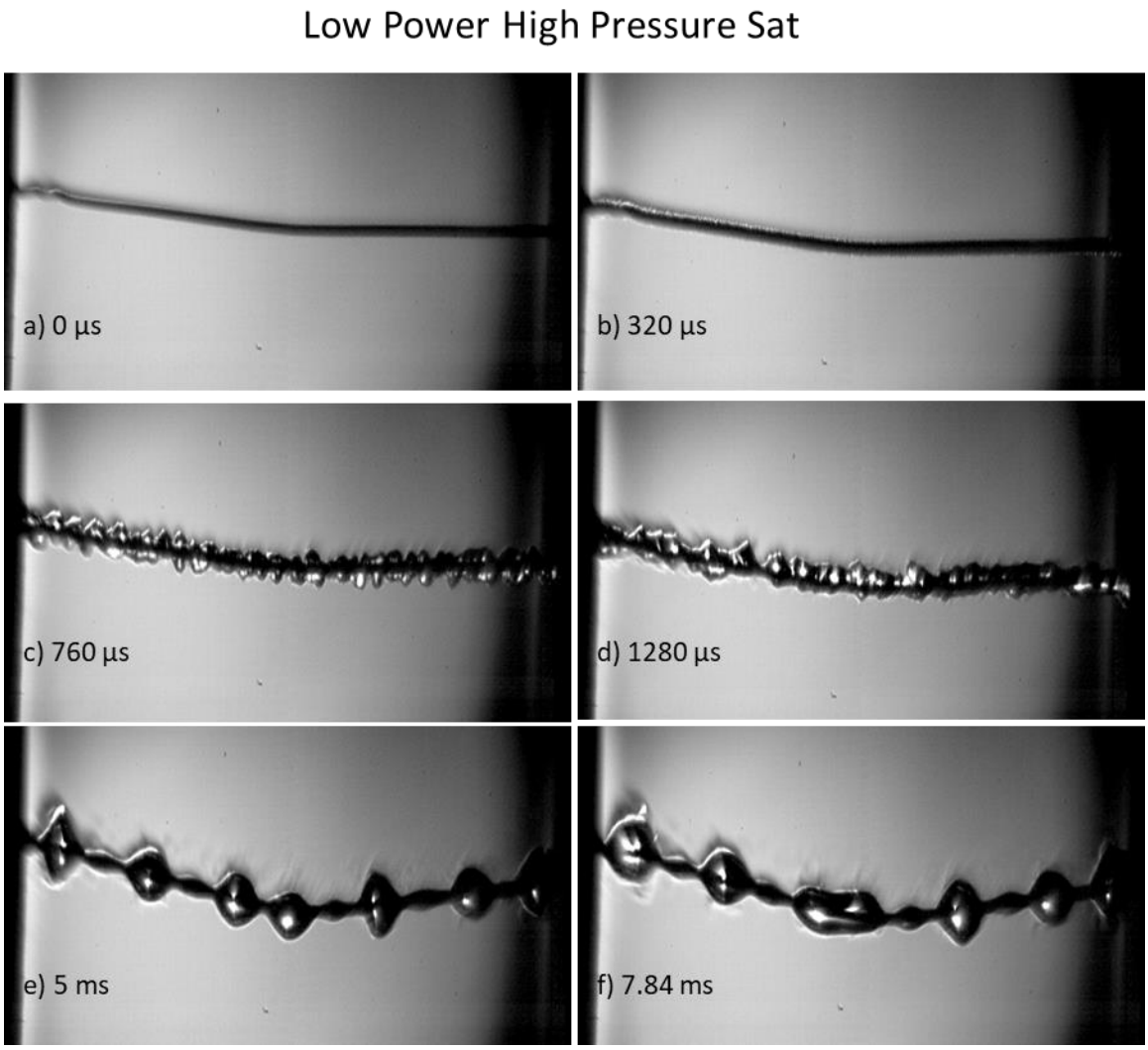

Appendix Figure 16: Smooth platinum under low power, high pressure, saturated condition with constant current heating bubbles is shown.

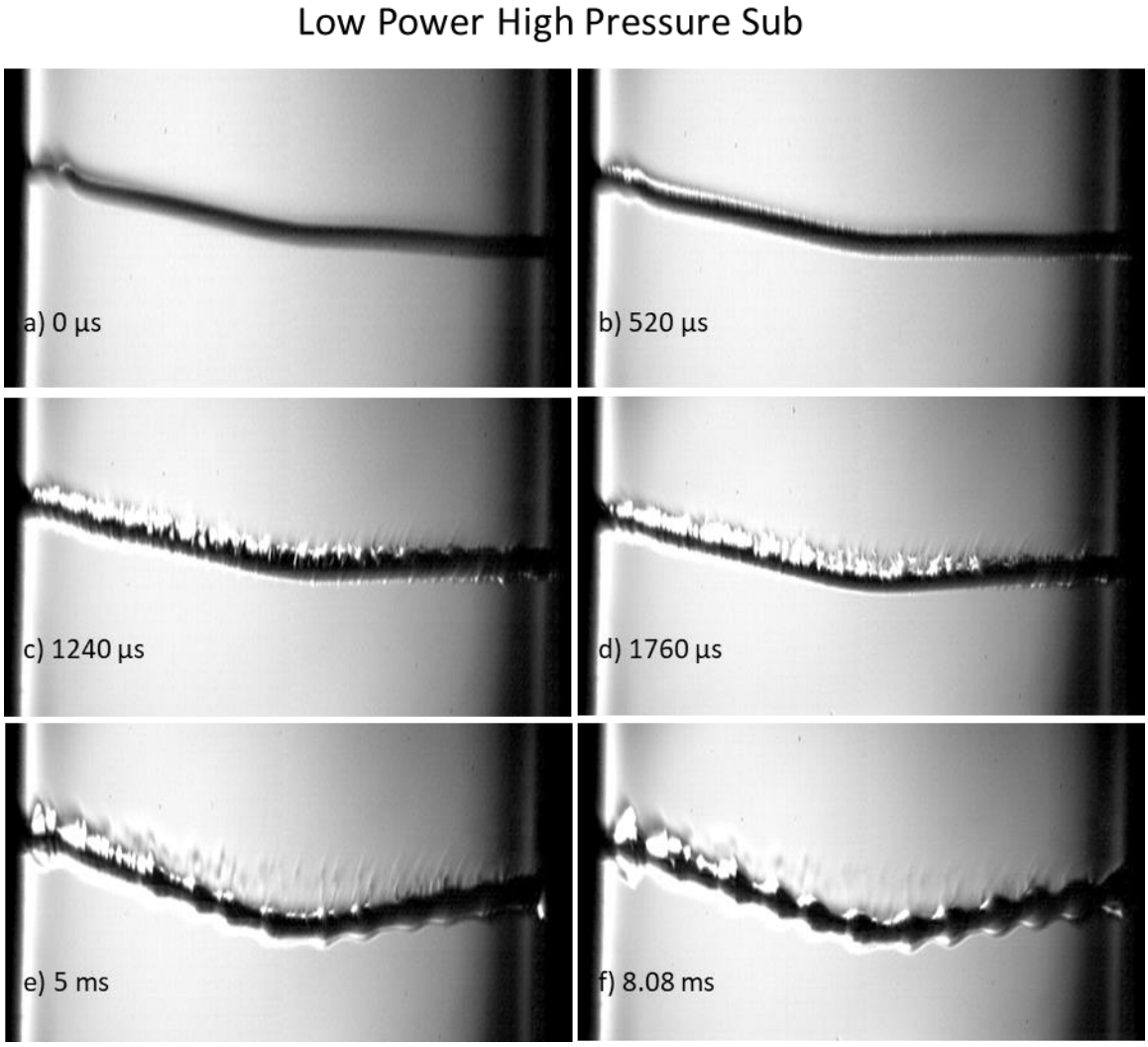

Appendix Figure 17: Smooth platinum under low power, high pressure, subcooled condition with constant current heating bubbles is shown.

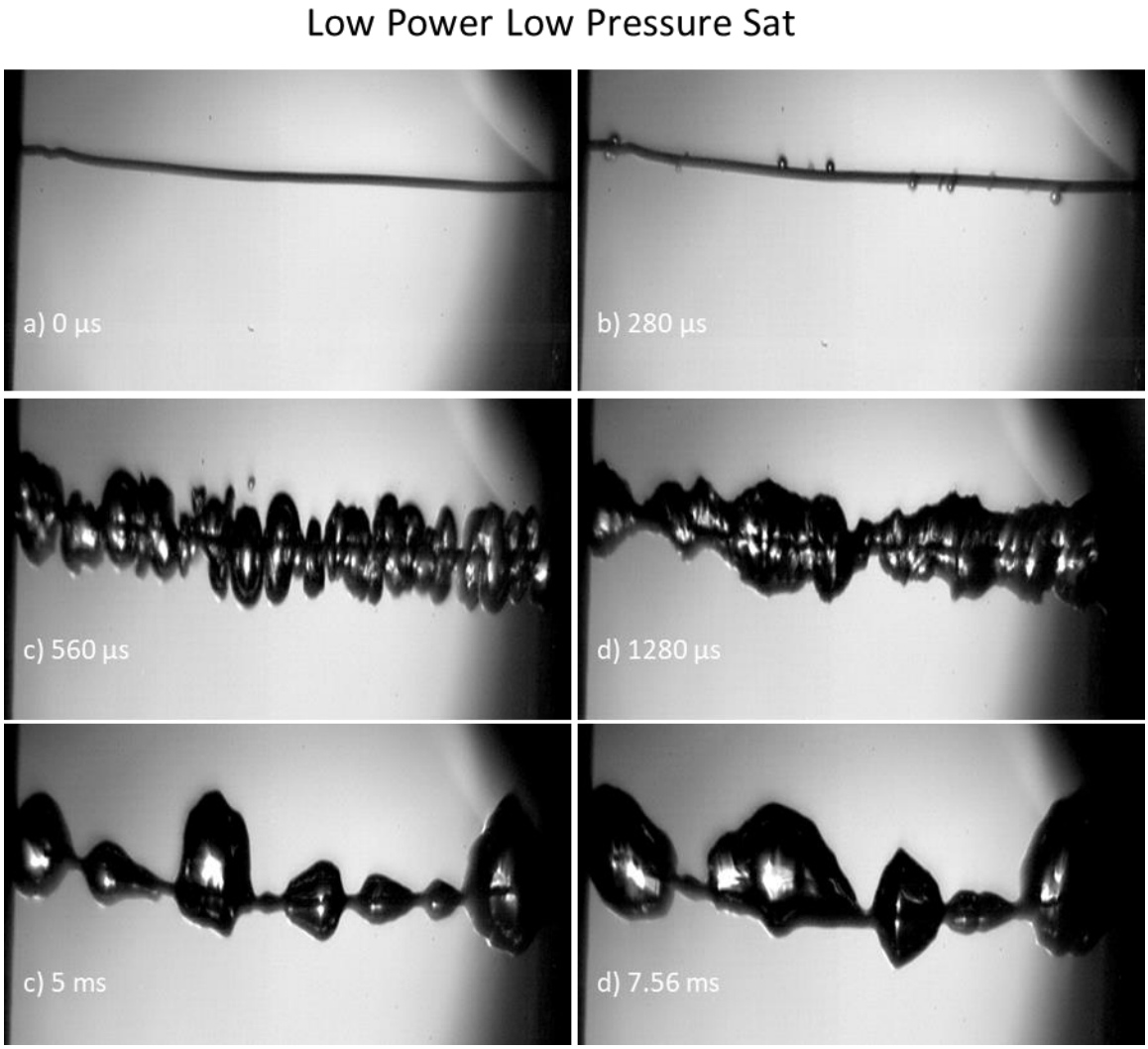

Appendix Figure 18: Smooth platinum under low power, low pressure, saturated condition with constant current heating bubbles is shown.

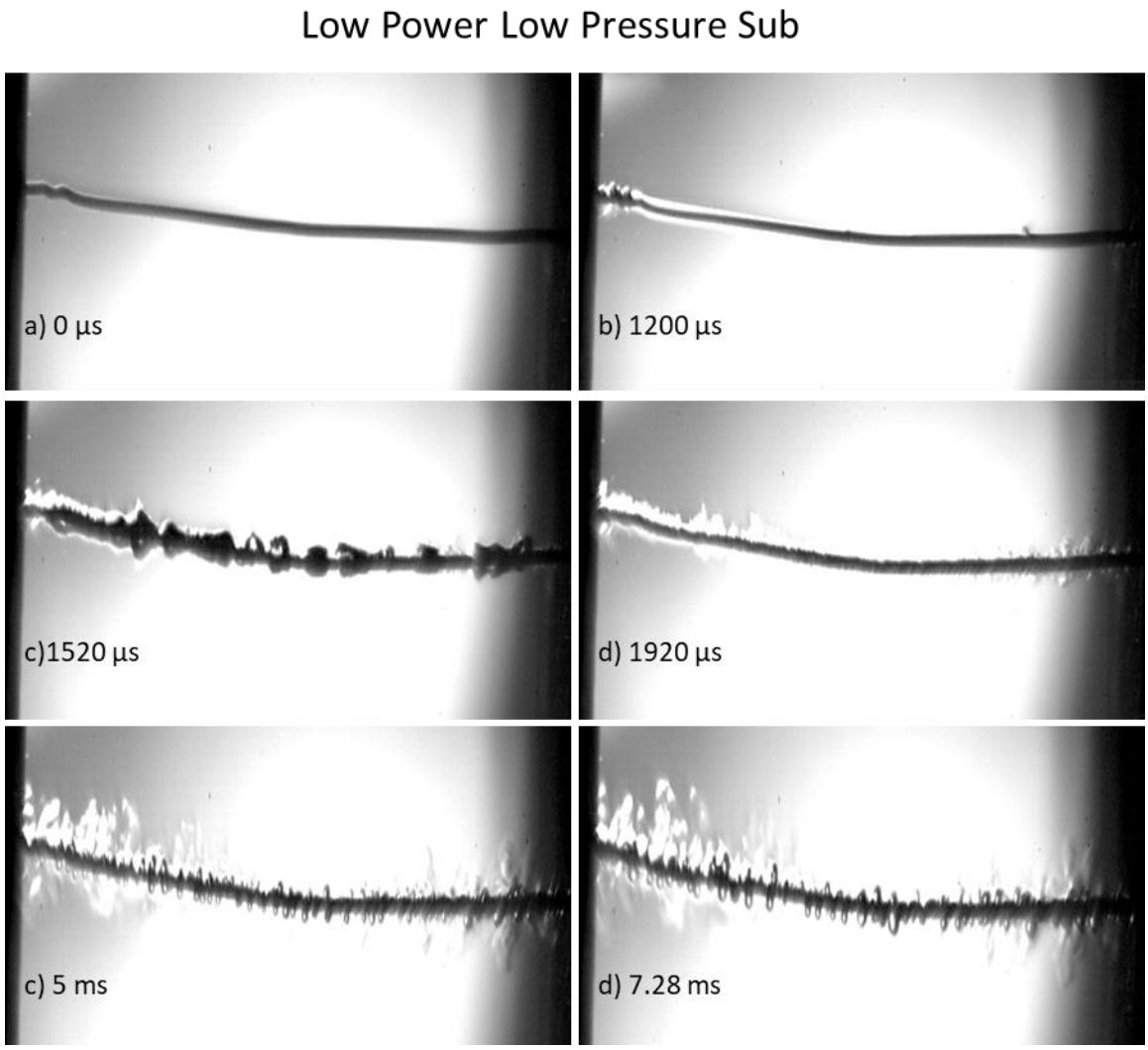

Appendix Figure 19: Smooth platinum under low power, low pressure, subcooled condition with constant current heating bubbles is shown.

Appendix E.1.3 Smooth Platinum Under Pulse Increase Heating (exponential, the pre and post heating levels equal and nonzero)

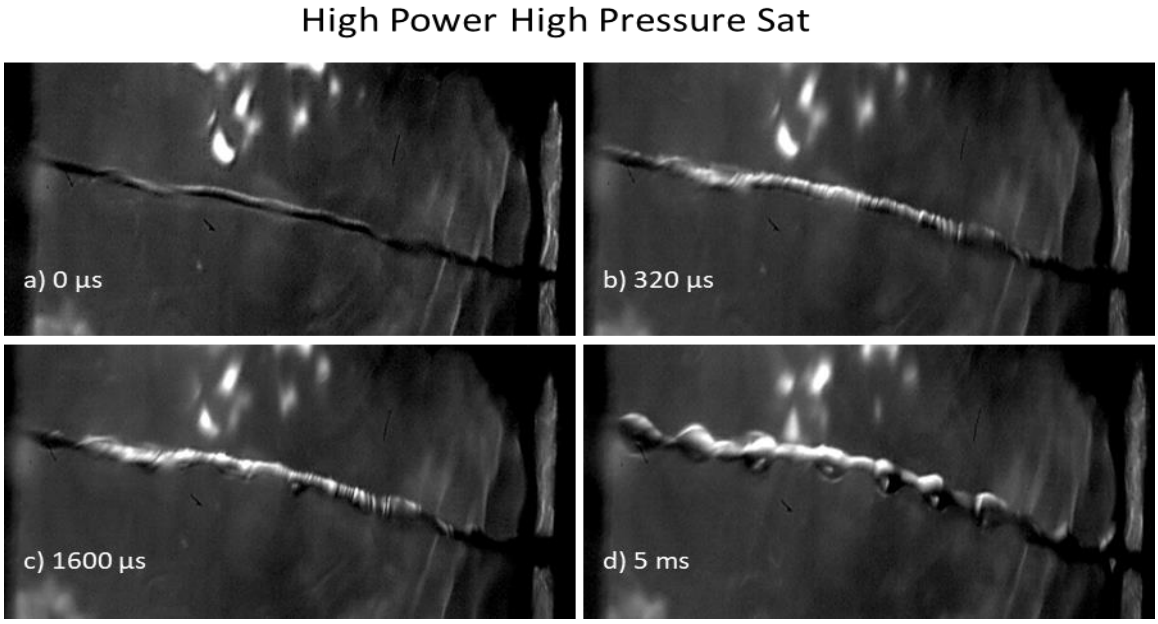

Appendix Figure 20: Smooth platinum under high power, high pressure, saturated condition with pulse increase heating bubbles is shown.

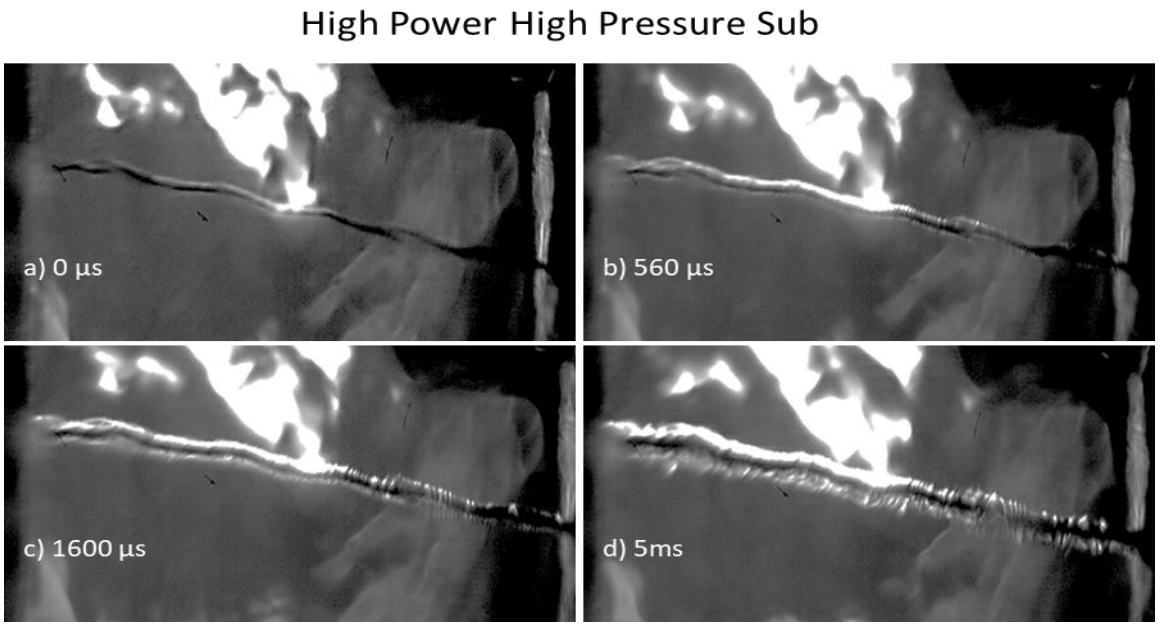

Appendix Figure 21: Smooth platinum under high power, high pressure, subcooled condition with pulse increase heating bubbles is shown.

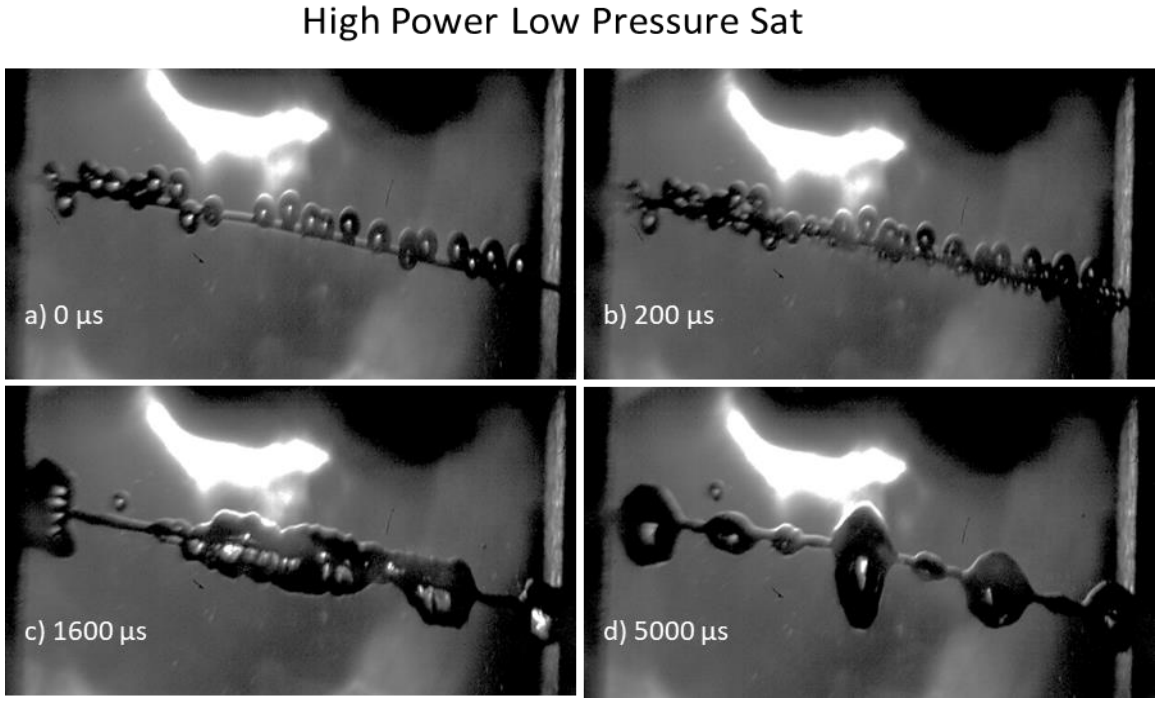

Appendix Figure 22: Smooth platinum under high power, low pressure, saturated condition with pulse increase heating bubbles is shown.

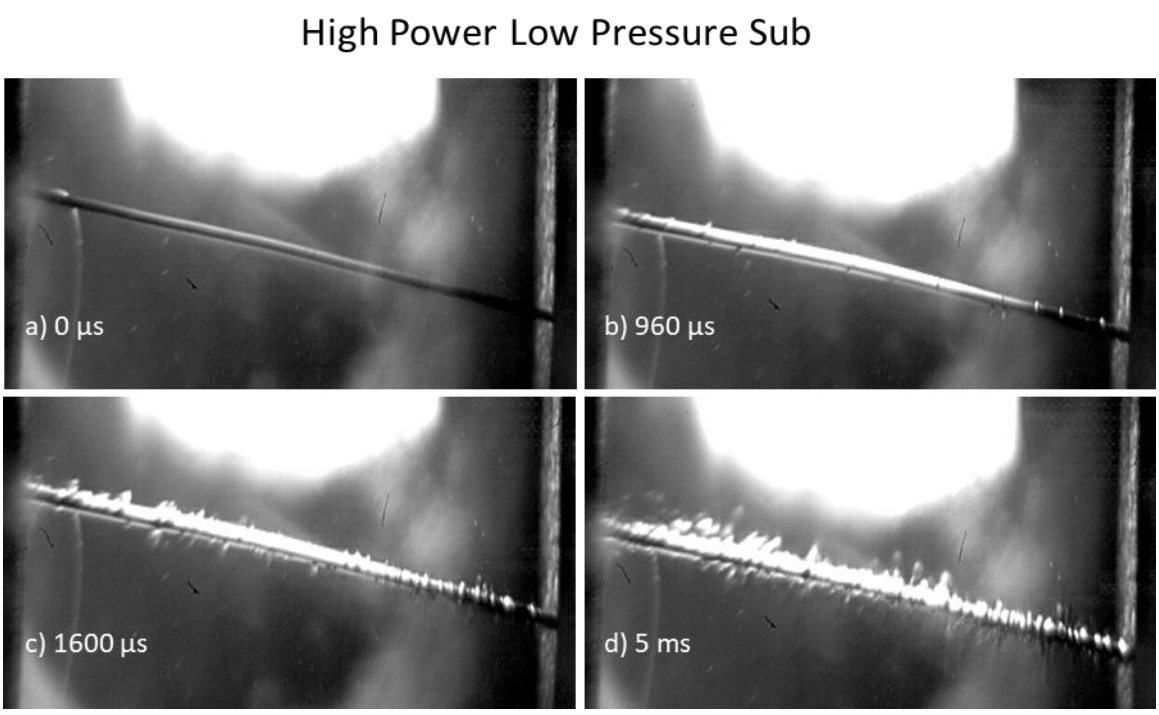

Appendix Figure 23: Smooth platinum under high power, low pressure, subcooled condition with pulse increase heating bubbles is shown.

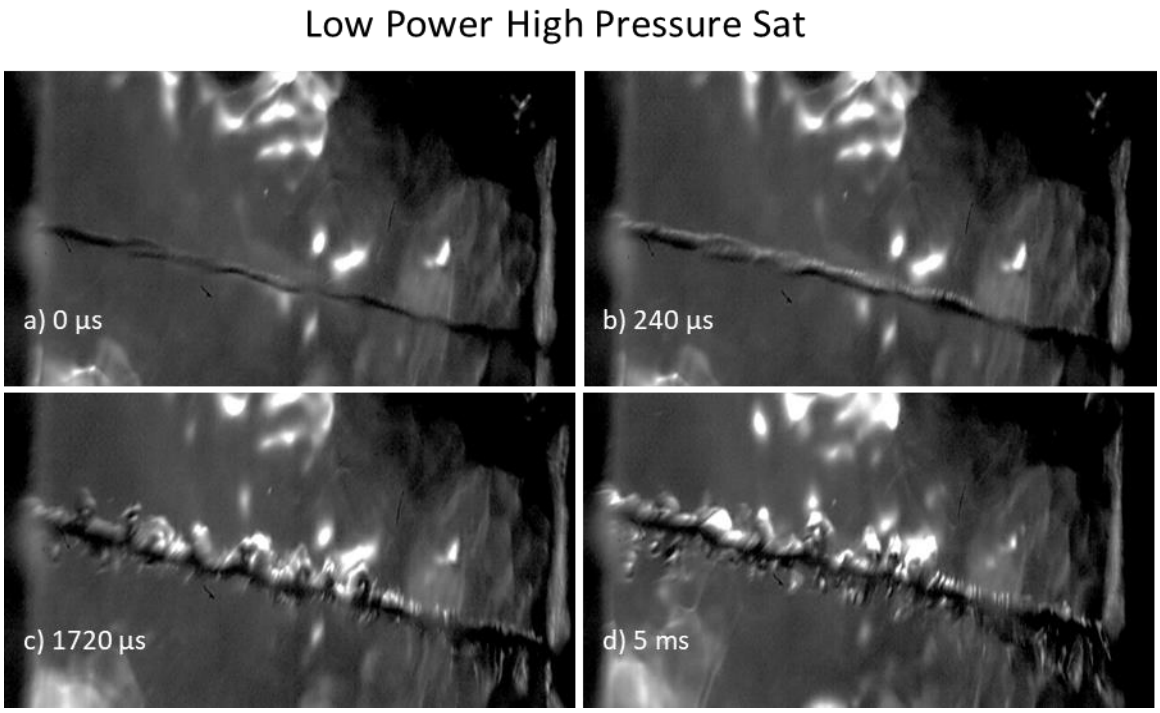

Appendix Figure 24: Smooth platinum under low power, high pressure, saturated condition with pulse increase heating bubbles is shown.

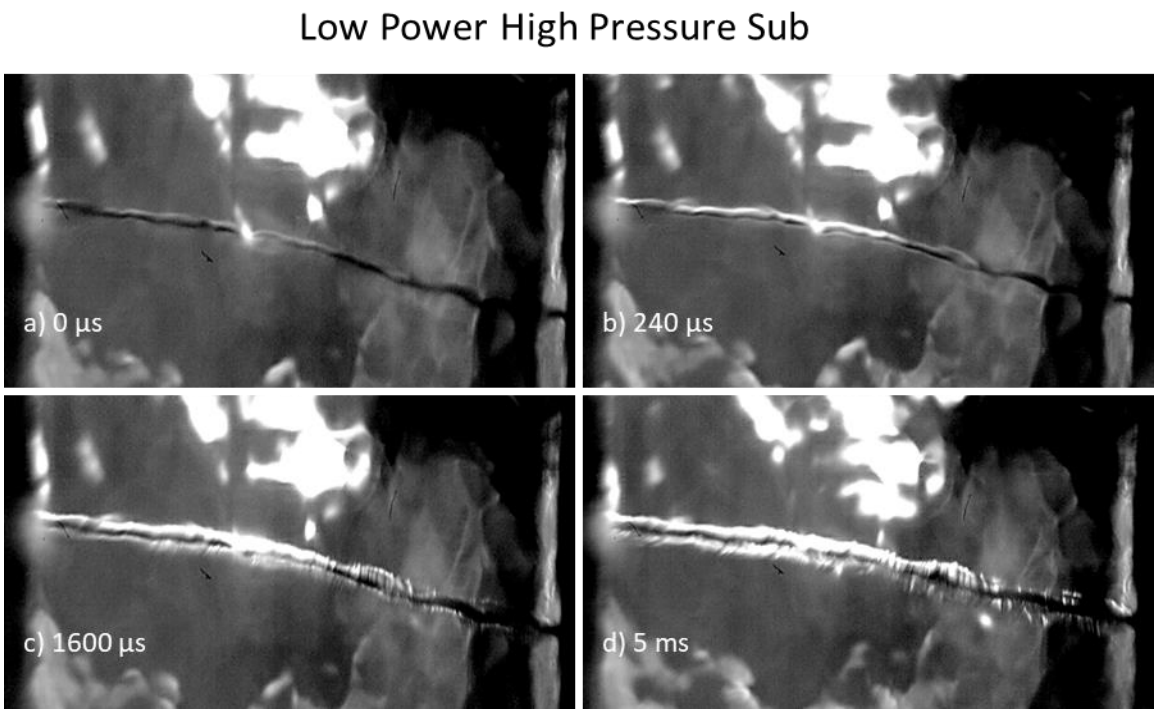

Appendix Figure 25: Smooth platinum under low power, high pressure, subcooled condition with pulse increase heating bubbles is shown.

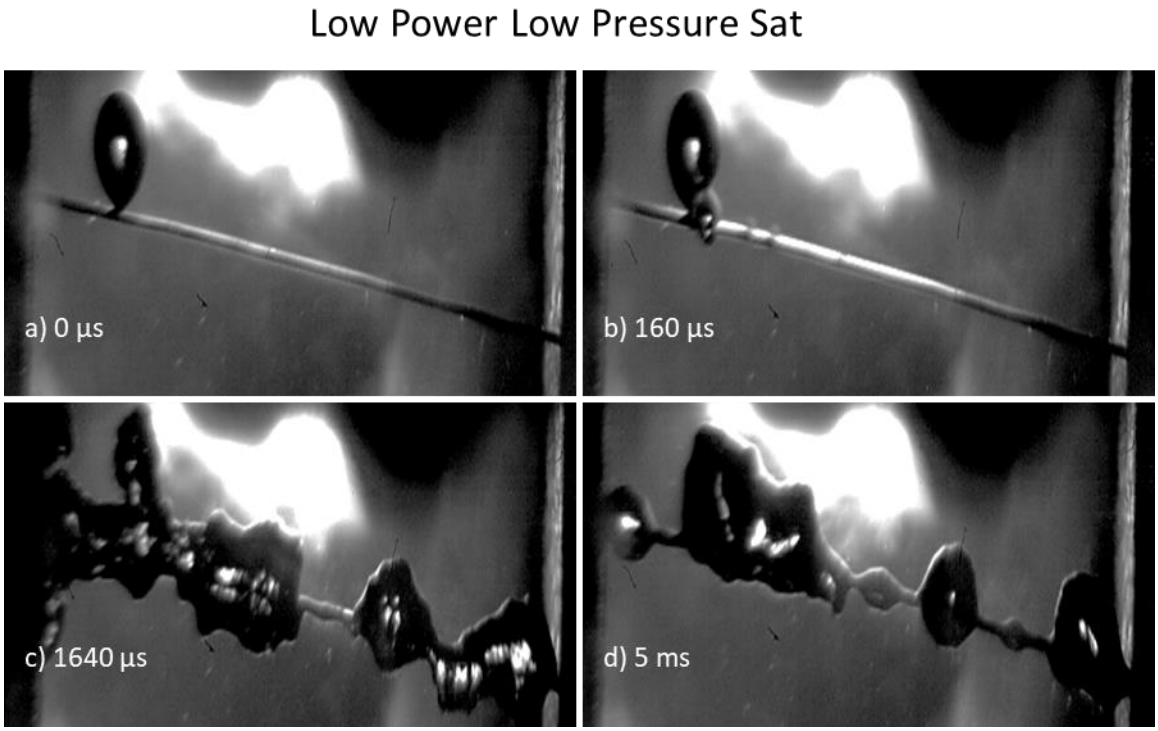

Appendix Figure 26: Smooth platinum under low power, low pressure, saturated condition with pulse increase heating bubbles is shown.

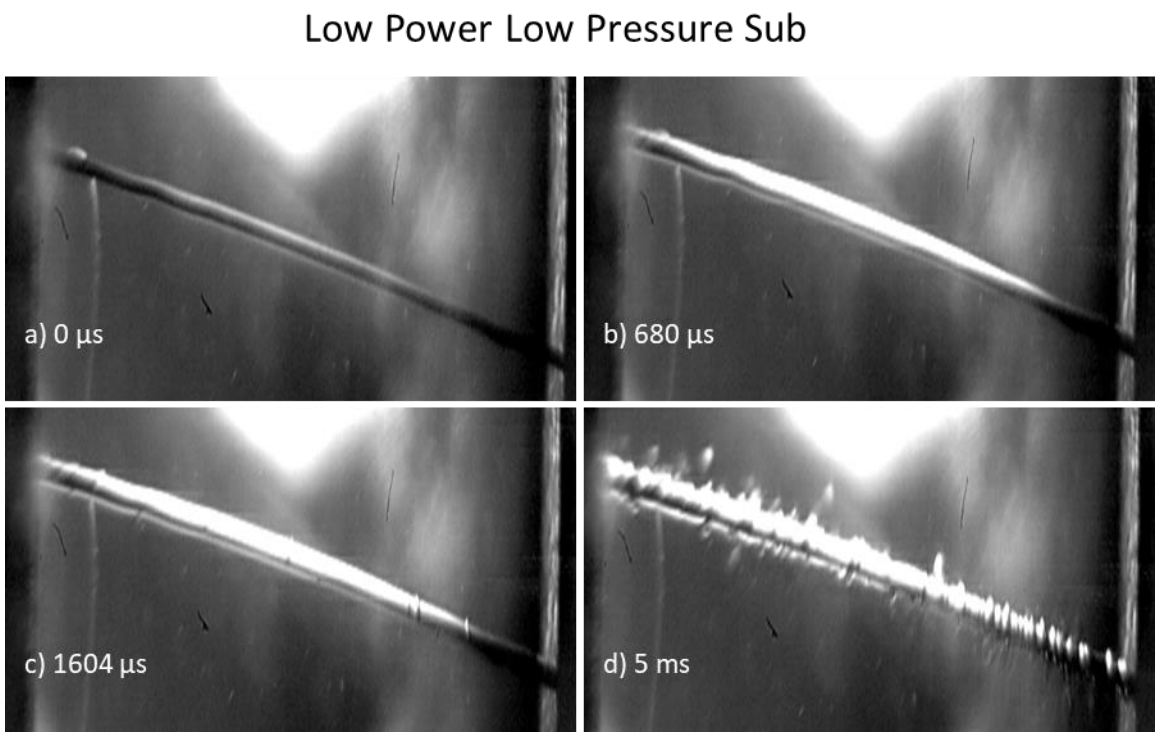

Appendix Figure 27: Smooth platinum under low power, low pressure, subcoooled condition with pulse increase heating bubbles is shown.

Appendix E.1.4 Rough Platinum Under Constant Voltage Heating (exponential, no initial pulse)

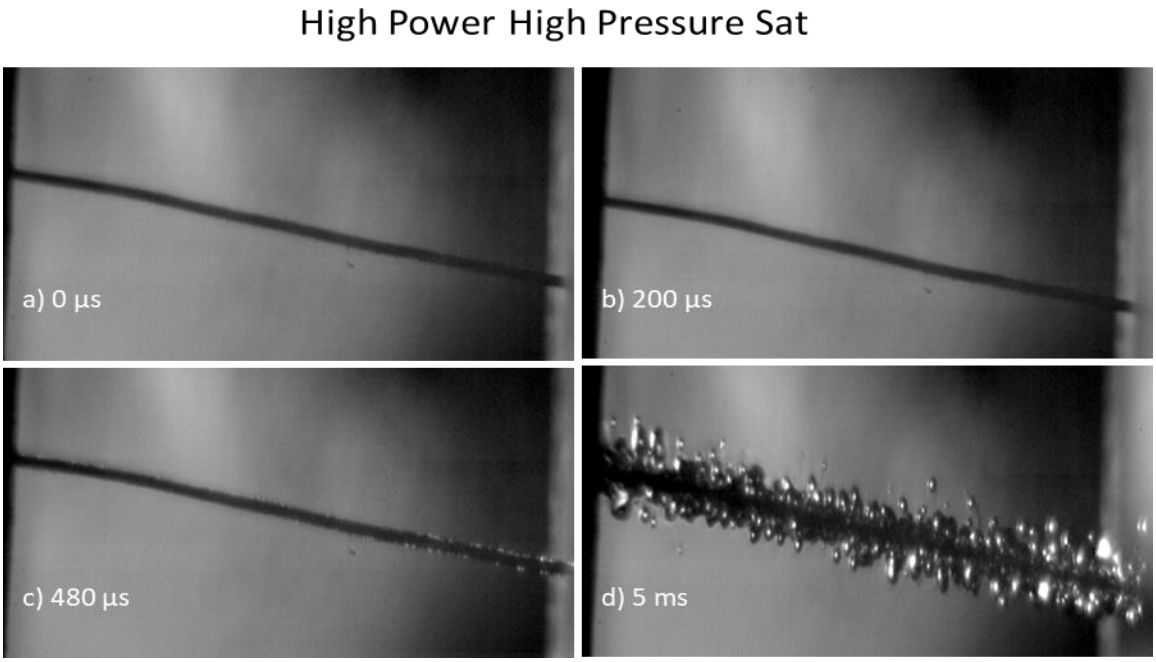

Appendix Figure 28: Rough platinum under high power, high pressure, saturated condition with constant voltage heating bubbles is shown.

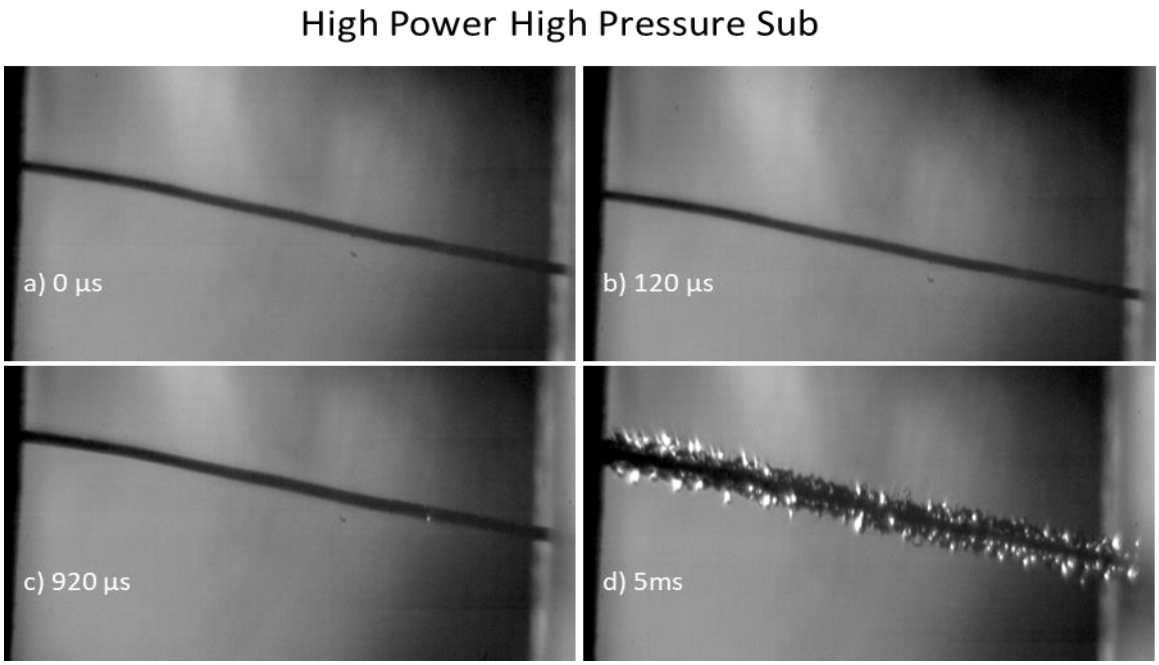

Appendix Figure 29: Rough platinum under high power, high pressure, subcooled condition with constant voltage heating bubbles is shown.

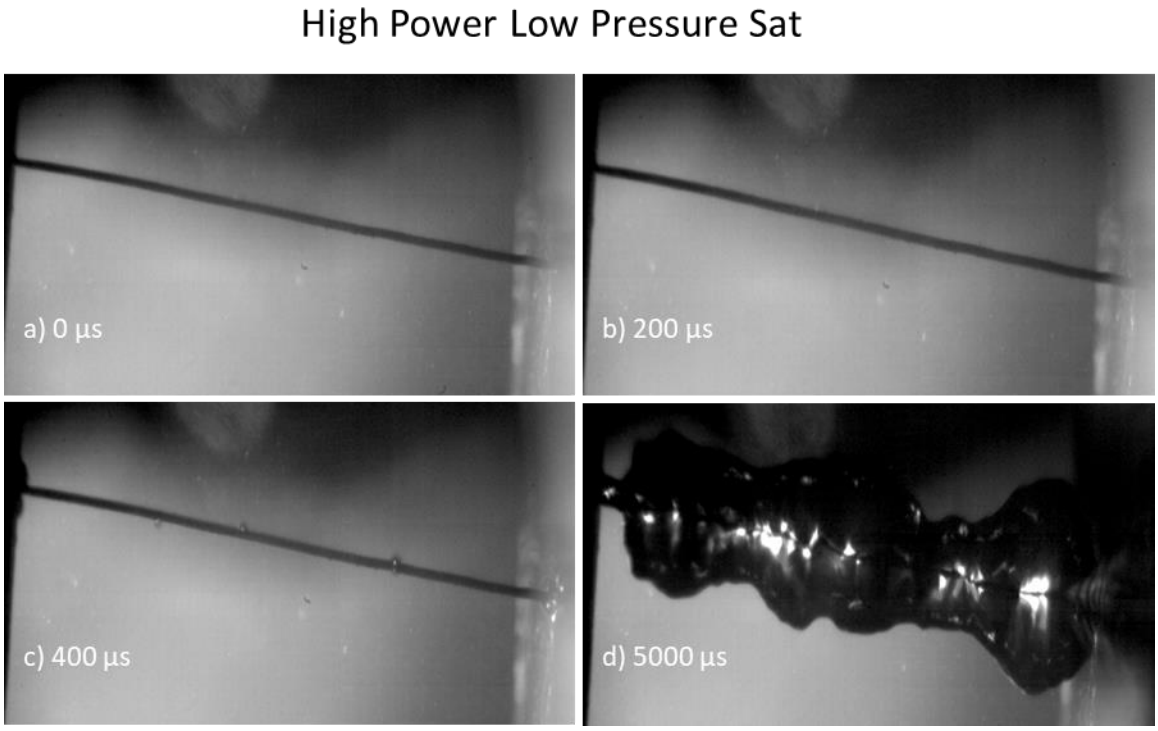

Appendix Figure 30: Rough platinum under high power, low pressure, saturated condition with constant voltage heating bubbles is shown.

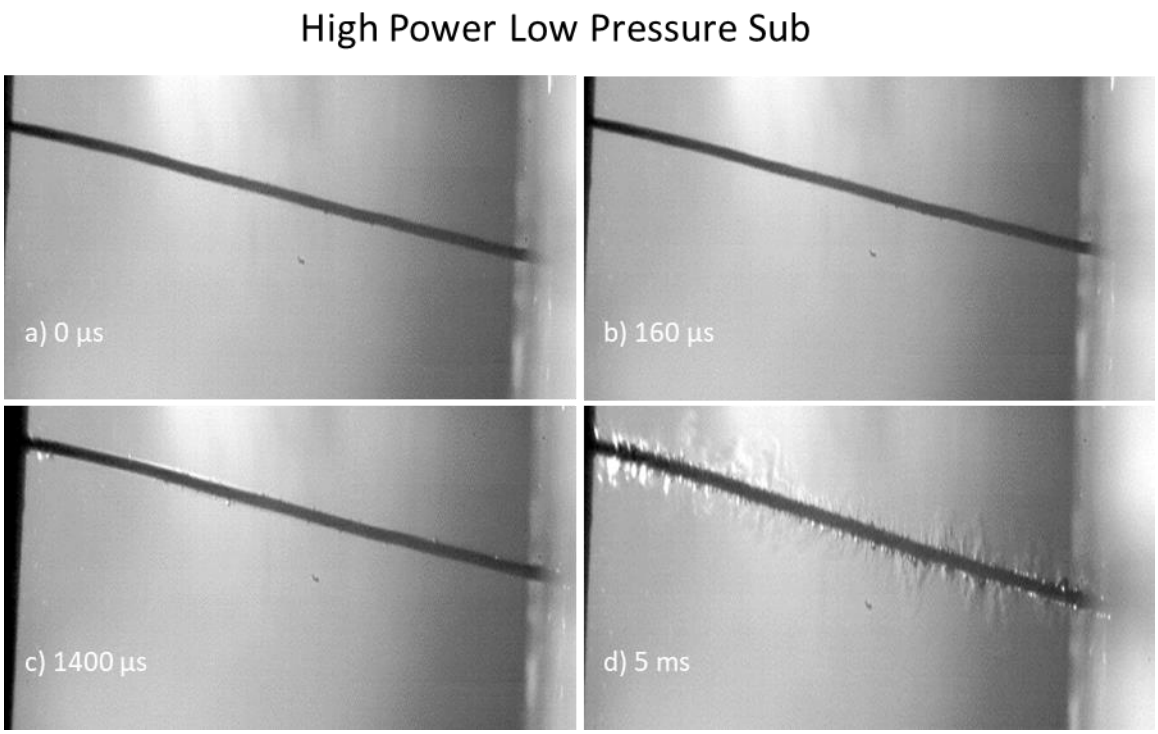

Appendix Figure 31: Rough platinum under high power, low pressure, subcooled condition with constant voltage heating bubbles is shown.

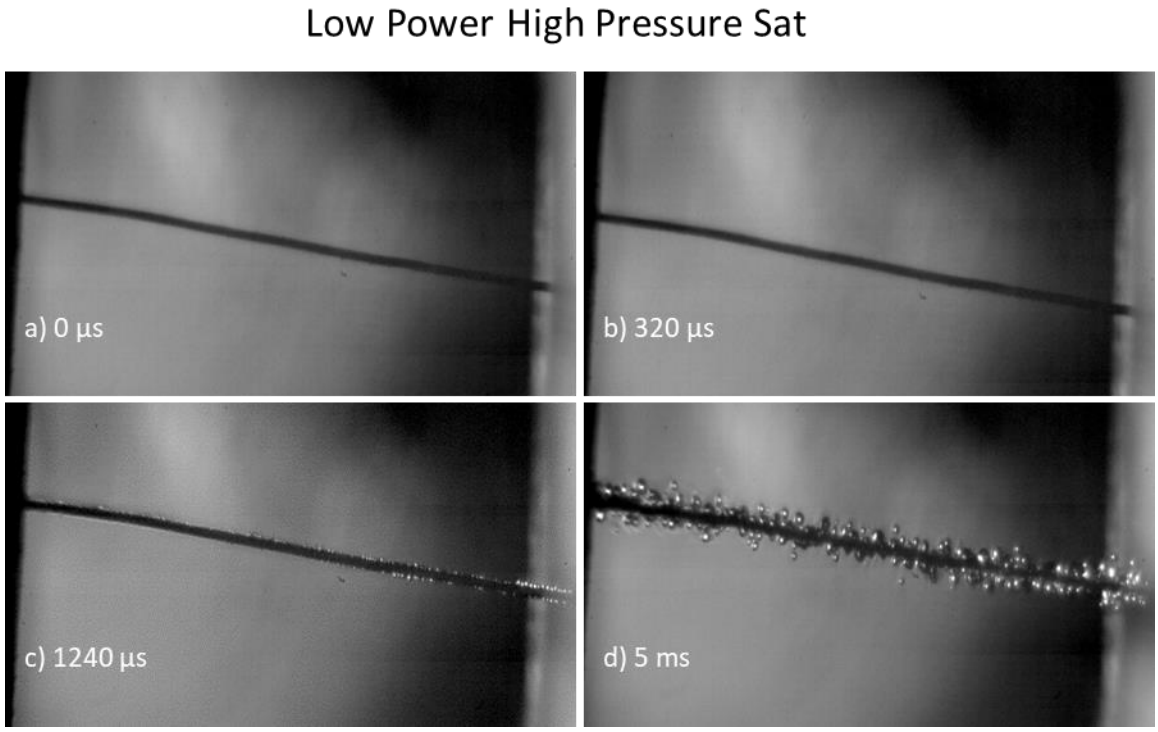

Appendix Figure 32: Rough platinum under low power, high pressure, saturated condition with constant voltage heating bubbles is shown.

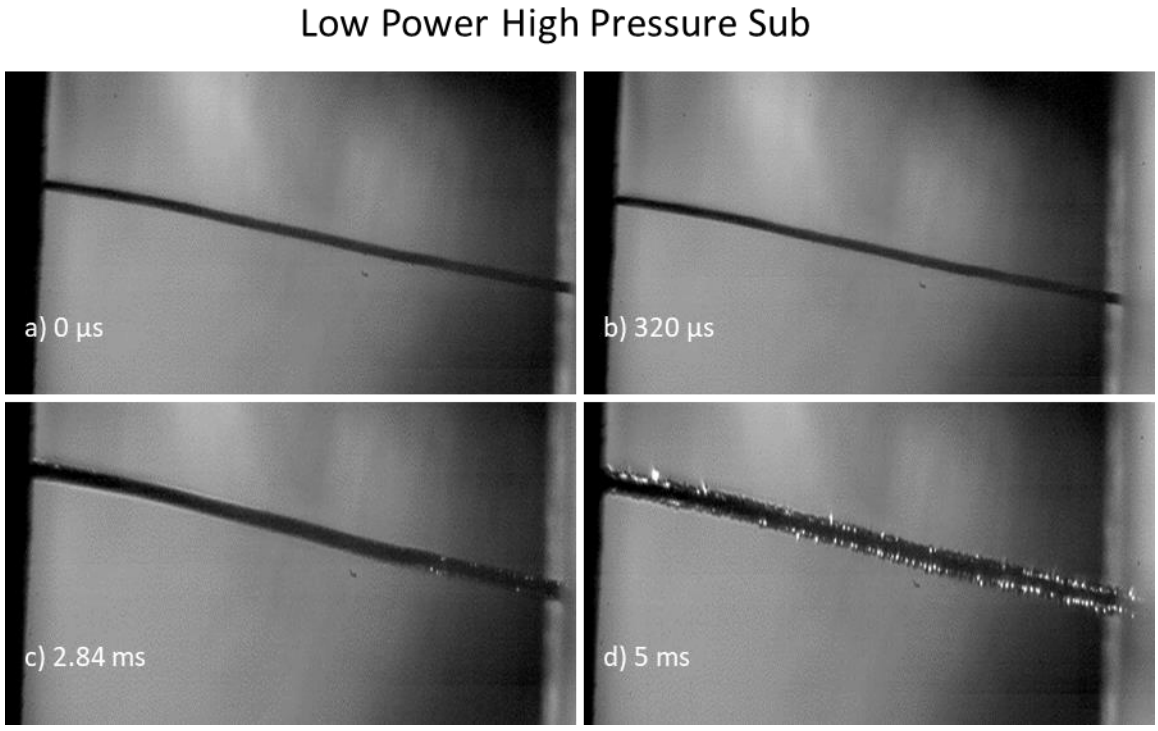

Appendix Figure 33: Rough platinum under low power, high pressure, subcooled condition with constant voltage heating bubbles is shown.

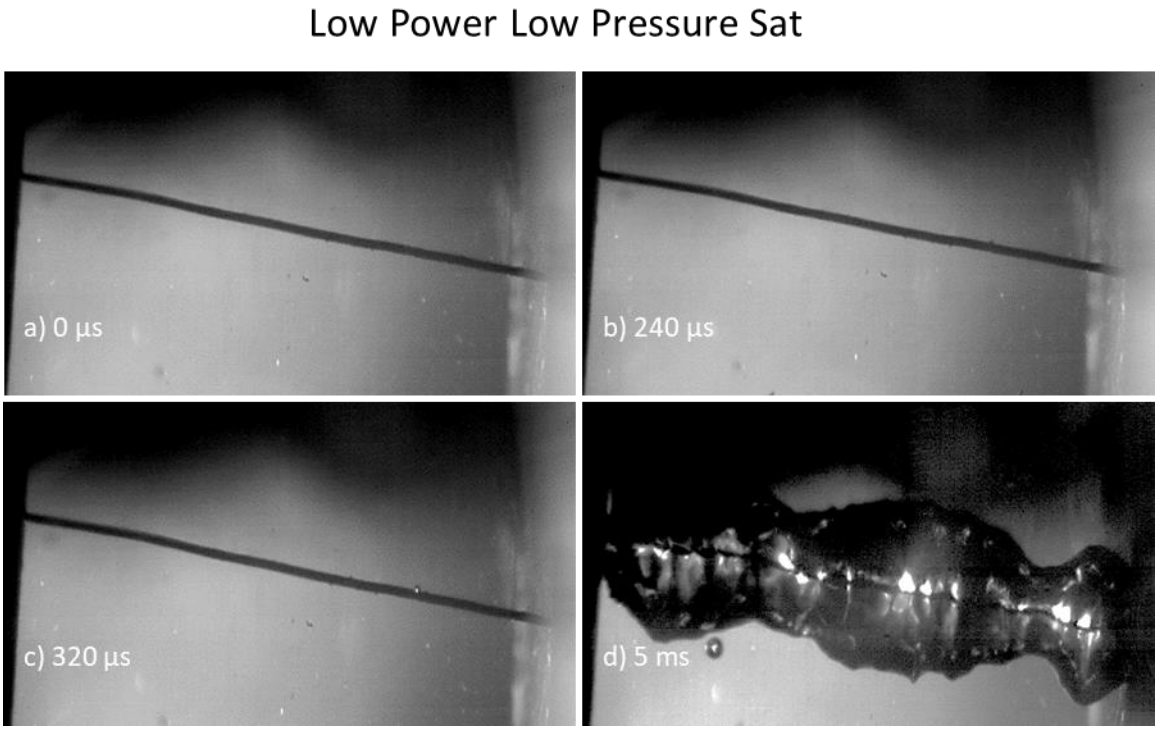

Appendix Figure 34: Rough platinum under low power, low pressure, saturated condition with constant voltage heating bubbles is shown.

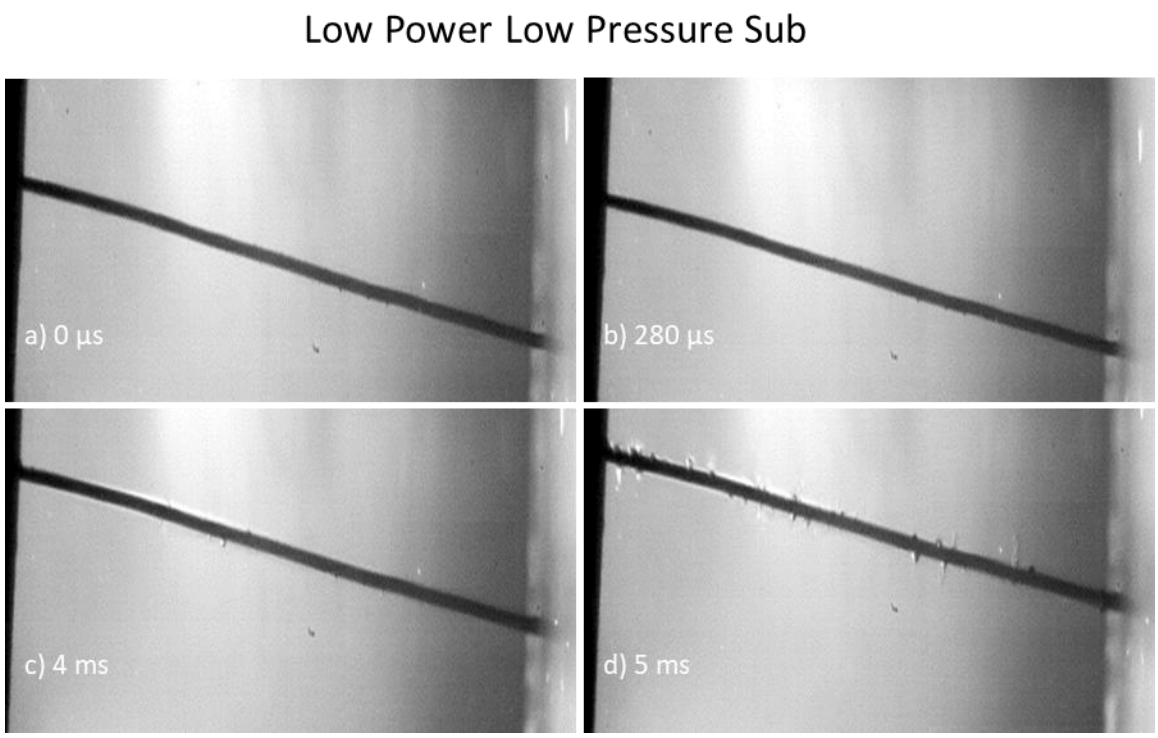

Appendix Figure 35: Rough platinum under low power, low pressure, subcooled condition with constant voltage heating bubbles is shown.

Appendix E.1.5 Smooth Zirconium Under Constant Voltage Heating (exponential, no initial pulse)

- Note: While the zirconium was unable to be accurately tested electrically at high pressure, boiling images were collected during calibration and present for visual comparison here.

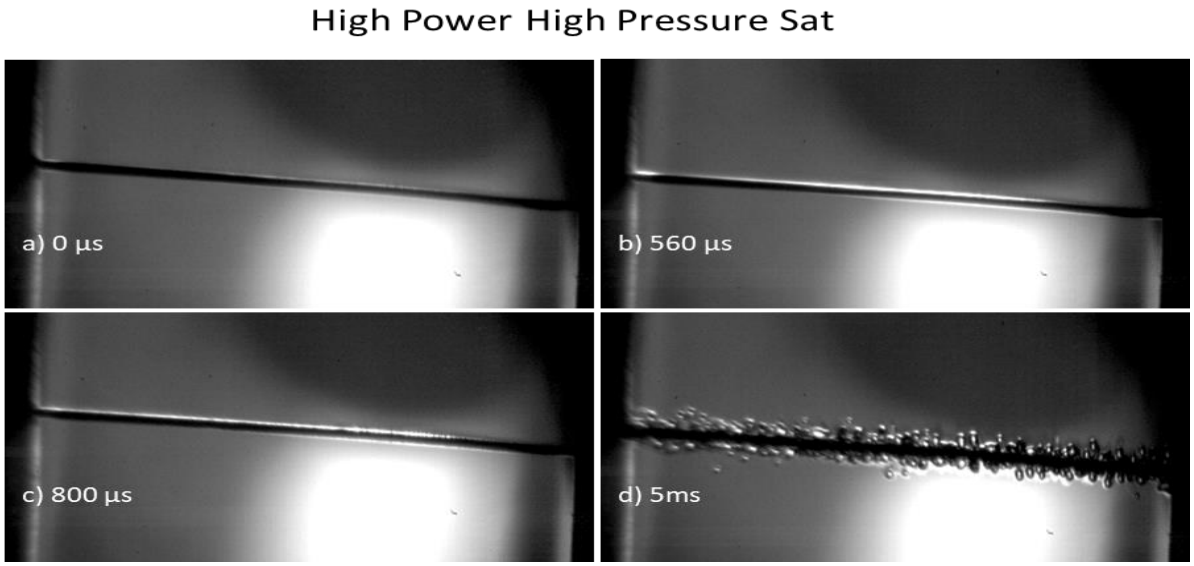

Appendix Figure 36: Smooth zirconium under high power, high pressure, saturated condition with constant voltage heating bubbles is shown.

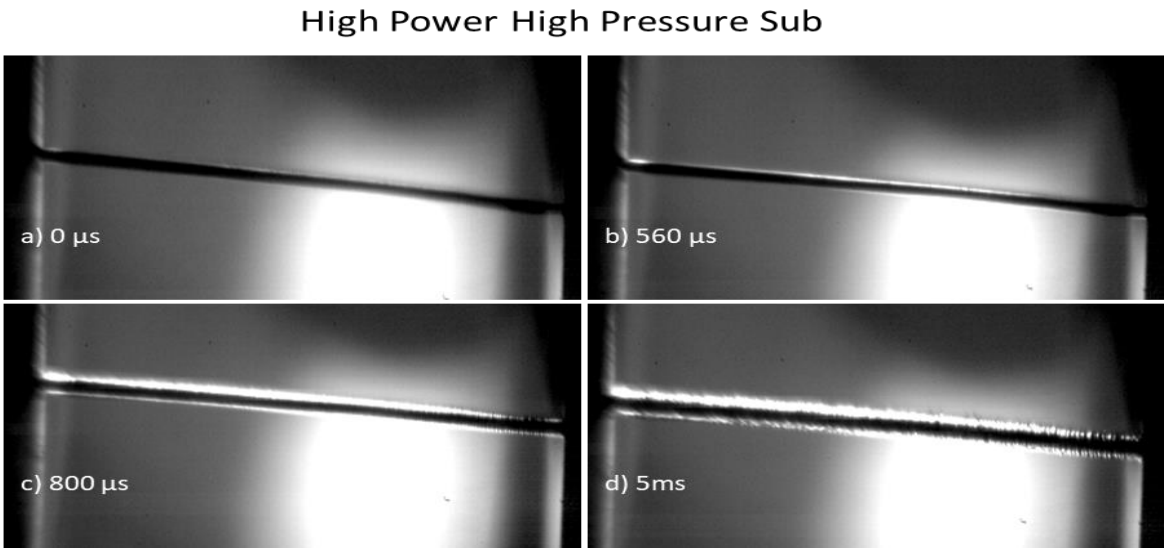

Appendix Figure 37: Smooth zirconium under high power, high pressure, subcooled condition with constant voltage heating bubbles is shown.

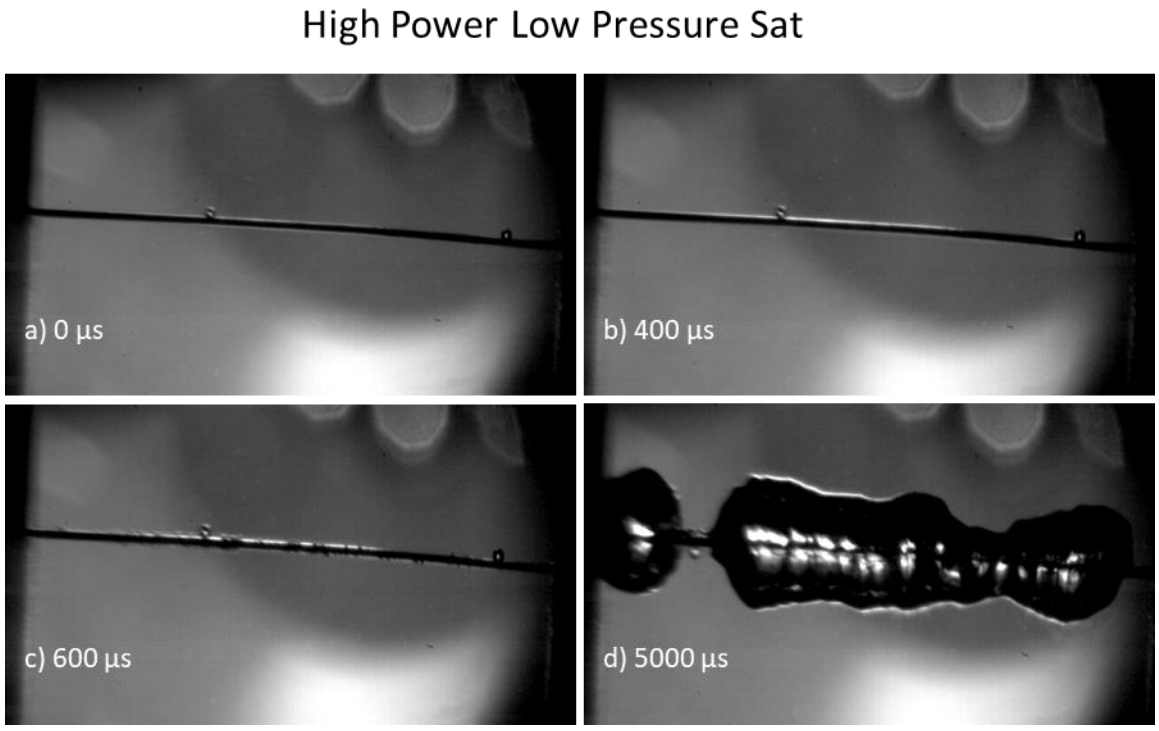

Appendix Figure 38: Smooth zirconium under high power, low pressure, saturated condition with constant voltage heating bubbles is shown.

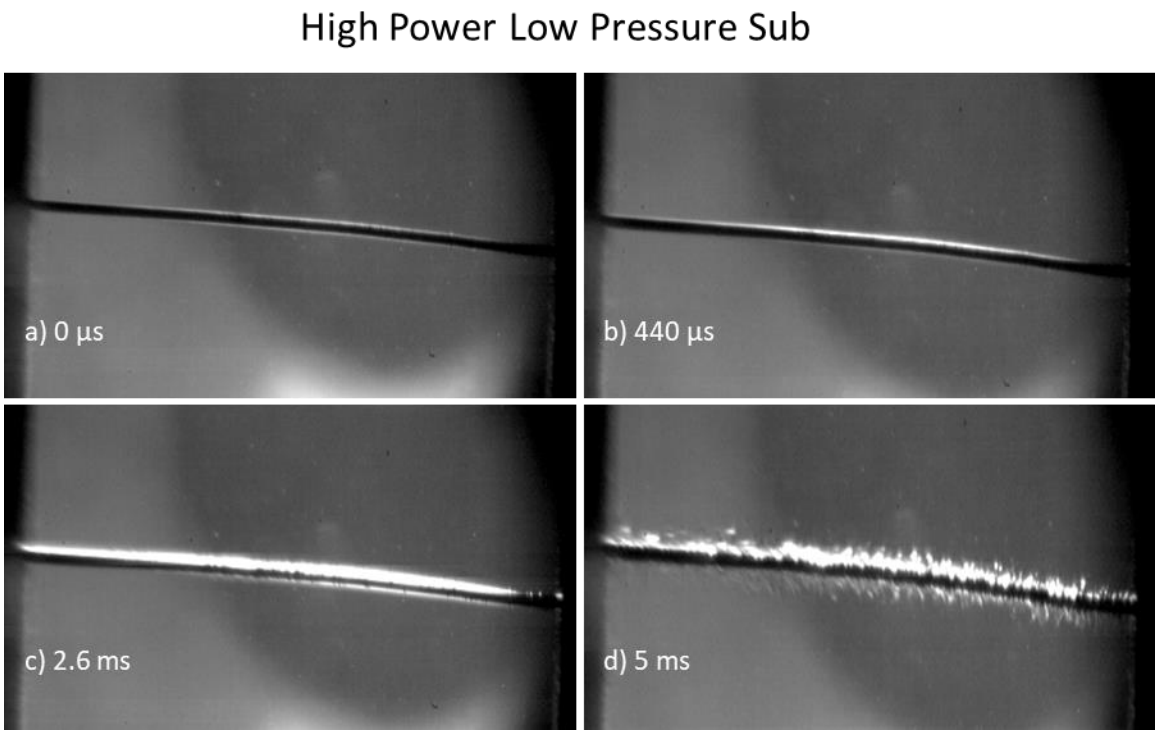

Appendix Figure 39: Smooth zirconium under high power, low pressure, subcooled condition with constant voltage heating bubbles is shown.

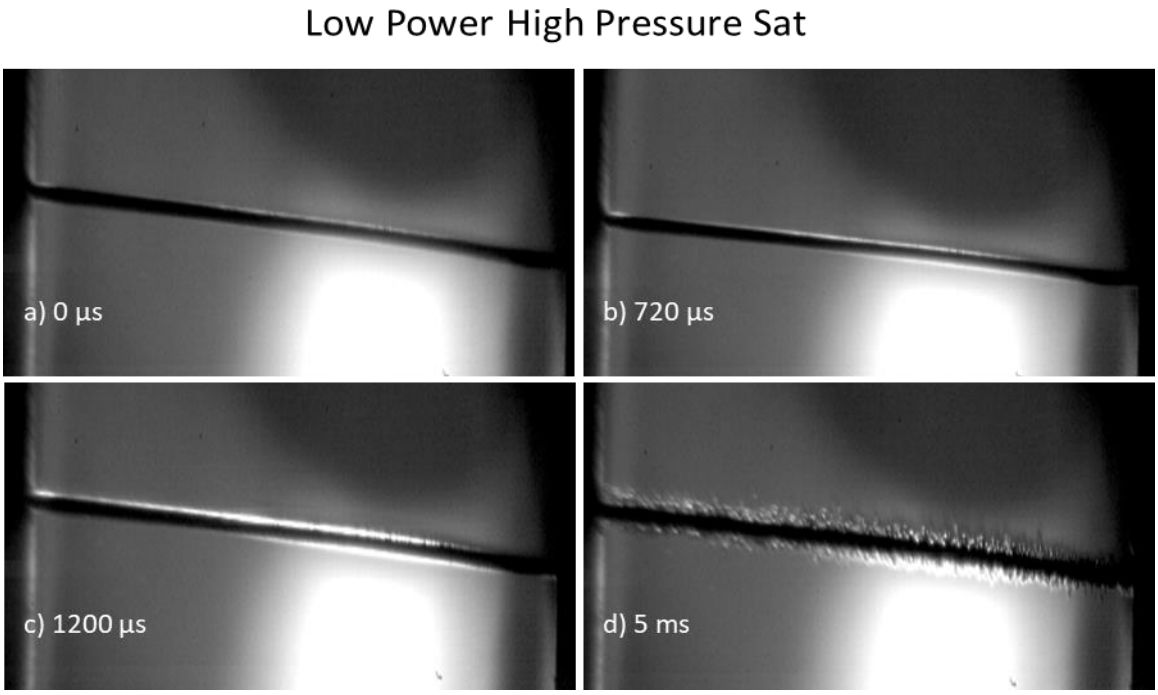

Appendix Figure 40: Smooth zirconium under low power, high pressure, saturated condition with constant voltage heating bubbles is shown.

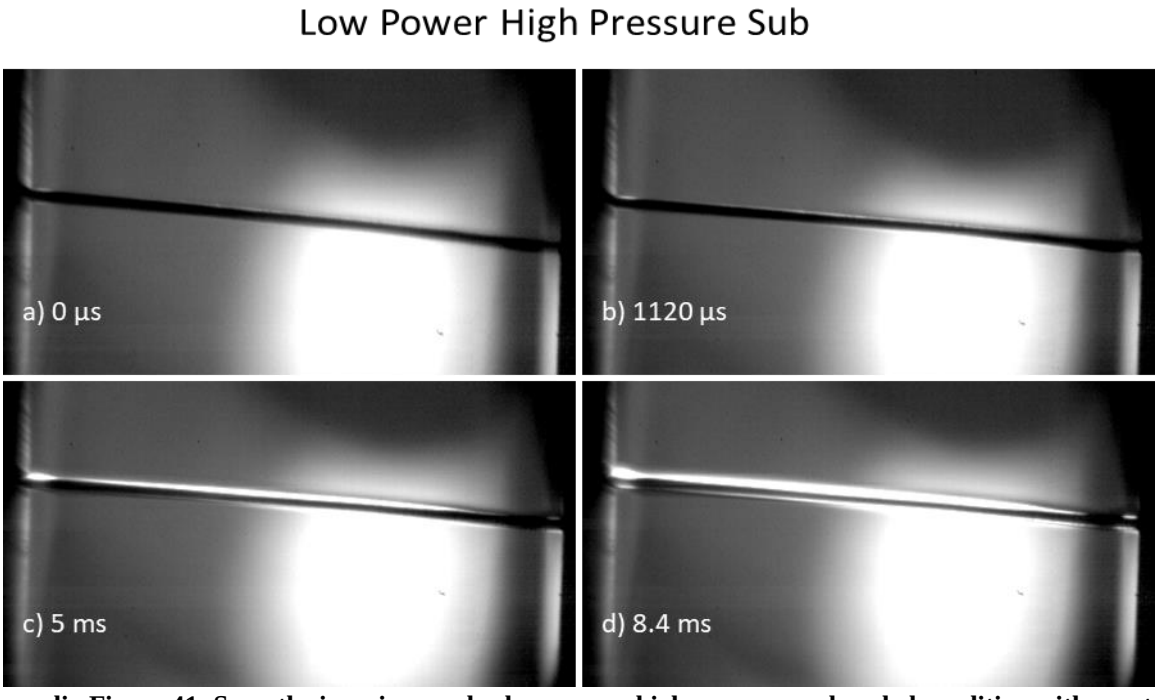

Appendix Figure 41: Smooth zirconium under low power, high pressure, subcooled condition with constant voltage heating bubbles is shown.

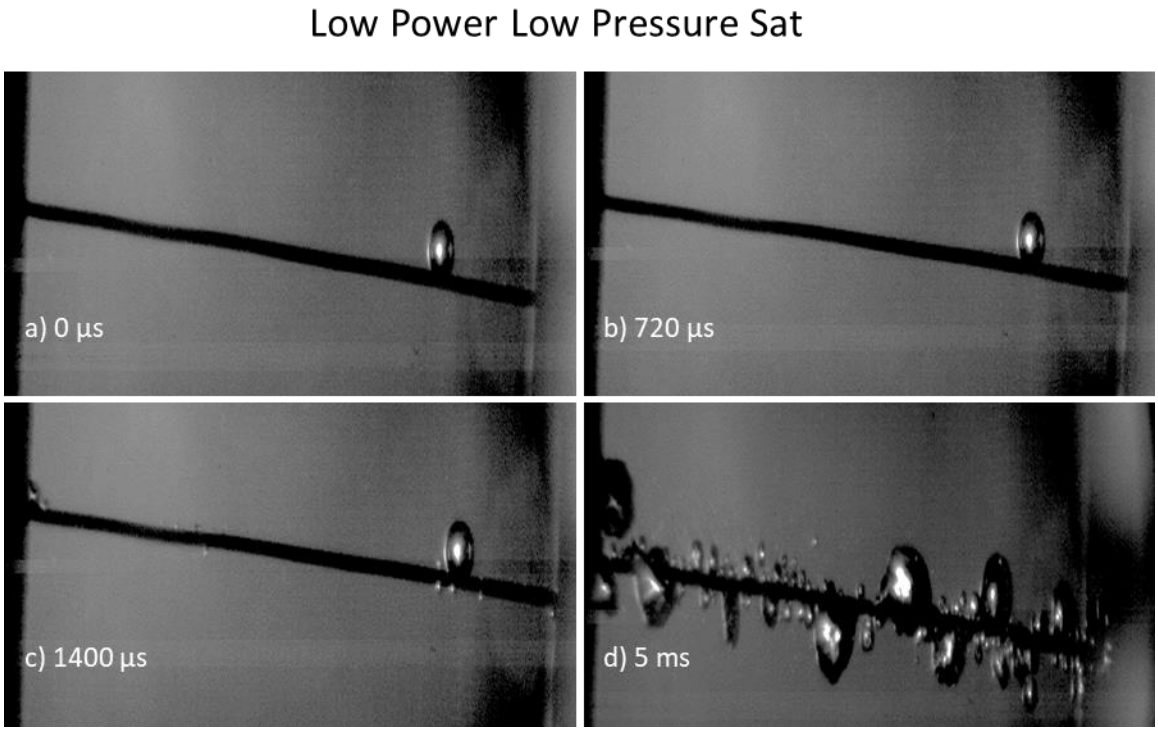

Appendix Figure 42: Smooth zirconium under low power, low pressure, saturated condition with constant voltage heating bubbles is shown.

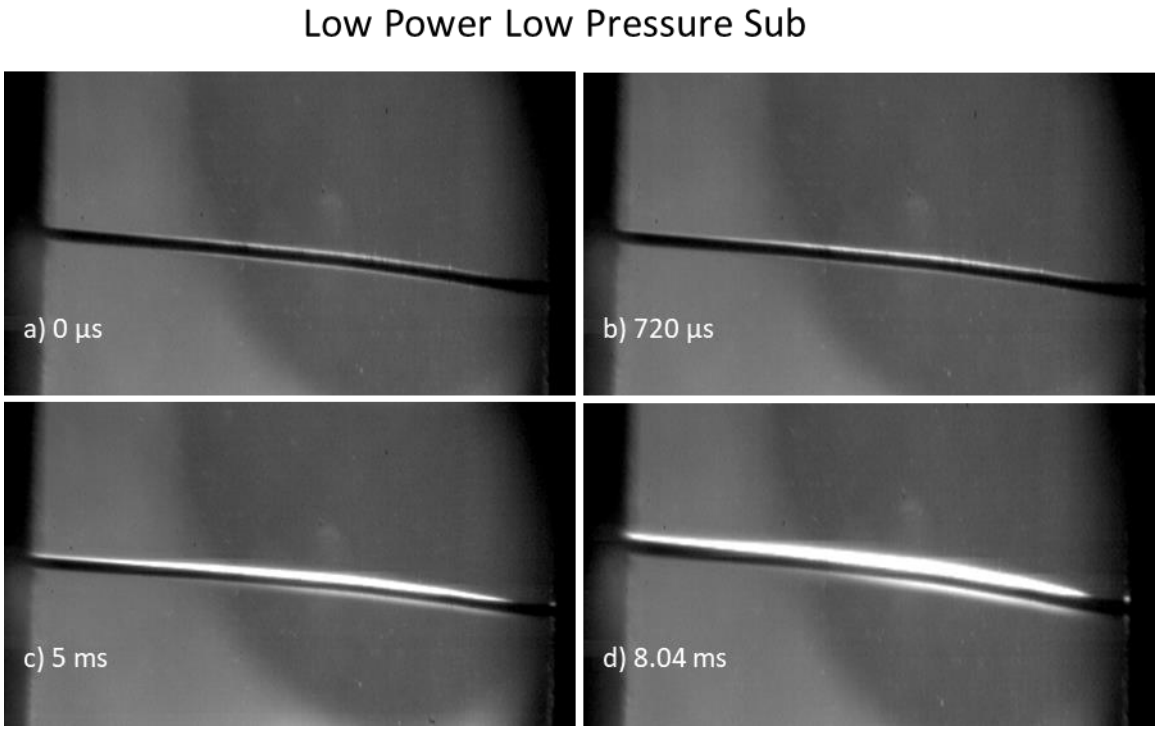

Appendix Figure 43: Smooth zirconium under low power, low pressure, subcooled condition with constant voltage heating bubbles is shown.

Appendix E.1.6 Rough Zirconium Under Constant Voltage Heating (exponential, no initial pulse)

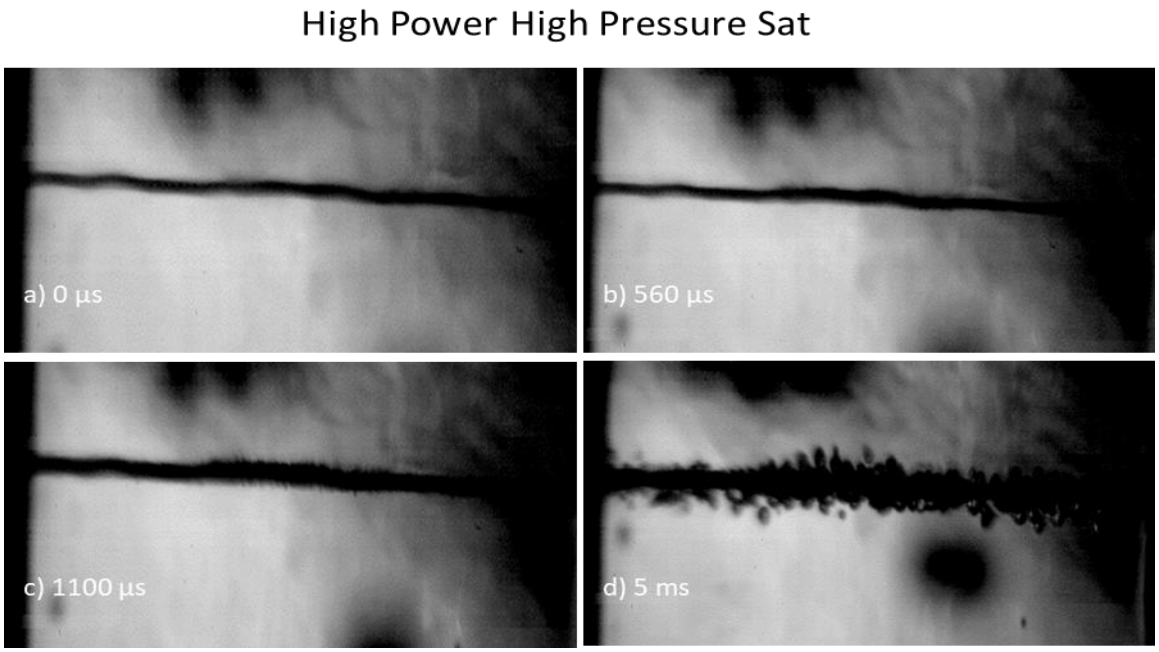

Appendix Figure 44: Rough zirconium under high power, high pressure, saturated condition with constant voltage heating bubbles is shown.

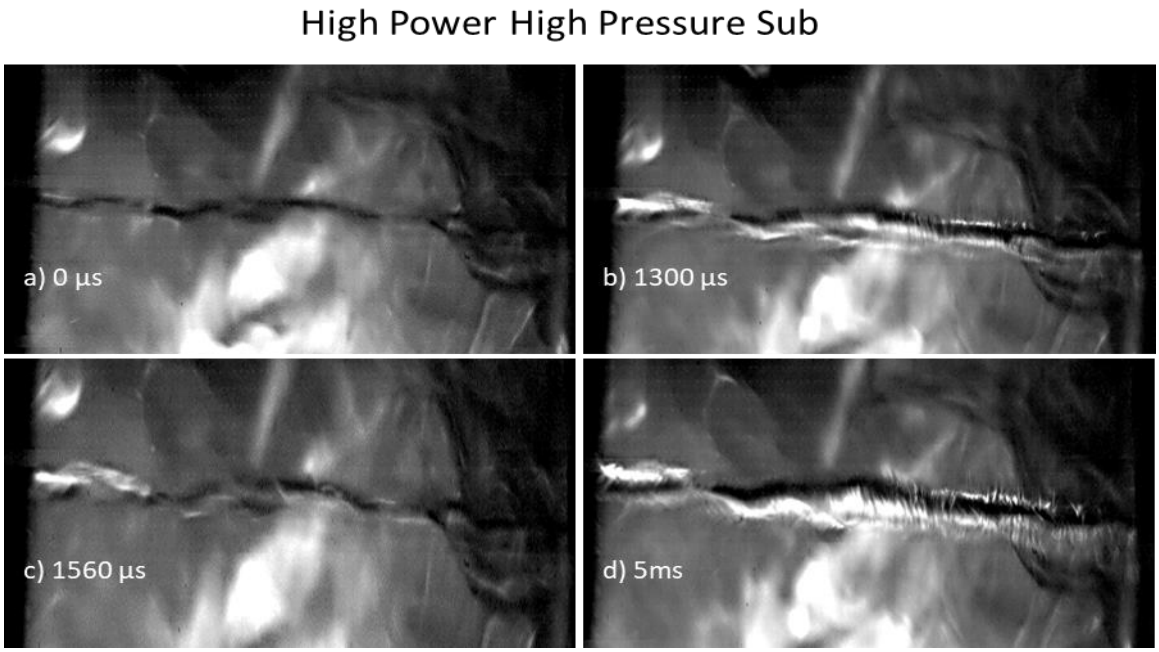

Appendix Figure 45: Rough zirconium under high power, high pressure, sabcooled condition with constant voltage heating bubbles is shown.

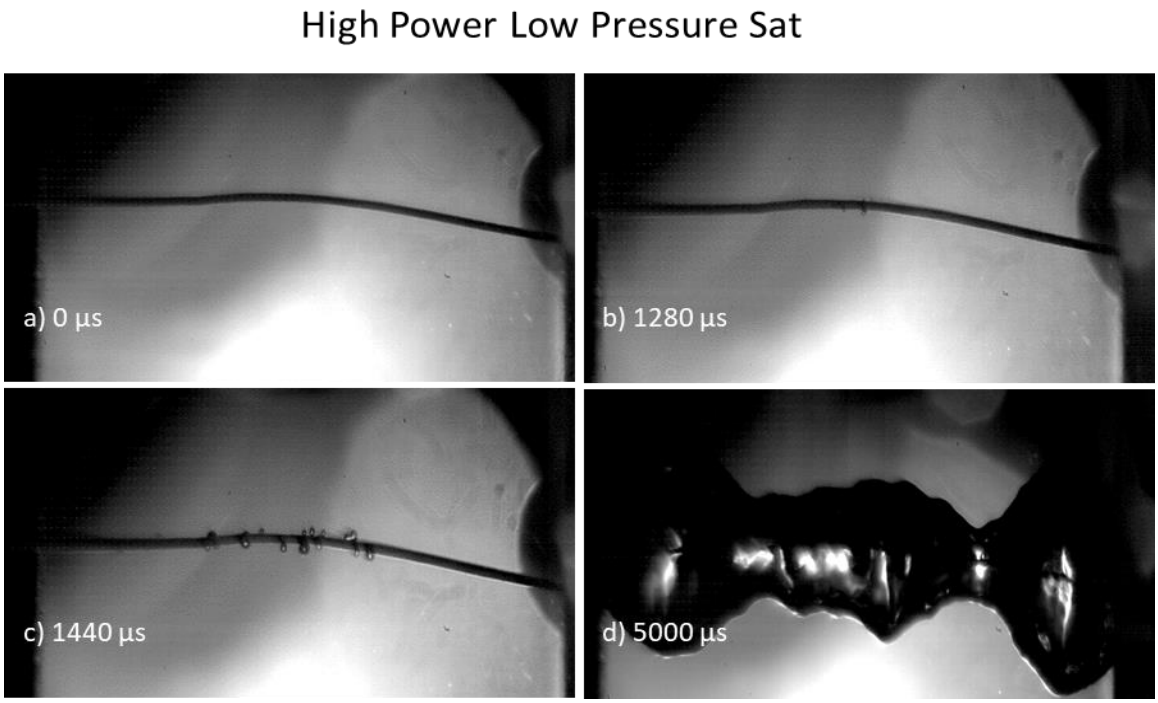

Appendix Figure 46: Rough zirconium under high power, low pressure, saturated condition with constant voltage heating bubbles is shown.

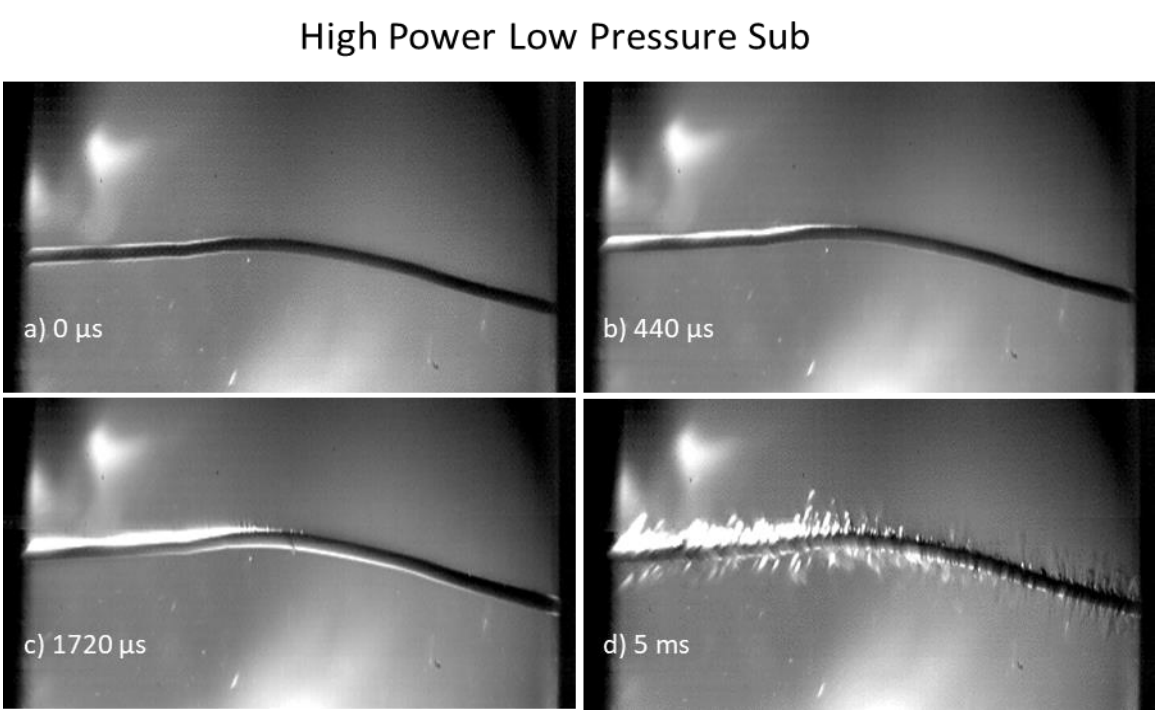

Appendix Figure 47: Rough zirconium under high power, low pressure, subcooled condition with constant voltage heating bubbles is shown.

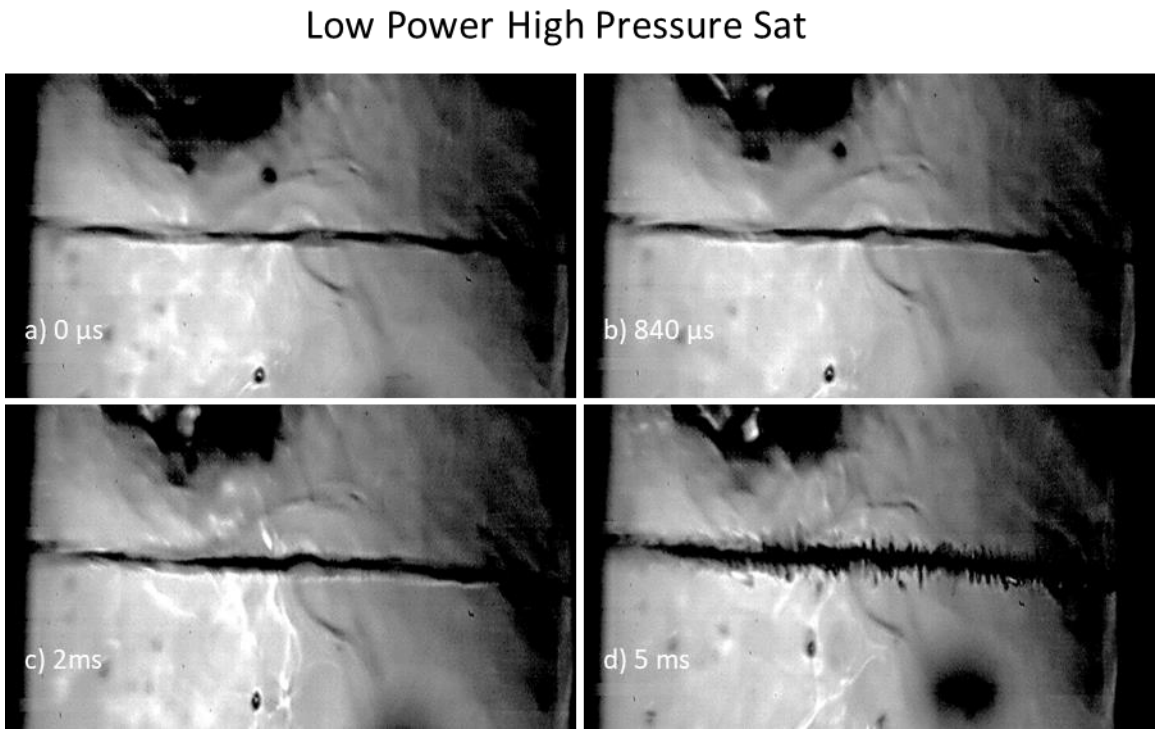

Appendix Figure 48: Rough zirconium under low power, high pressure, saturated condition with constant voltage heating bubbles is shown.

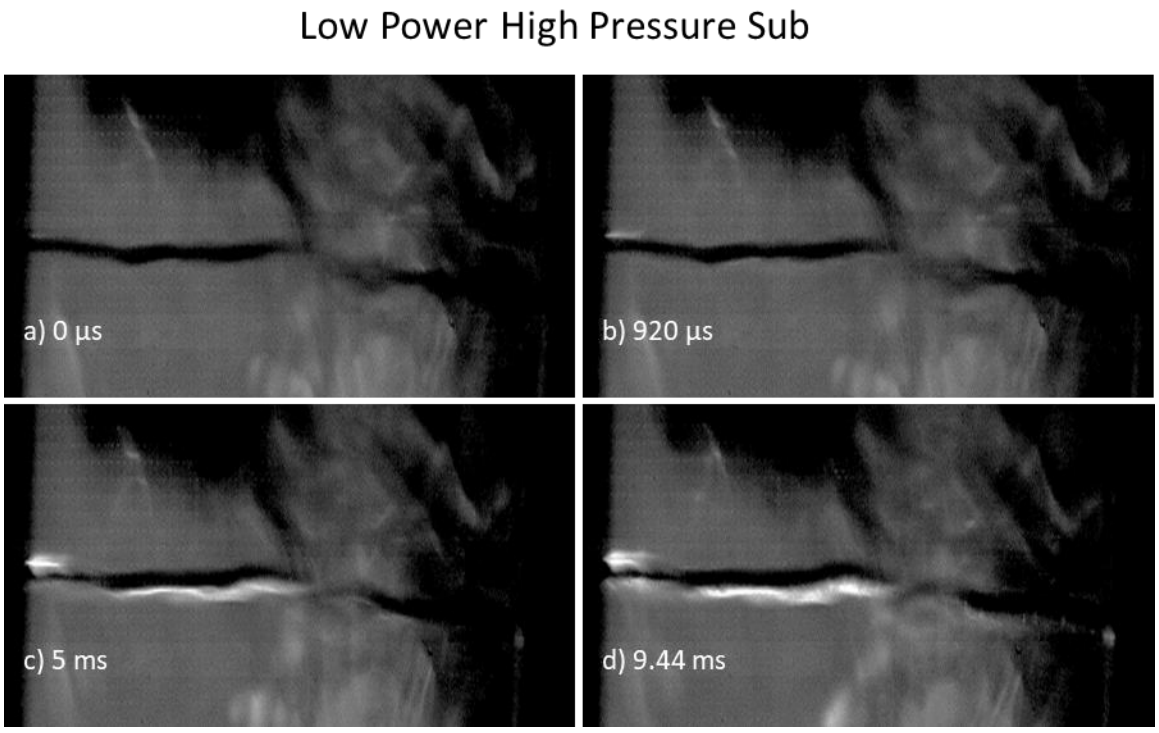

Appendix Figure 49: Rough zirconium under low power, high pressure, subcooled condition with constant voltage heating bubbles is shown.

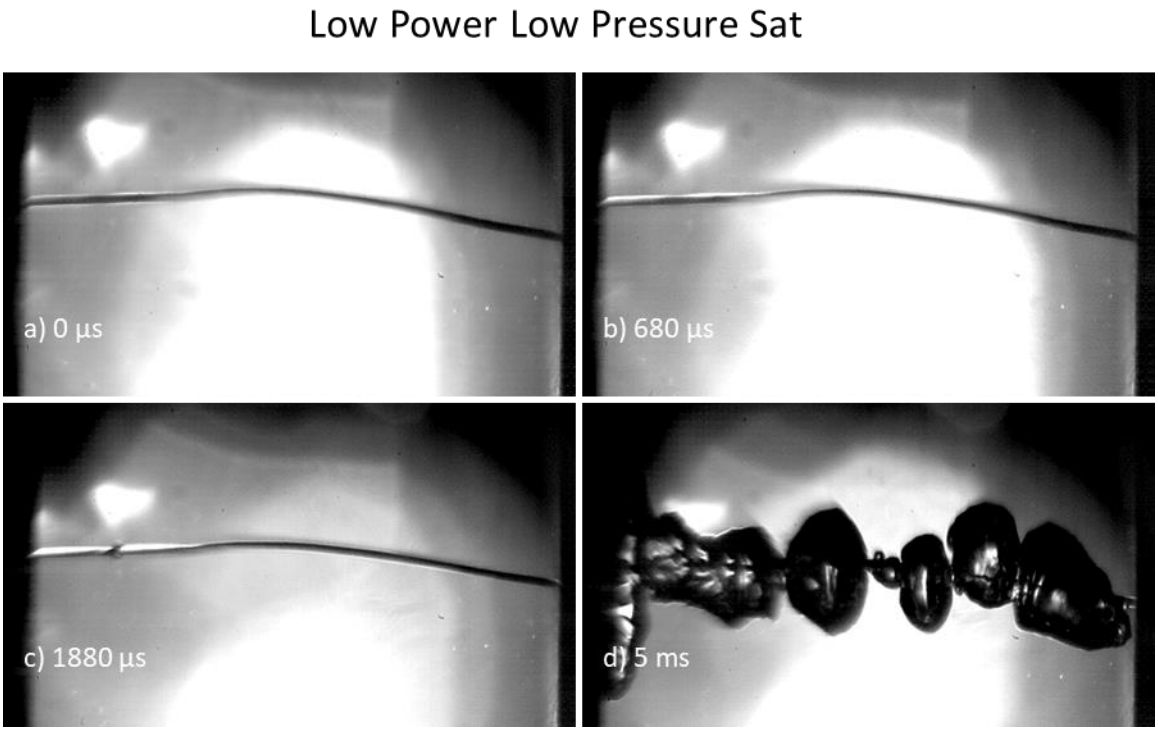

Appendix Figure 50: Rough zirconium under low power, low pressure, saturated condition with constant voltage heating bubbles is shown.

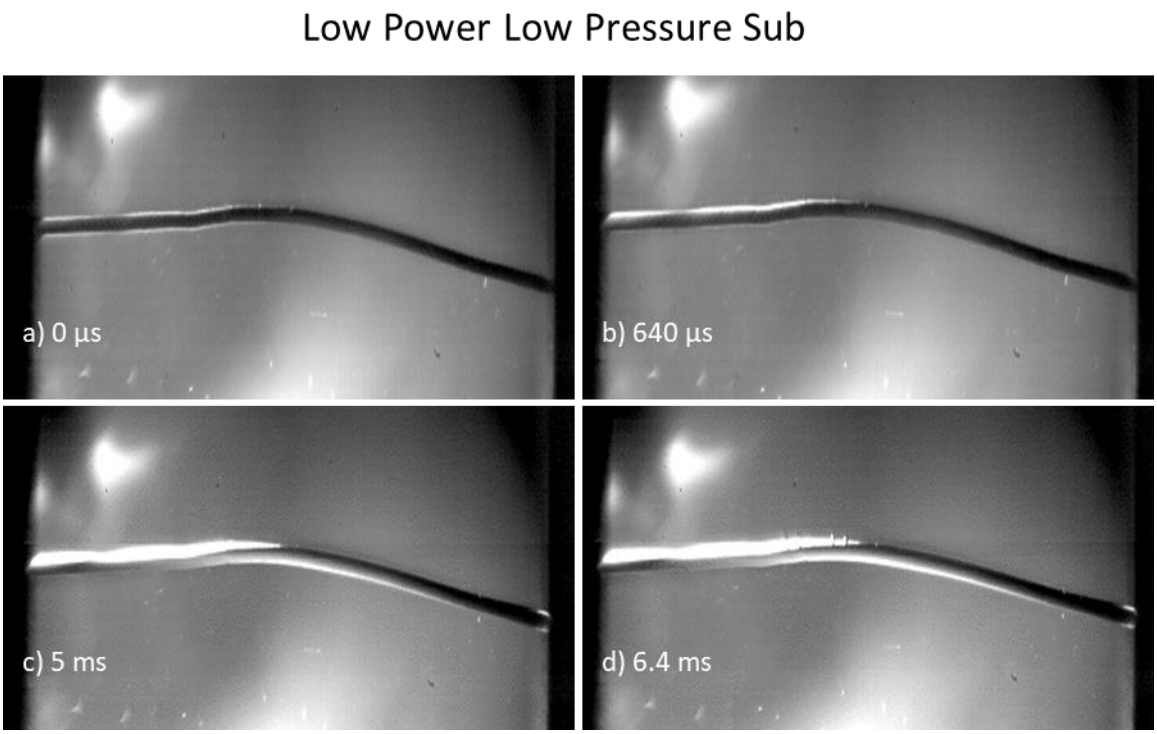

Appendix Figure 51: Rough zirconium under low power, low pressure, saturated condition with constant voltage heating bubbles is shown.

Appendix E.2 2^k Factorial Full Results

A variety of output parameters are compared and presented below. These are defined as follows:

Max Temp – The maximum temperature reached during the test pulse.

Min Temp – The minimum temperature reached during the test pulse.

Q Max– The maximum heat transfer reached during the test pulse.

Q Min– The minimum heat transfer reached during the test pulse.

h Max– The maximum heat transfer coefficient calculated from the test pulse.

h Min– The minimum heat transfer coefficient calculated from the test pulse.

T5 – The temperature at 5 ms.

Q5 – The heat transfer at 5 ms.

h5 – The heat transfer coefficient at 5 ms.

Tave – The average temperature value from 3ms to 6ms. (This time range was selected as the tests had reached a stead value, if such a steady value was going to be reached)

Qave – The average heat transfer value from 3ms to 6ms.

have – The average heat transfer coefficient value from 3ms to 6ms.

Qlocalmax – This is the heat transfer value found in the initial local maximum, typically occurring around 240 μs.

Qlocalmin – This is the heat transfer value found in the initial local minimum, typically occurring around 280 µs.

Appendix Table 2: The full results of the 2^k factorial study on plain platinum wire (Chapter 7).

	Subcooling (A)	Pressure (B)	Pulse Height (C)	AB	AC	BC	ABC
Max Temp	-154.7	-188.5	117.6	126.3	-96.9	-112.5	95.7
Min Temp	-57.7	-43.1	-51.5	-28.8	-6.0	-26.0	-32.3
Q Max	-77750.0	41250.0	5390250.0	321250.0	-180750.0	-161750.0	276250.0
Q Min	48275.0	96775.0	-408675.0	-983175.0	-184725.0	-424225.0	-1239175.0
h Max	512525.0	1958125.0	-133425.0	488125.0	-1617625.0	-679925.0	-1481025.0
h Min	-415872.5	-1571392.5	-1384912.5	-1406627.5	-491147.5	-428587.5	-1474352.5
T5	-98.3	-108.4	87.2	71.6	-64.3	-81.0	62.2
Q5	-37250.0	164750.0	5365750.0	280750.0	-185250.0	-144250.0	286750.0
h5	-8377.5	64417.5	43922.5	-27977.5	5937.5	36882.5	-14782.5
Tave	-122.6	-136.8	98.6	95.9	-82.4	-92.4	80.3
Qave	-71466.6	120542.4	5373034.4	314705.1	-208794.9	-151760.0	305049.4
have	-6216.8	67909.7	46036.3	-30311.8	6270.0	34672.5	-15162.1
Qlocalmax	129500.0	765000.0	4822000.0	63000.0	1000.0	289500.0	74500.0
Qlocalmin	130500.0	741000.0	4812500.0	57000.0	4500.0	282000.0	74000.0

Shading is from red (low) to blue (high) with the deeper the color the farther along that scale it is.

Appendix Table 3: The first half of the results of the 2^k factorial study on platinum wire testing pulse shapes with and without an initial power spike (Chapter 8).

	Max Temp	Min Temp	Q Max	Q Min	h Max	h Min
Subcooling (A)	-241.2	-100.8	-4.98E+05	-7.14E+05	2.60E+05	-2.04E+05
Pressure (B)	-312.8	10.1	1.39E+06	1.75E+06	9.81E+05	-7.86E+05
Pulse Height (C)	703.8	97.5	3.59E+06	2.49E+06	-9.44E+04	-6.97E+05
Pulse Shape (D)	892.5	289.6	1.22E+07	5.81E+06	-1.45E+06	1.25E+06
AB	70.9	23.0	6.99E+05	1.51E+06	2.39E+05	-7.04E+05
AC	-108.7	-37.8	-4.99E+05	-6.19E+05	-8.02E+05	-2.48E+05
AD	-86.5	-43.1	-4.20E+05	-7.62E+05	-2.52E+05	2.12E+05
BC	-324.3	1.6	-4.20E+05	1.07E+06	-3.49E+05	-2.09E+05
BD	-124.3	53.1	1.35E+06	1.65E+06	-9.77E+05	7.85E+05
CD	586.2	149.0	-1.80E+06	2.90E+06	3.90E+04	6.88E+05
ABC	-40.4	1.6	6.02E+05	8.51E+05	-7.43E+05	-7.32E+05
ABD	-55.4	51.8	3.78E+05	2.50E+06	-2.49E+05	7.02E+05
ACD	-11.8	-31.8	-3.18E+05	-4.34E+05	8.16E+05	2.43E+05
BCD	-211.8	27.6	-2.58E+05	1.49E+06	3.31E+05	2.20E+05
ABCD	-136.2	33.9	3.26E+05	2.09E+06	7.38E+05	7.42E+05

Appendix Table 4: The second half of the results of the 2^k factorial study on platinum wire testing pulse shapes with and without an initial power spike (Chapter 8).

	T5	Q5	h5	Tave	Qave	have
Subcooling (A)	-194.3	-1.28E+06	3.83E+02	-204.1	-1.15E+06	1.77E+03
Pressure (B)	4.8	6.89E+05	2.85E+04	-16.3	7.47E+05	3.03E+04
Pulse Height (C)	240.9	8.45E+06	2.46E+04	236.1	8.21E+06	2.59E+04
Pulse Shape (D)	413.8	4.54E+06	-5.17E+04	376.3	4.28E+06	-4.92E+04
AB	149.1	1.14E+06	-1.85E+04	159.6	1.03E+06	-2.00E+04
AC	-69.4	-1.10E+06	1.05E+03	-81.2	-9.94E+05	1.52E+03
AD	-96.0	-1.24E+06	8.76E+03	-81.5	-1.08E+06	7.99E+03
BC	-36.2	1.39E+05	2.01E+04	-46.5	2.09E+05	1.89E+04
BD	113.2	5.24E+05	-3.59E+04	120.5	6.27E+05	-3.76E+04
CD	153.7	3.09E+06	-1.94E+04	137.4	2.84E+06	-2.02E+04
ABC	47.5	5.56E+05	-5.83E+03	60.3	4.70E+05	-6.32E+03
ABD	77.5	8.55E+05	9.45E+03	63.7	7.11E+05	1.03E+04
ACD	-5.1	-9.16E+05	-4.89E+03	1.2	-7.85E+05	-4.75E+03
BCD	44.8	2.83E+05	-1.68E+04	46.0	3.61E+05	-1.57E+04
ABCD	-14.8	2.69E+05	8.95E+03	-20.0	1.65E+05	8.85E+03

Appendix Table 5: The first half of the results of the 2^k factorial study on platinum wire testing pulse shapes with and without power pulse step (Chapter 8).

	Max Temp	Min Temp	Q Max	Q Min	h Max	h Min
Subcooling (A)	-283.5	-119.9	-3.30E+05	-6.89E+05	-5.68E+05	-9.48E+05
Pressure (B)	-257.0	-43.6	5.18E+05	1.58E+06	1.78E+06	-5.03E+06
Pulse Height (C)	696.1	152.9	1.24E+06	2.50E+06	-1.56E+06	-2.34E+05
Pulse Shape (D)	-868.7	-309.2	5.79E+06	-7.27E+06	2.77E+06	-5.52E+06
AB	36.6	48.7	5.43E+05	2.03E+06	-1.31E+06	-4.71E+05
AC	-111.3	-57.9	-3.13E+05	-5.05E+05	1.35E+06	-4.70E+06
AD	44.2	24.0	5.88E+05	7.86E+05	-5.76E+05	-9.56E+05
BC	-240.8	52.7	-5.90E+05	1.20E+06	-2.23E+06	2.61E+05
BD	180.1	-106.8	-2.23E+06	-1.82E+06	1.77E+06	-5.03E+06
CD	-593.8	-93.6	-5.55E+05	-2.89E+06	-1.50E+06	-2.24E+05
ABC	-114.5	13.7	4.45E+05	1.50E+06	6.45E+05	-4.21E+06
ABD	21.0	-26.1	-5.35E+05	-1.97E+06	-1.30E+06	-4.69E+05
ACD	9.2	11.7	5.05E+05	5.49E+05	1.34E+06	-4.70E+06
BCD	295.3	23.6	8.75E+04	-1.36E+06	-2.21E+06	2.51E+05
ABCD	62.1	-21.8	-4.83E+05	-1.44E+06	6.50E+05	-4.22E+06

Appendix Table 6: The second half of the results of the 2^k factorial study on platinum wire testing pulse shapes with and without power pulse step (Chapter 8).

	T5	Q5	h5	Tave	Qave	have
Subcooling (A)	-224.2	-1.46E+06	4.27E+03	-224.2	-1.30E+06	4.49E+03
Pressure (B)	19.2	8.87E+05	2.66E+04	19.2	9.40E+05	2.58E+04
Pulse Height (C)	219.1	6.39E+06	-1.31E+04	219.1	6.23E+06	-1.08E+04
Pulse Shape (D)	-378.1	-6.60E+06	3.73E+04	-378.1	-6.30E+06	3.69E+04
AB	130.9	1.07E+06	-1.77E+04	130.9	9.32E+05	-1.78E+04
AC	-74.6	-1.04E+06	2.35E+04	-74.6	-9.21E+05	2.41E+04
AD	61.3	1.06E+06	-4.87E+03	61.3	9.33E+05	-5.27E+03
BC	21.8	2.51E+05	-1.91E+04	21.8	3.31E+05	-1.77E+04
BD	-85.0	-3.26E+05	3.40E+04	-85.0	-4.34E+05	3.31E+04
CD	-154.4	-5.15E+06	-1.83E+04	-154.4	-4.83E+06	-1.65E+04
ABC	-1.0	3.36E+05	2.25E+04	-1.0	2.45E+05	2.24E+04
ABD	-92.3	-9.15E+05	-8.66E+03	-92.3	-8.06E+05	-8.06E+03
ACD	5.4	9.75E+05	2.73E+04	5.4	8.58E+05	2.73E+04
BCD	22.3	-1.71E+05	-2.23E+04	22.3	-2.39E+05	-2.09E+04
ABCD	-41.3	-4.89E+05	1.94E+04	-41.3	-3.90E+05	1.99E+04

Appendix Table 7: The first half of the results of the 2^k factorial study on platinum and zirconium wire (Chapter 9).

	Max Temp	Min Temp	Q Max	Q Min	h Max	h Min
Subcooling (A)	-211.4	-49.3	-1.41E+05	2.78E+03	-4.40E+06	-2.93E+07
Pulse Height (B)	178.7	-8.9	3.77E+06	8.49E+05	3.02E+07	-6.36E+07
Roughness (C)	27.9	5.9	-5.37E+05	1.35E+06	-3.00E+07	6.36E+07
Material (D)	-178.1	20.3	-2.21E+06	2.50E+04	2.96E+07	-6.31E+07
AB	-157.7	9.1	-2.19E+05	2.53E+03	-4.48E+06	-2.93E+07
AC	-30.9	-7.9	9.98E+04	1.56E+05	4.39E+06	2.94E+07
AD	121.6	-8.5	1.14E+05	-4.94E+05	-4.38E+06	-2.98E+07
BC	34.5	4.8	-3.41E+05	1.12E+06	-3.00E+07	6.36E+07
BD	-113.0	6.7	-1.06E+06	-1.37E+04	2.97E+07	-6.31E+07
CD	1.6	-6.3	8.49E+05	2.97E+05	-2.98E+07	6.31E+07
ABC	-45.6	-2.5	2.33E+04	1.25E+05	4.39E+06	2.94E+07
ABD	110.0	-6.7	1.98E+05	-4.85E+05	-4.33E+06	-2.98E+07
ACD	21.1	3.9	-4.53E+04	6.90E+05	4.44E+06	2.98E+07
BCD	-27.1	-5.2	3.82E+05	2.72E+05	-2.99E+07	6.31E+07
ABCD	29.5	7.9	-1.68E+04	6.92E+05	4.40E+06	2.98E+07

Appendix Table 8: The second half of the results of the 2^k factorial study on platinum and zirconium wire (Chapter 9).

	T5	Q5	h5	Tave	Qave	have	Qlocalmax	Qlocalmin
(A)	-124.0	-7.41E+04	2.85E+04	-156.4	-6.36E+04	4.26E+04	4.03E+04	5.63E+04
(B)	108.9	3.63E+06	5.01E+04	130.7	3.60E+06	4.39E+04	3.40E+06	3.36E+06
(C)	13.7	-5.70E+05	-5.49E+04	12.9	-6.00E+05	-4.72E+04	-2.70E+05	-3.60E+05
(D)	-103.9	-2.27E+06	5.35E+04	-123.9	-2.33E+06	4.69E+04	-1.67E+06	-1.59E+06
AB	-89.5	-1.79E+05	3.33E+04	-113.8	-1.51E+05	4.52E+04	-5.50E+04	-4.80E+04
AC	-10.7	9.79E+04	-1.46E+04	-13.7	1.18E+05	-2.38E+04	3.88E+04	4.90E+04
AD	60.9	1.39E+05	9.51E+03	82.5	1.94E+05	1.78E+04	-6.78E+04	-8.43E+04
BC	8.2	-3.89E+05	-4.06E+04	13.6	-4.00E+05	-3.42E+04	-2.07E+05	-2.32E+05
BD	-68.9	-1.17E+06	4.27E+04	-80.8	-1.20E+06	3.34E+04	-6.78E+05	-6.71E+05
CD	9.9	7.25E+05	-5.34E+04	12.7	7.36E+05	-4.69E+04	5.83E+05	6.54E+05
ABC	-24.6	4.51E+04	-7.09E+03	-24.7	6.72E+04	-1.93E+04	4.50E+03	7.25E+03
ABD	73.3	2.77E+05	4.66E+03	84.7	3.18E+05	1.83E+04	3.45E+04	2.90E+04
ACD	4.4	-6.63E+03	-1.40E+04	6.6	-1.10E+04	-2.44E+04	-2.75E+03	-1.80E+04
BCD	-1.4	3.23E+05	-4.10E+04	-6.9	3.21E+05	-3.33E+04	2.47E+05	2.65E+05
ABCD	11.7	2.86E+04	-1.50E+04	11.1	2.18E+04	-2.48E+04	2.05E+04	1.48E+04

Appendix E.3 Zirconium Reduced Heating Discussion

The material change to zirconium, as seen in Chapter 9 presented another unexpected result. The zirconium wire has a lower maximum temperature and a lower maximum heat flux. The most likely conclusion on this result would be that the zirconium must have a higher heat capacity, meaning more energy is required to heat the wire to the same degree. This is true. The heat capacity of zirconium is more than double that of platinum ($0.285\frac{J}{gK}$ for zirconuim vs $0.133\frac{J}{gK}$ for platinum), but the density of platinum is more that three times that of zirconium ($21.45\frac{g}{cm^3}$ for platinum vs $6.5\frac{g}{cm^3}$ for zirconium). This means that for a given amount of heat, on a specified volume of wire, the zirconium wire would be expected to heat up more.

The flaw is the above logic is that the power supplied to the two wire ends up not being identical. These tests are operated in constant voltage mode allowing any amount of current needed to be drawn to maintain the voltage of the system. Because the resistances are not identical this leads to a difference between the power supplied of the two wires, as seen in appendix Figure 52 below. This is in agreement with the expected current from a supplied voltage on different resistors according to Ohm's law. It is noteworthy to state that the wire material did play a large role in the maximum heat that was transferred. The zirconium performed less well in its ability to transfer heat than the platinum. In every case, when viewed side by side, the bubbles around the zirconium wire were smaller and closer to the wire than those of the analogous platinum case. This could be due to the wettability of zirconium or simply that the specific heat of zirconium is larger meaning that more heat is required to go into the wire to heat it, and thus less is transferred out to the water.

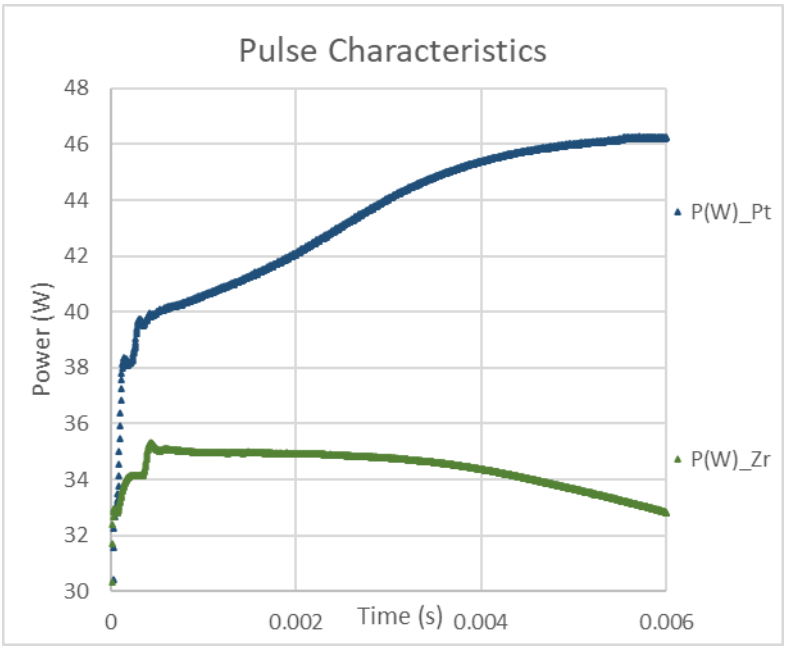

Appendix Figure 52: Zirconium vs platinum power shown under the same voltage heating settings

Bibliography

[1] S. Nukiyama, "The maximum and minimum values of the heat q transmitted," International Journal of heat and mass transfer, vol. 9, pp. 1419-1433, 1966.

[2] Nuclear Energy Agency (NEA), "Nuclear Fuel Behavior Under Reactivity Initiated Accident (RIA) Behavior," OECD Publishing, Boulogne-Billancourt, 2010.

[3] Nuclear Energy Agency (NEA), "Reactivity Initiated Accident (RIA) Fuel Codes Benchmark Phase II – Volume 1: Simplified Cases Results - Summary and Analysis," OECD Publishing, Paris, 2016.

[4] N. Baudin, "ÉTUDE EXPERIMENTALE ET MODELISATION DE L'EBULLITION," Institut National Polytechnique de Toulouse (INP Toulouse), 2015.

[5] V. Bessiron, "Modelling of Clad-to-Coolant Heat Transfer for RIA," Journal of Nuclear Science and Technology, vol. 44, no. 2, pp. 211-221, 2007.

[6] S. Guanyu, "Experimental Study of Transient Pool Boiling Heat Transfer under Exponential Power Excursion," Massachusetts Institute of Technology, 2015.

[7] R. Visentini, "Etude expérimentale des transferts thermiques en ébullition transitoire," Institut National Polytechnique de Toulouse (INP Toulouse), 2012.

[8] Y. Udagawa, T. Sugiyama and M. Amaya, "Heat transfer from fuel rod surface under Reactivity-Initiated accident condition," JAEA-DATA CODE, 2013.

[9] V. Georgenthum, N. Tregoures and Y. Udagawa, "Synthesis and Interpretation of Fuel Cladding Temperature Evolution under Reactivity Initiated Accident," 2014.

[10] M. He, E. Villarreal, H. Ban and M. Chen, "Boiling heat transfer experiments under power transients for LWRs: A review study," Progress in Nuclear Energy, vol. 141, pp. 1-22, 2021.

[11] R. Cole, "University Libraries UNT Digital Library UNT Libraries Government Documents Department This Report," National Advisory Committee for Aeronautics, Washington, 1956.

[12] M. W. Rosenthal, "An Experimental Study of Transient Boiling," Nuclear Science and Engineering, vol. 2, no. 5, pp. 1296-1307, 1957.

[13] F. Tachibana, M. Akiyama and H. Kawamura, "Heat Transfer and Critical Heat Flux in Transient Boiling, (I)," Journal or Nuclear Science and Technology, vol. 5, no. 3, pp. 117-126, 1968.

[14] H. Kawamura, F. Tachibana and M. Akiyama, "HEAT TRANSFER AND DNB HEAT FLUX IN TRANSIENT BOILING," in International Heat Transfer Conference 4, Paris-Versailles, 1970.

[15] A. Sakurai and M. Shiotsu, "Transient Pool Boiling Heat Transfer—Part 2: Boiling Heat Transfer and Burnout.," ASME Journal of Heat Transfer, vol. 99, no. 4, pp. 554-560, 1977.

[16] R. E. Faw, R. J. Vanvleet and D. L. Schmidt, "Pre-pressurization effects on initiation of subcooled pool boiling during pressure and power transients," International Journal of Heat and Mass Transfer, vol. 29, no. 9, pp. 1427-1437, 1986.

[17] K. Fukuda, M. Shiotsu and A. Sakurai, "Transient pool boiling heat transfer due to increasing heat inputs in subcooled water at high pressures," US Nuclear Regulatory Commission, Washington DC, 1995.

[18] K. Fukuda, M. Shiotsu and A. Sakurai, "Effect of surface conditions on transient critical heat fluxes for a horizontal cylinder in a pool of water at pressures due to exponentially increasing heat inputs," Nuclear Engineering and Design, vol. 200, pp. 55-68, 2000.

[19] J. Park, K. Fukuda and Q. Liu, "Effects of Surface Conditions on Transient Pool Boiling CHF in Various Liquids with Different Mechanisms Depending on Pressure and Subcooling," JSME International Journal Series B Fluids and Thermal Engineering, vol. 49, no. 2, pp. 318-325, 2006.

[20] J. Park, Q. Liu and K. Fukuda, "Transient CHF Phenomena Due to Exponentially Increasing Heat Inputs," Nuclear Engineering and Technology, vol. 41, no. 9, pp. 1205-1214, 2009.

[21] V. I. Sharma, J. Buongiorno, T. J. McKrell and L. W. Hu, "Experimental investigation of transient critical heat flux of water-based zinc–oxide nanofluids," International Journal of Heat and Mass Transfer, vol. 61, pp. 425-431, 2013.

[22] M. H. Htet, K. Fukuda and Q. Liu, "Experimental Study on Transient Boiling Heat Transfer and Critical Heat Flux on Horizontal Vertically-Oriented Ribbon with Different Surfaces under Atmospheric Conditions," Marine Engineering, vol. 50, no. 6, pp. 782-793, 2015.

[23] Y. Li, K. Fukuda and Q. Liu, "Steady and Transient CHF in Subcooled Pool Boiling of Water under Sub-atmospheric Pressures," Marine Engineering, vol. 52, no. 2, pp. 245-250, 2017.

[24] A. Ayoobi, A. F. Khorasani and M. R. Tavakoli, "The Effects of Subcooled Temperatures on Transient Pool Boiling of Deionized Water under Atmospheric Pressure," AUT Journal of Mechanical Engineeing, vol. 4, no. 1, pp. 67-78, 2020.

[25] L. Sargentini, M. Bucci, G. Su, J. Buongiorno and T. J. McKrell, "Experimental and Analytical Study of Exponential Power Excursion in Plate-Type Fuel," in Proceedings of the 2014 American Nuclear Society Embedded Topical Meeting on Advances in Thermal Hydraulics (ATH 14), Cambridge, 2014.

[26] G. Su, M. Bucci, T. McKrell and J. Buongiorni, "Transient boiling of water under exponentially escalating heat inputs. Part I: Pool boiling," International Journal of Heat and Mass Transfer, vol. 96, pp. 667-684, 2016.

[27] G. Su, M. Bucci, T. McKrell and J. Buongiorni, "Transient Boiling of Water Under Exponentially Escalating Heat Inputs Part II: Flow Boiling," International Journal of Heat Transfer, vol. 96, pp. 685-698, 2016.

[28] A. Walunj and A. Sathyabhama, "Transient CHF enhancement in high pressure pool boiling on rough surface," Chemical Engineering and Processing - Process Intensification, vol. 127, pp. 145-158, 2018.

[29] H. Auracher and W. Marquardt, "Experimental studies of boiling mechanisms in all boiling regimes under steady-state and transient conditions," International Journal of Thermal Sciences, vol. 41, no. 7, pp. 586-598, 2002.

[30] R. Hohl and H. Auracher, "Transient Pool Boiling Experiments," in Transient Phenomena in Multiphase and Multicomponent Systems: Research Report, 256, Wiley, 2000, p. 241.

[31] K. Fukuda and Q. Liu, "Steady and Transient Critical Heat Fluxes on a Horizontal Cylinder in a Pool of Freon-113," International Journal or Transport Phenomena, vol. 7, pp. 71-83, 2005.

[32] S. Mori and Y. Utaka, "Critical heat flux enhancement by surface modification in a saturated pool boiling: A review," International Journal of Heat and Mass Transfer, vol. 108, no. Part B, pp. 2534-2557, 2017.

[33] G. Liang and I. Mudawar, "Pool boiling critical heat flux (CHF) – Part 1: Review of mechanisms, models, and correlations," International Journal of Heat and Mass Transfer, vol. 117, pp. 1352 - 1367, 2018.

[34] S. K. Singh and D. Sharma, "Review of pool and flow boiling heat transfer enhancement through surface modification," International Journal of Heat and Mass Transfer, vol. 181, p. 122020, 2021.

[35] S. P. Fitri, K. Fukuda, Q. Liu and J. Park, "Transient Pool Boiling Critical Heat Flux of FC-72 Under Saturated Conditions," in Proceedings of the 14th International Conference on Nuclear Engineering. Volume 4: Computational Fluid Dynamics, Neutronics Methods and Coupled Codes, Miami, 2006.

[36] Y. Iida, K. Okuyama and K. Sakurai, "Peculiar bubble generation on a film heater submerged in ethyl alcohol and imposed a high heating rate over 107 K s1," International Journal of Heat and Mass Transfer, vol. 36, no. 10, pp. 2699-2701, 1993.

[37] H. Sakashita and A. Ono, "Boiling behaviors and critical heat flux on a horizontal plate in saturated pool boiling of water at high pressure," International Journal of Heat and Mass Transfer, vol. 52, no. 3-4, pp. 744-750, 2009.

[38] R. Séméria, "High-speed cinematography and pool boiling under high pressure," La Houille Blanche, vol. 49, no. 6, pp. 679-686, 1963.

[39] G. I. Bobrovich and N. N. Mamontova, "A study of the mechanism of nucleate boiling at high heat fluxes," International Journal of Heat and Mass Transfer, vol. 8, no. 11, pp. 1421-1422, 1965.

[40] S. Dahariya and A. R. Betz, "High pressure pool boiling: Mechanisms for heat transfer enhancement and comparison to existing models," International Journal of Heat and Mass Transfer, vol. 141, pp. 696-706, 2019.

[41] M.-G. Kang, "Effect of surface roughness on pool boiling heat transfer," International Journal of Heat and Mass Transfer, vol. 43, no. 12, pp. 4073-4085, 2000.

[42] J. Drelich, E. Chibowski, D. D. Meng and K. Terpilowski, "Hydrophilic and SuperhydroPhilic Surfaces and Materials," Soft Matter, vol. 7, no. 21, pp. 9804-9828, 2011.

[43] Z.-H. Liu, X.-F. Yang and J.-G. Xiong, "Boiling characteristics of carbon nanotube suspensions under sub-atmospheric pressures,," International Journal of Thermal Sciences,, vol. 49, no. 7, pp. 1156-1164, 2010.

[44] Z.-H. Liu, J.-G. Xiong and R. Bao, "Boiling heat transfer characteristics of nanofluids in a flat heat pipe evaporator with micro-grooved heating surface,," International Journal of Multiphase Flow,, vol. 32, no. 12, pp. 1284-1295, 2007.

[45] H. Jo, . S. Kim, J. Kin and M. H. Kim, "Nucleate boiling performance on nano/microstructures with different wetting surfaces," Nanoscale Research Letters, vol. 7, no. 242, pp. 1-9, 2012.

[46] A. Sakurai, "Mechanisms of transitions to film boiling at CHFs in subcooled and pressurized liquids due to steady and increasing heat inputs," Nuclear Engineering and Design, vol. 197, no. 3, pp. 301-356, 2000.

[47] M. He, M. Chen, E. Villarreal, H. Ban and R. B. Rebak, "Experimental investigation of power transient flow boiling," Experimental Thermal and Fluid Science, vol. 144, no. June, p. 110833, 2023.

[48] T. A. Kingston, J. A. Weibel and S. V. Garimella, "Time-resolved characterization of microchannel flow boiling during," International Journal of Heat and Mass Transfer, vol. 154, pp. 1-10, 2020.

[49] C. Xing, T. Munro, C. Jensen and H. Ban, "Analysis of the electrothermal technique for thermal property characterization of thin fibers," Measurement Science and Technology, vol. 24, no. 10, p. 105603, 2013.

[50] J. J. Stickel, "Data smoothing and numerical differentiation by a regularization method," Computers and Chemical Engineering, vol. 34, no. 4, pp. 467-475, 2010.

[51] I. Lightwave, "Callendar-Van Dusen equation and RTD temperature sensors".

[52] N. BAUDIN, "ÉTUDE EXPERIMENTALE ET MODELISATION DE L'EBULLITION," Institut National Polytechnique de Toulouse (INP Toulouse), 2015.

[53] V. BESSIRON, "Modelling of Clad-to-Coolant Heat Transfer for RIA," Journal of Nuclear Science and Technology, vol. 44, no. 2, pp. 211-221, 2007.

[54] S. Guanyu, "Experimental Study of Transient Pool Boiling Heat Transfer under Exponential Power Excursion," Massachusetts Institute of Technology, 2015.

[55] R. VISENTINI, "Etude expérimentale des transferts thermiques en ébullition transitoire," Institut National Polytechnique de Toulouse (INP Toulouse), 2012.

[56] Y. UDAGAWA, T. SUGIYAMA and M. AMAYA, "Heat transfer from fuel rod surface under Reactivity-Initiated accident condition," JAEA-DATA CODE, 2013.

[57] V. GEORGENTHUM, N. TREGOURES and Y. UDAGAWA, "Synthesis and Interpretation of Fuel Cladding Temperature Evolution under Reactivity Initiated Accident," 2014.

[58] B. J. Zhang, K. J. Kim and H. Yoon, "Enhanced heat transfer performance of alumina sponge-like nano-porous structures through surface wettability control in nucleate pool boiling," International Journal of Heat and Mass Transfer, vol. 55, no. 25-26, pp. 7487-7498, 2012.

[59] S. Glod, D. Poulilakos, Z. Zhao and G. Yadigaroglu, "An investigation of microscale explosive vaporization of water on an platinum wire," International of Heat Transfer and Mass Transfer, pp. 367-379, 2002.

[60] A. SAKURAI, "Mechanisms of transitions to film boiling at CHFs in subcooled and pressurized liquids due to steady and increasing heat inputs," Nuclear Engineering and Design, vol. 197, pp. 301-356, 2000.

[61] C. W. Corti, "Thermophysical Data on Platinum," Platinum Metals Rev., vol. 28, no. 4, pp. 164-165, 1984.

[62] R. S. Hixson and M. A. Winkler, "Thermophysical properties of liquid platinum," International Journal of Thermophysics, vol. 14, pp. 409-416, 1993.

[63] G. Y. Su, T. A. Moreira, D. Lee, D. Jena, G. Wang, A. Byers, B. Philips, Z. Karoutas, M. Anderson and M. Bucci, "Wettability and CHF limits of Accident-Tolerant nuclear fuel cladding materials in light water reactor conditions," Applied Thermal Engineering, vol. 216, no. November, p. 119018, 2022.

[64] P. E. MacDonald, S. L. Seiffert, Z. R. Martinson, R. K. McCardell, D. E. Owen and S. K. Fukuda, "Assessment of light water reactor fuel damage during a reactivity initiated accident," in IAEA CONF-800971--1 (CSNI Specialist Meeting on Safety Aspects of Fuel Behavior in Off-Normal and Accident Conditions), Espoo, 1980.

[65] P. Clifford, "Pressurized Water Reactor Control Rod Ejection and Boiling Water Reactor Control Rod Drop Accidents," US NRC Regulatory Guide DG-1327, New York, 2016.

[66] P. Rudling and L. O. Jernkvist, Nuclear Fuel Behaviour under RIA Conditions, Analysvägen: Advanced Nuclear Technology International, 2016.

[67] J. Schulthess, N. Woolstenhulme, A. Craft, J. Kane, N. Boulton, W. Chuirazzi, A. Winston, A. Smolinski, C. Jensen, D. Kamerman and D. Wachs, "Non-Destructive post-irradiation examination results of the first modern fueled experiments in TREAT," Journal of Nuclear Materials, vol. 541, no. December, p. 152442, 2020.

[68] J. Desquines, B. Cazalis, C. Bernaudat, C. Poussard, X. Avery and P. Yvon, "Mechanical Properties of Zircaloy-4 PWR Fuel Cladding with Burnup 54-64MWd/kgU and Implications for RIA Behavior," Journal of ASTM International, vol. 2, no. 6, pp. 851 - 872, 2005.

[69] A. M. Garde, G. P. Smith and R. C. Pirek, "Effects of Hydride Precipitate Localization and Neutron Fluence on the Ductility of Irradiated Zircaloy-4," ASTM International, no. January, pp. 407 - 430, 1996.

[70] R. S. Daum, S. Majumdar, Y. Liu and M. C. Billone, "Radial-hydride Embrittlement of High-burnup Zircaloy-4 Fuel Cladding," Journal of Nuclear Science and Technology, vol. 43, no. 9, pp. 1054 - 1067, 2006.

[71] K. S. Chan, "An assessment of delayed hydride cracking in zirconium alloy cladding tubes under stress transients," International Materials Review, vol. 58, no. 6, pp. 349 - 373, 2013.

[72] H. K. Yueh, R. L. Kesterson, R. J. Comstock, H. H. Shah, D. J. Colburn, M. Dahlback and L. Hallstadius, "Improved ZIRLOTM Cladding Performance through Chemistry and Process Modifications," Journal of ASTM International, vol. 2, no. 6, pp. 330 - 345, 2005.

[73] Maxim Integrated Products, "Line and Load Transient Testing for Power Supplies," 11 Feb 2005. [Online]. Available: https://www.analog.com/en/technical-articles/line-and-load-transient-testing-for-power-supplies.html. [Accessed 13 March 2023].

[74] A. Satou, Y. Maruyama and H. Nakamura, "A New Model for Onset of Net Vapor Generation in Fast Transient Subcooled Boiling," Journal of Power and Energy Systems, vol. 5, no. 3, pp. 263-278, 2011.

[75] U. Rohde, "The Modeling of Fuel Rod Behavior Under RIA Conditions in the Code DYN3D," Annals of Nuclear Energy, vol. 28, no. 13, pp. 1343-1363, 2001.

[76] J. Rempe and e. al, "New In-Pile Instrumentation to Support Fuel Cycle Research and Development," Idaho National Laboratory, Idaho Falls, 2011.

[77] Y. Maruyama, H. Asaka, A. Satou and H. Nakamura, "Single rod experiments on transient void behavior during low-pressure reactivity-initiated accidents in light water reactors," Nuclear Engineering and Design, vol. 236, pp. 1693-1700, 2006.

[78] J. D. Jackson, "Studies of nucleation and heat transfer during fast boiling transients in water with application to molten fuel-coolant interactions," Nuclear Energy, vol. 27, pp. 21-29, 1988.

[79] D. L. Moreira, T. A. Moreira, D. Lee, A. Jena, G. Wang, A. Byers, B. Philips, Z. Karoutas, M. Anderson and M. Bucci, "Wettability and CHF limits of Accident-Tolerant nuclear fuel cladding materials in light water reactor conditions," Applied Thermal Engineering, vol. 216, no. November, p. 119018, 2022.

[80] H. Wen, T. D. Topping, D. Isheim, D. N. Seidman and E. J. Lavernia, "Strengthening mechanisms in a high-strength bulk nanostructured Cu–Zn–Al alloy processed via cryomilling and spark plasma sintering," Acta Materialia, vol. 61, no. 8, pp. 2769-2782, 2013.

[81] J. Duan, H. Wen, L. He, K. Sridharan, A. Hoffman, M. Arivu, X. He, R. Islamgaliev and R. Valiev, "Effect of grain size on the irradiation response of grade 91 steel subjected to Fe ion irradiation at 300 °C," Journal of Material Science, vol. 57, pp. 13767-13778, 2022.

[82] A. K. Hoffman, Y. Zhang, M. Arivu, L. He, K. Sridharan, Y. Wu, R. K. Islamgaliev, R. Z. Valiev and H. Wen, "Novel effects of grain size and ion implantation on grain boundary segregation in ion irradiated austenitic steel," Acta Materialia, vol. 246, no. March, p. 118714, 2023.

[83] Department of Energy, "Mission," Energy.gov. [Online]. [Accessed 29 09 2017].